University of Bolton

Sunwater Project
- An Innovative Water Desalination System operated with Solar Thermal Energy

DOCTOR OF PHILOSOPHY

This thesis is submitted in partial fulfilment
of the requirements of University of Bolton, UK

This research programme was carried out in collaboration with the
South Westphalia University of Applied Sciences in Soest

Submitted by
Φ Daniel Buschert
from Recklinghausen, Germany

Soest, December 2014

Old Egyptian Sun God Re & Water God Sobek

Water, water, everywhere,
Nor any drop to drink.
- *Samuel Taylor Coleridge*

Bolton supervisor:	Prof. Dr. Danny Morton
Soest supervisor:	Prof. Dr.-Ing. Berthold Bitzer
Internal examiner:	Prof. Dr.-Ing. Egon Ortjohann
External examiner:	Prof. Dr. Naren Gupta

Abstract

key words: *solar energy and water shortness, water desalination, solar thermal, combination solar thermal and water desalination system, solar desalination, simulation, system model, demonstration plant, realisation, modelling, simulation results, measurement results, future prospects*

The present document is in the field of renewable energies in combination with an innovative water desalination unit (WDU). During this project a future proof and environmentally friendly solar desalination demonstration plant was planned, modelled and simulated in Germany and finally installed in Egypt. This includes a model of the solar thermal system and a model of the innovative water desalination unit, which works with evaporation. Additionally a few measurement and simulation results are presented and discussed. A connection is also given between both aspects. Furthermore a few future prospects are added, which can be used to improve later installations.
During this project it was shown, that it is possible to produce freshwater with state of the art technologies by using a solar desalination system. Solar energy can be tapped in a lot of areas to produce enough thermal heat to operate an evaporation desalination unit, which produces high-quality freshwater. The quality is high enough for the daily life in private homes and for the agriculture. If it should be used as drinking water it has to be accumulated with trace elements. During this project different difficult problems were found and solved, which should be taken into account during a later realisation and for a commercial use. One bigger problem is that the sun does not shine the whole day and therefore the produced thermal energy must be stored for a later usage, if the desalination unit should be operated 24 h/d. Another problem is the storage of the heat source itself, because the working temperature of the WDU is up to 95 °C and therefore the long-time storage is very difficult due to heat losses during the night and convection of hot and cold water. Additionally it is very difficult to adjust the output temperature of a huge solar thermal field to the desired operation temperature.
Finally the present document shows an innovative way for a worldwide future-proof freshwater supply, but the complete system is still optimisable and it could be very interesting to add new aspects in future projects.

My references

1. Daniel Buschert, *X-Band-ESR-Spektroskopie polarisierbarer Targetmaterialien bei tiefen Temperaturen*, diploma thesis, Ruhr-Universität-Bochum, Germany 2005
2. Daniel Buschert, *Optimization of energy parks with biomass plants and water desalination*, UPEC 2008, Padua, Italy 2008
3. Daniel Buschert, *Concept for optimization and simulation of renewable energy parks with desalination*, ICREPQ'09, Valencia, Spain 2009
4. Daniel Buschert, B. Bitzer, *Report 2: Analysis of the gathered data*, South Westphalia University of Applied Sciences, Campus Soest, Germany 2009
5. Daniel Buschert, *Modeling a solar desalination*, ICREPQ'10, Granada, Spain 2010
6. Daniel Buschert, *Water desalination with evaporation from environmentally friendly waste heat source*, UPEC 2011, Soest, Germany 2011
7. Daniel Buschert, *Sunwater and beyond*, ICREPQ'14, Cordoba, Spain 2014

Acknowledgements

At this point I want to say thanks to all people who gave me the possibility to write this PhD thesis at the University in Soest. Additionally I want to say thanks to all people who helped and supported me in the last years:

First and foremost, I would like to express my sincere gratitude to Prof. Dr. Morton from the University in Bolton for his encouragement, guidance and support. Without his help this PhD thesis would not have been possible.

Afterwards I want to say thanks to my internal examiner Prof. Dr.-Ing. Ortjohann and my external examiner Prof. Dr. Gupta for the pleasant atmosphere in the viva and the encouraging and constructive feedback. I am grateful for their thoughtful and detailed comments.

I would also like to express my sincere gratitude to Prof. Dr.-Ing. Bitzer at the SWU for his comments, valuable suggestions and the opportunity to initialise and work on this difficult and very interesting project. Many thanks for the incredible time and challenges during my time at the SWU.

A special thank goes to Prof. Dr. Amin and his project team at the HU. Without their help this Sunwater project would not have become reality.

I want to say thanks to Mr. Heyn, Mr. Schlickum and Mr. Siegmon from Terrawater for their help and contributions to the Sunwater project. Furthermore for a lot of interesting discussions which helped to finalise this innovative project.

My thanks goes to Prof. Dr. Virk from Endonergy and Mr. Kolhe from the SWU for the difficult work, which they undertook for this innovative and future oriented project.

Special thanks goes to Marga Taylor for her invaluable help concerning English language questions and for her support during this thesis.

I owe Mr. Vogelsang, Dr. Orlob and Dr. Johannsen a debt of gratitude for their support in Soest and the time we worked together in mathematics.

I also want to say thanks to Dr. Dominik Aufderheide, Prof. Dr. Dina Dreisbach and Mrs. Katrin Feldmann for their scientific help and the encouraging conversations during my time at the University in Soest. I wish them the best for their future work.

Furthermore I want to say thanks to my parents, my grandparents, my sister and their common-partners for their support in the last several years.

Finally, and last but not least, I want to thank all people who supported and helped me in the last years. This includes my close friends, for example Christian, Björn, Heiko, Jan and Lars and in particular Caroline, Christin, Claudia, Daniela, Kathrin, Nina and Sabrina. Thank you very much for the fantastic years which we had and which we will have in the future.

Finally my best wishes for all other people in Soest, my circle of acquaintances, my circle of friends and my family for the future.

Contents

List of Figures

List of Tables

List of Abbreviations

AM	- Air mass
CSP	- Concentrated solar power
DST	- Daylight saving time
ED	- Electrodialysis
EoT	- Equation of Time
HRA	- Hour angle
HU	- Helwan University
LST	- Local solar time
LSTM	- Local standard time meridian
LT	- Local time
MED	- Multi-effect distillation
MSF	- Multi-stage flash distillation
MSL	- Mean sea level
ODE	- Ordinary differential equation
PCM	- Phase change materials
PV	- Photovoltaic
RO	- Reverse osmosis system
SE	- Solar Egypt
ST	- Solar thermal
STR	- Solar thermal roof
SWU	- South Westphalia University in Soest
TC	- Time correction factor
THV	- Thermo-Hydraulic Vector
TW	- Terrawater
TW5	- Terrawater desalination unit for max. $5\,m^3/d$ freshwater
UTC	- Coordinated Universal Time
VC	- Vapour compression
WDU	- Water desalination unit

List of Symbols

s	- Scalar
$\vec{r}$	- Vector
$\underline{A}$	- Matrix
const.	- Constant value
$\exp(x) = \mathrm{e}^x$	- Exponential function
$\frac{\mathrm{d}}{\mathrm{d}i}$	- Total derivative for i
$\frac{\partial}{\partial i}$	- Partial derivative for i
i	- Imaginary unit
s'	- First derivative in x
$\dot{s}$	- First derivative in time
$\mathcal{O}(x)$	- Up to the order of x
$\hat{e}_i$	- Unit vector for the coordinate i
$\triangle$	- Delta
∇	- Nabla operator
$\Delta = \nabla^2$	- Laplace operator
$\mathrm{grad}\, s = \nabla s$	- Gradient of s
$\mathrm{div}\, \vec{r} = \nabla \cdot \vec{r}$	- Divergence of $\vec{r}$
$\mathrm{rot}\, \vec{r} = \nabla \times \vec{r}$	- Curl of $\vec{r}$
Q	- Volume flow rate
t	- Time
T	- Temperature or time of circulation
$\mathbb{N}$	- Natural numbers without 0
$\mathbb{N}_0$	- Natural numbers with 0
$\mathbb{Z}$	- Integers
$\mathbb{R}$	- Real numbers
Na^+	- Sodium kation
Cl^-	- Chloride anion

1. Prologue

This doctoral thesis follows the diploma thesis in physics with the translated title „X-Band-EPR-Spectroscopy for the polarized solid state target at very low temperatures“ [Bus05] which was in the field of nuclear and particle physics. It was written at the institute for Experimental Physics 1 AG at the Ruhr-Universität-Bochum, Germany. This doctoral thesis was written at the South Westphalia University for Applied Sciences at the campus in Soest, Germany, for the University in Bolton, UK. The present document is in the field of renewable energies in combination with an innovative water desalination unit (WDU). The desalination unit came from a German company in Kiel, named Terrawater. During this project a future-proof and environmentally friendly solar desalination demonstration plant was planned, modelled and installed in Egypt. Furthermore different theoretical considerations were aspired for this publication. Most of the work of the Sunwater project was done at the University in Soest. This PhD thesis is submitted in partial fulfilment of the requirements of Bolton University, UK for the degree of Doctor of Philosophy. It is part of the cooperation between the Universities in Bolton, UK and Soest, Germany.
This document is subdivided into several chapters. Chapter 2 gives a short overview of water shortages in the world, different water desalination technologies, the global solar radiation and the technology behind commonly used solar thermal and PV systems. Finally the idea of this innovative Sunwater project is described, which is the basis of this work. Chapter 3 gives the theoretical background for the calculation of the solar radiation and explains the difference between evaporation and boiling. The differences are important for the project and they are necessary to show the innovation of this project and its sustainable future. Chapter 4 explains components necessary for the realisation of the Sunwater project in Egypt. This includes the WDU, the solar thermal roof and other needed components. Additionally the complete intended realisation of the demonstration plant is presented. Chapter 5 discusses the realisation of the demonstration plant in Hurghada, Egypt. It also includes the control strategy of the system. Additionally the justification is given for the chosen location. Chapter 6 deals with the simulation of the demonstration plant. The model and the simulation of the solar thermal part and the whole water desalination unit are explained in detail. This includes physical models of different components. Furthermore different other aspects are discussed. Chapter 7 shows the measurement and simulation results of the demonstration plant. Furthermore an evaluation of this data is included. This chapter also includes discussions of improvements and other aspects. Chapter 8 deals with the summary of this project, possible optimisations and add-ons for later feasible studies and realisations. Annexes B till C give further information to the background and contains

necessary mathematical and physical information. A glossary and additional tables with needed information are included there.
This document is chronologically organised. The first chapters were done before or at the beginning of the project. The simulations and the evaluations were done in the middle of the project. The realisation and the measurements were at the end of the project. Future prospects were reviewed after the project. The order of the chapters does not reflect the order of writing.

1.1. Aims and objectives

The aim of the Sunwater project with partners from Germany, UK and Egypt was to install a solar thermal system in Egypt which can be used to operate an innovative evaporation desalination unit with solar thermal energy. Additionally an environmentally friendly backup system was considered to increase the efficiency of the whole system and to extend the working time after sunset. Unfortunately this backup system was not able to be installed within the timescale of this project.
At the moment most water desalination units are operated with fossil fuels. Further information can e. g. be found in [Qad09], [Daw12] and [Dar08]. Due to the carbon dioxide emissions this freshwater production accelerates the greenhouse effect and thus it is not future-proof. Due to the worldwide combination of water shortage and a high solar radiation this combination seems to be an innovative and future-proof approach. Based on this, the project team's first idea was to use solar energy in combination with a heat pump to produce enough thermal energy to operate a water desalination unit. At the beginning of the project life-cycle the combination of renewable energies and a water desalination unit was a novelty. In the last few years, however, more and more papers have been published concerning this topic. Papers are e. g. [Ire12], [Mdr12] and [Hoa09]. In 2007 the DLR (*Deutsches Zentrum für Luft- und Raumfahrt*) published a report which shows the theoretical possibility to combine solar thermal and water desalination, but a demonstration plant was not planned and installed [Aqu07]. [Pet03]. In this project one of the first commercial available systems were used.
At the moment the state of the art water desalination units are Reverse Osmosis (RO) or thermal desalination systems like Multi-Effect Desalination (MED) or Multi-Stage Flash Desalination (MSF) systems [Gtz09]. The thermal desalination systems work with distillation of saltwater. Due to this market dominance of these systems the idea was to use a complete different water desalination unit. The chosen water desalination unit came from the German company Terrawater [Ter10] and works with evaporation and therefore it is itself an innovative system. The advantage of this system is that the operation temperature is below the boiling point of water and it also works at ambient pressure and therefore it is user-friendly, and has a long life expectancy. Furthermore it has a very high efficiency which can be scaled to the available energy.

The project objectives were:

1. To determine a suitable location, to enable physical realisation of the solar thermal system, and typical of the environment where commercial systems would be viable. This required the availability of salt water and a relatively high level of solar radiation throughout the year.
2. To gather and analyse the location weather data, to enable simulations to be undertaken.
3. To simulate the operation of the solar system based on the available weather data.
4. To develop a control strategy, including the specification for sensors, pumps, solar panels and other hardware components.
5. To design and install a demonstration plant based on the simulation results and the devloped control strategy.
6. To test and gather data from, the prototype installation, in order to evaluate its efficiency, optimise its performance, and inform the design of a commercially realisable system.
7. To produce a specification for the design of commercial systems.

1.2. Contribution to knowledge

At the beginning of the project different components were available which have not been combined to such an innovative system. This were e. g. the evaporation desalination unit and the vacuum or flat plate collectors. They were installed side-by-side. At that time they were not combined in one system. Therefore this feasible study was done to show, if it is possible to combine both aspects in a new and extraordinary system. Later in the project life-time it was seen that it was more complicated than expected at the beginning. Different solutions must be found to plan and operate the system. This includes a method to control the energy harvesting, the storage of the solar thermal heat and the transfer of the energy to the water desalination unit. During the project life-time there was found a possibility to simulate the solar thermal system and additionally the new water desalination unit.
With this project it was finally shown, that it is possible to combine both aspects to produce usable freshwater, but in later realisations different modification could be made to raise the efficiency of the whole system. This includes the exchange of components and to include other components. This can for example be done in later feasible studies or in other projects.

2. Introduction

In the first sections of this chapter the background of the project is illuminated and summarised. This includes the demand on freshwater not only in the third world, but also the possibility to harvest enough energy with renewable energy sources for the operation of the demonstration plant. Additionally, different water desalination technologies are presented. Finally a short overview of the idea of the Sunwater project is given.

2.1. Water shortages in the world

Water is the foundation of the development and affluence in the world, however, this valuable resource is becoming more and more scarce [Gtz10], as can be observed in the daily news. Many people need to migrate, because of water shortages in their home countries. This is happening for example in Afghanistan or in East Africa like in Somalia at the moment [Wwf09].
On our blue planet there are 1.4 billion cubic meters of water, but only 2.5 % are freshwater and therefore directly usable for humans or animals. Of this 2.5 % round about 70 % is frozen in glaciers and ice caps. The remaining 30 percent is divided into 97 % ground water and 3 % surface water, like rivers, lakes or marshes. A detailed overview of the water distribution on Earth can be found in Fig. 2.1. As can be seen the amount of usable freshwater is negligible. Another problem is, that the freshwater resources are not equally distributed. At the moment a few countries have a huge freshwater reserve, but on the other side in a lot of countries they do not have enough freshwater for a daily freshwater supply. A short overview of the actual freshwater resources can be seen in Tab. 2.1. In a few countries, like in Saudi-Arabia, the total renewable water resources are vanishingly small, but in other countries the renewable water resources are significantly

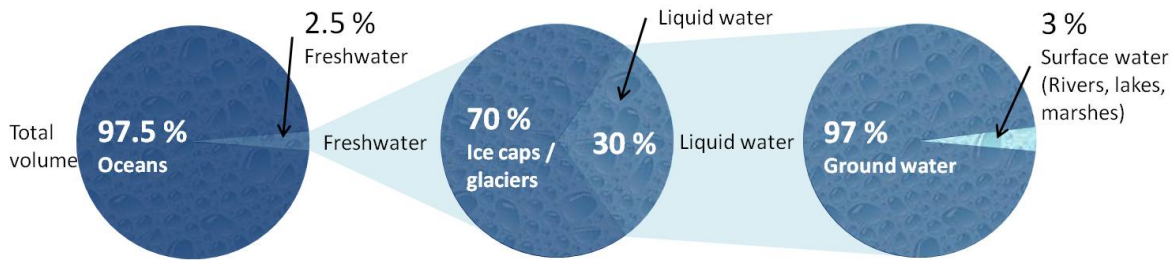

Fig. 2.1.: Saltwater and freshwater distribution in the world [Gtz10].

Tab. 2.1.: Freshwater resources and withdrawal for selected countries [Des10].

country	year	Renewable water resources		Water withdrawals
		total	per inhabitant	
		[bn m^3]	[m^3]	[m^3]
Australia	2002	492	25034	1218
Egypt	2002	57	786	937
Germany	2002	154	1873	473
Norway	2002	382	84178	483
Saudi-Arabia	2007	2	97	959
Spain	2002	112	2703	864
United States	2007	3069	9943	1550

high, as it is the case for example in Norway. In the country itself there could also be an unequal balance of the available freshwater resources. A good example for this is Egypt. Only close the Nile and in the Nile delta, there is enough freshwater, but in other parts, like in the Arabic and Libyan Desert, it is very hard to find freshwater. The first desert is right-handed of the Nile and the other desert is left-handed of the Nile. Sometimes freshwater resources are available in a depth between 6 m or 100 m, sometimes there is no freshwater available. Renewable water resources mean in this context the available freshwater feeding based on annual precipitations. In Germany only a few percent of the available annual resource is used. In other countries, however, there is a very low amount of renewable water resources available. Due to the low amount of renewable freshwater resources a lot of people do not have access to clean drinking water, furthermore many existing freshwater resources are polluted with waste water, which comes from the industry, agriculture or human beings. South of the Sahara Desert more than 43 % of the human populations have to live without clean water. Consequentially the death is very high, this is accompanied with malnutrition. This causes every fifth child to die before it is 5 years old. Worldwide more than 4500 children die every day, because they drink polluted water. Most people who do not have access to clean freshwater are living in unhygienic circumstances are located in Asia. In China and India alone more than 1.5 billion dispose the waste water without filtering and cleaning into the environment. Furthermore the ground water in Asia is contaminated with arsenic and fluorides and thus 50 million humans are in danger [Uni06]. Due to the expected global warming, the demand of freshwater will increase, because local mean temperatures increase and this has a direct effect on the freshwater demand. Countries which have just enough freshwater to live at the moment, may have a much bigger problem in the near future. One reason could be a lack of rainfall or an increasing freshwater demand.
Water is one of the most precious commodities of our time and it is needed for a lot of different applications. It is needed for cooking, preparing food and food manufacturing

in agriculture. Additionally it is needed in industries and private households. The demand of freshwater depends on the application. At the moment most water is needed for the agriculture. The water demand in Africa and Asia has risen to 85 % in this field. In other countries only two-third of the annual water consumption is needed for the irrigation. 20 % of the freshwater is needed for the industry and for households 20 % are estimated [Wel11].
Not only the direct use of water is important for the freshwater calculation, but also the so called virtual water must be considered during the life cycle. Virtual water is the water, which is used for the production of the product and which is not included in the final product. It varies extremely from product to product. For one 0.33 l Coca Cola can 70 l of virtual water is needed. For 1 kg corn 1400 l of freshwater are needed, 500 pages of DIN-A4 paper need 5000 l and for 1 kg beef 5000 l − 20 000 l of freshwater are necessary [Was11]. As be seen, the virtual water demand is much higher than the real water demand, but for the production of the commodity it is necessary. The demand could perhaps be somewhat reduced, but freshwater is always needed for the production. A German for example uses less than 130 l/d freshwater, but the virtual demand on freshwater, which is also called the virtual footprint is more than 4000 l/d. 50 % of the virtual water amount is imported.
Without sufficient freshwater supply, humans cannot survive. On average humans will only live for 3 days without freshwater. In contrast, they can live for a maximum of 3 weeks without food. This shows the importance of the commodity water. Therefore a possibility must be found to deliver clean freshwater to all humans and animals. In the next years the world population will rise and the demand on freshwater will also increase. The problem is that the water demand does not increase linearly, it increases much faster. Therefore a possibility must be found to produce the necessary freshwater in an environmentally friendly way. It makes no sense to produce a lot of carbon dioxide for the freshwater production, because carbon dioxide is responsible for global warming [Sol08].
Due to the shortfalls of water there is the fear, that there could be a lot of water wars in the world in the near future [N24]. It could for example happen in Africa. The Nile passes nine African states and it is the main freshwater supply in this region, especially in Egypt. 95 % of the Nile water is used for the freshwater supply in Egypt. In May 2010 Ethiopia and other countries decided to increase the withdrawal of water at the head water from the White and Blue Nile. The increased withdrawal of water can intensify the water problems in this region, because the actual water situation is already stressed. 85 % of Nile water comes from Ethiopia and the idea was to install irrigation systems and water power plants in Ethiopia, which could have a negative effect on the actual freshwater supply downriver and this effects not only Egypt. The difficult situation was appeased by the Egyptian government with favours and development policy promises. This problem cannot be solved by sitting it out and therefore other possibilities must be found to supply enough freshwater. The Egyptian government offers Ethiopia to help building new wells and irrigation systems, if they do not increase the water sampling in the head waters. Not only the Egyptians, but also other states think about how to secure their water resources with military missions and build-up of arms [Hei07]. Ad-

ditionally Egypt and other countries are deliberating, whether they should develop new water resources, including for example new and expensive water desalination systems like in other rich Gulf States. This is only one example for the aggravation of the actual situation. In the actual news further examples can easily be found.
Therefore new possibilities must be found to produce freshwater inexpensively and make it usable in a wide range of ways. Additionally the water production must be environmentally friendly. Not only the rich states need freshwater, but in particular poor countries in the third world need the possibility to generate freshwater for the inhabitants. One important possibility is to desalinate saltwater and the other possibility is to save the existing freshwater resources.

2.2. Water desalination technologies

Desalination means the production of freshwater or industrial water by reducing the salinity in the saltwater or brackish water. Freshwater distinguishes itself by the degree of purity, which includes a low salinity. In a lot of countries the allowable salt content in water is defined by directives and regulations. For example the Na^+ concentration in Germany must be below 200 mg/l and the Cl^- concentration must be below 250 mg/l [Tri01].
The kind of water is differentiated by the salinity. If the salinity is between 0.1 % and 1 % it is called brackish water, when the salinity is higher it is called saltwater. In the Anglo-Saxon the critical value for brackish water is sometimes up to 1.8 %. The name brackish comes from the Low German word Brack, which means the stirring of saltwater and freshwater. This happens for example after a crevasse in a newly formed lake. The salinity in saltwater can be from 1 % (1.8 %) up to 44.2 % in the Don-Juan pond, which is close to the west end of Wright Valley (South Fork), Victoria Land, Antarctica. The mean salinity in the seas is 3.5 %. In some areas it is necessary to use saltwater and brackish water for the freshwater production, because no other possibilities are available [Mic09]. Therefore this kind of water must be cleaned from salt and other impurities to use it as drinking water, otherwise it cannot be used. In Fig. 2.2 an overview of the global desalination capacity in 2005 can be found. In Saudi Arabia 18 % (6.5 million m^3/d) of water is converted. It is followed by 17 % (6 million m^3/d) in the USA, 13 % (4.8 million m^3/d) in the United Arab Emirates. Only 6 % (0.5 million m^3/d) and 5 % (0.4 million m^3/d) are desalinated in Spain and Kuwait. At the beginning of 2005 more than 10 000 desalting units larger than a nominal of 100 m^3/d were installed or contracted worldwide. The total freshwater capacity was about 36 million m^3/d from all sources. In 2000 the cumulative installed desalination capacity was round about 26 million m^3/day. This is a mean annual growth rate of 7 %. The global installed desalination plants only produce 0.3 % of the total worldwide demand on freshwater. Just in oil-rich Middle Eastern nations this freshwater production plays an essential role [Pac06].
The conversion of saltwater and brackish water is done with water desalination units. At the moment there are a lot of different possibilities to desalinate saltwater or brackish

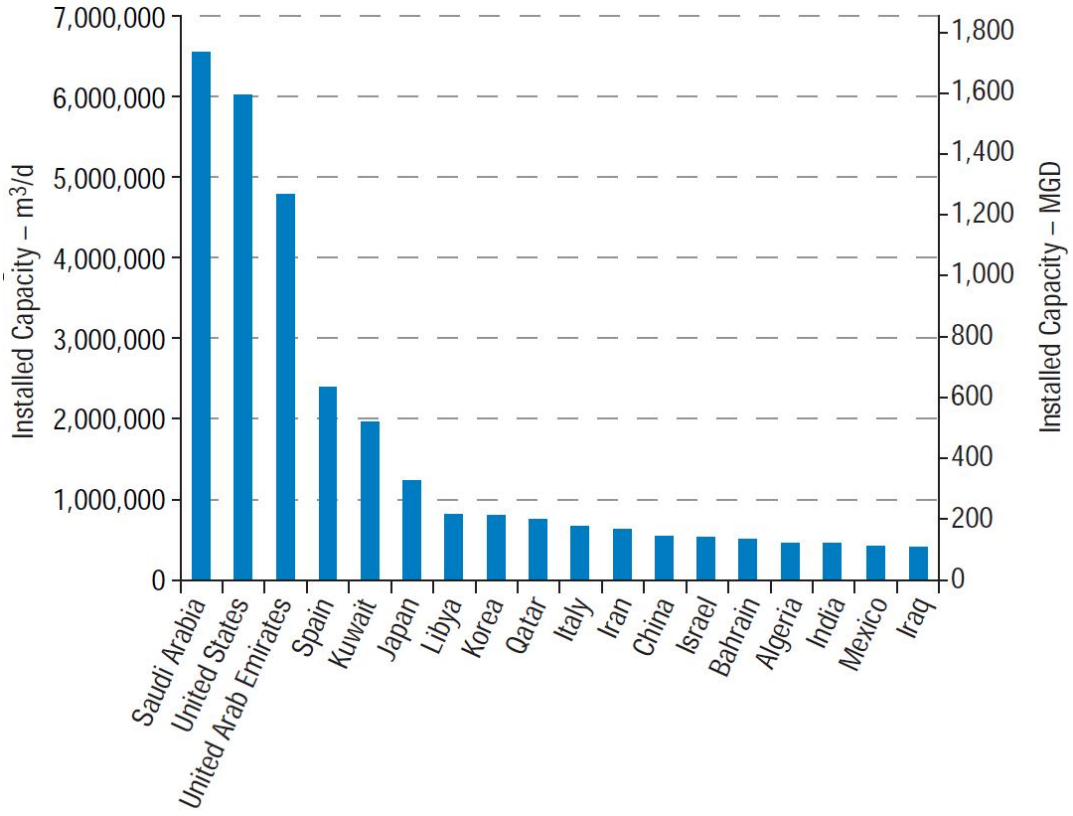

Fig. 2.2.: Countries with more than 1 % of global desalination capacity, January 2005 [Pac06].

Tab. 2.2.: Market share of the desalination technologies in 2005 [Gtz09].

Thermal desalination	Market share [%]	Membrane desalination	Market share [%]
Multi-stage flash distillation	36	Reverse osmosis	46
Multi-effect distillation	3	Electrodialysis	5
Vapour compression	5		

water to reduce the content of salts and minerals in the raw water. An overview and the market share of the most widely used desalination methods can be found in Tab. 2.2. 82 % of the freshwater is produced with multi-stage flash distillation (MSF) or with reverse osmosis (RO). Other desalination technologies do not play such an essential role at the moment. These are for example the multi-effect distillation (MED), electrodialysis (ED), vapour compression (VC) or evaporation systems. In the first order they can be divided into thermal and membrane desalination systems. The thermal desalination methods use high temperatures for the desalination process and the other systems use

Tab. 2.3.: Water desalination co-efficients [Gtz09, Ter10]

Technology	Max. salt concentration [g/l]	Water rate of yield [%]	Water quality [mg/l]
MSF	100	≤ 50	< 10
MED	100	≤ 50	< 10
VC	100	$30 - 50$	< 10
RO	45	≤ 50 $\leq 85^{\dagger}$	< 500
ED	3	$\leq 97^{\dagger}$	< 500
Evaporation	225	< 90	0

† Brackish water

membranes to separate the salt from the water. Thermal desalination technologies are for example MED or MSF. Membrane desalination systems are for example RO or ED. The different desalination technologies have different frame conditions for the needed saltwater and for the produced freshwater. An actual overview can be seen in Tab. 2.3. The maximum salinity of the raw water can be between 100 g/l for MSF and 3 g/l for ED. The water rate of yield also differs on the depending technology. The maximum rate of yield is 97 % for ED. Sometimes it must be separated between saltwater and brackish water. The ED can only be used to convert brackish water, because in normal saltwater the salinity is too high and therefore the efficiency is of no interest. The energy costs raise linearly with the salinity of the water.
During the desalination process not only freshwater is produced, but also brine. Brine is the remaining saltwater with a much higher salt concentration compared to the used raw saltwater, because it contains the salt, which was removed from the produced freshwater. Due to the higher salinity it cannot directly be depolluted in the seas or oceans because this could endanger and possibly destroy the environmental equilibrium. Brine is an ecological menace for the biota. Therefore other possibilities must be found to depollute it which is a product of all desalination systems. A final and environmentally friendly solution has not yet been found. Possibilities are for example to use the brine for the common salt production or it can be mixed up with added saltwater from the sea to reduce the salt concentration. Then it can be transferred back to the sea with a lower environmental impact, but this water with a higher salinity still increases the salt concentration locally in seas and oceans. It could not be a final solution.
As can be seen in Tab. 2.3 the maximum salt concentration of evaporation desalination units is much higher than the salt concentration of any other desalination unit. Therefore there is the possibility to use the evaporation desalination units to convert brine into freshwater which comes from reverse osmosis systems for example. Due to the connection in series the efficiency can be raised, and another advantage is that the amount of brine which must be disposed off can be reduced. This highly concentrated saltwater

can be easily used to produce common salt for example. Another advantage of the evaporation desalination is that water resources can be used for freshwater production, if the concentration of salt is too high for common reverse osmosis or other desalination systems.
In the following section different desalination technologies are presented. This is just a short summary of actual desalination technologies. The following sections are just an overview without any guaranty of completeness. A few desalination systems are still in development and could become important in the next years.

2.2.1. Membrane desalination

The desalination systems can be separated into systems with membranes and systems without membranes. Two good examples for desalination systems with membranes are RO and ED. In both systems membranes are used to separate the salt from the water to generate freshwater. After the desalination process, brine is left which must be disposed off in an environmentally friendly way. In the following paragraphs an overview of a few membrane desalination systems is given.

Reverse osmosis

With reverse osmosis, the saltwater or the brackish water is compressed with high pressure through a semipermeable membrane. The high pressure is necessary to overcome the osmotic pressure. Osmosis makes it possible that two fluids with different concentrations equalize through a semipermeable membrane. This is done with a rectified flow through this membrane. After the concentrations are equal in both fluids, the rectified flow stops. The process is very important in nature and in particular in cells and plants. The theoretical description is part of the statistical mechanics and right now it is still part of the actual research work. With reverse osmosis the above-mentioned method is inverted. The water in the saltwater passes the semipermeable membrane. The semipermeable membrane only lets the water pass and holds back the salts, bacteria, virus limes and poisons like heavy metals. The necessary pressure in the system depends on the salinity. For a lower salinity, like in brackish water, a lower pressure is necessary and for saltwater with a higher salinity higher pressure is needed. The pressure ranges from 10 bar to 15 bar for brackish water and from 50 bar to 80 bar for seawater. The pressure for saltwater with a salinity of 35 g/kg is 25 bar [Aqu07]. This technology is also used for separating processes in the medical sciences and process engineering.
The osmotic pressure raises with the salinity of the water and therefore the saltwater is replaced during the desalination process. Otherwise the desalination would stop at a particular salt concentration, which depends on the adjusted pressure. The higher the salinity, the higher the pressure in the system must be and therefore the energy requirements increase. Furthermore the sulphuring of the salt must be avoided and therefore the brine is exchanged. The pore diameters in the membranes are between $5 \cdot 10^{-7}$ mm

and $5 \cdot 10^{-6}$ mm and the membranes are made of polyamide for example or in actual research projects with nano tubes [Hei07, Mit11].
At the moment RO systems are one of the main desalination technologies to convert saltwater into freshwater and in the next years a rapid growth is expected. The actual size of desalination systems varies between 100 m^3/d up to 400 000 m^3/d. This can be achieved with a modular construction technique. Additionally for private and mobile usage there are systems with only 2 l/min. In 2005, in Ashkelon, Israel the world's largest RO plant has built. The daily freshwater capacity is 395 000 m^3/d [Pac06]. Efficient water desalination units have a power consumption between 2.5 kW h/m^3 and 7.5 kW h/m^3. Highly efficient plants shall have a consumption of 2 kW h/m^3 [Gtz09].
The reverse osmosis membranes are susceptible to pH, oxidisers, algae, bacteria, depositions of particulates, fouling and other organics. For the secure operation of a reverse osmosis system the raw water must be preprocessed and this can have a significant impact of the energy consumption and costs. This could for example be an extensive filtration or additions of chemicals like Ca or Na salts. This is necessary to stabilise the pH value of the saltwater. Additionally dangerous ingredients must be removed from the saltwater and later from the remaining brine. The pretreatment process depends on the necessary freshwater quality, the raw water quality or the freshwater production. Additionally the membranes must be flushed out and exchanged on a regular base. Furthermore pressure changes at the membranes must be avoided, otherwise they can be damaged.

Electrodialysis

Another desalination system is the electrodialysis which works with a membrane. With this desalination technology, electrical power is used to separate the salt from the saltwater. As can be shown, the mean salinity in the oceans is 3.5 %. In 1 kg liquid 96.5 % or 965 g is water (H_2O) and the rest is salt (35 g). The main ions in the saltwater are sodium Na^+ and chloride Cl^- with 30.6 % and 55 %. The other common ions are sulphate SO_4^{2-} with 7.7 % and magnesium Mg^{2+} with 3.7 %. Other particles in the water have a lower density. Due to the high sodium and chloride ions the most ions crystallise as cooking salt, when the water volatilises during heating. Without water the salt crystal is a solid, when it has contact with water it dissociates

$$NaCl_{(s)} \longrightarrow Na^+_{(aq)} + Cl^-_{(aq)}.$$

The index s means that it is a solid state body and the aq that the salt crystal is dissolved (hydrates) in water. As can be seen on the right side of the equation the salt crystal dissociates into an anion and a kation. Therefore it is possible to desalinate saltwater with electrical power. The anion moves to the anode and the kation moves to the cathode. For this reason, the salt concentration is reduced inside the saltwater. During the movement, the ions pass semipermeable membranes and crystallise at the electrodes. This desalination technology works with an ion exchange. As can be seen, the electrical power is proportional to the salinity of the water. The higher the salt concentration, the

higher is the demand of the electrical current. Therefore this desalination technology is only interesting for a low salinity in the process water, for example for brackish water. The advantage is that ED can produce more freshwater compared to RO systems out of the same amount of saltwater or brackish water.
An improved electro-dialysis system uses a regular polarisation change of the anode and the cathode. It is more complex, but the different membranes are cleaned and therefore a higher efficiency can be reached and in addition the covering of the membranes can be reduced. This improved system can effectively be used for water with a higher salinity [Opp86].

2.2.2. Thermal desalination

Next to the membrane desalination systems, thermal desalination is very important right now. In all thermal desalination systems, the temperature is raised to a necessary value. In some systems, the pressure is reduced or raised as well to increase the vaporisation of the saltwater. This is be done in the multi-stage flash distillation (MSF) and the multi-effect distillation (MED) for example. In contrast to these desalination technologies, the pressure does not have to be reduced in evaporation desalination systems. In evaporation systems, the water temperature is only raised to a temperature below the boiling point of the saltwater. In MSF and MED, the temperature of the saltwater is raised to or higher than the boiling point at ambient pressure and this costs more energy in comparison with the evaporation systems. Finally, the electricity consumption of MSF and MED is independent on the salinity of the saltwater, this is in contrast to the RO systems [Aqu07]. In the following paragraphs, the different thermal desalination systems are briefly presented.

Multi-stage flash distillation

A short overview of the MSF technology can be found in Fig. 2.3. It is a distillation process to convert saltwater or brackish water into freshwater. For this desalination process, the saltwater is heated up to a temperature close to the boiling point of water. Sometimes the pressure in the system is raised to increase the maximum liquid water temperature which at that point is higher than 100 °C. Afterwards the hot water enters a chamber with a lower pressure. Due to the lower pressure, the water starts boiling and only a small percentage of the water vaporises in this first chamber. The water vapour rises in this chamber and then at the top it will be cooled down with the saltwater feed, which is heated up later to the maximum temperature. It is also a preheating of the saltwater and due to this concept, the efficiency of the system is raised. During the cool-down period the freshwater condenses and then the condensed freshwater is extracted from this chamber. It can now be used as freshwater. The remaining brine is reused in the next chamber as a freshwater source. After the last chamber, the brine must be discharged. The amount of the vaporised water depends on the temperature of the

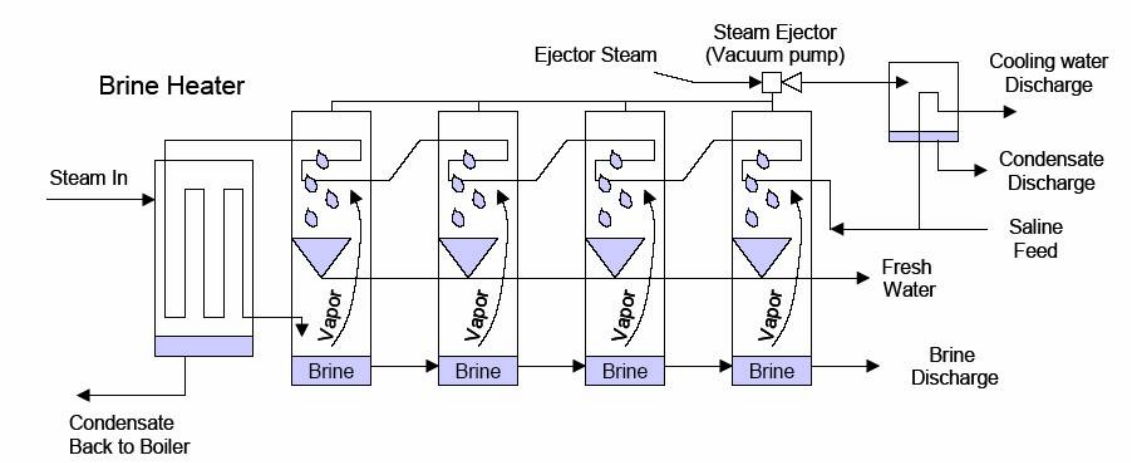

Fig. 2.3.: Principle of Multi-Stage Flash Desalination (MSF) [Aqu07]

saltwater and the pressure in the chamber. Until an equilibrium between the water temperature and the pressure is reached, the saltwater vaporises. When the saltwater enters the chamber, it immediately starts boiling, almost exploding or flashing. Therefore this desalination system is called flash distillation. The hotter the water and the lower the pressure in the system, the better is the rate of yield, but due to the thermodynamics it is better for a high efficiency of the system to pass different equilibrium conditions. For this reason different chambers are used to desalinate the water. It can reach up to 40 stages with different pressures and water temperatures. For the different pressures in the chambers, a vacuum pump or steam ejector is needed.
MSF desalination units are often combined with steam or gas turbine power plants. This is for example done in the Middle East, like Saudi Arabia, the United Arab Emirates and Kuwait [Ett06]. It is used especially in those countries because the necessary fossil fuels for the operation are relative cheap at the moment. It will change in the next decades because their sources are decreasing [Faz06]. In these power plants, the fossil fuels are burned, and with this combustible a gas turbine is used to produce electricity. Afterwards the temperature is high enough to operate the water desalination unit. The extracting steam needs a temperature between 90 °C and 120 °C and then it can be used for the MSF distillation.
For the desalination with MSF 330 kJ/kg of heat is required for the product. The electricity demand is in the range between 3 kW h/m^3 and 5 kW h/m^3. Furthermore 6 kW h/m^3 to 8 kW h/m^3 are lost in the electricity generation, because of the higher temperatures which are needed for the hotter gas turbine steam [Aqu07]. Due to the energy losses for the power generation, the size of this power plants must be designed larger.

Multi-effect distillation

Fig. 2.4 gives an overview of this distillation process to generate freshwater. The saltwater enters a chamber (effect) at the top and is sprayed or distributed inside this chamber.

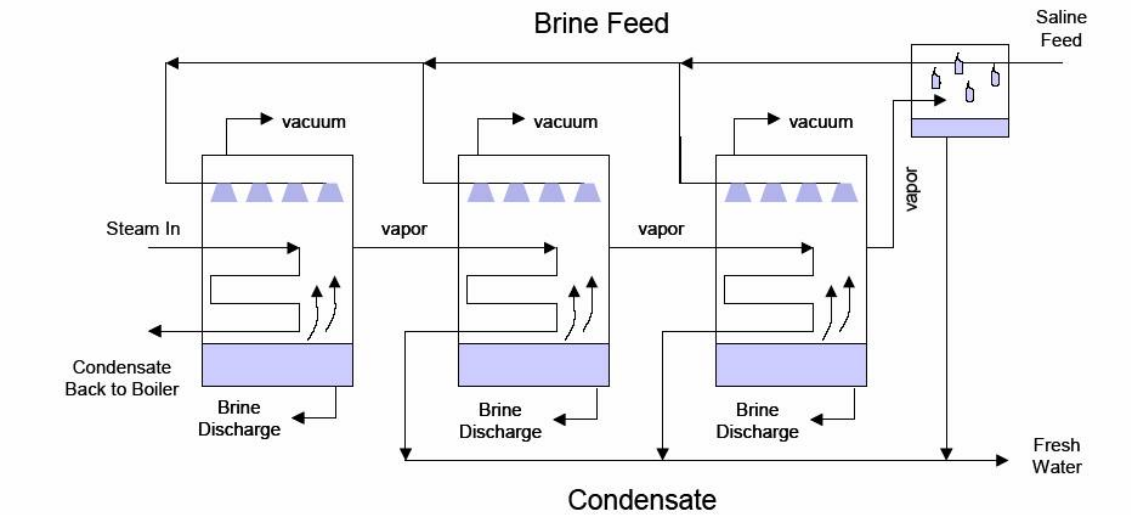

Fig. 2.4.: Principle of Multi Effect Desalination (MED) [Aqu07]

It is normally distributed onto the surface of tubes. In the first stage, the sprayed saltwater is heated up to the boiling point with an external hot steam or from a boiler. The vaporised water leaves the first chamber and is used inside the next chamber as a heating source for the next vaporisation. In the first stage and in the next stages the remaining brine leaves the chambers at the bottom and then it must be disposed off. During the temperature release, the water vapour condenses and leaves the second chamber as freshwater. The sprayed saltwater in the second chamber is vaporised and will again be used in the next chamber. The chambers are called effects. This can be repeated up to 16 times. The disadvantage is that in every successive chamber the pressure must be lower than in the foregoing effect, otherwise less freshwater is produced, because the water will not boil. If the water is not boiling, the freshwater is not produced with distillation. The vapour from the last effect is cooled down with the incoming saltwater. This is also a preheating of the saltwater. The heating source in the first effect can come from a power plant or from a boiler. The temperature can have a wide range and it is also possible to operate this desalination system with temperatures lower than 70 °C, but the pressure in the system must be reduced accordingly. Lower temperatures have the advantage that corrosion and scaling is reduced and that low temperature heating sources can be used. Therefore MED allows the usage of low-waste heat sources. If it is coupled to a steam cycle, the power losses are much lower compared to a MSF plant.
The heat consumption of the MED is in the range from 190 kJ/kg to 390 kJ/kg at less than 0.35 bar. The electricity consumption is between 1.5 kW h/m^3 and 2.5 kW h/m^3. MED has gained attention due to a better thermal performance compared to MSF.

Evaporation desalination

Instead of an operation with overpressure and underpressure which is generated with a vacuum pump and to raise the temperature to or higher than the boiling point at ambient pressure, the above-mentioned systems can be slightly modified. An innovative idea is to heat up the saltwater not to the boiling point, but to a desired temperature close to the boiling point. This is done at ambient pressure. Therefore the evaporation desalination unit does not need a reduced operation pressure inside the evaporation chamber. This is in contrast to the MSF and MED, where the pressure is reduced for the operation. The complete system can be operated at ambient pressure and thus a vacuum pump or a steam ejector is not necessary. For example the vacuum pumps are prone to damage and therefore a damageable component can be economised. This has the advantage that the operation of an evaporation desalination unit is safer compared to systems with a vacuum pump.
An overview of the used evaporation desalination system can be found in Fig. 6.1. The volume flow is explained in that chapter, because this detailed information is needed for modelling and simulation.
The hotter the saltwater in the system, the more water evaporates in the system. The vaporisation of water is described with the vapour pressure curve of water (3.42). Therefore a temperature close to 100 °C is preferable, but it is not necessary for an operation. The evaporated water is cooled down with the incoming saltwater and the condensate leaves the system and is useable as freshwater. For drinking water it must be accumulated with trace elements, otherwise an excessive consumption can cause a water intoxication in humans, because the necessary electrolytes are missing. Furthermore the system can be combined with a heat recovery, because the leaving brine could have a temperature of more than 30 °C. In this case less energy is lost during the desalination process.
For the Sunwater project a water desalination unit was chosen which works with evaporation. It is a very innovative and future-proof technology and additionally it is not state of the art at the moment. The most widely used desalination systems are RO or MSF. Furthermore the WDU used is not so prone to damage, because no vacuum pumps are needed and the other components are durable and cannot corrode. Another advantage is that the system can be self-sustaining. Additionally the operation temperature is below the boiling point of water at ambient temperature and therefore solar collectors can be used to deliver thermal heat for the operation. The necessary electrical energy for the pumps and the monitoring can be taken out of the grid. The usage of this desalination unit is very promising and future-proof. Furthermore, the system is still under development and will be enhanced in the next years.

2.3. Global solar radiation

As a renewable energy source, different possibilities are of interest. The system can be operated with geothermal, biomass or solar energy for example. Due to the fact that the freshwater demand and the global solar radiation are coexistent, a combination of solar energy and water desalination was chosen. Most countries with a high solar radiation have also a high demand for freshwater. This can be seen by the worldwide distribution of freshwater and the daily solar radiation for example.
This section briefly describes the background information of the global solar radiation. This includes the energy generation and why the solar radiation differs on earth during one year on the same location. Furthermore it compares different energy densities at different locations. It also shows that a few areas are more predestined for solar installations than other areas.
It is commonly known that solar radiation comes from the Sun and the energy is produced in the core with thermonuclear fusion of hydrogen. During the year the Earth runs on a elliptical orbit around the Sun. The Sun is located at one of the focal points. Due to the elliptical orbit, the speed of the Earth and the distance to the Sun varies throughout the whole year. In mean the distance is $r = 1.496 \cdot 10^6\,\mathrm{km} = 1\mathrm{AE}$. Furthermore the axis of rotation of the Earth is not perpendicular on the orbit of the Earth. Therefore the solar radiation varies during the whole year. If the Earth would be on a circular orbit and the axis of rotation of the Earth would be perpendicular on this orbit, the amount of the solar radiation would be theoretically the same during the whole year. The Sun emits not only electromagnetic radiation, but also charged and uncharged particles. They reach the Earth through the vacuum. The charged particles are diffracted from the Earth's magnetic field[1] and thus the Earth is shielded. The most charged particles are for example electrons e^-, protons p^+ and α-particles ${}^4_2\mathrm{He}^{2+}$. It is therefore a plasma. Most uncharged particles are neutrinos ν, in particular the electron neutrinos ν_e. They have a maximum mass of $m_\nu = 0.2\,\mathrm{eV/c^2}$ and a velocity close to the speed of light c.[2] Most pass the Earth without interaction, because they interact only with the weak interaction and thus the interaction is very low. Therefore it is very difficult to detect them, but a few possibilities exist at the moment. These are for example the Super-Kamiokande in Japan or the IceCube at the South Pole. The detectors detect neutrinos with Tscherenkow-Light or with the usage of scintillators for example.
Due to diffraction of the charged particles and the passing of the neutrinos, only the electromagnetic radiation reaches the surface of the Earth. The highest intensity is in the area of the visible light. With the assumption that the Sun is nearly a black body with a temperature of 5800 K the maximum radiation is at 500 nm, which is the colour green in the visible spectrum. The Sun's surface temperature can be calculated with the Stefan-Boltzmann law and the wavelength can be calculated with the Wien's displacement law. The complete wavelength of the Sun is in the range between hard x-rays

[1] A Pole Shift is not expected within the next 2000 a.
[2] Newer measurements show that neutrinos ν do not have a velocity fast than the speed of light c. In contrast to 2011 [Phy11, Nat11, Cer11], when a few measurements showed that it could be possible.

and long radio waves. At the position of the Earth, the long standing, seasonal mean of the solar radiation is 1367 W/m^2. This value is without the Earth's atmosphere and it was assigned by the World Meteorological Organization (WMO / OMM) in Geneva in 1982. It is also called solar constant [Chi04]. Since 1978 the solar constant is measured in space and it is the perpendicular radiation on a plane surface, without consideration of the atmosphere.
The solar radiation passes the Earth's atmosphere. During the passing of the air mass, which is dependent on the zenith angle, a part of the solar radiation is scattered and absorbed. The global solar radiation is the radiation which reaches the surface of the Earth. It consists of the direct solar radiation and the scattered radiation, the indirect solar radiation. It can for example be scattered in the atmosphere directly from dust particles or small water drops. The total solar radiation varies from 0 W/m^2 at night and up to values higher than 1000 W/m^2 in a few areas around the equator. Just 110 W/m^2 is the mean value in Germany during one year. This is justified with the shadowing effects of clouds, fogs and vapours. The annual sum of the solar radiation in Germany is between 900 kW h/(m^2 a) and 1200 kW h/(m^2 a). This value is measured on a horizontal area. In Spain the global solar radiation is round about 2000 kW h/(m^2 a) and in the Sahara 2500 kW h/(m^2 a). With this high daily solar radiation, in particular around the equator, it is possible to produce a lot of energy which can for example be used for electricity or for thermal energy generation. In Germany only 18 % of the time is there a high amount of a global solar radiation during the year, this amounts to only 1550 h/a. Therefore it is more interesting and effective to install solar collectors in the sunbelt of the Earth, these are for example the southern countries in Europe and for example in North Africa, Australia, America or Asia [DPG10]. In these countries the factor is sometimes 2.5 times higher compared to Germany. Therefore less modules or absorber areas are needed to generate the same amount of energy. There is less area demand for the same capacity, due to the higher solar radiation and the longer incident solar radiation during the daytimes. Another advantage is for example that the investment costs are lower compared to Germany and furthermore there is no conflict between shadowing effects, in particular with actual agricultural use. The installation of collectors and the associated shadowing effect could have additional advantages for agriculture, because in the time dependence shadows, plants can easily be grown.
The first steps have been accomplished with the Desertec project [Des11]. It is a concept to produce renewable energy with solar energy, wind energy and PV in deserts. For this a few studies were done to show the possible realisation of this intention. This includes for example solar thermal power plants with Concentrating Solar Power (CSP) or photovoltaics (PV). For the CSP, mirrors are used to reflect the solar radiation and to focus it on a local point to reach high temperatures. With these high temperatures and a good heat transfer medium a few steam turbines could be operated to generate electricity. The sunlight is reflected with a lot of heliostats to a fixed point and there is a fluid that is heated. The temperature of the fluid can go higher than 1000 °C and this energy can finally be used to produce water or oil vapour. This vapour can be used to operate an electrical generator. If the energy is produced in deserts, the generated elec-

trical energy must be transmitted over long distances to the consumers. For an energy transport over long distances HVDC transmission lines are considered. Furthermore the usage of superconductive high voltage transmission lines is also possible, but it is still in the state of research [Bac11].

2.4. Solar systems

At the moment there are a lot of different possibilities to produce thermal and electrical energy with the Sun. Photovoltaics (PV) are used for the generation of electricity, and other collectors are used for the heat production. At the moment thermal energy is for example used to heat up the tap water or to support the heating system in buildings. In the following section a rough overview of the predominating used technologies are given. This includes PV, flat plate collectors and vacuum tube collectors. An overview of the conversion factors, thermal dissipation factors and the temperature ranges of different solar thermal collectors can be found in C.1.

Photovoltaic modules

Photovoltaics are the possibility to convert solar radiation into electric energy. This is directly done without producing thermal heat. In Germany and in many other countries it is already used to generate electrical energy. Most PV panels are installed at the roof of the building, but other installations are also possible. They can for example be included in the building walls or on the ground. The angle of setting depends on the region. The higher the latitude the higher is the angle of setting to gain the best performance from the collectors. The best angle depends on the course of the Sun during the whole year. With photovoltaics, direct current (DC) is produced at a low voltage. This can be stored in accumulators or it can be fed into the local grid. For the feed the direct current must be changed into alternating current (AC). This can be done with 50 Hz inverters, but the losses in the electronic power energy conversion can be higher than 7 %. A few actual inverters have an efficiency of 97 % with gallium nitride transistors. They work up to 600 V and the idea is to increase the efficiency up to 99 % in the next years [Phy12].
The photovoltaic effect was discovered in the year 1839 by Alexandre Edmond Becquerel. In 1883 the first conventional photo cell was built of selenium and in 1893 the first solar cell was built. round about sixty years later high purity silicium could be manufactured, which is the basis for the actual solar cells. 55 years later a worldwide globally significant industry was established in Germany. The existence of this sector is well-grounded with the massive (German) market support. PV is in network-bound renewable systems far removed from economic efficiency. Therefore it is very important to reduce costs and to become competitive in comparison to other systems. The nominal PV potential on buildings in Germany is up to 161 GW [Loe10]. This is the annual mean effective

electricity power. In the summer the value is higher, but in the winter the value is much lower. The total generated electrical power is only 10 % of the nominal power. Compared to thermal base load power stations with more than 90 %, it is a very low value. The nominal power installed in 2007 was 4550 MW, but only 456 MW was collected and in 2013 the nominal installed capacity was 36 GW. The reason is that in the night no Sun shines and the output in the morning and the evening is relative low. Furthermore nearly zero energy is produced in the winter. The load profile of the PV systems is different, therefore the main energy demand in the winter, in the evening and in the morning must be covered with alternative energy sources. Another aspect is that other power plants must be operated with a fluctuation of the energy production and this has the negative effect that the efficiency of this power plants is reduced. Sometimes they are operated with part or light load and thus the efficiency is reduced compared to the full load. In summary, PV is not as good as it seems.
In 2010 the worldwide production of photovoltaic cells and modules were 23.5 GW. This is twice as much as in 2009. Most modules are from China which together with Taiwan delivers more than 60 % of the worldwide production. In 2010 more than 77 % of the worldwide modules were installed in Europe with a total capacity of 13.5 GW. The leading position with 7.4 GW is held by Germany followed by Italy with 2.5 GW. This is more or less the same amount as in Japan, the USA and China put together [Phy11]. 90 % of the installed PV modules are made of silicium. Most systems are made of multicrystalline cells, this is in contrast to monocrystalline cells. Actual commercially available cells have an efficiency between 14 % and 19 % [Ebe11]. The typical thickness of the silicium cells is 180 µm. This is due to mechanical stability, but thicknesses of 100 µm or down to 10 µm are possible [DPG10].
The functionality of the PV modules is a p-n junction made of silicium. The photons from the Sun are absorbed and create a hole and a free electron. This is physically described with the photoelectric effect. In the ground state this electron is in the valence band. When the energy of the absorbed photon is high enough the electron excites into the conduction band. Now the electron is moveable in contrast to the ground state. An electron-hole pair is created, which is movable in the solar cell. For the generation of electricity, an internal electric field is necessary and this is created with the p-n junction. n doping means, that donors are included in the silicium crystal which have an odd electron (pentavalent) and in the p layer there is an acceptor included which has an electron less than silicium (trivalent). This material can for example be produced with particle accelerators. The two layers are layered on the top of each other. The boundary layer can be smaller than 10^{-4} cm. The electrons are accelerated to the n layer and the holes are accelerated to the p layer, this is based on the charged double layer in the crystal. A few electrons and holes recombine during their passage and are lost as heat. The remaining photocurrent can directly be used by the consumers. For a standard cell the output voltage is just 0.5 V.

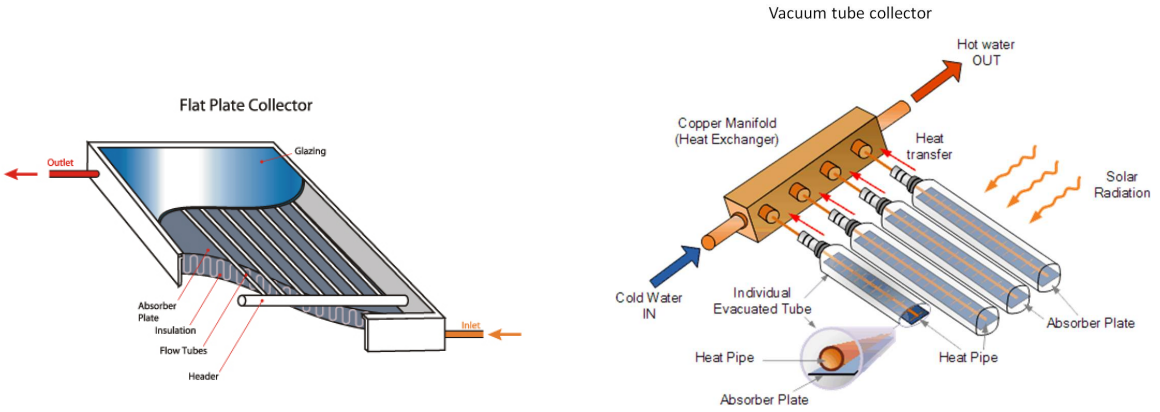

(a) (b)

Fig. 2.5.: a) Comparison between flat plate collector [Gre14] and b) vacuum tube collector [Aet14].

Flat plate collectors

In contrast to the PV modules, the flat plate collectors can be used to generate heat at a relative low temperature. At the moment the most flat plate collectors are used in the building service. The most collectors are used to generate thermal heat to support the heater or to heat up the tap water. Currently most collectors are installed on the roof of the building. For the best operation, they need the same spatial arrangement as the PV modules. The best installation angle could be slightly different compared to the already installed PV modules, because the most hot water is needed in the winter time instead of in the summer time. Due to the lower curve progression of the Sun the installation angle could be a little bit lager based on the normal vector of the horizontal plane. In Germany it is orientated towards the south with a special angle, which depends on the location and on the course of the Sun during the whole year. This can for example be seen in the following section 3.1.
With flat plate collectors the nearly entire solar spectrum is dissipated into thermal energy. This is done with a relative high efficiency. The efficiency depends on the kind of solar collector and can be up to 90 %. An overview of the technical background can be found in Fig. 2.5a. The solar collector absorbs the solar radiation, which passes the transparent cover (glazing). The better the absorber and the insulation, the higher is the generated temperature with the flat plate collectors. Most absorbers are made of black chrome, black nickel or nickel pigmented aluminium oxide which is galvanically applied on the absorber. Newer collectors have a titan-nitride-oxide-coating which is vacuum coated. The radiation is absorbed and therefore it is heated up to a higher temperature compared to the ambient temperature. Due to a better efficiency, the absorber is installed in a housing which is thermally isolated against the environment. Insulation materials are for example mineral rock wool or polyurethane foam. Alternative insulation materials could also be glass wool or glass fibre for example. The insulation

material is necessary to prevent convection of the produced thermal heat with the environment. The heat is extracted from the absorber with a heat carrier pipe, whereas a solar fluid streams inside of this pipe. Between the transparent cover and the absorber, an artificial greenhouse effect is created which also increases the temperature. Due to the transparent cover the thermal emission is reduced, but the most solar radiation can pass it and only a slightly amount is reflected.
For a higher temperature the volume between the absorber and the transparent cover can be evacuated, but to keep the better performance the evacuation process must regularly be repeated. The interval is between 1 year and 3 years. These collectors are called vacuum flat plate collectors. Based on their affordability and high price performance ratio it is very interesting to install them to support the heater.

Vacuum tube collectors

Fig. 2.5b demonstrates a scheme of a vacuum tube collector. The vacuum tube collector can also be used to generate thermal heat, but in contrast to the flat plate collectors, higher temperatures and higher efficiencies are possible. Temperatures up to a few 100 °C are generatable and therefore it can be used to generate process heat for a lot of different applications. The first absorbers were made of coated copper strips, which were inserted into an evacuated glass pipe. Due to the vacuum inside the pipe the thermal convection is minimised. Newer systems use a fluid stream in a U-pipe or in a pipe-in-pipe system which are installed in an evacuated glass pipe. In the second combination, the outer face of the inner glass pipes is coated and thus it absorbs the solar radiation and due to this reason the fluid is heated up to very high temperatures. The second technology is realised with a counter flow technology and in the best case it is constructed as a thermos flask. The heated fluid inside the vacuum tube collectors rises to the heat exchanger at the top of the vacuum tubes. The stored heat is extracted with a heat pipe and therefore the fluid cools down and can be reheated again. The heat is transferred via a heat exchanger to the convector fluid in the manifold. For an operation of the vacuum tube collectors, the collectors must be installed at minimum with a minimal angle. If the collectors are installed even with the ground or with a negative angle, the fluid inside the collectors cannot circulate, because the natural convection is disabled. Inside the vacuum tubes no pumps or ventilators are installed to generate the flows. Due to the higher temperatures the density of the hotter fluid is lower. Therefore the hottest water rises to the highest point in the system and this must be the heat exchanger in the system. Otherwise the system can be damaged and can become inoperable. The heat transfer medium streams to the heat storage tanks or it can be used directly. Normally a few vacuum tube collectors are combined in an array to reach higher temperatures and higher volume flows.
The manifold is insulated to reduce the temperature losses during the transport. At the moment there are two different connection types for the heat exchangers. The dry junction connects the heat exchanger indirectly with the manifold via a heat transfer medium and in the case of a wet junction, the heat exchanger is extended into the

manifold. The advantage of the dry junction is that the pipes can be exchanged without draining the heat transfer medium in the manifold, this is in contrast to the wet junction. For higher performances, a parabolic reflector can be used to increase the light intensity at the absorber, because the diffuse solar radiation is reflected to the absorber and more effective absorber area can be used.

2.5. Project idea

As can be seen in the previous chapters there are a lot of people in the world who do not have a sufficient freshwater supply in their daily life. They use polluted freshwater for cooking and drinking with serious consequences. Many nations use desalination units for freshwater production, but in most cases fossil fuels are needed for this freshwater production. The combustion of fossil fuels produces a lot of carbon dioxide, which is responsible for global warming. Due to global warming more and more freshwater may be needed for the daily life, especially for irrigation in agriculture, because wide swath of land will be drying out in the future. This freshwater production is therefore a double-sided sword. On the one hand, the freshwater is needed for the production of food and on the other hand the actual production of freshwater is very energy-intensive and environmentally damaging. For an energy equilibrium it is best, when the energy comes from environmentally neutral energy sources. For example these can be renewable energy sources like wind, solar, biomass or others. Biomass energy sources only produce as much carbon dioxide during the application as they have absorbed before. Therefore no dangerous carbon dioxide is emitted, which accelerates global warming. Due to this equilibrium they are future-proof.
On the other hand it can be seen in the first sections, there are many areas and entire countries which have a very high daily solar radiation. Most areas are located around the equator. In these regions, the daily solar radiation is sometime higher than $1000\,\mathrm{W/m^2}$ for a short period during a few days in the year. Additionally these areas are not only somewhere in the desert, they are also close to seas, like the Red Sea. These energy densities are high enough to harvest enough usable energy for applications like the generation of electricity or the production of thermal energy for a large number of different utilisations. At the moment only a very low percentage of the incoming daily solar radiation is used and thus a huge energy potential is untapped. Furthermore the usage of solar radiation can provide secure jobs in those countries for a long time. This could stabilise these areas and countries. In addition it can improve the financial situation not only in those countries.
After a short consideration, beginning in 2007, there was the obvious and innovative idea in Soest to produce freshwater with a renewable energy source. At the beginning there was the idea to produce freshwater with biomass, but later this author changed his mind about the energy production for the Sunwater project. The new innovative idea was to use solar thermal energy for the production. This combination fits very well, because in a lot of countries both circumstances are coexistent and thus it has many

advantages, because most countries with an actual and future freshwater problem have very high daily solar radiation, like for example Egypt or parts of Spain. Furthermore the harvested solar energy can directly be used to operate a desalination unit, because this thermal energy form does not have to be converted to another energy source. The conversion from one energy source to another energy source is accompanied with a big loss of energy. With this direct usage the energy losses can be minimized and the effectiveness can be raised. One problem in this case is that the thermal energy collected must be stored during the noonday to extend the working time between sunset and sunrise. Without the storage the water desalination unit can only be operated with thermal energy during the sunshine hours. For a longer operation it must be hearken back to other energy sources and this is contradictory to the project idea of an energy-friendly freshwater production. Therefore different ideas must be reevaluated to solve this and other problems.
During the planning phase of this innovative project, different partners were sought at SWU in Soest who could contribute to it. After a long search a partner was found in Kiel which produces a water desalination unit which works with evaporation. This technology is very innovative and rarely used and therefore a good basis for a future-oriented desalination project. Most thermal desalination units work with distillation and this makes a huge difference, because the working temperature varies and also the technology behind the water desalination unit is different. In addition a partner was found in Egypt, who wants to contribute to this project. The Egyptian partner also has good contacts to the solar industry and holiday industry in that country. These contacts were very helpful during the project planning phase and during the project duration. With this consortium the project could be realised.
The initial idea was to install an environmentally friendly desalination demonstration plant in Egypt which works with evaporation. The system was installed in the touristic area in Hurghada close to the Red Sea. It was installed at one of the five-star hotels of Sunrise. This site was chosen, because on the one hand the Egyptian partner has had good contacts to the hotel operator and on the other hand it could be incorporated into an existing RO system. This has the advantage that the saltwater from the reverse osmosis system can be used to generate freshwater with the WDU. The remaining brine, water with higher salinity, from the freshwater production can be depolluted with the existing system. This has the advantages that no saltwater supply and no brine disposal system must be installed and thereby effectively reducing costs. Another aspect for this building site was the high daily solar radiation. It is higher than $1000\,\mathrm{W/m^2}$.
The produced freshwater can be delivered with the existing piping system to the consumers. The RO system has been installed to supply the complete hotel complex with freshwater. The freshwater production is $400\,\mathrm{m^3/d}$. This amount is used for the primary service of the holiday maker and all other demands in the hotel like the irrigation and the swimming pools. With the evaporation desalination system only a small percentage of the daily freshwater demand is produced and in the case that the system stops working, the freshwater supply is not in danger and this is very important for the hotel complex and for the tourists. This project is just a feasibility study to show that the production of freshwater is possible with solar energy.

3. Theoretical background

In this chapter the theoretical background for the installation of the demonstration plant will be discussed and presented. In some instances, difficult and interesting calculations are necessary. This requires good mathematical background knowledge. It will be presented in a way that most important equations and identities are mentioned which are used in the mathematical conversions. Most calculations are presented step by step and so they can be understood by the reader. The following sections include for example the calculation of the daily solar radiation with the associated Equation of Time (EoT) A.7. Furthermore they give an introduction into evaporation and energy and heat transfer in fluids. This chapter starts with the rough calculation of the global solar radiation and for this the Equation of Time is necessary. This equation will be derived from the basic geometry of the solar system and the complete calculation can be found in chapter A.

3.1. Calculation of the global solar radiation

For the simulation of the demonstration plant, a rough calculation of the amount of the solar radiation is necessary. At the beginning of the project there were no data available and so another way had to be found to generate the needed data. Later in the project life time, a few data were bought from a weather institute in Germany, which also contains the daily solar radiation, but these were also calculated and not measured data. Additionally a few measurements were done at the building site in Egypt. For this a solar radiation sensor was installed and evaluated by a controller. This will be compared in a later section with the calculated data.
The Earth is divided into more than 24 time zones. Beginning with $-12\,\mathrm{h}$ and ending with $12\,\mathrm{h}$. This is based and defined on the $24\,\mathrm{h}$ rotation of the Earth. The time zones are arranged with the longitudes and normally the time difference from time zone to time zone are complete hours, but sometimes the difference is just $30\,\mathrm{min}$ like in Australia. The time zone zero is around the longitude of $0°$ and has a theoretically width of $15°$. The width of the most time zones differs a little bit, because of political and cultural interests. Good examples are the time zones in Europe. Due to this organisation different countries have the same uniform times and the same uniform dates. This has political, economic and practical reasons.
Now the global solar radiation is calculated. For this calculation the equation (A.84) is needed and furthermore different geometrical aspects must be considered. The calculation of the solar radiation at the place of installation is necessary, because there were no

exact data available which reflect the actual solar radiation at this place and finally the amount of the produced process heat depends on it. For a later simulation an hourly overview is needed and only with this simulation of the solar radiation the necessary data can be generated. In literature only mean values for several days or mean values for a lot of years can be found. The data published are given in $\mathrm{kW\,h/m^2}$, but for the simulations hourly values in $\mathrm{kW/m^2}$ are necessary. The Carnot-toolbox needs values in $\mathrm{kW/m^2}$ for the simulation and they must be given on the hour. Other values cannot be used . A back calculation with the given data is very difficult and only possible in a statistical way and this is uninteresting for the simulation of the demonstration plant. Later in the project life time a few data were bought from a German weather institute, but this was too late for the first simulations. Another problem was that the bought global solar radiation data were also calculated and the information on how it was calculated was not presented by the weather institute. Another aspect which must be considered in the simulation for the installation is that the solar radiation differs during the day and the year. In the summer a higher solar radiation is on the northern hemisphere compared to the winter. On the southern hemisphere it is vice versa. Another problem is that the global solar radiation differs from place to place. Close to the equator is a higher solar radiation than in Germany or Iceland on the same day and at the same local time. Additionally the solar radiation depends also on the mean sea level (MSL). The higher the location, the higher is the solar radiation. A short visualisation can be seen in Fig. 3.1. Only the Earth's view is from [Jax11]. For a first-order series approximation the solar radiation reaches the Earth parallel. If the solar radiation has a perpendicular incidence at the equator, this happens two times a year, the solar radiation reaches the Earth's surface in the North or in the South under a lower angle. The bigger the distance from the equator, the flatter is the angle of incidence. The more tilted the angle of incidence is, the larger is the irradiated area for the same sized light beam. Additionally the larger the distance from the equator, the longer is the distance through the atmosphere. Due to many dependencies, this includes clouds and dust particles, only a rough approximation is possible for the calculation of the solar radiation at the Earth's surface right now. Furthermore the coverage with clouds has an essential effect on the actual solar irradiation. For example these aspects cannot be included into the simulation of the global solar radiation, because it has a chaotic behaviour and it is dependent in time. This approximation of the global solar radiation will be explained in the following section. The calculation is based on [Pvc11], but a few modifications were included in the calculations. With these modifications a better result for the approximation should be possible.

The solar radiation comes from the Sun, the centre point of the solar system. The energy is produced with fusion of hydrogen. The solar radiation is emitted spherically and therefore only a minimum value reaches the Earth and the difference is lost in space. The mean global solar constant is

$$E_0 = 1367\,\frac{\mathrm{W}}{\mathrm{m^2}} = 1367\,\frac{\mathrm{J}}{\mathrm{m^2\,s}}. \tag{3.1}$$

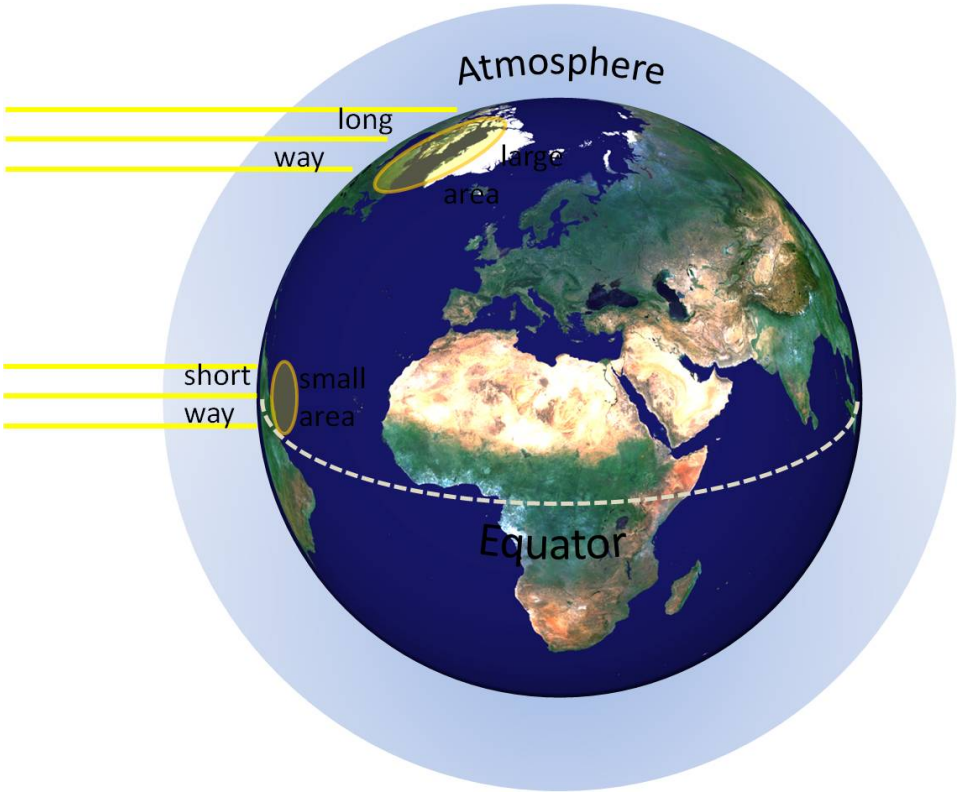

Fig. 3.1.: Dependency of the airmass and the angle of incidence at different locations on the Earth's surface. The Earth's view is from [Jax11].

This value was defined in 1982 in Geneva by the World Meteorological Organization (WMO). This is the mean solar radiation at the position of the Earth without consideration of the atmospheric interaction. Due to the elliptical orbit of the Earth around the Sun the global solar radiation varies throughout the whole year. At the perihelion with $147.1 \cdot 10^6$ km distance is the irradiation density $1420\,\mathrm{W/m^2}$ and at the aphelion with $152.1 \cdot 10^6$ km is the irradiation density $1325\,\mathrm{W/m^2}$. This is a difference of 3.4 % above in the perihelion and 3.3 % below the yearly mean value in the aphelion. This is a variation of almost 7 % during the whole year. Due to long measurements the curve behaviour can be described as

$$E_\odot = 1367\frac{\mathrm{W}}{\mathrm{m^2}} + 48.5\cos(0.01721d - 0.25815)\frac{\mathrm{W}}{\mathrm{m^2}}. \tag{3.2}$$

Where $\odot$ is the sign for the Sun. This is based on measured data in the last years, where d is the actual day in the year and it reflects the irradiation on a horizontal plane compared to the light incidence [Gas96]. If it is on a slope the irradiation density is lower. Since 1978 the irradiation density is measured in space with the space probe Solar and Heliospheric Observatory (SOHO). The used radiometer is called VIRGO (Variability of Solar Irradiance and Gravity Oscillations). With this sensor it is possible to measure the solar constant without an impact of the Earth's atmosphere. Due to the air mass the light is scattered, absorbed and reflected and therefore the measured value at the

surface is lower compared to the solar constant. The main effects of the irradiation density variations at the Earth's surface can be summarised as:

- atmospheric effects, including absorption and scattering
- local variations in the atmosphere, such as water vapour, clouds and pollutions
- latitude of the location
- the season of the year and the time of day

These effects also depend at the wavelength λ of the solar radiation spectra and therefore for the energy $E = \hbar\omega = h\nu = {}^{hc}/_{\lambda}$ and the momentum $\vec{p} = \hbar\vec{k}$ with $|\vec{k}| = {}^{2\pi}/_{\lambda}$ of the photons, where

$$h = 2\pi\hbar = 6.63 \cdot 10^{-34}\,\mathrm{J\,s} = 4.14 \cdot 10^{-15}\,\mathrm{eV\,s} \tag{3.3}$$

is the Planck's constant, ν the frequency of the photon, $\vec{k}$ the wave vector and

$$c = 299\,792\,458\,\mathrm{m/s} \tag{3.4}$$

the speed of light in vacuum. In matter the speed of light is lower compared to the speed of light in vacuum, but for the vacuum the value is exactly defined and has no error. This constancy is very important in the relativistic, because no causation can bear on with a higher speed. This is considered in the Lorentz transformation (B.21) in contrast to the Galilei transformation (B.20). Due to de Broglie a photon has a momentum and due to Einstein a photon has an energy value. It will be absorbed by the gasses in the air, when the energy is close to the bond energies of these ingredients. The specific gases are for example ozone O_3, carbon dioxide CO_2 and water vapour $H_2O_{(g)}$. Infrared light above $\lambda = 2\,\mu\mathrm{m}$ is absorbed by water vapour and carbon dioxide. Ultraviolet light below $\lambda = 0.3\,\mu\mathrm{m}$ is absorbed by ozone. If the particles are small against λ it is Rayleigh scattering otherwise the radiation is scattered at the surface of the particles. Due to the frequency depending scattering of light in the atmosphere the dusk and dawn can be reddish coloured. This is also dependent on the path length of the solar radiation through the atmosphere. During the day the sky is bluish coloured, because of the highly scattered blue light compared to the red light. Therefore the sky appears blue during the day and contrary to expectations, this colour is not based on the oceans on the Earth. Additionally the light is mostly polarised perpendicularly to the plane established between the Sun, the observer and the line of sight. This can easily be tested with a polarisation filter [Ger02].
In the morning and the evening the path length of the solar radiation through the atmosphere is longer than at noon and thus the light is more effectively absorbed and scattered. This is one reason why the Sun has a lower intensity during the evening hours and the morning hours. Furthermore the angle of incidence is lower in the morning and the evening compared to noonday. The flatter the angle of the solar radiation, the lower is the intensity of the incident solar radiation. This is not only valid during the day, but also one effect on the movement of the location alongside the latitude. The dependency can be seen in Fig. 3.1. The higher the latitude, the lower is the solar radiation.

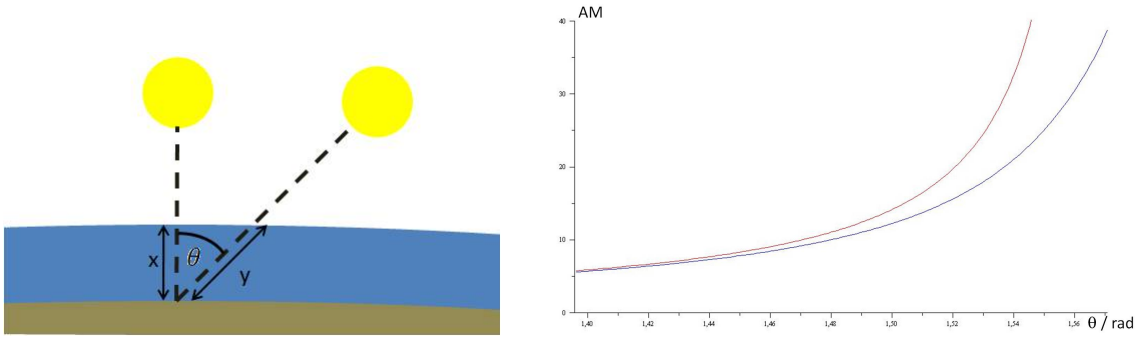

(a) (b)

Fig. 3.2.: a) Definition of the air mass with the angle θ. b) Difference between plane-parallel atmosphere (red) and Pickering's approximation (blue) between 80° and 90°.

At a single location the daily amount of solar energy can vary lastly during one year. This is based on the length of the day, the amount of clouds on the sky and the time of the day. In Germany it varies between $0\,\mathrm{W/m^2}$ during the night and several $100\,\mathrm{W/m^2}$ on sunny days. On cloudy days less than $200\,\mathrm{W/m^2}$ are also possible at noon. Another limitation is the total turbidity factor of the air. It differs from location to location and from season to season. In industrial areas this factor is higher compared to larger towns, rural districts and high mountains. The factor decreases in this sequence. Furthermore this total turbidity factor is higher in the summer than in the winter. It varies between 1.5 and 5.8. The value 1 is valid for the atmosphere, when it only consists of ideal gases without contaminations [Gas96].
The solar radiation received at a place on the Earth is composed of direct and scattered solar radiation. The scattered solar radiation is also called diffuse solar radiation. The amount of the scattered and absorbed solar radiation depends on the optical path length through the atmosphere, the longer the way through the atmosphere, the more solar radiation is scattered and absorbed. The attenuation of the solar radiation depends on the so called air mass. In the simplest way the air mass can be defined as

$$\mathrm{AM} = \frac{1}{\cos(\theta)} = \sec(\theta), \tag{3.5}$$

where θ is the angle from the vertical (zenith angle). With $\theta = 0$ the Sun is perpendicular on the Earth's surface and this is at noonday. With this simple approximation the Earth's surface at MSL and the atmosphere are plane-parallel. An overview can be seen in Fig. 3.2a and it is proportional to y/x. The spherical appearance of the Earth is ignored in this approximation and thus this formula can only be used for small angles $\theta \leq 60°$. Without an impact of the atmosphere the air mass (AM) is defined as 0, with an AM of 1 the minimum air mass is passed ($\theta = 0$), an AM of 1.5 has a zenith angle of

round about $\theta = 48°$. For $\theta = 90°$ the air mass is indefinite and therefore it is not a good approximation. A better approximation for the AM is the Pickering's approximation

$$\mathrm{AM} = \frac{1}{\cos\left(\theta - \frac{61}{45}\frac{\pi}{165+47\left(90-\frac{180\theta}{\pi}\right)^{1.1}}\right)}, \tag{3.6}$$

where θ is the zenith angle in radiant [Pic02]. The original form of the air mass equation was taken from [Raw92], but the constants were recalculated by the method of least squares. A comparison between (3.5) and (3.6) in the range between 80° and 90° can be found in Fig. 3.2b. The curve of the plane approximation is indefinite for 90°, but with the Pickering's approximation the air mass at 90° is not indefinite and therefore it is a better formula. A value of 38.7 is calculated with this angle. θ varies during the whole day and therefore this angle is time-dependent $\theta(t)$. At exactly 12 o'clock, respectively apparent local time, the Sun has the highest position in the sky. This is the so called local solar time (LST). The local time (LT) normally varies from LST, because of global time zones on the Earth, which also includes the daylight saving time (DST). Furthermore the eccentricity of the Earth's orbit is also important for the calculation, which was reviewed in the previous section. The LST depends on the Equation of Time (EoT) (A.84) and the local standard time meridian (LSTM). The LSTM is a reference meridian in every time zone of the Earth. It is similar to the UTC time zone, which comes from the zero meridian, which runs through the district Greenwich in London. UTC is an acronym for Coordinated Universal Time and Temps Universel Coordonné. Due to the fact that the Earth rotates in approximately 24 h around its own axis (2π), the LSTM can be calculated as

$$\mathrm{LSTM} = \frac{2\pi}{24\,\mathrm{h}}\Delta T_{\mathrm{UTC}} = \frac{\pi}{12\,\mathrm{h}}\Delta T_{\mathrm{UTC}}, \tag{3.7}$$

where ΔT_{UTC} is the difference between the local time and UTC in hours. This are 15 °/h. Most time zones can be calculated with adding or subtracting a number of whole-numbers hours. For the wintertime in Germany it is $\Delta T_{\mathrm{UTC}} = +1$ and for the summertime (DST) it is $\Delta T_{\mathrm{UTC}} = +2$. The time zones are regulated by the government and have the same time and the same date. People who live in the same areas, have the same local time and a regulated time has a lot of ecological and economic advantages. Without these regulations, time agreements and determinations would be very difficult. Furthermore the natural sciences, especially Physics, need an exact time measurement. In the early past it happened, that worldwide measurements could not be evaluated, because of inexact time measurements at different locations. For the calculation of the solar radiation another time correction factor (TC) must be included

$$\mathrm{TC} = \frac{720\,\mathrm{min}}{\pi}(\lambda - \mathrm{LSTM}) + \mathrm{EoT}, \tag{3.8}$$

where λ is the longitude of the location in radian between $-\pi$ and π. During $^{720\,\mathrm{min}}/_{\pi}$ the Earth sweeps one radian. This are 4 min/°. The longitude must be considered in the

calculation, because the most locations have a longitude variation based on the LSTM. With (3.7) and (3.8) the local solar time can be calculated as

$$\mathrm{LST} = \mathrm{LT} + \frac{\mathrm{TC}}{60\,\mathrm{min/h}}. \tag{3.9}$$

LT is between 0 o'clock and 24 o'clock.
By definition the hour angle (HRA) is 0°=0 rad at noon, because the measuring of the noon is easier compared to the midnight. Due to the hourly rotation of the Earth the HRA differs from hour to hour and from minute to minute. In the morning the angle is negative and in the afternoon it is positive. The HRA is calculated in dependency of the LST and converts the hourly movement into a number of radians, which the Sun runs across the sky

$$\mathrm{HRA} = \frac{\pi}{12\,\mathrm{h}}(\mathrm{LST} - 12\,\mathrm{h}). \tag{3.10}$$

The declination angle of the sun $\delta_\odot$ is different during the year, as was mentioned in subsection A. At the moment the Earth's declination angle is between $\pm 23.439° = \pm 0.041$ rad. Due to the movement of the Earth around the Sun the angle varies throughout the whole year. In the northern summer it reaches its maximum and in the winter it reaches its minimum. Only at the spring and the autumn equinox the angle is 0°. An easy approximation of the declination is for example

$$\delta_\odot = \frac{23.439°\pi}{180°} \sin\left(\frac{2\pi}{365\,\mathrm{d}}(d - 81\,\mathrm{d})\right), \tag{3.11}$$

where d is the day in the year, beginning at 1. January and ending 31. December. A better expression for the declination can be found in [Spe71] and it is given as

$$\begin{aligned}\delta_\odot = {} & 0.006918 - 0.399912\cos(\gamma) + 0.070257\sin(\gamma) - 0.006758\cos(2\gamma) \\ & + 0.000907\sin(2\gamma) - 0.002697\cos(3\gamma) + 0.00148\sin(3\gamma),\end{aligned} \tag{3.12}$$

with

$$\gamma = \frac{2\pi}{365}(d - 1) \tag{3.13}$$

and where d is the day of the year like in (3.2). Another angle is the elevation angle h, which must be considered for the calculation of the global solar radiation. It is also called the altitude angle. It defines the angle measured from the idealized horizon to the position of the Sun. Between the zenith angle θ and the elevation angle h is the dependency

$$\theta = \frac{\pi}{2} - h. \tag{3.14}$$

Therefore θ varies throughout the whole day, it depends also on the latitude of the location and the day of the year. Concerning Fig. 3.2a h is the angle between y and the Earth's surface. It can easily be calculated with [Mee98]

$$h = \arcsin\left(\sin(\delta_\odot)\sin(\varphi) + \cos(\delta_\odot)\cos(\varphi)\cos(\mathrm{HRA})\right), \tag{3.15}$$

where φ is the latitude of the location. $\delta_\odot$ is given in (3.12) and HRA is given in (3.10). Between the Tropic of Cancer and the Tropic of Capricorn, it is possible during a few days in the year, that during the noon time the elevation angle h is larger than 90°. This has the effect that the Sun can shine on a few places on a few days in the year from the North and for the other days from the South and vice versa. Northern the Tropic of Cancer and southern the Tropic of Capricorn the Sun is always in the South or in the North. Right now enough information are available to calculate the sunset and the sunrise. At the sunrise and the sunset the elevation can be set and it is defined as $h = -0.0145$, where this value is a special horizon altitude for the sunrise and the sunset [Bar10]. This is used in (3.15) and with (3.10) and (3.9), now it can be solved for the LT:

$$\text{Sunrise} = 12\,\text{h} - \frac{12\,\text{h}}{\pi} \arccos\left(\frac{\sin(-0.0145) - \sin(\varphi)\sin(\delta)}{\cos(\varphi)\cos(\delta)}\right) - \frac{TC}{60\,\text{min/h}} \tag{3.16}$$

$$\text{Sunset} = 12\,\text{h} + \frac{12\,\text{h}}{\pi} \arccos\left(\frac{\sin(-0.0145) - \sin(\varphi)\sin(\delta)}{\cos(\varphi)\cos(\delta)}\right) - \frac{TC}{60\,\text{min/h}} \tag{3.17}$$

Due to the symmetry between the solar noon at the sunrise and the sunset, the sign can be exchanged. For the sake of the completeness the azimuth angle can also be calculated. The azimuth angle is the direction from which the Sun comes during the day and it also varies throughout the whole day. The values differ from day to day and they depend on the latitude. On the northern hemisphere above the tropic at noon the Sun is exactly in the South and on the southern hemisphere below the tropic the Sun is in the North. At the equinoxes the sunrise is exactly at 90° and the sunset is exactly at 270°. With the above formulas the azimuth angle can be calculated as

$$\text{Azimuth} = \arccos\left(\frac{\sin(\delta_\odot)\cos(\varphi) - \cos(\delta_\odot)\sin(\varphi)\cos(\text{HRA})}{\cos(h)}\right). \tag{3.18}$$

It must be considered, that the real value of the azimuth angle depends on the calculated HRA:

$$\text{Azimuth}_r = \begin{cases} \text{Azimuth} & \text{HRA} \leq 0 \\ 2\pi - \text{Azimuth} & \text{HRA} > 0 \end{cases} \tag{3.19}$$

Now all information are collected to calculate the solar radiation in dependency of the location, the day and the time. In the following the daylight saving time (DST) is not considered. If the DST should be considered, only a time shift for one hour must be included into the calculation. The exact date of the start and the end of the DST differs from country to country. There is no worldwide uniform regularisation. For example in 2011 there was no DST in Egypt, but in Germany and other European states there was the so called summer time. The direct solar radiation on a perpendicular plane can now be calculated with

$$I_D = E_\odot \cdot 0.7^{\text{AM}^{0.678}}, \tag{3.20}$$

where $E_\odot$ is defined in (3.2) and AM in (3.6). The 0.7 is based on that just 70 % of the solar radiation reaches the Earth's surface and 0.678 is an empirical value, which fits to

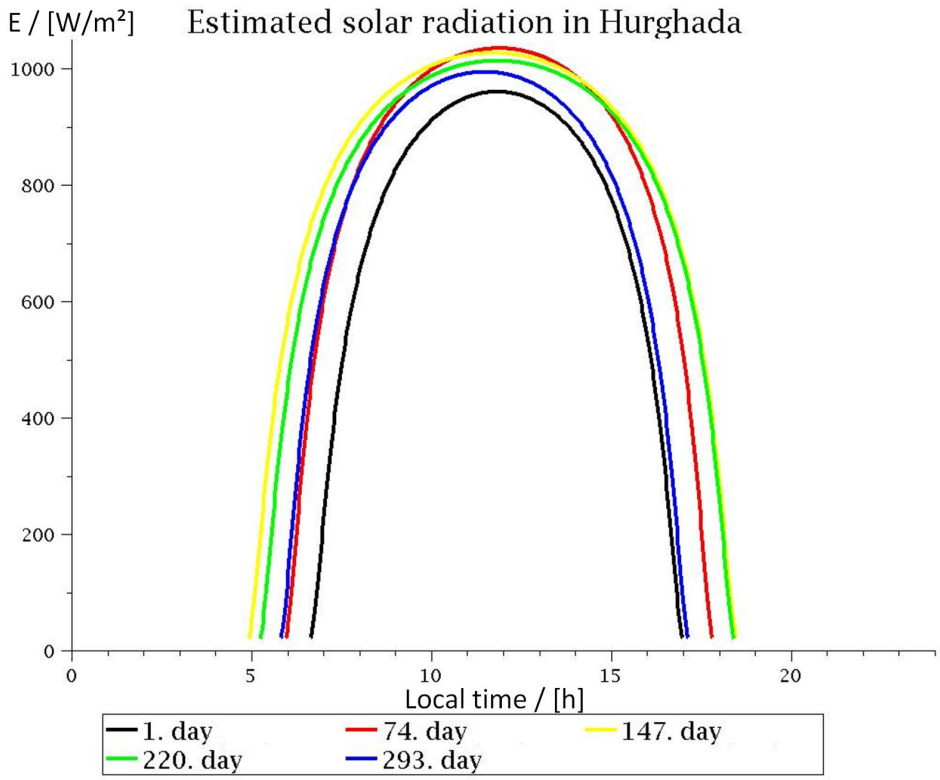

Fig. 3.3.: Approximation of the solar radiation in Hurghada on a few selected days during the year.

the measurements. It considers the non-uniformities in the atmospheric layers. For a location higher as the MSL, the above equation must be slightly modified

$$I_D = E_\odot \cdot \left((1 - aH)0.7^{\mathrm{AM}^{0.678}} + aH\right), \tag{3.21}$$

where H is the height in kilometres of the location above sea level and $a = 0.14$ is an empirical constant. The diffuse solar radiation is about 10 %, but only on days with a clear sky. Therefore the complete solar radiation can be approximated as

$$I_G = 1.1 \cdot I_D. \tag{3.22}$$

Hurghada has the coordinates:

$$\text{Longitude: } \lambda = 33°48'42'' \text{ E} \tag{3.23}$$

$$\text{Latitude: } \varphi = 27°15'28'' \text{ N} \tag{3.24}$$

With this values and the time difference to UTC the solar radiation with the above equations can be calculated. Fig. 3.3 shows the approximated solar radiation on a few days in the year. These are the days with the numbers 1, 74, 147, 220 and 293. The maximum value is more than 1000 W/m^2 and the lowest value at noon is round

about $900\,\mathrm{W/m^2}$. The time with a low solar radiation is at the beginning of January and the highest solar radiation is in the time between June and August. Compared to Germany these values are very high. These are values which are really expected and measured at this location. The left intersection with the x-axis is the sunrise and the right intersection is the sunset. In this figure the DST is not considered. Compared to Germany the sunrise is very early in the morning (5 o'clock - 7 o'clock) and the sunset is also very early in the evening (17 o'clock - 19 o'clock). In Egypt the day is more or less split into 12 h daytime and 12 h nighttime. In the ancient Egyptian culture this value has a matter of special importance. It appears on a lot of different wall paintings in a lot of different gravesites.

3.2. Introduction to theoretical mechanics and thermodynamics

Fluids are made up of a vast amount of molecules and atoms. They stream for example in pipes or they are transported through the air. Every of the N particles can be described with a coordinate-triple x_1, x_2 and x_3 in the Cartesian Coordinate System. The coordinates for the N particles are

$$x_n = x_{3\nu+j-3} = \vec{r}_\nu \cdot \hat{e}_j \quad (\nu = 1, \ldots, N,\ j = 1, 2, 3,\ n = 1, \ldots, 3N). \tag{3.25}$$

Therefore it is theoretically possible to solve the Newton equations with the associated frame conditions. The Lagrange equation of the first kind is in this case:

$$m_n \ddot{x}_n = F_n + \sum_{\alpha=1}^{R} \lambda_\alpha \frac{\partial g_\alpha(x_1, \ldots, x_{3N}, t)}{\partial x_n} \qquad (n = 1, 2, \ldots 3N) \tag{3.26}$$

$$\text{with} \qquad g_\alpha(x_1, \ldots x_{3N}, t) = 0 \qquad (\alpha = 1, 2, \ldots, R) \tag{3.27}$$

The variable g_α represents the frame condition of the system, like the gravitation and infinity potentials. These are $3N + R$ equations ($3N$ ODE 2^{nd} order and R algebraic equations) for $3N + R$ unknown functions $x_n(t)$ and λ_α. The forces F_n are known. Due to the high amount of particles it is very difficult and time intensive to solve this system of ODEs, but in most cases it is of very little interest to know the position $\vec{r}$ of every particle at a desired time t. Instead of mass points, the mass density ϱ of fluids is used in calculations:

$$\varrho(\vec{r}, t) = \frac{\sum_\nu m_\nu}{\triangle V} = \frac{\triangle m}{\triangle V} = \frac{\text{Mass}}{\text{Volume}} \tag{3.28}$$

In this equation the ν runs over all atoms and molecules $(1, ..., \triangle N)$ which are located in the volume element $\triangle V$ at the position $\vec{r}$. The volume element $\triangle V$ must be a specific size so that $\triangle N \gg 1$ and also a size so that the microscopic characteristics in $\triangle V$ are more or less the same for all particles. $\triangle V$ could for example consist of $\triangle N = 10^7$ and then the volume element is more or less independent in $\varrho(\vec{r}, t)$. The size of the volume

element is for example $(\triangle V)^{1/3} \sim 10^{-5}\,\mathrm{cm}$ for fluids and $(\triangle V)^{1/3} \sim 10^{-4}\,\mathrm{cm}$ for gas. Instead of independent velocities $\vec{v}_\nu$ of different particles, a velocity field is used:

$$\vec{v}(\vec{r},t) = \frac{1}{\triangle N}\sum_{\nu=1}^{\triangle N}\vec{v}_\nu = \langle\vec{v}_\nu\rangle \tag{3.29}$$

This is the mean velocity of the particles in the volume element $\triangle V$ and furthermore the pressure is defined as

$$p = p(\vec{r},t) = \frac{\triangle F}{\triangle A} = \frac{\text{Force}}{\text{Area}}. \tag{3.30}$$

If $\triangle V$ was chosen in the right size, it is independent in $\varrho(\vec{r},t)$, $\vec{v}(\vec{r},t)$ and $p(\vec{r},t)$. Ideal gases can be described with these variables. For real fluids and other gases it is a good approximation.
In fluid streams the amount of particles are constant and therefore it is valid

$$\oint\limits_{F(V)} \varrho(\vec{r},t)\vec{v}(\vec{r},t)\cdot\,\mathrm{d}\vec{F} = -\frac{\mathrm{d}}{\mathrm{d}t}\int\limits_V \varrho(\vec{r},t)\,\mathrm{d}^3r = -\int\limits_V \frac{\partial\varrho}{\partial t}\,\mathrm{d}^3r. \tag{3.31}$$

The left integrand reflects the flow

$$\vec{j}(\vec{r},t) = \varrho\vec{v} = \text{Flow density} = \frac{\text{Mass}}{\text{Area}\cdot\text{Time}}, \tag{3.32}$$

which passes the surface area $F(V)$ of the constant and static volume V. The flow, which leaves the volume V, must reduce the mass inside the volume in time and vice versa. This is equal to the second part in (3.31). And due to the static system the last step is possible. This can now be rewritten with the Gauss theorem (B.22)

$$\int\limits_V \left(\frac{\partial\varrho(\vec{r},t)}{\partial t} + \nabla\left(\varrho(\vec{r},t)\vec{v}(\vec{r},t)\right)\right)\mathrm{d}^3r = 0. \tag{3.33}$$

This is valid for all volumes which are larger than $\triangle V$, and therefore the integrand disappears. The final continuity equation is

$$\frac{\partial\varrho(\vec{r},t)}{\partial t} + \nabla\left(\varrho(\vec{r},t)\vec{v}(\vec{r},t)\right) = 0. \tag{3.34}$$

Another important equation for the calculations is the Euler equation of the hydrodynamics

$$\varrho\left(\frac{\partial\vec{v}}{\partial t} + (\vec{v}\cdot\nabla)\,\vec{v}\right) = -\nabla p + \vec{f}. \tag{3.35}$$

The derivation is based on Newton's 2nd axiom and it can also be found in [Fli01]. Now 4 partial ODEs for 5 fields $\varrho(\vec{r},t)$, $\vec{v}(\vec{r},t)$ and $p(\vec{r},t)$ exist and thus another equation is necessary to solve this system of equations. The missing equation is the constitutive equation

$$p = p\left(\varrho(\vec{r},t)\right). \tag{3.36}$$

Tab. 3.1.: A few examples for the exponent γ in the polytropic, constitutive equation.

γ	System
∞	incompressible liquid
$\gg 1$	real liquid
1	ideal gas, isotherm
c_p/c_V	ideal gas, adiabatic
$5/3$	Fermi gas, $T \approx 0\,\mathrm{K}$, non relativistic
$4/3$	Fermi gas, $T \approx 0\,\mathrm{K}$, relativistic

This is an equation which combines the pressure and the density of a fluid. The dependency is determined by the kind of matter. For polytropic, constitutive equations can be used

$$p = \text{const.} \cdot \varrho^{\gamma} \tag{3.37}$$

An overview of the values of the constant factor γ can be found in Tab. 3.1. It differs from matter to matter. But with this approach a lot of different problems can be covered. With the constitutive equation follows the compressibility

$$\kappa = -\frac{1}{V}\frac{\partial V}{\partial p} = \frac{1}{\varrho}\frac{\partial \varrho}{\partial p} = \frac{1}{\gamma p}. \tag{3.38}$$

For fluids a pressure change has just a minor change in the density $\gamma \gg 1$ and ideally it is $\gamma = \infty$ and thus incompressible. Therefore it is valid $\varrho = \text{const.} \cdot p^{1/\gamma} = \text{const.}$
For an ideal gas the constitutive equation is

$$pV = Nk_BT, \tag{3.39}$$

where $k_B = 8.617 \cdot 10^{-5}\,\mathrm{eV/K}$ is the Boltzmann constant and N the amount of the gas particles with the mass m. For an isothermal volume change follows $p(\varrho) = \text{const.} \cdot \varrho$, therefore $\gamma = 1$ and $\kappa_T = 1/p$. For an adiabatic volume change follows $\gamma = c_p/c_V$ and finally

$$\kappa_S = \frac{1}{\varrho}\left(\frac{\partial \varrho}{\partial p}\right)_S = \frac{c_V}{c_p p}, \tag{3.40}$$

where c_p is the heat capacity at constant pressure and c_V the heat capacity at constant volume. The S in the index implicates, that the entropy is constant.

3.3. Evaporation and boiling of water

The state of aggregation of a substance depends on the pressure and the temperature and it describes the physical state of this substance. An overview of the different states can be found in Tab. 3.2. Furthermore the names of the phase changes between the

Tab. 3.2.: Description of intermediate states between different states of aggregation

initial	final state		
state	**Solid**	**Liquid**	**Gas**
Solid	– – –	Melting	Sublimation
Liquid	Freezing	– – –	Boiling / Evaporation
Gas	Desublimation	Condensation	– – –

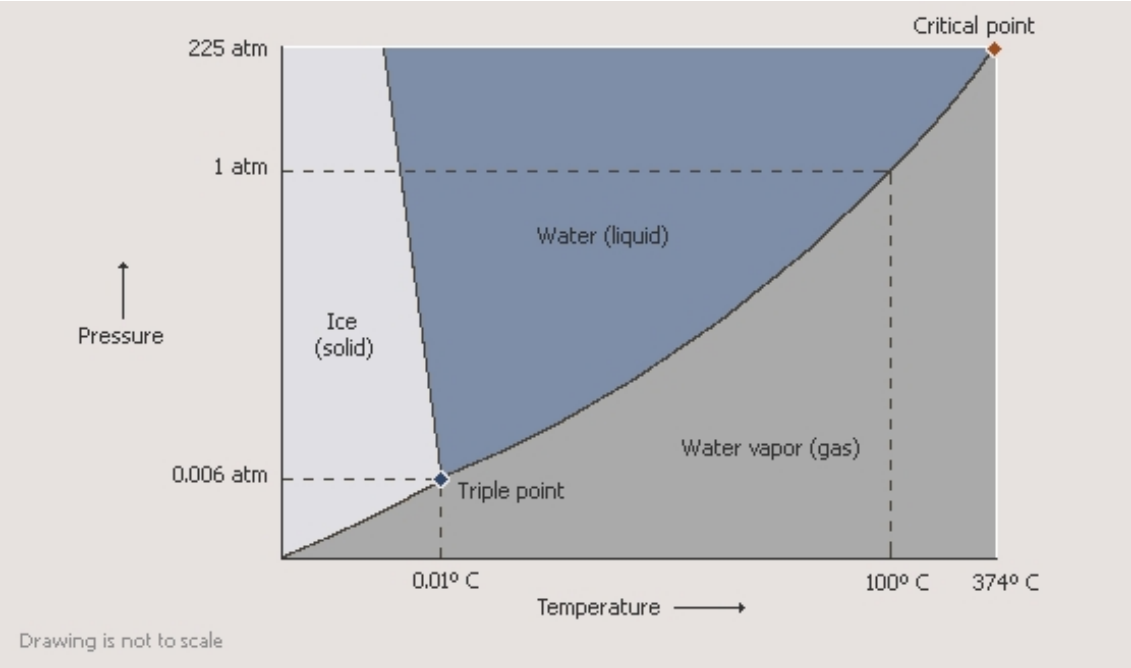

Fig. 3.4.: Phase diagram of water with important points [Aki11]. Drawing is not to scale.

different states are also included in this table. At standard pressure and a very low temperature all substances are solid with the exception of helium, which is liquid. Only at a very high pressure and a very low temperature it is freezing[1]. For this publication the phase change of water from liquid to gas and from gas to liquid is important, because the water desalination unit works in the temperature range between 0 °C and 100 °C at ambient pressure. In the one direction it is called boiling and evaporation and in the other direction it is called condensation. It must be distinguished between boiling and evaporation, because the physical background is different. Sometimes it is mixed up in the literature. A graphical overview of the phase diagram of water can be found in Fig. 3.4. The internationally accepted triple point of water is at 0.01 °C (273.16 K) and 611.657 Pa with an error of ±0.01 Pa. It is the optimum value which was measured by

[1] 2.5 MPa and 1 K

Guildner, Johnson and Jones in the year 1976 [GJJ76]. At the triple point all three phases like gas, liquid and solid are coexistent and they are in an equilibrium state. Small phase changes are possible, but in mean the amount of the different phases are constant. At this state sublimation is also possible. If the frame conditions are changed, the equilibrium state is moved for the benefit of other states.
During the evaporation the temperature at the set pressure is below the boiling temperature. In this state the temperature of the liquid can be increased. It can be increased up to the boiling temperature. This is in contrast to the boiling temperature. At this temperature level, which depends on the pressure, an energy addition has no effect on the temperature of the liquid. It reaches a fixed temperature level and it stays at this value. The additional energy is necessary for the phase change from liquid to gas. It is called the boiling energy. The boiling temperature can only be changed by changing other environmental conditions. In this case it is the pressure or it is also possible to add additives.
During the evaporation only as much water evaporates as an equilibrium between the water temperature and the vapour pressure curve is reached. The molecules in the air and in the liquid have different velocities. A few are faster and a few are slower. Therefore it is possible that molecules can leave the liquid and resolve the intermolecular forces. Other molecules in the air enter the liquid, because their speed is too low for the gas phase and to escape the intermolecular attractive force. In closed bins an equilibrium between leaving and entering molecules is reached. If the bin is opened the equilibrium between the two phases is destroyed and much more molecules can leave the liquid. Thus the liquid evaporates. It can also be explained in that way, that the partial pressure of the liquid in the air is lower than the saturation pressure curve. Until the value is lower the liquid evaporates and if the equality is reached the evaporation stops.
At the moment there are a few possibilities to calculate the saturation vapour pressure curve. One possibility is to calculate it with the Magnus-equation

$$e_s = 6.112\,\mathrm{hPa} \cdot \exp\left(\frac{17.62T}{243.12\,^{\circ}\mathrm{C} + T}\right), \tag{3.41}$$

where T is a temperature in the range between $-45\,^{\circ}\mathrm{C}$ and $60\,^{\circ}\mathrm{C}$. Due to the reason that the WDU can be operated in a temperature range between $0\,^{\circ}\mathrm{C}$ and $100\,^{\circ}\mathrm{C}$ this easy equation cannot be used. Instead of this equation the more complex equation of Goff and Gratch is necessary, which is a polynomial of the 6^{th} order with a logarithm in the temperature T.
The following equation calculates the water vapour pressure above a water surface as a function of the water temperature. It was invented by Mr. Goff and Mr. Gratch and it was later modified by Mr. Goff (1957) and the World Meteorological Organization (2000) [Gof46]

$$e_s = e_{st} \cdot 10^{z}, \tag{3.42}$$

with

$$z = a\left(\frac{T_s}{T} - 1\right) + b\log\left(\frac{T_s}{T}\right) + c\left(10^{d\left(1-\frac{T}{T_s}\right)} - 1\right) + f\left(10^{h\left(\frac{T_s}{T}-1\right)} - 1\right), \tag{3.43}$$

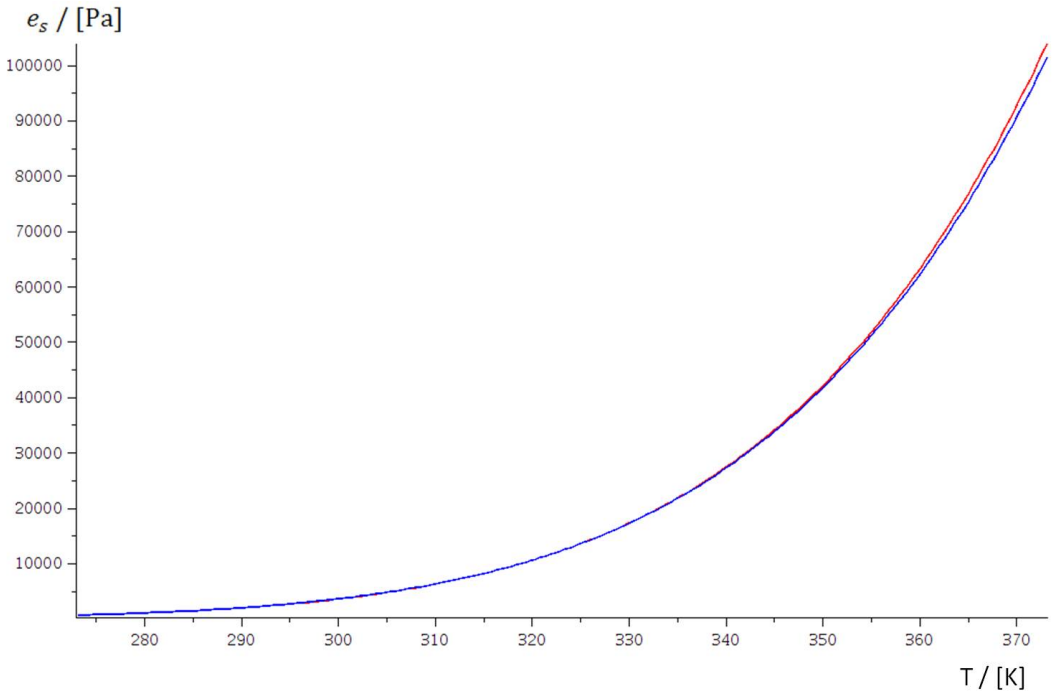

Fig. 3.5.: Comparison between Magnus (red) and Goff-Gratch (blue) equation in the temperature range between 273 K and 373 K.

where T is the actual temperature in Kelvin, $e_{st} = 1013.25\,\text{hPa}$ is the steam-point pressure and $T_s = 373.16\,\text{K}$ is the steam-point temperature for example at ambient pressure 1013.25 hPa. The other characters are constant and have the values:

$$\begin{array}{lll} a = -7.90298 & b = 5.02808 & c = -1.3816 \cdot 10^{-7} \\ d = 11.344 & f = 8.1328 \cdot 10^{-3} & h = -3.49149 \end{array} \tag{3.44}$$

A comparison between the Magnus-equation and the modified Goff-Gratch-equation can be found in Fig. 3.5. The equations are plotted in the range between 273 K and 373 K. As it can be seen in this figure, the Magnus equation calculates a too high value especially in the temperature higher than 350 K. It is just a small difference, but in the sum and for a huge amount the difference adds up. Therefore the Goff-Gratch-equation is used in the following chapters.
Evaporation is one of the most important aspects in the nature. An overview can be seen in Fig. 3.6. The complete water cycle on Earth is founded on evaporation. The water evaporates from seas, rivers and landscapes. Salts which are for example stored in oceans stay there. The necessary energy for the evaporation of the water comes from the Sun. The evaporated water rises in the atmosphere and in the higher atmosphere the water condenses and it is transported with the wind to all locations around the Earth. It condenses, because of lower temperatures and lower pressures. Due to the fact, that the system is not closed, there is normally no equilibrium state between condensation and evaporation. Therefore a lot of water is evaporated every day. Later the evaporated water precipitates as rain or snow over the landscapes or over oceans. A part of the

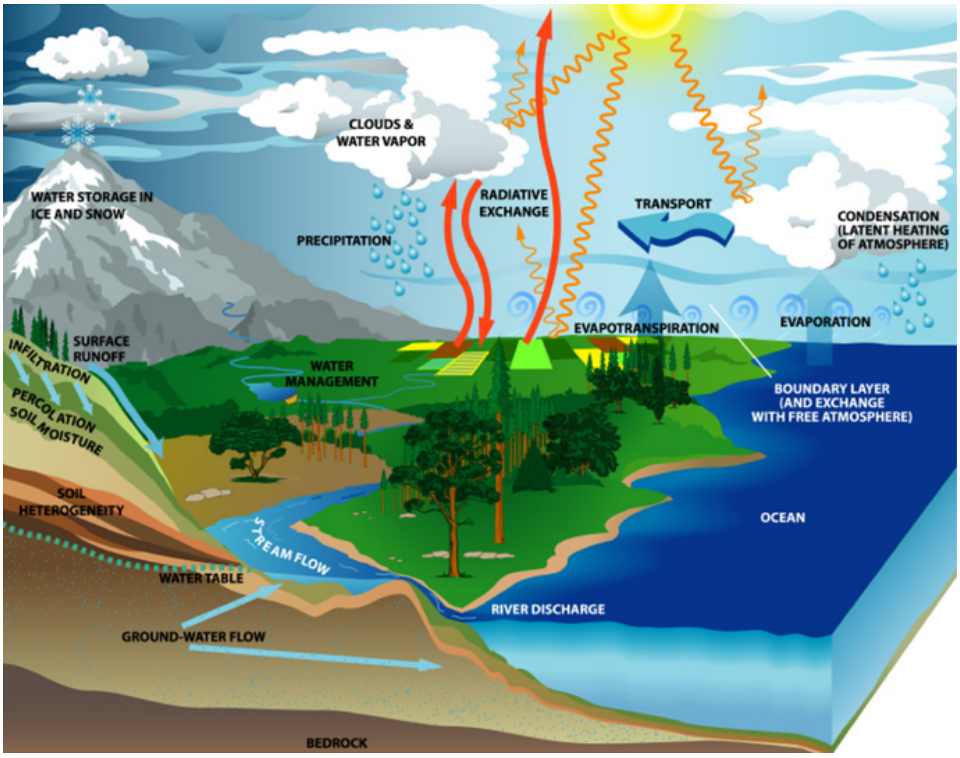

Fig. 3.6.: Overview of the evaporation and water transport in the nature [Twt11].

water is stored in ice and snow and other parts stream back into seas and oceans. Other parts are stored in the ground water which also could flow back into rivers and oceans. The most rivers end also in seas or larger rivers. An exceptional case is the river Jordan which ends in the Dead Sea which has a very high salinity. The salinity is up to 33 %. The salt mixture in the Dead Sea differs from the salt mixture in the oceans. It is 50.8 % $MgCl_2$, 14.4 % $CaCl_2$, 30.4 % NaCl and 4.4 % KCl. The rest are other trace elements. Due to the continuous water exchange, salts are washed out from stones and from the landscape. It is flushed into seas and oceans and therefore the salinity has increased over several million years. As was shown above, evaporation is one of the most important aspects in nature. Without evaporation there would be less life on Earth, because no new freshwater would be produced which is necessary for the daily life, for example for plants and animals.

4. Sunwater project

In the following chapter the innovative and future-proof Sunwater project is presented. It starts with the idea behind the demonstration plant which consists of a solar thermal part and a water desalination unit. This chapter is subdivided into the initial concept and the final concept of the whole system. Furthermore the design and the idea behind the system is discussed. At the end of this chapter the main components will be presented, which were needed and were bought in different countries to operate the demonstration plant and to produce freshwater with solar energy.

4.1. Demonstration plant

The idea behind the project Sunwater is, as mentioned before, that freshwater is produced in an environmentally friendly and future-proof way. At the moment there are a lot of different possibilities to convert saltwater into freshwater. A few possibilities were shown in section 2.2. It can be converted with reverse osmosis systems, multi-stage flash distillation or evaporating systems. The second main aspect of the Sunwater project was that freshwater is produced in an environmentally friendly way with renewable energy sources. These are energy sources which do not pollute the environment or accelerate the green house effect. Therefore it is very interesting for the future [Gre11]. At the beginning of the project it was clear that the demonstration plant should be operated with solar energy. At the moment there are two different technologies which can be used for this project. An overview of the different technologies was given in section 2.4. The first technology is used to produce the necessary electrical energy for the desalination. This can be done with photovoltaics, but the efficiency of the PV modules is very low. The second possibility is to generate heat with solar thermal, which has a much better efficiency compared to PV. Another advantage is that this thermal heat can directly be used for a special kind of desalination process. Other possible energy sources like geothermal, biomass or wind energy are also possible, but they were not considered during the initial phase of this project. The reason was that one project partner came from Egypt and in a few areas of this country, there is a very high daily solar radiation. Hurghada has for example the world highest solar radiation and therefore it should be possible to operate a desalination demonstration plant with solar energy.
At the beginning of the project there was the idea in Soest to store the surplus energy in heat storage tanks to extend the working time of the demonstration plant or to bridge the time, when the solar radiation drops during the day. One big problem could for

example be clouds, but in Hurghada, the location of the demonstration plant, there are just a few days in the year with clouds and thus it is predestined for the installation. Furthermore the idea was to use another green technology to extend the operation time of the demonstration plant. The first idea was to use a heat pump. The advantage is that the heat pump produces more thermal energy compared to the deployed electrical energy [Hep08]. The difference is taken from the environment and so this energy source can be more or less defined as environmentally friendly. With this background knowledge it is possible to include in this project the innovative desalination unit from a company in Kiel, Germany, which works with evaporation. See subsection 2.2.2. The necessary thermal energy can be generated with the solar thermal roof or the heat pump and it can directly be used for the desalination. Another innovative advantage of this idea is that less energy is squandered during the conversion between two different energy forms. Normally a lot of energy is lost, for example by the conversion between sunlight and electrical energy with PV or from thermal energy to electrical energy in conventional power plants. In this project the necessary electrical energy for pumps or controllers came from the grid, but compared to the needed thermal energy this amount was insignificantly low.
The first innovative and unique concept of the demonstration plant can be found in Fig. 4.1. It was conceived by this author. As be seen in this picture the needed thermal energy will be produced with a solar thermal roof (STR) of round about 240 m^2. Water is pumped through the roof by using a pump which is controlled by a ST-controller. The water enters the panels with a low temperature and then it leaves the roof with a much higher temperature. It will directly be heated up by the Sun. The idea is that the temperature is heated up to 90 °C or a little bit higher, but the water temperature must be below the boiling point, because the whole system is operated with normal pressure and not with overpressure. Therefore the maximum water temperature in this system is just 100 °C. If the water should be heated up higher than the boiling point at normal pressure, the complete system must be operated with overpressure, but this is more complex and much more expensive. This is due to the innovative and completely new system too complicated for a first project and therefore the system is operated under normal pressure. The operation with overpressure could be the next step and can be realised in another project. This could have the advantage, that less heat storage volume is needed for the same time of operation. The hotter water can be mixed up to the necessary water temperatures and volume flows and consequently the operation time of the demonstration plant can be extended. If the water temperature rises above the boiling point, the water starts cooking and vaporises. Due to the vaporisation of the water in the pipes, the volume of the water rises extremely. Without safety measures the pressure increases in the closed system and then the complete system can be damaged. Without safety equipment the system can explode and the hot water and / or parts can hurt people, who work at or visit the system. So the idea is that the pump must be controlled by the ST-controller in a way that the temperature never reaches the boiling point. If the temperature in the system is too high, different safety arrangements must automatically be activated. This safety aspects must be included in the planning and the control programme of the system.

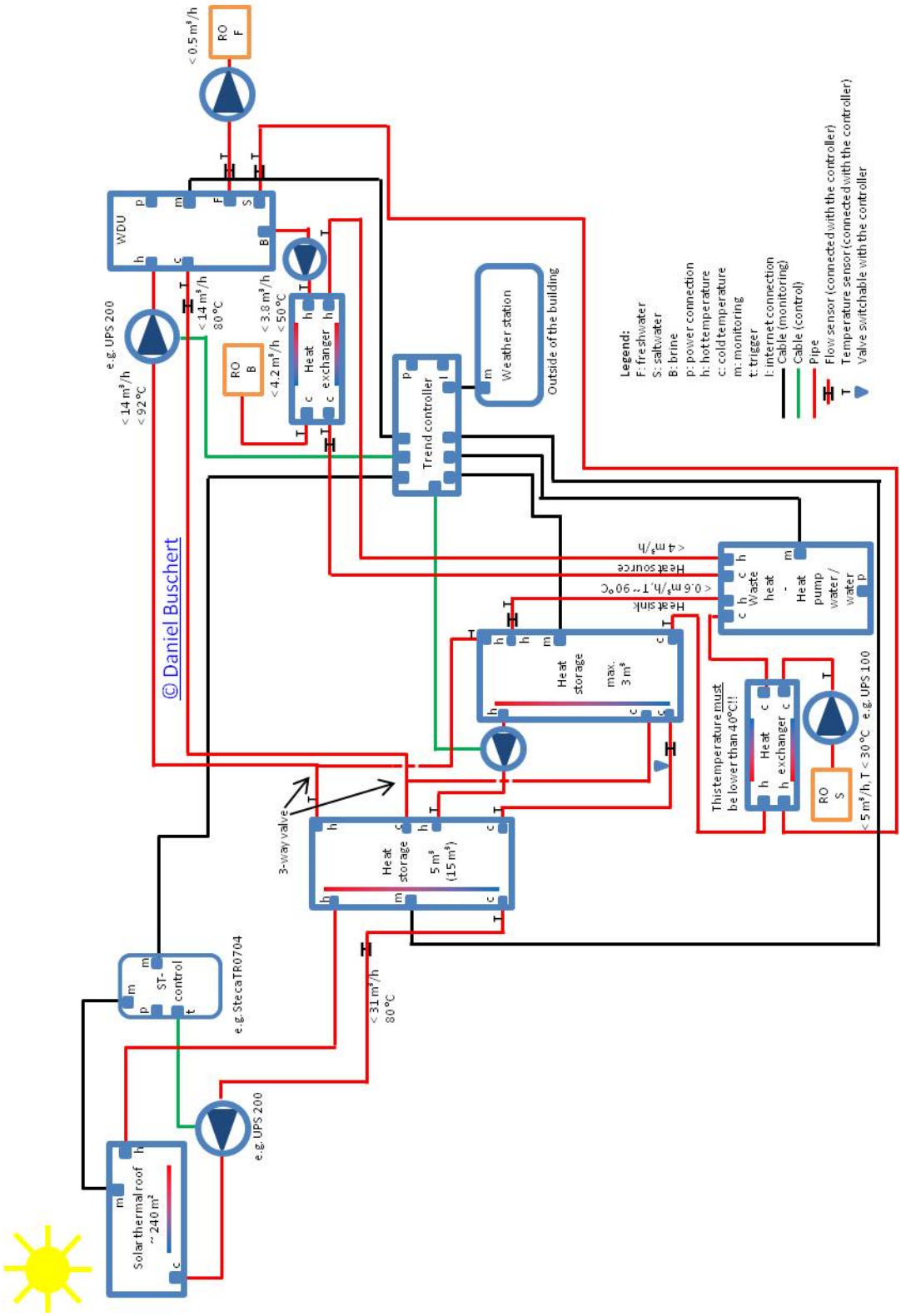

Fig. 4.1.: First concept of the demonstration plant in Egypt.

The produced hot water will be buffered in the first larger heat storage tank with the size of 5 m^3 or maybe up to 15 m^3. Inside the heat storage tank there are different temperature layers. At the top is the layer with the highest temperature and on the bottom is the layer with the lowest temperature. For this reason only the coldest water in the heat storage tank is transported from the heat storage tank to the solar roof and thus the temperature increases in the system. Furthermore different temperature sensors are installed inside the heat storage tank, which will be evaluated by the Trend controller. It can be found in the right middle of Fig. 4.1. Another idea was to install a level meter inside the heat storage tank to control the water level in the system. When the water level drops, a few parts in the system could be damaged or another aspect could be, that too much water is vaporised in the system. This level meter is included as a security measure and it could be used to keep the amount of water at the right level. It could for example be combined with an automatic refill for the process water. The water temperature of the system is increased by the STR, and if there is enough thermal energy available in the system, the desalination unit can be started. The energy amount in the system is equivalent to the temperature stratification in the heat storage tank and the pipes. The hotter the water in the heat storage tank, the more energy is available in the system. It is pumped from the large heat storage tank to the desalination unit. In this case the pump is controlled by the controller from Trend. The Trend controller was used again, because in the former Endohouse project [End05] a kind of this controller was already installed and therefore important basics and hardware were available in Soest. The hot water enters the WDU and the energy is used to convert the saltwater into freshwater and brine. The entering water leaves the WDU at a lower temperature and then it is transported back to the heat storage tank. From the heat storage tank it will be pumped again through the solar thermal roof and there it will be heated up to new hot process water.
For the desalination inside the WDU, the energy from the heat source is transported to the saltwater by using a heat exchanger[1]. The desalination of the saltwater starts and the brine and the freshwater leave the unit. The problem is, that the temperature of the brine and the freshwater are relatively high. Due to the internal procedures the temperature of the brine is much higher compared to the freshwater. This principle will be explained in section 4.2. Therefore a lot of energy is squandered. At this point a completely new aspect is included in the already innovative concept. This idea also comes from the author. The remaining energy in the brine can be reused by using a waste heat heat pump. This is a heat pump which recovers the stored heat in the brine and / or the freshwater and this energy is transferred back to the solar thermal system. Therefore it is called a waste heat heat pump in this application. With this heat pump the temperature in the brine will be reduced and the energy which would normally be lost is returned in the solar thermal part of the system and can be reused for the desalination. The energy from the brine to the heat source of the heat pump is again transferred by using a heat exchanger. This heat exchanger can be found in the upper right part of

[1] In subsection 6.5.1 an idea behind the simulation of a heat exchanger can be found. Furthermore the mathematical background is also illuminated.

Fig. 4.1. The hot brine enters the heat exchanger and leaves it at a lower temperature. Additionally the cold water enters the heat exchanger from the other side and due to the second law of the thermodynamics the heat is transferred from the hot medium to the cold medium [Fli04]. Therefore the water from the heat pump leaves the heat exchanger with a higher temperature. A part of the energy is taken from the brine and with the mentioned heat pump the energy is shifted to a higher temperature level. For the system a temperatures close to 90 °C is required. Therefore a special heat pump is necessary which has a desired sink temperature. The produced hot water is buffered in the second and smaller heat storage tank, which can be found in the middle of Fig. 4.1. This size is only 3 m^3. Inside this heat storage tank, there are also temperature sensors and a level meter installed. The components are also evaluated by the installed Trend controller. These information are needed for security reasons and the control of the solar thermal system. In case when the solar radiation drops or during the night, the hot water in the second heat storage tank can be used to operate the desalination unit.
During the night the temperature drops normally in the large heat storage, because the water is not heated up by the Sun and due to physics the temperature drops exponentially (6.101). In this case the heat pump can be used to hold the solar thermal system at a relatively high temperature. The advantage is that in the next morning, when the Sun rises, less energy is needed to raise the temperature inside the solar thermal system to the necessary operation temperature. Therefore the desalination unit can be started much faster and produce more freshwater during the whole day.
As it was mentioned a special heat pump is necessary for the operation of the solar thermal system. Most existing heat pumps have only a flow temperature of 65 °C or 75 °C, but for this project the temperature must be higher, for example between 90 °C and 95 °C. Other temperature ranges are counterproductive, because the whole system is operated at a temperature range between 75 °C and 95 °C. Normally the temperature should not drop below this temperature. After a difficult worldwide search only one company in Germany was found which can produce such a heat pump [The10], but for the operation of this heat pump the input temperature of the heat sink must be below 40 °C. Therefore another heat exchanger is necessary to cool down the temperature below the maximum input temperature of the heat pump. This heat exchanger can be found in Fig. 4.1 in the lower centre. The hot water which enters the heat pump, is cooled down with the entering saltwater. The saltwater will somewhat be preheated, but the advantage is that less energy is necessary later to heat up the saltwater to the needed operation temperature needed for the best desalination results. Therefore the transferred energy is not lost, it is only shifted to the incoming saltwater and thus it stays in the system.
The smaller and larger heat storage tanks are connected with a bypass. It can also be controlled with the Trend controller. First of all the switchable valve must be opened. This is necessary to prevent convection of hot water in the system, this is based on different temperatures and thus variable densities and it separates the heat storage tanks from each other. Afterwards the pump can be used to transport the hot water from the smaller heat storage tank to the larger heat storage tank. This is helpful to hold the water in the larger heat storage tank at a higher level, when for example the solar

radiation drops or during the night. Furthermore two 3-way-valves are included into the system. This can be used to select the energy source for the desalination. This could for example be the larger heat storage tank which is directly connected with the solar roof or the smaller heat storage tank which is connected to the heat pump. It is also possible to use the hot water in the smaller heat storage tank via the larger heat storage tank, but the disadvantage is that the volume flow produces turbulences in the heat storages and thus the hot water is mixed up with colder water and therefore a water temperature drop is inevitable in the system.
Additionally there are also other components installed inside the ST plant to monitor and control the system. This includes different flow meters, temperature sensors and of course a weather station. One flow meter can be found between the larger heat storage tank and the solar thermal roof. The other volume flow meter is between the WDU and the heat storage tank. The first sensor is installed in the supply pipe of the solar thermal roof and the second sensor is installed in the return pipe of the WDU, because the temperatures are lower compared to the corresponding pipes on the other side. Due to the continuity equation (3.34) the volume flow of water is the same in both pipes. A few temperature sensors are installed between the components of the system. Different sensors are needed to monitor and control the system. The measuring results are evaluated with the Trend controller and important decisions could be met for the control of the system. Furthermore the Trend controller is connected to the internet and the system can be monitored and controlled from all over the world.
Outside of the building, where the complete system is included, there could be a weather station installed. This station measures all needed environmental data which are necessary to operate and optimise the system. The measuring data are for example wind direction and wind speed, air temperature and solar radiation. All sensors are connected with the Trend controller and the controller also evaluates and uses different measuring results for the control of the whole system.
In this concept, the necessary saltwater comes from an existing reverse osmosis water desalination system which was built up near the hotel in Egypt. The saltwater is taken out of a saltwater well and then it is transported into the water desalination. Before it enters the WDU it passes the first heat exchanger. Inside the WDU, it is converted into freshwater and brine. The brine passes the second heat exchanger. It is used to reduce the remaining thermal energy in the brine. This energy is returned to the solar thermal system by using the heat pump. Therefore the efficiency of the whole system can be raised, because otherwise the energy would be lost. Finally the brine is returned to the existing osmosis system and there it is depolluted into another existing well. The produced freshwater is transported to the present freshwater piping system and then it can be used by humans or for other applications.
During the planning of the whole system, this includes the consideration of the available project budget and the gettable components, it was discovered that the demonstration plant must be modified and cannot be installed like in Fig. 4.1. One problem is that vacuum tube collectors are necessary for this project, because the inquiries at different companies all over the world showed, that no one has the experience nor can give the guarantee, that normal flat plate collectors can be used to heat up water up to 90 °C or

higher. Therefore more expensive vacuum tube collectors are needed to produce water in this temperature range. With vacuum tube collectors it is no problem to reach these temperatures. It is also possible to reach temperatures higher than 95 °C without considerable problems. The advantage of the vacuum tube collectors is that the efficiency in this temperature range is much higher compared to flat plate collectors. The difference in the budget was solved in a way that the money for the planned heat pump was used to buy the vacuum tube collectors. Before this decision was taken, the heat pump manufacturer had been contacted several times and after a few consultations it was clear that they were not interested in such a project which was undertaken in Egypt or outside Germany at the moment. The problem for the company is that this kind of heat pump is very innovative and the technology is in its infancy. Based on this, the money for the heat pump could easily be transferred to the solar thermal roof. With the additional money the needed vacuum tube collectors could be bought. Another problem is that the 15 m^3 heat storage tank is not available at the moment and therefore two smaller heat storage tanks must be installed in Egypt. Each has a volume of 5 m^3. Fig. 4.2 shows the idea how the solar desalination demonstration plant could be installed in Egypt. This idea of the demonstration plant was also invented by this author and was approved by other partners, but the Egyptian partners installed the demonstration plant in a different way. This was done without consultations.
In this concept the thermal energy comes from vacuum tube collectors. The volume flow of the water, which is pumped through the collectors, is controlled in that way, that the temperature is as long as possible 90 °C at the output of the solar thermal roof. For this the input temperature and the output temperature of the water is measured. With this information and the information of the actual solar radiation, the solar thermal pump can be controlled and adjusted to the needed volume flows. This is done with the associated inverter for the pump. The inverter is otherwise controlled with the Trend controller. It continuously evaluates the different temperatures of the STR, weather conditions and the volume flows. The volume flow is measured with an ultrasonic volume flow sensor, which is installed before the solar thermal roof. With this information the solar thermal pump can be adjusted via the inverter to the right volume flow. For the actual measured solar radiation, the right volume flow through the STR can be calculated if the input and output temperature of the STR is considered. There is an easy relation between these variables. This information is additionally helpful to calculate the amount of energy in the system and to find the right moment to start the desalination process.
The hot water can be buffered in the two heat storage tanks. The distance between both heat storage tanks and the solar thermal roof must be the same. If the distance were different, the temperature layering and the volume flows inside the tanks would be different. If the temperatures are different and the water is later transported in pipes with an equal length from the heat storage tank to the WDU, the water is mixed up and then the temperature in the volume flow from the tanks to the WDU drops by a few degrees. Due to the fact that two heat storage tanks are installed, the incoming volume flow must be split into two equal volume flows, which enter the different heat storage tanks. For buffering, loading or other situations the right solar thermal part

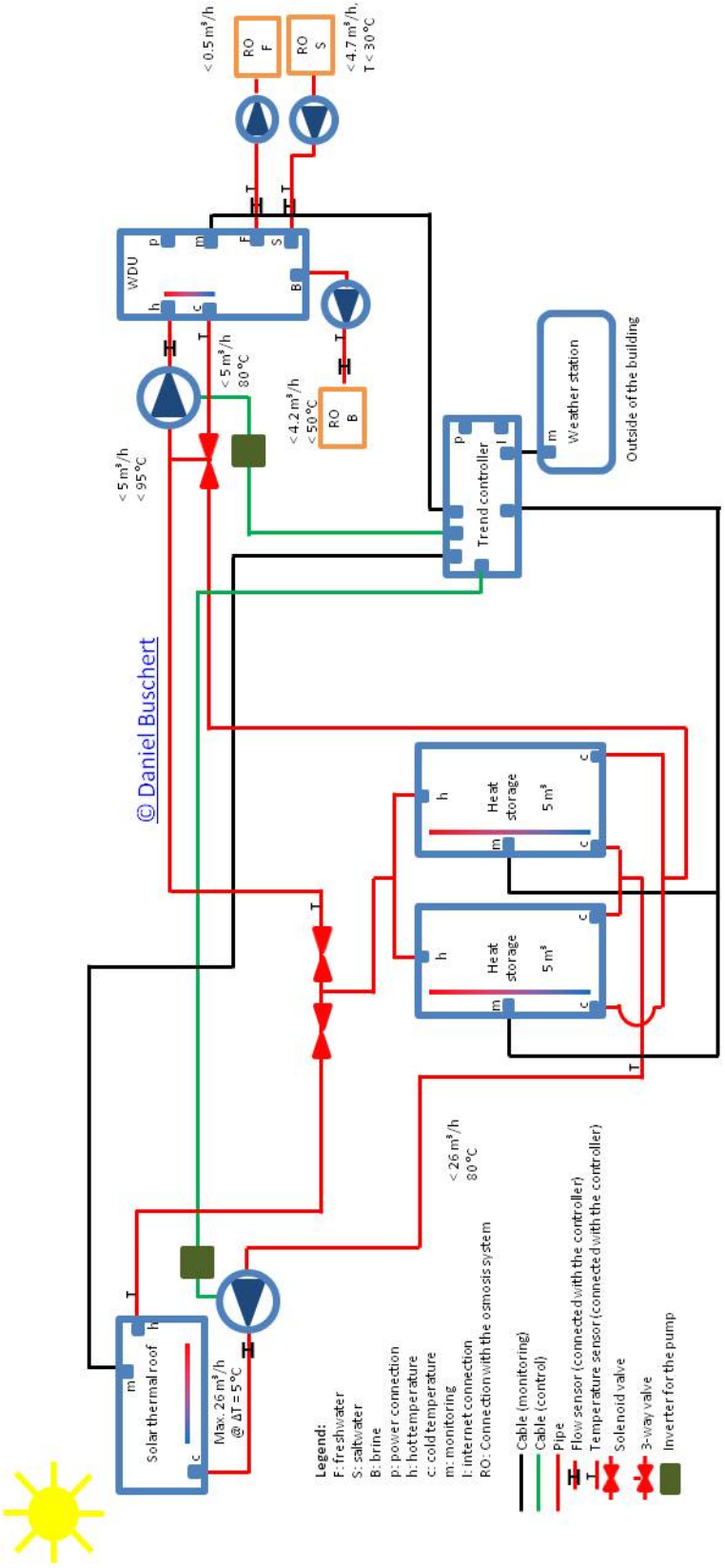

Fig. 4.2.: Final concept of the demonstration plant in Egypt.

with the WDU can be separated from the rest of the system. This can be done with the installed solenoid valve, which is on the right in Fig. 4.2. It could be very interesting in the morning, when the volume flow from the STR is not high enough to operate the WDU. The energy, which is gathered, can be used later during the day. Furthermore convection of the hot water is avoided in the system, which would decrease the efficiency. If the right solenoid valve is closed, it cuts off the right part from the left part. When the solar thermal pump is running, the left solenoid valve in Fig. 4.2 must be opened. The same is true for the heat delivery pump and the right solenoid valve. Otherwise no water can be transported in the system and the pumps could be damaged. Both solenoid valves are controllable via the Trend controller with just a digital signal. The hot water enters the heat storage tanks at the top and at the same time the cold water leaves the heat storage tanks at the bottom. Due to the continuous volume flow different layers are loaded inside the two tanks. The hottest layer is on the top and the coldest layer is at the bottom. Each heat storage tank has 3 temperature sensors and a level meter, which are also evaluated by the Trend controller. With the temperature sensors the amount of energy in the system can be calculated. The distance from both heat storage tanks to the solar thermal roof must once again be the same. If the distance is different the volume flows inside the tanks will vary.
When enough energy is available the desalination process can be started. For the start the right solenoid valve must be opened and then the heat delivery pump must be activated. This pump is controlled with the measured volume flow, because for the best operation of the WDU, it needs a constant flow rate. The flow rate is measured with another ultrasonic volume flow meter and is once again evaluated by the Trend controller. The Trend controller controls the pump via another inverter. The water enters the WDU with a temperature between 90 °C and 95 °C at maximum. Inside the WDU the thermal energy is transferred with a heat exchanger from the solar thermal or process water to the saltwater. Then it leaves the WDU with a lower temperature, e.g. 80 °C. Now the water flows back to the heat storage tank. The inlet of the water into the heat storage tank is at the bottom. The distance between the hot water and the colder water is as large as possible. This has the advantage, that the cold water is not mixed up with the hotter water at the top. The coldest water is taken from the bottom of the heat storage tank and it is transferred back to the solar collectors to be heated up again. The distance between the inlet of the hot and the inlet of the cold water should be as large as possible and then only small turbulences can evolve from the volume flows inside the tanks. If the distance is too short, the cold water from the WDU can again be transferred to the WDU and then the temperature drops again and finally the temperature is not high enough to operate the WDU. In this case two independent cycles can be generated in the heat storage tanks. One for the WDU and one for the solar thermal roof. If this is the case the whole system cannot be used to generate freshwater.
Fig. 4.2 also shows a 3-way-valve. This is used to control the input temperature of the WDU. It can mix the returning heat flow from the WDU into the flow for the heat delivery. With this valve it should be possible to adjust the input temperature of the WDU to a specified temperature level in case that the output temperature of the WDU should be the same. The energy demand of the WDU varies during its operation. The

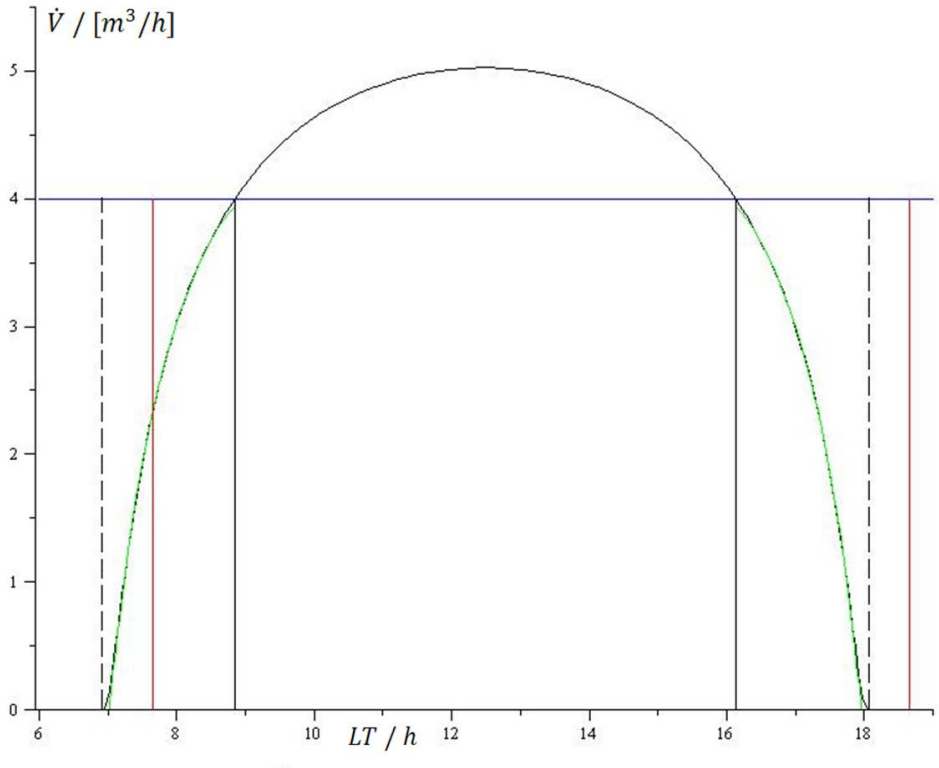

Fig. 4.3.: Relationship between the heat source and the operation of the WDU. Between the two perpendicular red lines the WDU can be operated.

less energy is needed, the higher is the output temperature of the process water and the more energy is needed, the lower is the temperature. These temperature differences can be compensated with this 3-way-valve. If the water from the returning flow is mixed up with the other volume flow, less energy is taken from the heat storage tanks or from the solar thermal roof. Due to the lower volume flow, more hot water can be stored in the heat storage tanks and additionally the turbulences can be reduced in the system, which has a positive effect on the storage capacities and working times of the WDU. The 3-way valve can also be used as a safety equipment. If the temperature of the heat delivery volume flow is too hot, the returning water can be used to cool down the process water to the needed operation temperature of the WDU.
During the operation different volume flows from the STR must be considered. An overview can be seen in Figure 4.3. In the morning the volume flow from the solar thermal roof is very low. Therefore the water is directly transferred into the heat storage tanks, which are used as a buffer. Later the volume flow of the solar thermal roof increases. Then the water inside the heat storage tank and the water from the solar roof can be used to deliver the needed thermal energy to the WDU. The operation time of the WDU starts at the first perpendicular red line in Fig. 4.3. It consists of the water from the solar roof and the buffered hot water inside the heat storage tank. Later the volume flow from the solar roof is high enough to operate the WDU. This is between the

two intersections between the horizontal line at 4 m^3 and the curve. The idea is that the hot water from the solar roof is split into two volume flows. The needed constant volume flow for the desalination is directly delivered to the WDU and the other is buffered in the heat storage tanks. It is advisable that the hot water comes from the solar roof, passes the T-piece in Fig. 4.2 and is directly transferred to the WDU. During this time the surplus hot water can be buffered with the T-piece inside the heat storage tanks for a later usage. This hot process water is needed after sunset or at a point of time with a low solar radiation. Later the volume flow from the solar roof drops below the demand of the WDU and then the water from the heat storage tank is added to generate the needed volume flow demand of the WDU. At the end the hot water from the roof runs dry and then the whole water for the desalination must be provided by the heat storage tanks. In this case the left solenoid valve in Fig. 4.2 must be closed to prevent convection of hot water through the collectors. Freshwater can be produced until the temperature in the system drops below a certain level. Then the heat delivery pump and the WDU must be switched off. Furthermore the right solenoid valve in Fig. 4.2 should also be closed to prevent convection of hot water through the WDU. This has also the effect that the temperature level in the system is more stable compared to a system either without or opened solenoid valves.
The working time of the WDU depends certainly on the volume flow during the whole day and the capacity of the heat storage tanks. The ideal case would be that during the whole time the necessary volume flow with the necessary temperature is produced with the solar roof, but this is only possible for a short time period every day, as can be seen in the Fig. 4.3. The ideal case can only be reached when a constant (waste) heat source is available. This could be geothermal or the waste heat from power plants like nuclear power plants or from industrial waste heat from steelworks for example.

4.2. Water desalination unit (WDU)

The desalination unit used comes from the German company Terrawater [Ter10]. This company was founded in the year 2007 in Kiel. They produce a water desalination unit, which works with evaporation. For the Sunwater project they contribute their water desalination unit and their expertise. The complete system was build in Kiel and was transported to Egypt with a freight container. At the building site the staff members of this company installed the water desalination unit and initialised the system for the freshwater production. A typical picture of this innovative and future-proof desalination unit can be found in Fig. 4.4. The innovation of this desalination unit is that the saltwater and / or the brackish water is desalinated with evaporation and not with distillation. The difference between evaporation and distillation was explained in section 3.3. Both are responsible for the volatilisation of water, but the difference is that during the distillation the temperature is at the boiling temperature of the fluid, but the evaporation takes part at a temperature below the boiling temperature. Therefore less (thermal) energy is necessary for evaporation and the production of freshwater. This is compared

Fig. 4.4.: Water desalination from Terrawater which is used in the project in Egypt [Ter10]. The photo was taken at the company in Kiel.

to other distillation technologies. Due to distillation, the phase change from liquid state to gaseous state costs a lot of energy, similar is the phase change between ice and liquid water [Tip00]. Another advantage of the WDU is, that no filters or membranes are necessary for the desalination compared to other desalination systems and this reduces the operation costs of the whole system. Filters and membranes do not need to be exchanged like in the RO systems. Additionally no chemicals or additives must be used for the desalination process and this also has a cost saving aspect. Furthermore it is not so prone to fouling and other damage. If the amount of freshwater should be raised and enough thermal energy is available, a vast number of water desalination units can be combined for the freshwater production. This can be done for example in a freight container or locally in buildings. Thus the system is very modular and if the system is installed in a freight container the system can be transported within a short time period anywhere in the world. Finally the system can help to reduce the water shortages all over the world.
For the operation of this desalination unit a heat source at a special temperature level is necessary. It enters the WDU and the stored energy is transferred via an external heat

exchanger from the heat source to the saltwater. Thus the heat source cools down to a lower temperature and leaves the WDU. The heat source can be obtained for example from the industry, from geothermal or from solar thermal sources. The best value is when the temperature of the heat source has at minimum 90 °C, but lower temperatures are also possible. If the temperature is higher than the boiling point of water and higher than the specifications of the used external heat exchanger, the heat source must be cooled down to the maximum possible operation temperature. This can for example be done by cooling down the heat source or by mixing it up with a colder fluid, which can for example be the returning fluid from the water desalination unit. The entering saltwater is heated up with the heat source to a temperature close to the boiling point, because the evaporation is more effective at higher temperatures compared to lower temperatures. The water vapour pressure curve has an exponential slope (3.42) and therefore it is very important to raise the temperature of the saltwater as high as possible. The higher the temperature, the higher is the amount of the evaporated water. Later the evaporated water is cooled down and then it condenses as freshwater which can be used. An innovation of this desalination unit is that there are a few bypasses included in the system, which raise the efficiency of this system. Therefore most energy in the system stays in the system and only a relative low amount leaves it as a temperature rise in the brine and in the freshwater. The temperature rise of the brine and the freshwater can be higher than 15 °C compared to the entering saltwater, but it is adjustable to different needs. This energy, which raises the temperature in the brine and freshwater, is normally lost and must be supplied with the external heat source.
This TW water desalination unit is controlled with a controller from Beckhoff. It controls for example different pumps and valves in the system and regulates the volume flows inside the system. This also includes different bypasses. Furthermore different temperature sensors and volume flow meters are included in the system, which are evaluated with this controller and which are necessary for the operation. The controller is also connected with the internet and can be controlled and configured from all over the world. Additional software updates can also be implemented. Further technical data can be found in Tab. 4.1.

4.3. Solar thermal roof

With the solar thermal roof, the needed thermal energy for the desalination is produced. The idea was to install the solar field at the roof of a building in Hurghada, Egypt. Hurghada was chosen, because it has the world's highest solar radiation. The maximum daily solar radiation is higher than 1000 W/m^2. With this high solar radiation it should be possible to produce enough hot water in the range of up to 95 °C, which can be used to operate the water desalination unit.
At the beginning of the project flat plate collectors were considered to heat up the process water for the desalination. During the normal operation the temperature must normaly be heated up in the range from 70 °C until 80 °C up to 90 °C or 95 °C. Only at the start-up or after a long shut down of the system the temperatures in the system must be raised

Tab. 4.1.: Technical data of the water desalination unit from the German company Terrawater [Ter10].

Parameter	TW5 design	Remarks
Raw water temperature (RT)	$> 0\,°C$	frost free, max. $70\,°C$
Grain size of raw water	$< 0.5\,mm$	max. $1\,mm$
Ambient temperature	$21\,°C$	max. $50\,°C$
Salinity	$< 50.000\,ppm$	max. $300.000\,ppm$
Daily output	$5\,m^3$	max. $6\,m^3$ in $24\,h$
Hourly output	$209\,l/h$	max. $250\,l/h$
Temperature input	$95\,°C$	min $50\,°C$, max. regardless
Temperature output	$85\,°C$	depends on mass stream
Thermal power per hour	$50\,kW_{th}$	min. $10\,kW_{th}$, max. $90\,kW_{th}$
Mass stream of thermal power	$3.4\,m^3/h$	depends on energy and temperature difference
Power input	$0.7\,kW_{el}$	
Electrical energy / m^3	$3.2\,kW_{el}$	
Recovery rate	adjustable	min. $10\,\%$, max. $95\,\%$
Product water temperature	RT + $15\,°C$	max. brine loop
Brine temperature	RT + $15\,°C$	max. brine loop
(Raw water) / (m^3 product water)	adjustable	depends on recovery rate

from ambient temperature to the operation temperature of the WDU, because the water temperature is filled in with ambient temperature or it cools down at worst to the local ambient temperature, which is between $10\,°C$ and $40\,°C$. Therefore the collectors need a high efficiency at high temperatures. The usage of plat plate collectors were considered during the planning, because they are much cheaper than other available possibilities. Later it was discovered, that the flat plate collectors have relative low efficiencies at these temperature ranges. Additionally there was the fear that the flat plate collectors cannot heat up the process water to the needed operation temperatures. Experimental data were not available during the project life-time, especially at the beginning of the project. One Egyptian partner tried to take a few measurements, but the results were never presented to other project partners. From Germany a few suggestions for different measurements were given to the Egyptian partner but they were not realized there. Therefore the more expensive vacuum tube collectors were bought for the project. The difference from the planned budget in the project proposal to the expensed budget was

Tab. 4.2.: Technical data of the utilised vacuum tube collectors from the German company AkoTec [Ako09]

Collector	Dimension [cm]	Gross area [m^2]	Aperture area [m^2]	Weight [kg]	Peak power [W_p]
Vario 3000	$225 \times 220 \times 12$	4.9	4.4†	67.5	3312

† with reflector

taken from the planned heat pump, which had not been installed. The collectors are installed like in a matrix $\underline{A}$. The complete field consists of different rows and each row consists of a few solar collectors. The collectors in the columns are needed to heat up the water to temperatures higher than 90 °C and the rows are needed to increase the volume flow of the complete field. The maximum volume flow of one row is not high enough to operate the WDU, therefore several parallel branches must be installed to generate a volume flow, which is high enough for an operation. If the volume flow would be too low, the WDU can either not be operated at all or just for a few short periods during the day. If the volume flow is too low for a continuous operation, there is the possibility to buffer the whole hot process water in the heat storage tanks and when the heat storage tanks are fully loaded, the WDU can be started. Due to different time intervals, the operation is very inefficient, because the water inside the WDU must always be heated up to the operation temperature and this is very energy-intensive, because during the inoperative times the water in the WDU cools down.
The vacuum tube collectors are installed at the roof of the building in Egypt. They are southerly orientated for a better performance. The technical data of the collectors can be found in Tab. 4.2. The collectors also came from the German company AkoTec, but they were directly bought from the Egyptian partner and were installed by another Egyptian partner. The vacuum tube collectors used are OEM vario 3000. They have a double-sided coating of TiNOX, a stagnation temperature of 192 °C and a maximum operation pressure of 10 bar. The efficiency of the collector with a reflector is $\eta_0 = 75.2\,\%$. For this collector the absorption coefficient is $\alpha = 96\,\%$ and the emission coefficient is $\epsilon = 4\,\%$. The pipe connection is $^3/_4''$ and the fluid volume is just 3.96 l.

4.4. Trend controller and touch screen

To control the solar thermal part of the demonstration plant, a controller from Trend (IQ3XCITE / 96 / 100-240) with 3 add-on modules were scheduled to be installed at the building site. A picture of the Trend controller with one add-on module can be found in Fig. 4.5. The main controller consists of 10 universal inputs and 6 analogue voltage outputs. One add-on module is for digital output signals (XCITE / IO / 8DO) and two other modules are for universal inputs (XCITE / IO / 8UI). The universal inputs can be used to measure voltages, currents, thermistors and digital signals. The analogue

Fig. 4.5.: Trend controller with one add-on module for the control and monitoring of the solar thermal part of the system [Tre11].

voltage signals could be in the range between 0 V and 10 V and have an input resistance of 200 kΩ. The switchable analogue current input is in the range between 0 mA and 20 mA with a resistance of 240 Ω. The bridge resistor for the thermistor input is 10 kΩ with a bridge voltage of 5 V and the digital input is a potential-free contact with a counting rate of 30 Hz. This input is fed with 5 V and 3 mA. In contrast to the digital inputs the current, voltage and thermistor inputs have a resolution of 20 bit (4096 data). The analogue outputs are in the range between 0 V and 10 V with a maximum of 20 mA and a resolution of 11 bit. The digital outputs have the states high and low. With the circuit points at the Trend controller there are overall 26 universal inputs, 8 digital outputs and 6 analogue outputs available to control and measure all components in the solar thermal part of the demonstration plant. For a basic operation of the demonstration plant these inputs and outputs should be enough. In later realisations the amount of inputs can be reduced or the focus can be different. It can be optimised to the given situation and the target of the next realisation.
All measurement and control components are installed inside or close to the building, with the WDU. Furthermore a touch screen (IQVIEW4 / 24) is installed for on-site monitoring and presenting purposes. The picture of the touch screen can be found in Fig. 4.6. The Trend controller and the touch screen are directly connected with a RJ232 cable and the touch screen is mounted at the front door of the switch cabinet. The Trend controller and the add-on modules are installed on a DIN rail inside a standard switch cabinet from Rittal. Furthermore the power supply for the touch screen can also be installed inside the switch cabinet. With the controller the different temperature sensors and flow meters of the solar thermal part can be evaluated and the results can be presented at the touch screen and / or it can be observed via the internet. A few settings can additionally be changed via the touch screen. With evaluation of the temperatures, volume flows and the weather sensors of the system, the two pumps and the solenoid valves must be controlled. This can be done with control logics. The programme can be generated at a PC and it can be uploaded onto the Trend controller. This can be done directly with a cable or over the internet. Furthermore an interconnection with the Beckhoff controller inside the WDU is planned with two digital signals on each side. One is for the status and one is in the case of an error. The Trend controller was used in this project, because this kind of controller was already used in the former

Fig. 4.6.: IQview4 touch screen for the on-site monitoring and presentation [Tre11].

Tab. 4.3.: Technical data of the components from Trend [Tre11].

Trend	Weight [g]	Height [mm]	Length [mm]	Width [mm]
IQ3XCITE / 96 100-240	702	263	150	46
Add-on module IQ3XCITE	332	130	150	46
IQ4View touch screen	1160	185	155	40

Endohouse project [Hep08]. The advantage is that existing hardware and knowledge from the old project can be reused in this project and therefore less time is needed for the implementation of new control strategies for the water desalination demonstration plant in Hurghada.
The controller can be operated with 100 V and 240 V at 50 Hz. The maximum demand for the main controller is 46 VA. In contrast to the controller the display must be operated with 24 V. It has a maximum demand of 3 W. For this reason an additional power supply is needed for the operation of the touch screen, because the internal power supply of the Trend controller does not have the power to supply the touch screen self-sufficiently. This power supply is also installed inside the switch cabinet for the Trend controller. All components can be operated in the temperature range between 0 °C and 45 °C with a maximum relative humidity of 90 %. Further technical data can be found in Tab. 4.3. The digital outputs in the add-on module are needed to activate and deactivate the solenoid valves, the signal exchange with the Beckhoff controller, which is responsible for the operation of the WDU, and for the activation of the solar thermal and heat delivery pump in the system. The universal inputs are needed to measure different volume flows, the temperatures in the system and the heat storage tanks and

Fig. 4.7.: GSM router ER75i from the company Lucom [Luc10].

also to evaluate the signals, which are sent from the Beckhoff controller to the Trend controller. Furthermore the status of the pumps can be controlled and in the case of a problem, it can directly be solved with the Trend controller, or the project team can be informed via eMail or other communication channels. With the analogue outputs at the Trend controller, the speed of the pumps and the orientation of the 3-way valve can be adjusted for the best operation.
The Trend controller is connected with the internet via an installed GSM router and therefore the router can be accessed from the internet from all over the world. A picture can be found in Fig. 4.7. Now different process data can be analysed and the control programme can be changed, for example improved from a member by the University in Soest.
A GSM router was used to connect to the internet, because the demonstration plant is installed in the tourism area in Hurghada in Egypt. Normally there is a mobile network available and hence it is an easy and inexpensive opportunity to monitor and control the system via the internet. The GSM router bought is the Lucom ER75i and this component was also bought in Germany and was sent together with the other components from Trend to Egypt.

4.5. Other components

In the following subsection other components of the demonstration plant, which should be installed at the building site in Egypt, are summarised and explained. This includes for example different sensors like volume flow sensors and the weather station. These are important components for an operation of the demonstration plant, but these are not the main components. They are important for the measurement and adjustment of the demonstration plant, but in later realisations they can be exchanged or downsized.

Fig. 4.8.: Typical ultrasound flow meter from Kobold [Kob11].

4.5.1. Volume flow meters

In the solar thermal part of the Sunwater project two volume flow sensors are installed. In Fig. 4.2 they are marked with a rotated *H*. One sensor was planned between the heat storage tanks and the solar thermal roof and the other sensor between the heat storage tanks and the water desalination unit. Both sensors are directly connected with the Trend controller and therefore the data could easily be gathered and evaluated. The volume flow sensors are from the German company Kobold. They were bought in Germany and were transported to Egypt and installed at the building site in Hurghada. The flow meters used are DUK-21G9HL343L and DUK-21G8HL343L. A typical picture of the used ultrasound flow meters can be found in Fig. 4.8. The water enters the flow meter on the left and it leaves it on the right. In the orange box, the electronic for the sensor is located, which is used for the evaluation of measuring heads. On both sides of the brass pipe there are two ultrasound sensors installed. One is at the front and one is at the back, but they are sidewise moved a little bit. Both work as an emitter and receiver. With a delay time calculation the volume flow inside the pipe can be calculated. If the volume flow is zero, both signals have the same running time. With a volume flow through the flow meter the running time of both signals is different, because the sonic velocity is constant in liquids. The two signals are shifted with the fluid and thus there is a time difference between the different signals. The running time in flow direction is therefore shorter than the running time in the counter flow direction. With the delay time calculation the right volume flow can now be calculated. For the project two special high temperature volume flow sensors were bought. This technology is itself very innovative and not state of the art at the moment. These kind of volume flow sensors were made available after a personal enquiry at the company Kobold [Kob11]. During the project life-time they were not regularly available.
They have a maximum working range between −20 °C and 120 °C. This temperature range is high enough, because the water inside the solar thermal part should only be heated up to 95 °C at maximum. It should not be cooked with the solar thermal roof. Further technical data of both sensors can be found in Tab. 4.4.
The sensors are connected with the Trend controller by using a standard L343 electrical connector. It is a 3-wire connector with ground, phase and an output with the analogue

Tab. 4.4.: Technical data of the volume flow sensors from Kobold [Kob10].

Flow meter	Connection [″]	Span [l]	Weight [g]	Height [mm]	Length [mm]	Width [mm]
DUK-21G8HL343L	1 1/2	0.6 - 150	2350	89.5	190	90
DUK-21G9HL343L	2	1 - 250	3800	94.5	238	97

Fig. 4.9.: Temperature sensors and immersion temperature sensors from Trend [Tre11].

measuring signal. The sensors are operated with 24 V and the analogue output signal is in the range between 4 mA and 20 mA, where the first value is the minimum volume flow and the second value is the maximum volume flow of each sensor. The sensors can be externally powered or they can be powered with the Trend controller.

4.5.2. Temperature sensors

For the operation of the demonstration plant and the control of the pumps, different temperature sensors are indispensible. For this project the temperature sensors are from Trend in Germany [Tre11]. An overview of the different temperature sensors can be found in Fig. 4.9. It contains the immersion temperature sensor, which has a nail and the strap-on temperature sensor. The sensors are delivered with a junction box. The installed sensors are NTC temperature sensors with 10 kΩ at 25 °C. The temperature sensors are measured and evaluated with the Trend controller. These sensors are mounted directly on the pipes or inside the heat storage tanks of the solar thermal parts of the system. An overview of the locations of the different temperature sensors can be found

in Fig. 4.2. They are marked with a T. At every interconnection between two elements a temperature sensor is installed. For example one is at the outlet of the heat storage tank and another is at the exit of the solar thermal roof. These sensors are needed to control the solar thermal pump. With the input temperature and the measured solar radiation the volume flow can be controlled in a way that the output temperature is as high as possible, but not higher than 95 °C. Furthermore there are temperature sensors at the outlet of the WDU and at the outlet of the heat storage tanks. These temperature sensors are used to compare the input and the output temperatures of the WDU with each other. This temperature difference is an indicator for the actual energy demand of the WDU. The lower the temperature of the water output, the higher is the actual energy demand of the WDU.
Inside the heat storage tanks there are also temperature sensors installed. In each tank are 3 NTC temperature sensors. All in all there are 6 immersion temperature sensors. They also have 10 kΩ at 25 °C. The immersion sleeve is 465 mm long. One is at the top, one is in the middle and one is at the bottom. These sensors are also evaluated with the Trend controller and each is installed in its own casing, which is embedded in the heat storage tanks. These sensors can also be used to calculate the amount of stored hot water in the two tanks. For this a linear interpolation can be used, because the theory is that hot water is at the top and the lowest temperature is at the bottom. Because of the layering a linear model is possible. Later it can be exchanged with another polynomial or completely different model which may be more suitable for the particular situation. With the linear model and the geometry of the heat storage tanks used the amount of hot water can be calculated. If enough hot water is buffered and the volume flow from the solar thermal roof is high enough, the Trend controller can activate the WDU by sending a wake up signal to the Beckhoff controller, which is responsible for the operation of the WDU. When the WDU is ready for operation, the Trend controller can open the right solenoid valve in Fig. 4.2 and start the heat delivery pump for the hot water. Furthermore the 3-way valve can be adjusted for the best operation of the WDU.

4.5.3. Solenoid valves

Inside the demonstration plant two solenoid valves are planned. The first one is between the solar thermal roof and the heat storage tanks and the other is between the heat storage tanks and the WDU. These positions can be found in Fig. 4.2. One sensor is marked with two red triangles. The valves come from the German company Buschjost and the sensors bought are G043.001408.010.009.010 and G043.001715.010.009.010. The idea behind the left solenoid valves is that the hot water cannot circulate in the system during the night or during times with a low solar radiation. The problem is that the hot water inside the heat storage tanks can climb inside the pipes from the heat storage tanks to the solar thermal roof, because this is the highest point in the solar thermal part. There the water cools down to ambient temperature and then it flows back to the heat storage tanks. Due to this continuous circulation, the energy, which is stored in the

Fig. 4.10.: Solenoid valve from the company Buschjost [Bjo11].

system, is reduced and in addition the stored energy is dissipated to the environment and therefore it is lost. In the next morning the lost energy must be collected again and this takes a lot of time. When this solenoid valve is closed, a circulation can be prevented. This valve is controlled via the Trend controller. Before the pump starts the solenoid valve must be opened and after the pump stops it must be closed.
The other solenoid valve is also used to prevent circulation of hot water through the WDU and furthermore it can be used as a safety device. When the temperature in the system reaches a critical value, this solenoid valve can be closed and then the WDU is protected and it cannot be damaged with the hot water from the solar thermal roof. A typical picture of the bought solenoid valves can be found in Fig. 4.10. In idle position the valve is closed, because the membrane is force pilot operated. The included solenoid opens the membrane itself or with the help of the pressure of the flow medium. For the operation a pressure difference Δp is not necessary. The operation temperature of the solenoid valve is between $-10\,°C$ and $130\,°C$ with a maximum ambient temperature of $35\,°C$. Both valves are made of brass and they are operated with $24\,V$. Further technical data can be found in Tab. 4.5.

Tab. 4.5.: Technical data for the solenoid valves from the company Buschjost [Mag10].

Solenoid valve	Pressure range [bar]	Connection [″]	Seat ⌀ [mm]
G043.001408.010.009.010	0 – 3	1 1/2	40
G043.001715.010.009.010	0 – 2	2	50

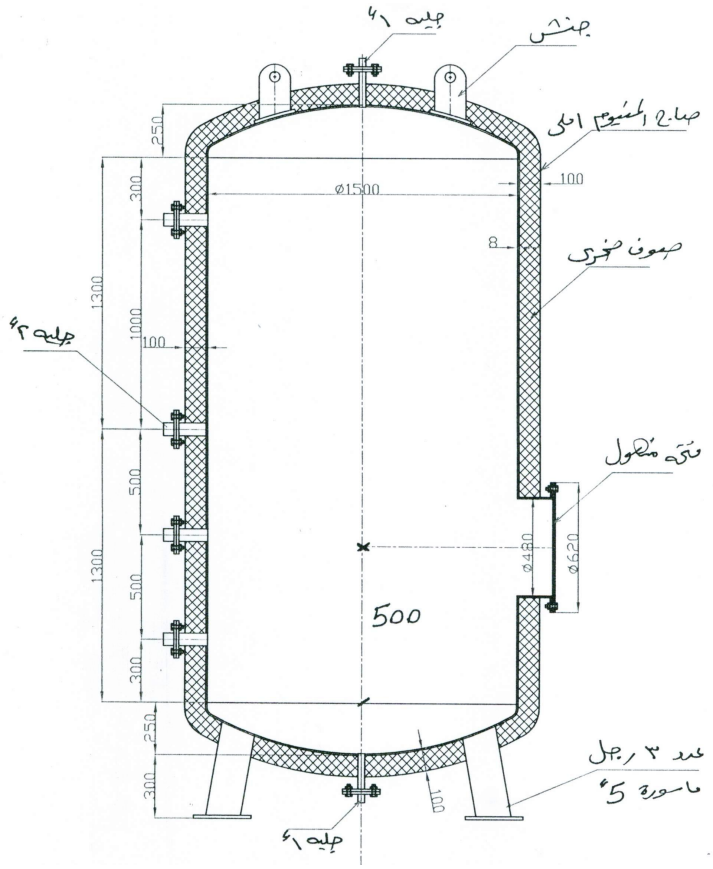

Fig. 4.11.: Heat storage tank used for the Sunwater project in Egypt [Sol10].

4.5.4. Heat storage tank

As a heat buffer in the solar thermal part of the system, two heat storages are considered. A technical drawing can be found in Fig. 4.11. The size of the cylindrical heat storage tank is 3600 mm with an inner diameter of 1500 mm and an outer diameter of 1700 mm. The material is epoxy coated steel. The volume of the heat storage tank is 5 m^3. For a good heat insulation the thickness of the insulation is 100 mm and it is made of rock wool. The tank has several circuit points for water sampling and water intake. One is at the top and one is at the bottom. Furthermore there are circuit points at the side and a maintenance access on the other side. The 2 heat storage tanks are installed edgewise on legs. For monitoring three immersion temperature sensors are installed in each tank, which are not shown in this Figure. One is installed at the upper third, one in the middle and one in the lower third. For each installation a hole is drilled and then a immersion sleeve for the temperature sensor is inserted and fixed. Furthermore there was the idea to include a level meter at the top of the heat storage tank, which is also not shown in Fig. 4.11. For the Sunwater project two 5 m^3 heat storage tanks are installed outside the building with the WDU. Two tanks are installed, because there had been inconsistent information on the expected volume flows from the solar thermal roof. The range of the

volume flows at the temperature of 90 °C varies from a few litres per hour to several litres per hour. No exact data were available during the planning of the demonstration plant.
The tanks have more than one justification. During the morning they should store the hot water, which comes from the solar thermal roof, because the volume flow is not high enough to supply the water desalination unit. Therefore this water is stored or better buffered in the heat storage tanks for later usage. It makes no sense to start the solar thermal pump only in the case, when enough hot water can be produced. Otherwise the water would boil in the collectors, when the volume flow stops. The hot process water produced during the morning is therefore buffered in these tanks. Later during the day the collectors should produce more hot water than the WDU needs for operation. The surplus energy is also stored in the tanks. The stored water can be used to operate the WDU in this demonstration plant in the afternoon, in the evening and maybe through a few hours during the night. An overview of the theoretical hot water output of the solar collectors can be found in Fig. 4.3. The working time depends considerably on the sunshine duration and other weather conditions of the actual day.
As can be seen in Fig. 4.11 the tanks have a lot of different circuit points. For the operation of the STR the circuit points at the top and at the bottom are very interesting. At the top the hot water, which comes from the solar roof, enters the heat storage tanks. It enters it at the top, because hot water has a lower density compared to colder water. If the hot water would enter the heat storage tanks at the bottom, it would rise to the top. Due to the rise of the hot water, turbulences are generated inside the tanks and therefore no layering can be established in the system. The hot water is otherwise mixed up with the colder water. Due to the high water intake a layering in the heat storage tank is possible. This is justified, because the cold water outlet is at the bottom of the heat storage tanks. The water level drops during the operation of the STR, but it is filled with hot water, which comes from the solar thermal roof. Another advantage of this concept is, that the turbulences between the inlet and outlet can be avoided, because the distance is as large as possible. The hot water for the desalination is taken from the top of the heat storage tank. The returning water from the WDU enters the heat storage tanks at the bottom. It should enter the tank as low as possible. It makes no sense that the hot water in the heat storage tanks have a separate water outlet for the WDU and that the returning water enters the tank in the middle, because it can happen that the cold water leaves the tank immediately via the hot water outlet of the WDU and thus the water will not be heated up in the collectors. An own circuit between the heat storage tank and the WDU is possible with the effect that the WDU cannot be operated, because the temperature drops below the needed operation temperature. In addition another unwanted separate circuit can be generated between the STR and the heat storage tanks. In this case the hot water enters the tanks at the top and leaves it at the bottom to be heated again. Therefore the maximum passable temperature in this circuit can be reached and in an extreme case the system, in particular different sensors, can be damaged. Both circuits are not teethed and thus the system cannot be used to produce freshwater.

4.5.5. Pump, inverter and 3-way valve

As can be seen in Fig. 4.2 there are two pumps in the solar thermal part of the system. One pump is used for the solar thermal roof and the other pump is used for the heat delivery to the WDU. Both pumps are controlled via inverters and the inverters are connected to the Trend controller. It evaluates the measuring results from different sensors. These are for example the temperature sensors, the volume flow sensors and the weather sensors. The weather sensors are summarised in the next subsection.
In this case pumps from Grundfos and inverters from LG were used, because they are low priced and directly available in Egypt. For this feasibility study these pumps are sufficient. In later realisations other pumps with a better control methodology can be installed, but in the most cases they are more expensive. It could also be interesting to operate the solar thermal roof with higher temperatures and higher pressures and then better pumps are required.
The pump for the solar thermal roof is adjusted in a way that the output temperature is as high as possible, but not higher than 95 °C. Otherwise the system can be damaged, because of excessive temperature and overpressure. During the night the solar thermal pump is shut down, because it makes no sense to pump the stored hot water through the collectors. The hot water would be cooled down and this is counterproductive to the complete concept of the desalination plant. Collected energy during the whole day would be wasted during the night. In the morning, when enough solar radiation is available, the pump must be started with the minimum transport capacity to prevent overheating in the collectors. When the solar radiation raises the volume flow must be adjusted with the solar pump in a way, that the maximum temperature of 95 °C is not exceeded. In the afternoon and during a low solar radiation the pump speed must be reduced to hold the temperature of the fluid at a desired working temperature of the WDU.
In contrast to the solar pump the other heat deliver pump must be activated, when enough hot water is available in the system. The WDU needs a constant volume flow of less than $5\,m^3/h$. The volume flow can also be adjusted with the inverter for the pump by evaluating the volume flow sensor with the Trend controller. The volume flow may change slightly, when the volume flow of the solar pump varies during the day, because the pressure in the system changes during the different operation states. This can for example be compensated by controlling the heat delivery pump to the needed constant volume flow. Furthermore different temperatures of the fluid can also be responsible for changes in the volume flows.
The two pumps come from Grundfos and they were bought in Egypt and were installed at the building site by an Egyptian project partner. A typical picture can be found in Fig. 4.12. For the heat delivery and the solar roof pump the UPS 32-120 F are considered. The operation temperature range of the liquid is between −10 °C and 120 °C with an ambient temperature working range between 0 °C and 40 °C. The maximum operation pressure is 10 bar and the maximum power demand of this 3-phase pump (400 V − 415 V) is 400 W at a frequency of 50 Hz. The energy label of the pump is *C*. Further data can be found in Tab. 4.6.

Fig. 4.12.: Utilised pump UPS 32-120 F from the company Grundfos for heat delivery and solar collectors [Gru11].

Tab. 4.6.: Technical data of the Grundfos pump UPS 32-120 F [Gru10]

pump	net weight [g]	height [mm]	length [mm]	width [mm]
UPS 120-32 F	17300	324	220	245

The inverters for the pumps are from LG Industrial Systems and were bought in Egypt. They were also installed by an Egyptian partner at the building site in Hurghada. The inverters used are from the iG5 series. The 3-way valve, which can be found on the right in Fig. 4.2, was bought from the water desalination unit manufacturer in Germany and was installed in Egypt by an Egyptian partner. The idea is that energy delivery to the WDU can be controlled to some extent. If less energy is needed for the operation of the WDU, part of the returning water, which flows back to the heat storage tanks, can be mixed up with the volume flow, which comes from the heat storage tanks. Therefore the water input temperature of the WDU can be reduced and thus the output temperature of the WDU is adjustable. Furthermore the 3-way valve can be used as a security installation. When the incoming water is too hot for the operation, the incoming water can be cooled down to the right operation temperature and thus the external heat exchanger of the water desalination unit is not in danger.

4.5.6. Weather station

For the measuring of the weather data, different weather sensors from the German company Toss were bought and transported to Egypt. The weather sensors are an ultrasonic wind sensor for measuring the wind direction and wind speed, an air pressure sensor,

(a) (b)

Fig. 4.13.: a) Wind direction and wind speed sensors. b) Solar radiation sensor from the German company Toss [Tos11].

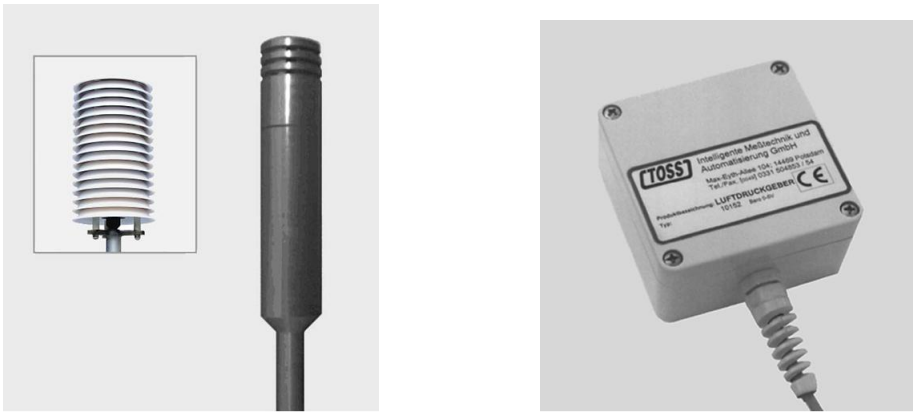

(a) (b)

Fig. 4.14.: a) Air temperature and relative humidity sensors. b) Air pressure sensor from the German company Toss [Tos11].

a global solar radiation sensor, a temperature sensor and a humidity sensor. The wind speed, wind direction and the solar radiation sensors can be found in Fig. 4.13a and Fig. 4.13b. The innovation of the wind sensor is that no movable parts are used to measure the wind direction and wind speed like in other standard wind speed and wind direction meters. Therefore this sensor has a long life time and is not prone to damage. The values are also calculated based on a delay time calculation of the ultrasonic signals from the North to the South and from the West to the East. Its functionality is similar to the ultrasonic flow meters in subsection 4.5.1. A picture of the ambient temperature sensor, the relative humidity sensor and the air pressure sensor can be found in Fig. 4.14a and Fig. 4.14b. The ambient temperature and relative humidity sensors are combined and protected from the Sun with a radiation protection.
All sensors are installed outside the building and are connected with the Trend controller for evaluation. With the evaluation of the different sensors the weather conditions of the

building site can be collected. For the calculation of the water output temperature of the STR, it is important to know the actual solar radiation, the ambient temperature, the wind direction and the wind speed. All conditions influence the output temperature of the water from the solar thermal roof and in addition the ambient temperature is responsible for the decrease of the temperature of the stored water in the heat storage tanks and the pipes. The hotter the ambient temperature, the slighter the temperature decrease in the heat storage tanks and the pipes. The higher the actual solar radiation, the higher the possible output temperature of the fluid from the solar collectors. Furthermore the output temperature depends of course on the wind speed and the ambient temperature. The higher the wind speed and the lower the ambient temperature, the lower the expected water output temperature of the collectors.
All sensors can be evaluated with the Trend controller, because the sensors have a current output in the range between 4 mA and 20 mA with an operation voltage in the range between 15 V and 30 V. The spectral range for the solar radiation sensor is between 350 nm and 1100 nm (at 10 % of S_{max}) with a maximum sensitivity at 850 nm. The settling time for the solar radiation sensor is smaller than 1 min. Further technical data can be found in Tab. 4.7.

Tab. 4.7.: Technical data of the weather sensors from the company Toss in Germany [Tos10].

Weather sensor	Measuring range	Error	Temperature working range
Wind direction	0° ... 360°	1°	−35 °C ... 70 °C
Wind speed	0 m/s ... 60 m/s	0.01 m/s	−35 °C ... 70 °C
Solar radiation	0 W/m^2 ... 1200 W/m^2	1 %	−25 °C ... 70 °C
Air pressure	900 hPa ... 1100 hPa	1 hPa	−20 °C ... 50 °C
Air temperature	−40 °C ... 60 °C	0.3 °C	−40 °C ... 60 °C
Rel. humidity	0 % ... 100 %	3 %	−40 °C ... 60 °C

5. Realisation of the demonstration plant

In the following chapter the realisation of the demonstration plant in Egypt is discussed. It starts with the description of the location and the weather conditions at the building site. Then the local installation of different components is presented and explained in detail. Finally the realised control strategy of the solar thermal part is explained. A short overview of all components are also shown, which were finally planned and installed at the building site. This author searched for most components and was directly involved in the tender procedures.

5.1. Location of the demonstration plant

The location of the building site in Egypt can be found in Fig. 5.1. Egypt is located at the Mediterranean Sea and has the neighbouring states Libya in the West, Sudan in the South and Israel and Saudi Arabia in the East. The country is split along the Nile into two parts. In the West is the Libyan Desert and in the East is the Arabian Desert.

Fig. 5.1.: Location of the demonstration plant in Egypt. Hurghada is at the Red Sea and is marked here with an *A* [Goo11].

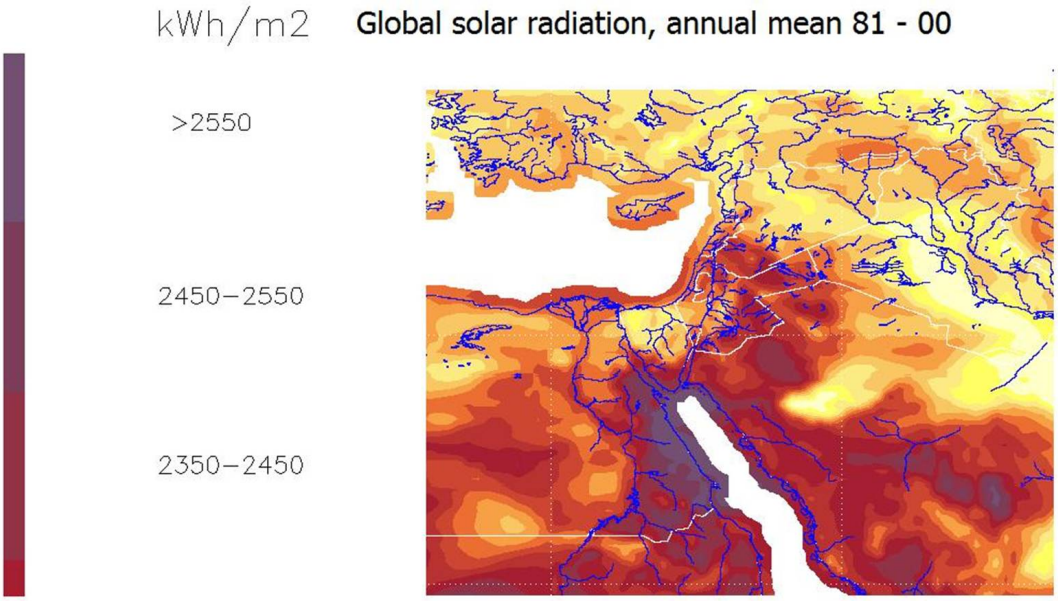

Fig. 5.2.: Global solar radiation in Hurghada, annual mean 1981 - 2000 [Met07]

The Nile and the Nile River delta are the lifeline of this country. Most of the 83 million people live in these areas. The location of the demonstration plant is in Hurghada, it is on the left coast of the Red Sea, which can be found in the middle of Fig. 5.1. The town is marked with an *A*.
The decision for the location of the Sunwater demonstration plant was carefully made. The requirements were that there is a relative high daily solar radiation at the building site during the whole year, because it makes no sense, if only on a few days during the year there is a relatively high value and on the other days there is just a low amount of solar radiation. This could for example happen, when there are a lot of clouds on the sky or maybe dusts or sandstorms. Additionally the ambient temperature should be high enough to operate the desalination unit. The access of the demonstration plant for the Sunwater project members and the financial possibilities are also an important reason. Furthermore the availability of saltwater is a very important aspect for the operation of the desalination unit.
At the building site in Hurghada there is a very high daily solar radiation. The annual mean of the global solar radiation is higher than 2550 kW h/m^2, as can be seen in Fig. 5.2. The areas with a very high daily solar radiation are coloured in violet and areas with a solar radiation between 2450 kW h/m^2 and 2550 kW h/m^2 are coloured in dark red. On the west side of the Red Sea it is violet coloured. Therefore this location is predestined for a realisation of the demonstration plant. An Egyptian project partner has additional good contacts to different local companies and a residential hotel chain and thus there was the possibility to install the solar desalination demonstration plant in and next to a building with an existing RO system. This has the advantages for the project, that the existing saltwater supply and the freshwater and brine disposal can be included in the project. In the already installed RO system the saltwater comes from a saltwater

well and the brine is depolluted into another well. This must be done in this way due to governmental regulations. The usage of the existing infrastructures reduces the costs for the Sunwater project. Without this preparation it would not have been possible to realise this innovative project and to stay additional within the project budget.
The freshwater is transferred to the hotel and there it can be used by the tourists or employees. The associated hotel has 400 rooms. The total daily amount of the desalinated water is 400 m^3 and for the next years is the idea to extend the daily amount by 200 m^3. 600 m^3 are enough to supply the complete hotel and all extensions with needed freshwater. The needed saltwater comes from the Red Sea and at the moment it is converted with the installed reverse osmosis system.
The Sunwater components were installed at the roof and close to the building with the RO system. In the building a power supply with 380 V and 220 V with 50 Hz is available for the operation of the WDU, the controllers and all other components. Compared to the daily freshwater demand, the new system only produces a few percent freshwater a day. In case that there is a problem with the new system, the freshwater supply can be covered with the existing osmosis system as it was done before. The new system is just an add-on and a feasible study to show the possibility to produce freshwater which relies on solar energy.
The roof of the building with the existing RO system is used for the solar collectors. It is only 40 m × 40 m. Furthermore there is the possibility to extend the solar thermal area to an additional 40 m × 40 m, which is at the roof of an existing freshwater storage tank. The freshwater storage tank is 12 m away from the building. For the installation of the WDU inside this building, there is only the space of 4.5 m × 3 m, but an extension to 4.5 m × 3.7 m is possible. Additionally there are two smaller unused freshwater storage tanks close to the building [Ami09, Bus09b].

5.1.1. Weather data of the building site

During the preparation phase and in the first months of this project, different already available weather data were collected to create a data base for the project and the simulations. The weather data are needed for calculation of the possible volume flows, to design the complete desalination plant and to get a feeling for the options to realise the demonstration plant. Important are data like daily solar radiation, the expected sunshine duration during the whole year and the ambient temperature. Therefore different sources were tapped to get the needed information. A few data came from the Egyptian partners or directly from the Internet. Other information were bought from a weather institute, because the information had not been available online, which was checked in a large number of different documents. A summary of this data can be found in Tab. C.2. The needed data set was bought from the Meteo Group for every first day of every second month in 2009. The data bought can be found in Tab. C.3 until Tab. C.8. The most data are measured which are shown in these tables. Only the hourly solar radiation values in kW/m^2 were calculated. All values are tabulated hourly from zero o'clock until 23 o'clock for 6 different days in 2009. Due to the situation, that the solar radiation is

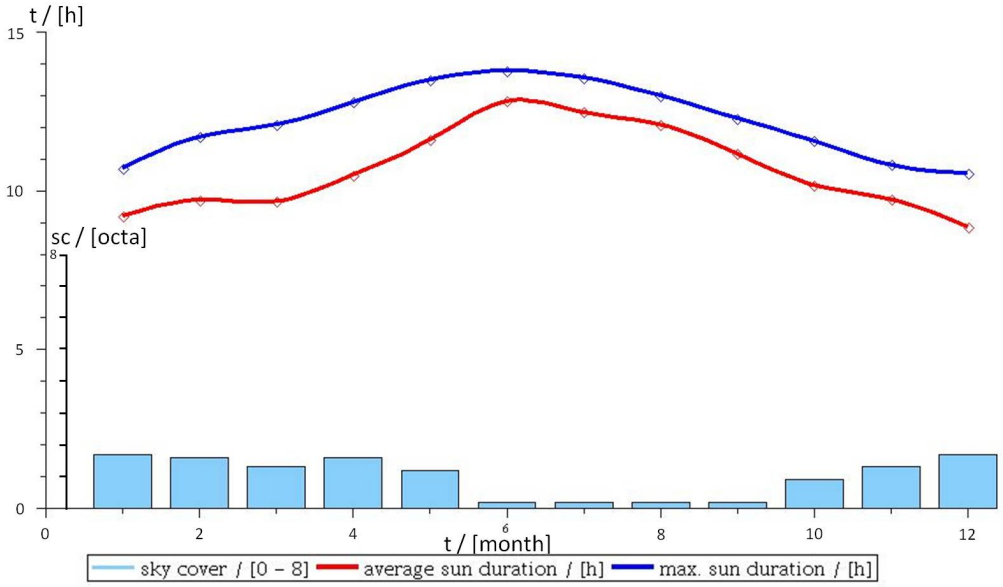

Fig. 5.3.: Maximum and average sun duration and sky cover in Hurghada during the year [Ami09, Aeg11], where 0 reflects that there are no clouds on the sky.

calculated it must be proved with the simulated and measured data during the project life-time.
As can be seen in Fig. 5.3 the yearly average sun duration in a day is between 8.85 h and 12.81 h. At the beginning and at the end of the year the sun duration is shorter than in the summer and this is a indication that Hurghada is located in the northern hemisphere. The possible sun duration in the whole year is between 10.54 h and 13.77 h. The difference between these two values is for example based on clouds. In the winter time it is most cloudy. In Germany there is sometimes only a mean value of less than 4 h per day [Dwd11]. At the beginning of the year and at the end of the year there are more clouds in the sky compared to midsummer. This can also be seen in Fig. 5.3. If there are more clouds in the sky, there is a higher difference between the average and maximum sun duration compared to times with less clouds. At the beginning of the year the coverage is less than $^{2}/_{8}$, but in the midsummer the coverage is close to zero. As can be seen in Tab. C.2 the mean cloud coverage in a month is not higher than $^{1.7}/_{8}$, where $^{0}/_{8}$ is no clouds and $^{8}/_{8}$ is completely covered. An octa is in meteorology an unit of measurement used to describe the amount of cloud cover at a given location. With this long sunshine duration, low cloud coverages and the high solar radiation during the whole year, Hurghada is predestined for solar thermal and photovoltaic installations. In other countries, for example in Germany, it is completely different.
Fig. 5.4 shows the air and the water temperatures in Hurghada during the whole year. The minimum air temperature with only 9.7 °C is in the winter and the minimum air temperature in the summer is 25.2 °C. These are the minimum temperatures during the night, when the environment has cooled down. The maximum daily temperature in the winter is 21 °C and in the summer 33.3 °C. During the year the water temperature of

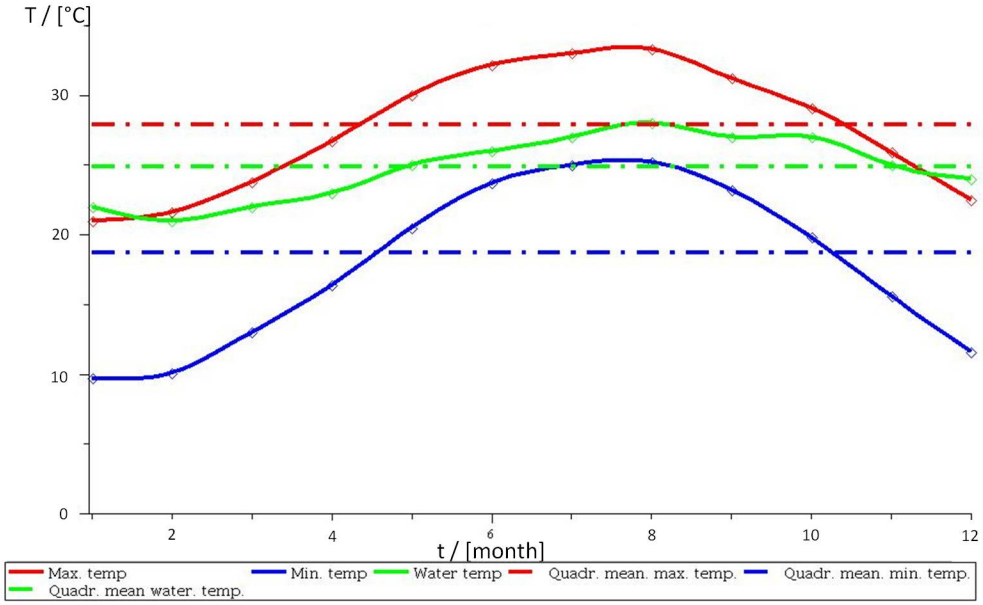

Fig. 5.4.: Air and seawater temperatures in Hurghada during the year [Ami09, Aeg11].

the Red Sea varies in the range between 21 °C in the winter and 28 °C in the summer. Furthermore Fig. 5.4 shows the quadratic mean of the maximum temperature $T_{\max}$, the minimum temperature $T_{\min}$ and the seawater temperature T_{sw}. During the whole year the behaviour of the air temperature in the night and the day are the same. At the beginning and at the end of the year, there are the lowest temperatures and in the summer there are the highest temperatures, as it is normally expected in the northern hemisphere. The curve progression of the water is slightly different. At the beginning of the year the water temperature has its lowest value. Until the summer the temperature increases continuously. This curve progression is similar to the air temperature. In July and August the highest temperatures are reached. Later in the course of the year the water temperature drops, but it does not drop as fast as the maximum daily ambient temperature. At the end of the year the water temperature is higher than the maximum ambient temperature. This could be effected by the high heat capacity of the saltwater in the Red Sea. Due to different temperatures the wind direction varies during the day and the night. During the day there is normally sea breeze (onshore wind) and during the night land breeze (offshore wind), but at the end of the year, when the water temperature is always higher than the ambient temperature, the wind could blow the whole day from the land to the sea (land breeze). Furthermore the quadratic mean of the water temperature is also included in this figure. The mean water temperature is closer to the maximum ambient temperature than to the minimum ambient temperature. It reflects the high heat capacity of the saltwater and the long sunshine duration on every day. In Egypt the day splits in mean into 12 h night and 12 h day.
Fig. 5.5 shows other local weather data of Hurghada. The global solar radiation in Hurghada is between 3.91 kW h/(m^2 d) and 8.27 kW h/(m^2 d). During the year the mean

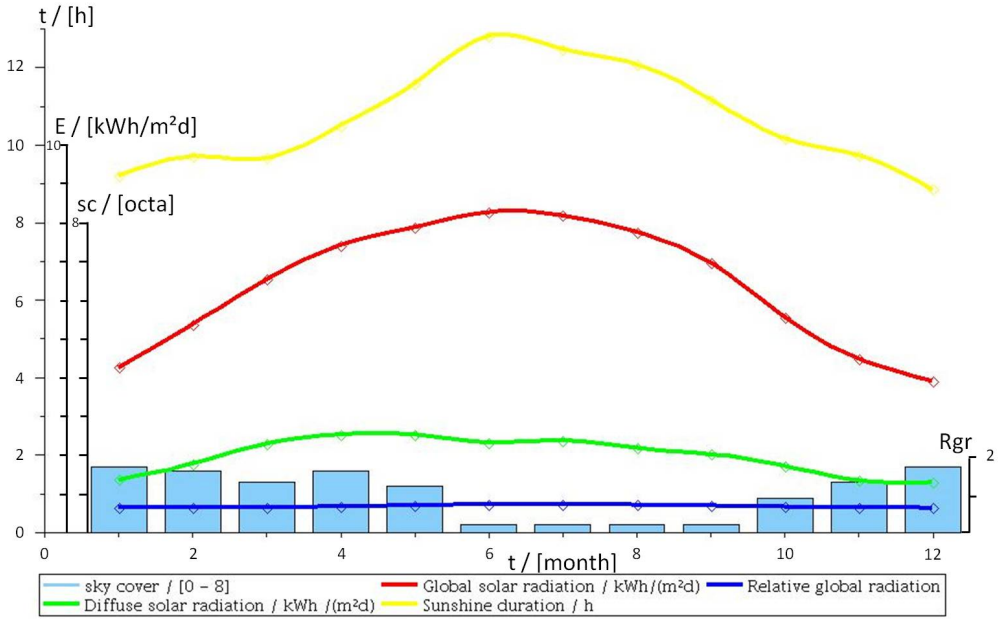

Fig. 5.5.: Solar radiation and sunshine duration in Hurghada throughout the year [Ami09, Aeg11].

value is 6.38 kW h/(m² d). Again it can be seen in Fig. 5.5, that in the beginning of the year and the end of the year there are more clouds in the sky. During the summer there are less clouds and this has a direct effect on the solar radiation, but this is just one aspect. Further dependencies are presented in section 3.1. At the beginning of the year the solar radiation is lower than in the summer. The measured global and diffuse solar radiation increases in the first half of the year and decreases in the second half of the year. Diffuse solar radiation is the radiation which reaches the surface of the earth after it was scattered from e. g. molecules in the atmosphere. The maximum diffuse solar radiation is reached in April and May with 2.52 kW h/(m² d). The lowest value is reached in December with 1.29 kW h/(m² d) and the mean value is 1.97 kW h/(m² d). As can be seen the diffuse solar radiation and the global solar radiation have a similar curve progression, but the diffuse solar radiation does not increase as much as the global solar radiation. Additionally it can be seen, that the clouds have a direct effect on the amount of the diffuse solar radiation. When there are less or no clouds on the sky, there is a small drop in the measuring curve. Furthermore the relative global radiation (the clearness index) G/G_0 is also shown in this figure, where G is the global solar radiation and G_0 is the possible extra-terrestrial global solar radiation. The value of this ratio is relatively constant during the whole year and compares the maximum extraterrestrial solar radiation value with the value which can be harvested at the Earth's surface. The minimum value is 0.63 and the maximum value is 0.72. This shown measurements are just a few arguments in favour for the usage of Hurghada as the location for the Sunwater building site. With this high solar radiation and the long sunny days over the whole year, the final decision was to install the water desalination unit with the associated solar thermal roof close to the Red Sea.

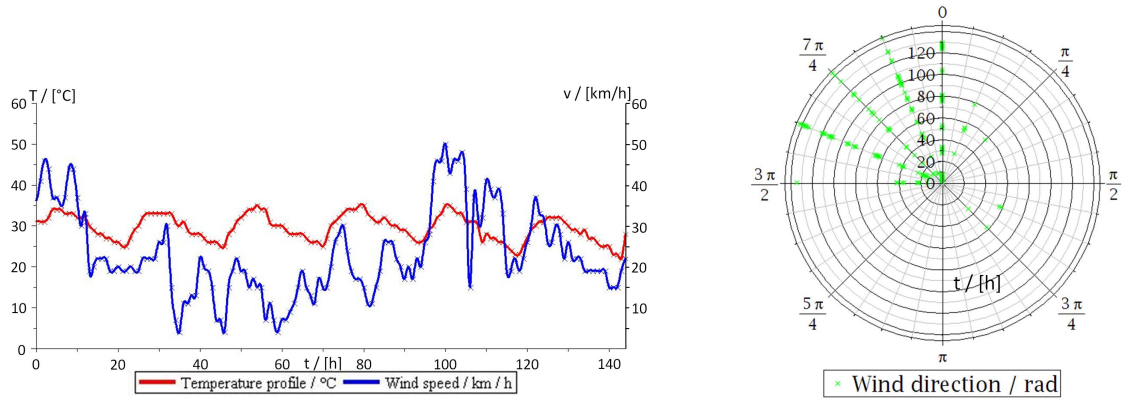

(a) (b)

Fig. 5.6.: a) Hourly temperature and wind profile for Hurghada. b) Radial wind direction for Hurghada [Wet09].

Fig. 5.6a shows the temperature and wind profile in Hurghada between 19.09.09, 9:00 until 25.09.09, 8:00 [Wet09]. The temperature varies on those days between 20 °C in the night and up to 35 °C during the day. As can be seen in this figure the temperature has a consistent behaviour. During the morning the temperature rises until its maximum value is reached. Afterwards the curve drops. It is very interesting that the temperature rises more faster and drops slower during the afternoon and the night. In the morning the minimum temperature is reached and the maximum temperature is reached in the early afternoon. Furthermore it can be seen in this figure that the wind speeds differ during the different days. In contrast to the ambient temperature no consistent behaviour is visible. The minimum wind speed is below 5 km/h and the maximum is around 30 km/h. Fig 5.6b shows a radial plot of the wind directions on the same days. It is plotted in that way, that 0 rad is the North and π rad is the South. The radial direction is the time axis. At the point of origin is the start point of the measurements and points with a bigger distance to the centre were measured later. The main wind direction on these days is between West and North. During a long period of almost one year, for more than 80 % the wind had a direction between West and North. Other directions are insignificant, because the relative frequencies are below 3 %.
The daily solar radiation spanning almost an entire year is shown in Fig. 5.7. It starts at the beginning and it ends at the end of the same year. During this time for every first day of every second month the measured daily solar radiation was bought from [Met09] and the data were plotted into this graph. On the x-axis the day of the year can be found, on the y-axis is the time in hours and on the z-axis the solar radiation in W/m^2 can be found. For a better overview the different points are connected with cubic splines. As can be seen in this figure, at the beginning of the year and at the end of the year there is a relatively low solar radiation in Hurghada. During the other times the radiation is much higher. The maximum is up to 1046 W/m^2 and this value should be high enough for an operation of the water desalination unit. The times of the sunrise and the sunset

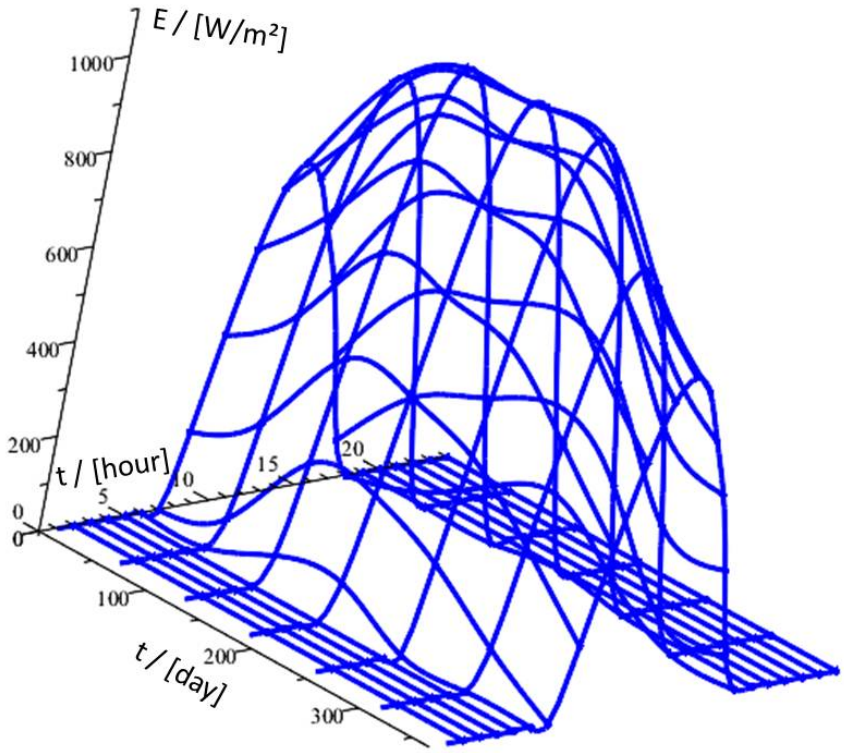

Fig. 5.7.: Solar radiation in Hurghada for selected days in the year 2009. The highest value is above 1000 W/m^2 [Met09].

vary slightly during the whole year. It is very interesting that in the middle of the year a solar radiation drop can be found. It is similar to the simulation, which can be seen during a continuous simulation of the solar radiation, which was explained in section 3.1.

5.2. Local installation

In the following section the installation of the demonstration plant at the building site is discussed. An overview of all components, which are installed in Egypt, is shown in Fig. 5.8. It summarises all components, which are necessary for the operation of this demonstration plant. These are for example the heat storage tanks, different temperature and volume flow sensors, control units, pumps and the module for the connection with the internet. Furthermore the amount of the components can be seen and where and how they are connected.
As was mentioned before the installation was done by the Egyptian partner, only the WDU was installed by the German project partner. The Egyptian partner received

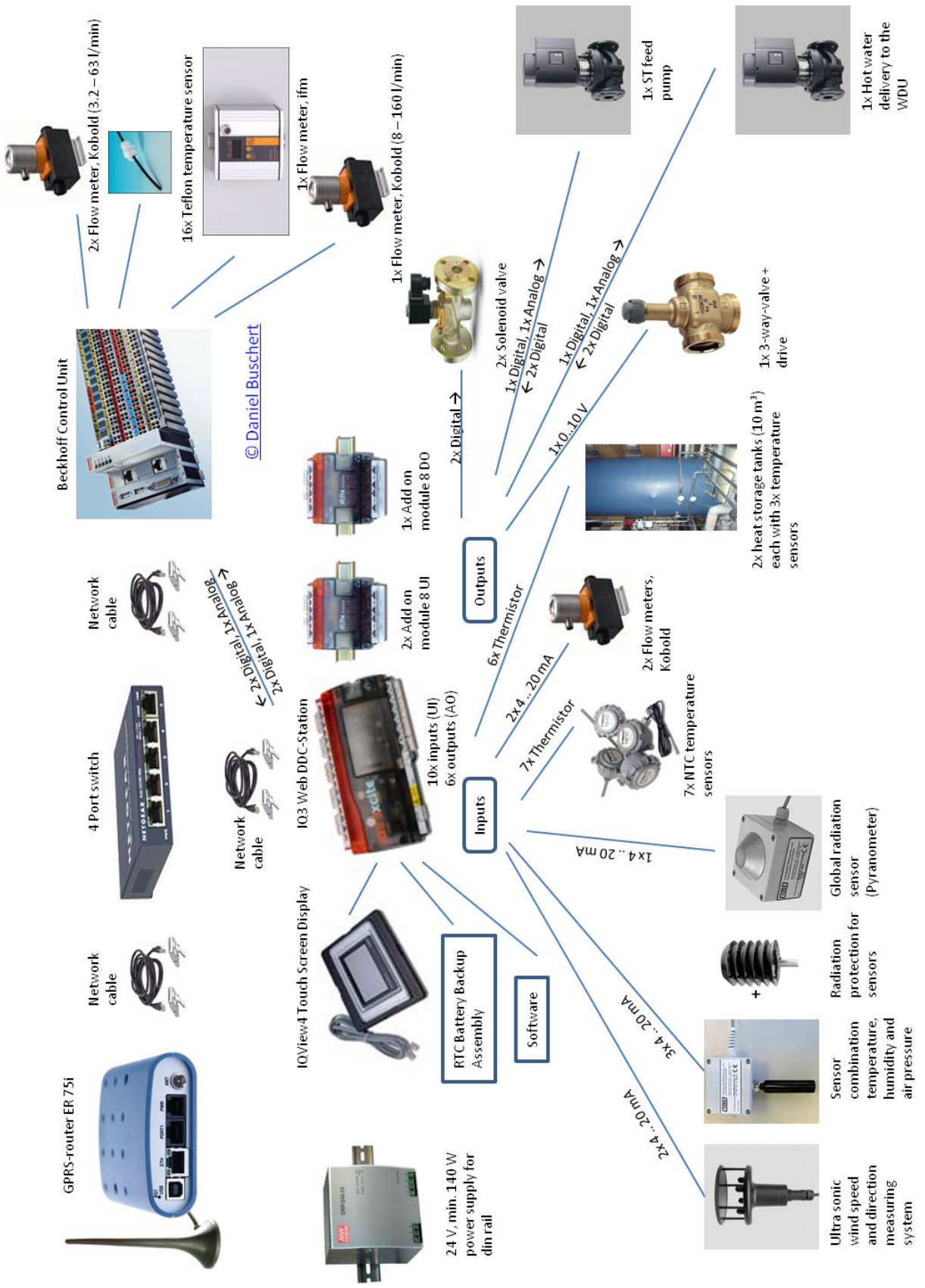

Fig. 5.8.: Overview of the components used for Sunwater which should be installed at the building site in Egypt.

Fig. 5.9.: Building site of the demonstration plant with two Sunwater heat storage tanks.

detailed installation information from the other project partners in Germany. The instructions were given in detail, but the Egyptian partners were not able to follow these specification and installed a few of the components in a different way. Due to this a few problems prose during the running of the demonstration plant. These problems will be discussed during the evaluation of the demonstration plant in a later chapter. In this section only the installation is described. Fig. 5.9 shows a photo of the building site. Close to the building with the existing reverse osmosis water desalination unit two large heat storage tanks were installed. They are installed on a white painted concrete foundation and they are connected with different pipes, which come from the solar thermal roof or from the project's water desalination unit. One pipe is connected close to the top of the heat storage tanks, another one is installed a little bit lower, the third pipe is also installed in the middle of the heat storage tanks. The fourth and final pipe is installed at the bottom. In each heat storage tank there are also three immersion temperature sensors which can be found on the left side of each heat storage tank. They are directly connected with the Trend controller, which is installed in a switch cabinet inside the building on the right. The red jar in the background is an equalising tank and furthermore a few overpressure valves were installed in the solar thermal system. The Egyptian team did not felt that these components were so important at the beginning, but later they have installed these components. After the initialisation of the complete demonstration plant, it was seen, that there was a pressure increase in the system, while the temperature increases and therefore the equalising tank and the over pressure valves were installed.

Fig. 5.10.: Installation of the vacuum tube collectors at the roof of the building. In the background at the left is the weather station.

The water desalination unit was installed inside the building. Furthermore inside the building, there can be found the saltwater and freshwater buffer tanks for the WDU. The pumps and inverters, which control the volume flows for the solar thermal roof and the heat delivery source of the WDU, are installed at the outer wall of the building. The inverters are also installed in an additional switch cabinet. The volume flow sensors, which were planned in Soest, are also installed at this outer wall, but the planned and ordered solenoid valves were not installed. The Egyptian team did not recognise the importance of this components. All pipes have cut-off valves for security, later modifications and reparations. From this position two pipes go to the roof of this building, because the vacuum tube collectors were installed there.
A picture of the solar thermal roof can be found in Fig. 5.10. They have been installed on a white tiled ground. The setting angle in this installation is negligible, because they are directly installed on the ground. Only a small setting angle is visible. This relevance was explained in section 2.4, because an installation angle is necessary for the operation of the vacuum tube collectors. For a better performance of the collectors the angle should be a little bit larger. It should be based on the curve progression of the Sun at noon. If the angle is larger the solar radiation during the noon time is perpendicular on the solar collectors. In this case the rate of yield is better. The best angle depends on the orbit of the Sun. If more hot water is needed in the winter the installation angle must be different compared to the situation that more hot water is needed in the summer. This dependency on the orbit of the Sun can be seen in section 3.1. As can be seen in Fig. 5.10 the highest point of the solar collectors is in the middle between both rows.

(a) (b)

Fig. 5.11.: a) Weather station with different sensors at the roof. b) Switch cabinet with the Trend controller and the touch screen in the building.

An exclusion zone is in the back on the left. At this point the hot process water rises to the highest point and there it cannot be extracted. The produced energy in this part of the collector is lost. The collectors are installed in a way that the water flow has always the same distance to bridge. If the distance is different the output temperatures differ from collector to collector. In the worst case part of the water is boiling and another part of the water could have a temperature below 80 °C and this is not desirable for the operation of the WDU. It can also be seen in this figure, that one pipe comes from the front and ends at the last row. The other pipe starts at the first row and goes to the background and then it comes back on the left outside of the left collector column. The vacuum tube collectors are connected to this two pipes. In one pipe is the cold water from the heat storage tanks and in the other pipe is the hot water, which goes back to those tanks. This pipe layout was implemented by the Egyptian. It was mentioned, that the pipe lengths between the collectors and the heat storage tanks must be the same. Without this important information the Egyptians would have had installed the collectors in a different way.
The back left in Fig. 5.10 shows the installed weather station. A closer picture can be found in Fig. 5.11a. At the top the wind sensor is installed, which measures the wind direction and the wind speed on ultrasonic base. The wind speed and direction is calculated with a delay time calculation. On the right side there is the solar radiation sensor. On the left in the two housings the temperature, the relative humidity and the air pressure sensors are installed. An overview and more details of these sensors can be found in subsection 4.5.6. All components are also connected with the Trend controller, which is inside the building. A picture of the installed Trend controller can be found in Fig. 5.11b. The Trend controller with just two add-on modules are at the top. The third module is on the second din-rail. Inside the door the touch screen for monitoring is implemented. Furthermore a power supply is also included in the switch cabinet, it is for example necessary for the touch screen. On the right there are a few safety devices. Close to the switch cabinet and also inside the building, the used water desalination unit was installed.

5.3. Control strategy of the demonstration plant

The control strategy of the whole demonstration plant was implemented by the Egyptian partners in cooperation with a person from the SWU, but it was implemented in another way, than it was planned by this author before. In contrast to measuring the actual solar radiation and the input and output temperatures of the collectors, the middle temperatures in the heat storage tanks were considered for the control of this pump. An already planned safety switching was included into the programme for the solar thermal roof. The first safety aspect was that the solar thermal pump starts, when a special limit of the solar radiation is reached. Another aspect was, that the pump switches into an emergency mode, if the temperature at the output of the solar thermal roof reaches a temperature level higher than a special limit, for example higher than 93 °C. In this emergency mode the volume flow of the pump was increased to its maximum value. The argument is to stop heating and to start cooling the water inside the solar thermal roof. If it reaches higher temperatures than considered during the planning, the water starts boiling and the solar collectors or the sensors could be damaged. In this demonstration plant the water temperature in the external heat exchanger of the WDU must be below a certain value, otherwise it could be damaged. One volume flow sensor was for example damaged during the operation, due to the fact, that the water temperature reaches an excessive value. The sensor was sent back to Germany and then to the manufacturing company. There it was repaired and was once again sent back to Egypt. Finally it was once again included into the demonstration plant.
During the planning stage a data interchange between the Trend controller and the Beckhoff controller was considered with 2 digital signals each. One to show the readiness and the other signal was the emergency signal for both controllers. This data exchange was discussed and approved during one meeting in Kiel. Later merely one signal per controller was implemented into the final system. The other signal was neglected. Only with this single signal the two controllers must be harmonised.
Due to the fact, that the solenoid valves were not installed in the system, the associated control signal was not included into the control routine of the demonstration plan. Due to the fact that the solenoid valves were not installed there was a very high temperature drop in the system during the night. It can be seen in section 7.5. Warm water rose in the system and during the night it was cooled down in the solar collectors. This could have been prevented, if the solenoid valves had been installed at the building site in Egypt.
These were the serious changes in the implementation of the demonstration plant. The solar thermal pumps were still controlled by the Trend controller and the other sensors were also evaluated by it. Additionally a few minor changes were made in the control structure to optimise the solar thermal part of the demonstration plant.

5.4. Excessive temperature in the system

On days with a very high solar radiation it could happen that the water inside the solar thermal roof is heated up to temperatures higher than 90 °C. If the output temperature is higher, it is possible to increase the volume flow through the collectors to lower the temperature. If enough energy is in the system, the WDU can be operated, but if its energy demand is lower than the energy production with the solar roof, the surplus energy is stored in the heat storage tanks. If this period of time is too long, the heat storage tanks are fully loaded at any time and the output temperature of the collectors can no longer be reduced, because the stored hot water from the heat storage tanks and the used process water from the WDU are heated up again with the collectors. The temperature increases slowly in the system and reaches its maximum technical value. Due to this temperature rise a few components in the system could be damaged. This includes for example the volume flow meters and the external heat exchanger of the WDU. To prevent this, there is the possibility to cool down the process water with the WDU. The stored energy in the solar thermal system can be depolluted with the saltwater. In this case the energy is transferred from the process water to the saltwater and then the saltwater leaves the WDU immediately. For this the bypass in the WDU must be deactivated. With this possibility the stored energy in the system can be lowered, but this has the negative effect, that the efficiency of the WDU drops and the freshwater output is reduced.
Another solution to increase the storage capacities in the system could be to cool down the water in the heat storage tanks during the night to a lower temperature. For this the hot water must be circulated through the collectors during the night, like in the Endohousing project [End05]. At this time the energy is dissipated to the environment and the water cools down. It can be cooled down to the ambient temperature. During the next day the water must again be heated up to the operation temperature and therefore more energy can be stored in the solar thermal part. If this is not a solution and the temperature rises again to the maximum temperature level, this problem can only be solved by adding another heat storage tank or by reducing the solar thermal area. To add another WDU is also possible.
During the project planning phase it was not expected that such a high volume flow can be generated with the small solar thermal area and therefore this safety arrangement was never tested.

6. Simulation of the demonstration plant

In the this chapter the simulation of the demonstration plant is shown. The main aspect in this chapter is the water desalination unit, which is one important component in the whole solar desalination system. It starts with the explanation of the volume flows of the fluids and the calculation of the distributions inside the WDU. Later the densities of different fluids are examined in this chapter. Another important part in this chapter is the simulation of the complete WDU with all needed components in Simulink. The last point in the following chapter will be the simulation of the complete demonstration plant. This includes the solar thermal roof, heat storage tanks and other components needed for the operation.

6.1. Water transport inside the water desalination unit

In the following section the volume flow inside the water desalination unit is observed and calculated. The volume flow is defined as $Q = \dot{V} = \frac{\mathrm{d}V}{\mathrm{d}t}$. This is the volume of a fluid, which moves through a profile with the size A in a time period t. Fig. 6.1 gives a short overview of the volume flows inside the water desalination unit with the associated variables T_i, $\dot{V}_i$, ϱ_i and v_i, which are the different temperatures, volume flows, densities and velocities of the saltwater $_S$, the air $_L$, the freshwater $_F$ and the thermal heat source $_w$. The state variables are numerated and they could be different in all included points. Sometimes there is just a change in the temperatures or the densities. In most included points more than one state variable is different from a previous point. Furthermore the flow directions of the air, the saltwater and the heat source are included with coloured arrows. For a better differentiation they are coloured in blue, black, red and green. The ϵ describes if in the evaporation and condensation chambers is a fluid source or a fluid sink. For $\epsilon < 0$ it is a sink, for $\epsilon > 0$ it is a source and for $\epsilon = 0$ it is neither a sink nor a source. Additionally the size of the WDU is shown. The height of the WDU is 2 m, the width is 1.7 m and the depth is 0.75 m. The ventilator used has a diameter of 0.155 m and the shown pipe in the right has diameter of 0.04 m. Additionally two pumps are included in this figure. One for the saltwater delivery and one for the bypass. The coordinate system is needed for later calculations.
The water enters the WDU on the right side, it goes through the complete system and this water leaves the WDU on the left side. Inside the water desalination unit there

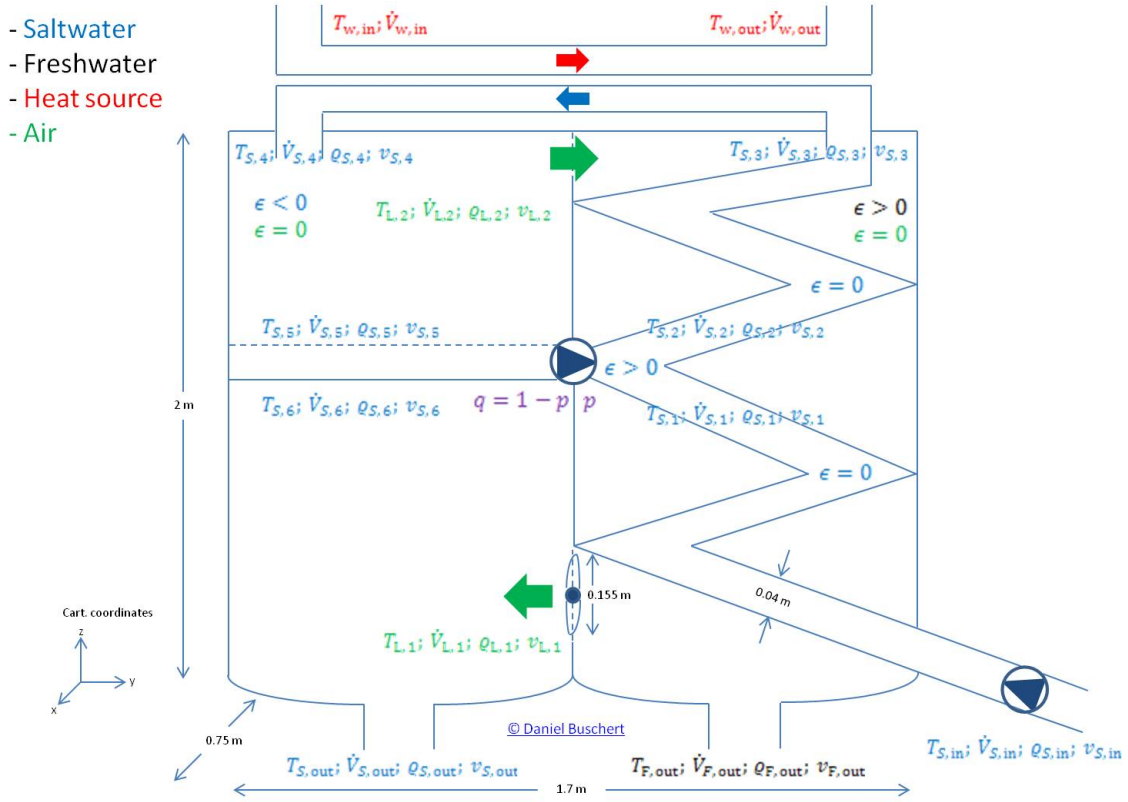

Fig. 6.1.: Saltwater, freshwater and air volume flows inside the WDU with coloured differentiations. Most important variables are shown.

on the left hand side a flow diverter is included. This flow diverter takes a constant percentage p of the streamed in water and delivers it through a bypass to the right side of the WDU. On the right side the volume flow from the bypass and the entering volume flow, which enters the WDU, are combined in a flow mixer. This water heats up the incoming saltwater and it streams again through the WDU. Then the combined volume flow goes through the system, it is again heated up in the external heat exchanger and it is separated again in the flow diverter. p in % stays in the water desalination unit and $q = 1 - p$ in % leaves it. The question is how much water stays and how much water leaves the water desalination unit? For this a constant volume flow V_0 is considered, which enters the water desalination unit. Furthermore the flow diverter has also a fixed diversion rate p. For the calculation the following constant values are considered:

$$Q_0 = 2\,\mathrm{kg/s} \tag{6.1}$$

$$p = 50\,\% \tag{6.2}$$

During this calculation the evaporation is not considered, but in a static situation it is only a constant value, which depends on the saltwater temperature and the volume flow of the air. The first step is to calculate the volume flow $\dot{V}_{in} = Q_{in}$, which stays inside the water desalination unit and the volume flow $\dot{V}_{out} = Q_{out}$, which leaves the WDU.

With the constant numerical values (6.1) and (6.2) an estimation for both volume flows is possible. This will be done by a time critical model with the result:

T_{cycle} [time]	Q_{in} [kg/s]	Q_{out} [kg/s]
-1	$0+0=0$	0
0	$2+0=2$	0
1	$2+1=3$	1
2	$2+1.5=3.5$	1.5
3	$2+1.75=3.75$	1.75
4	$2+1.875=3.875$	1.875
5	$2+1.9375=3.9375$	1.9375
6	$2+1.96875=3.96875$	1.96875
$\vdots$	$\vdots$	$\vdots$
N	$2+2=4$	2

(6.3)

As can be seen in this table the maximum volume flow, which leaves the WDU, converge against 2 kg/s. This is the same numerical value as the volume flow which enters the WDU (6.1). Inside the WDU the volume flow Q_{in} seems to converge against 4 kg/s. For the calculation with other p-values a short program with a graphical output was written in Maple [Maple]. The figures with different volume flows inside the WDU, which depend on p, can be found in Fig. 6.2 and the different volume flows, which leave the WDU, can be found in Fig. 6.3. The range of the p was between 0 % and 90 %. As can be seen the step size was 10 %. The volume flow, which stays inside the WDU, increases with increasing p. The higher the p, the higher the amount of water inside the WDU, but for all p the volume flow inside the WDU converges against a constant value, which depends on the value of p. For 10 % the constant value seems to be close to 2 kg/s and for 90 % it seems to be close to 20 kg/s. For other values of p the volume flows inside the WDU are between these two limit values. As can be seen in Fig. 6.3 the volume flow, which leaves the WDU, converges for all values of p against 2 kg/s. This is the same value as the volume flow, which enters the WDU. The time to reach the constant value depends on p. The higher the p, the longer the time. One interesting aspect of this figure is that for all p the maximum volume flow is always the same, but the curves and time constants are different. It has the same value like the input volume flow (6.1).

For a common description the input volume flow is described with V_0 and the constant diverter ratio is described with p. The value of p is between $0 \leq p < 1$. If p has the value 0, all water leaves the WDU and if p has the value 1 all water stays inside the unit. The value of 1 makes no sense in this calculation, because this would have the effect, that an infinity volume for the storage is necessary and this is not practical. Therefore the maximum value is reduced to a value below 1.

The first step is to calculate the volume flow V_{in} inside the WDU after N complete cycles T. Where T is the time for one cycle. For these calculations the position of the flow

mixer on the right side is considered. The different volume flows are added, which enter the WDU and which come from the flow diverter. The exact position of the flow mixer is shown in Fig. 6.1. In the following calculations it is mathematically examined for a

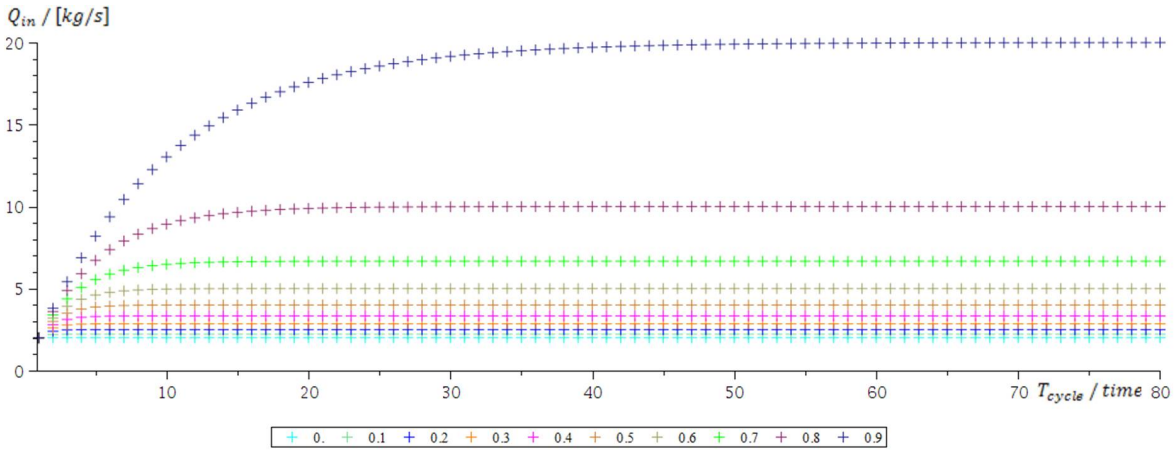

Fig. 6.2.: Water amount inside the WDU for different p.

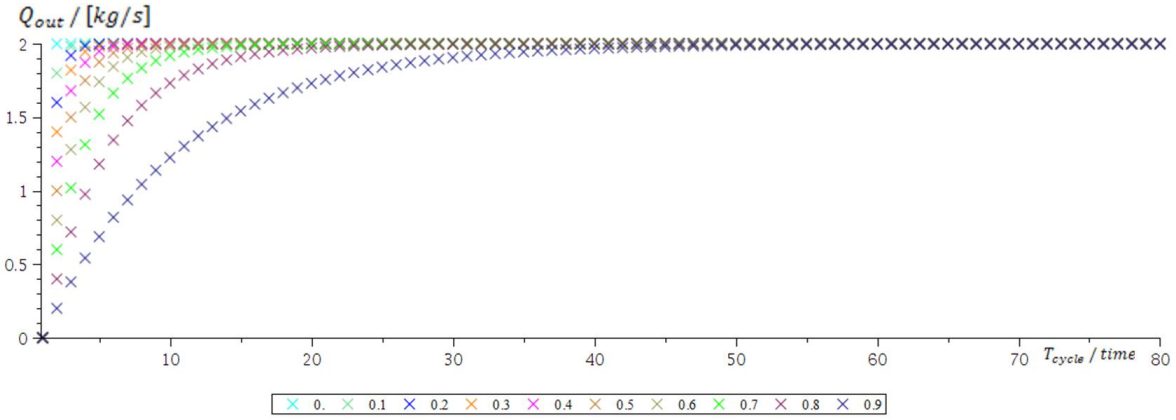

Fig. 6.3.: Water amount for different p which leaves the WDU.

constant volume flow Q_0. In the first table the behaviour of the volume flow is analysed and the water inside the WDU is calculated:

T [time]	Q_{in} [kg/s]
0	$Q_0 = Q_0 + 0 = Q_0$
1	$Q_1 = Q_0 + pQ_0$
2	$Q_2 = Q_0 + pQ_1 = Q_0 + p\,(Q_0 + pQ_0)$
3	$Q_3 = Q_0 + pQ_2 = Q_0 + p\,(Q_0 + p\,(Q_0 + pQ_0))$
4	$Q_4 = Q_0 + pQ_3 = Q_0 + p\,(Q_0 + p\,(Q_0 + p\,(Q_0 + pQ_0)))$
$\vdots$	$\vdots$
N	$Q_N = Q_0 + pQ_{N-1}$

(6.4)

This tabular can be simplified with an expansion of the different terms:

T [time]	Q_{in} [kg/s]
0	$Q_0 = Q_0$
1	$Q_1 = Q_0 + pQ_0$
2	$Q_2 = Q_0 + pQ_0 + p^2Q_0$
3	$Q_3 = Q_0 + pQ_0 + p^2Q_0 + p^3Q_0$
4	$Q_4 = Q_0 + pQ_0 + p^2Q_0 + p^3Q_0 + p^4Q_0$
$\vdots$	$\vdots$
N	$Q_N = Q_0\left(1 + p + p^2 + \cdots + p^N\right)$

(6.5)

For $T \to \infty$ respectively $N \to \infty$ the equation in tabular 6.5 can be written as an infinite sum:

$$Q_{in} = Q_\infty = \sum_{n=0}^{\infty} Q_0 p^n = Q_0 \sum_{n=0}^{\infty} p^n \tag{6.6}$$

The equation for Q_N in tabular (6.5) is used for an easier description

$$Q_N = Q_0 + pQ_0 + p^2Q_0 + p^3Q_0 + \cdots + p^NQ_0. \tag{6.7}$$

Now this equation is multiplied by p

$$pQ_N = pQ_0 + p^2Q_0 + p^3Q_0 + \cdots + p^{N+1}Q_0 \tag{6.8}$$

and the next step is to subtract (6.8) from (6.7)

$$Q_N - pQ_N = Q_0 - p^{N+1}Q_0. \tag{6.9}$$

Finally it is solved in Q_N

$$Q_N = Q_0 \frac{1 - p^{N+1}}{1 - p}. \tag{6.10}$$

This equation is only valid for fixed integers N, and with $N \to \infty$ it can be written with (B.25) as

$$Q_\infty = \lim_{N\to\infty} Q_0 \frac{1-p^{N+1}}{1-p} = Q_0 \frac{1}{1-p}. \tag{6.11}$$

As can be seen in this equation the final value of Q_∞ depends only on the value of p. For $p = 0$ is the maximum value inside the WDU just Q_0, for $p = 0.9$ is the volume flow inside the WDU $Q_0/0.1$. Due to this scaling excessive value of p cannot be adjusted for the bypass, because only a special and definite volume is available inside the WDU. For $p = 1$ the equation is indefinite. If the value of p is too high all entering saltwater cannot be stored inside the WDU. The maximum value of p depends on the incoming saltwater flow and the available volume. The higher the saltwater flow, the lower must be the value of p as long as the available volume inside the WDU stays constant.
The next step is to calculate the value of Q_{out}. For this calculation a position after the flow diverter is considered. If p is separated from the volume flow, only $q = 1 - p$ leaves the WDU and it is similar calculable like in (6.4). For the result (6.5) is used:

T [time]	Q_{out} [kg/s]
0	$Q_{O,0} = qQ_0 = (1-p)Q_0$
1	$Q_{O,1} = qQ_1 = (1-p)(Q_0 + pQ_0)$
2	$Q_{O,2} = qQ_2 = (1-p)(Q_0 + pQ_0 + p^2Q_0)$
3	$Q_{O,3} = qQ_3 = (1-p)(Q_0 + pQ_0 + p^2Q_0 + p^3Q_0)$
$\vdots$	$\vdots$
N	$Q_{O,N} = qQ_N = (1-p)Q_N$

(6.12)

This equation can also be simplified:

T [time]	Q_{out} [kg/s]
0	$Q_{O,0} = qQ_0 = Q_0(1-p)$
1	$Q_{O,1} = Q_0 + pQ_0 - pQ_0 - p^2Q_0 = Q_0 - p^2Q_0 = Q_0(1-p^2)$
2	$Q_{O,2} = Q_0 - p^3Q_0 = Q_0(1-p^3)$
3	$Q_{O,3} = Q_0 - p^4Q_0 = Q_0(1-p^4)$
$\vdots$	$\vdots$
N	$Q_{O,N} = Q_0 - p^{N+1}Q_0 = Q_0(1-p^{N+1})$

(6.13)

For $T \to \infty$ respectively $N \to \infty$ the last equation in (6.13) can also be written with (B.25) and $p < 1$ as an infinite sum:

$$\begin{aligned} Q_{out} = Q_{O,\infty} &= \sum_{n=0}^{\infty} Q_0 \left(p^n - p^{n+1}\right) = Q_0 \sum_{n=0}^{\infty} p^n - Q_0 \sum_{n=0}^{\infty} p^{n+1} \\ &= Q_0 \lim_{N\to\infty} \left(\frac{1-p^{N+1}}{1-p} - p\frac{1-p^{N+1}}{1-p} \right) \end{aligned} \tag{6.14}$$

With the limit laws it can be written as

$$Q_{out} = Q_0 \left(\frac{1}{1-p} - p\frac{1}{1-p} \right) = Q_0 \left(\frac{1-p}{1-p} \right) = Q_0. \tag{6.15}$$

As can be seen in this equation the volume flow, which leaves the WDU, has always the same value like the input value, because it is independent on p. With the results of (6.11) and (6.15) the Fig.'s 6.2 and 6.3 are confirmed.
In the next paragraph the maximum speed of the waterdrops inside the WDU is calculated. The saltwater leaves the external heat exchanger at the top with the highest temperature in the system and rains down in the left chamber of the WDU. This can be observed in Fig. 6.1. The air streams upwards, which comes from the bottom of the WDU and which was accelerated by the ventilator. For a constant velocity of the air a Galilei transformation (B.20) could be used to transform from a laboratory coordinate system into the body fixed coordinate system of the air. Due to different velocity directions both fluids are in a counterflow and caused on the air resistance only a maximum fall velocity is possible for the saltwater. It is the same for a sky diver in the air. They can only reach a maximum velocity in the air, which depends mainly on his or her body resistance in the air. The waterdrops in the WDU are also accelerated due to gravity. If the speed of the air inside the WDU is too high the waterdrops may raise and will not fall to the bottom. In the worst case the saltwater is transported from the left chamber to the right chamber and will pollute the produced freshwater in the condensation chamber. Therefore it is very interesting to find the maximum speed of the air flow inside the WDU. Furthermore the advantage is, that if the waterdrops stay for a longer time in the left chamber, more water can evaporate. The residence time of the saltwater drops in the left chamber can be adjusted by the velocity of the air. In the following part a rough approximation of the maximum speed is calculated. For the calculation the balancing of forces

$$\vec{F} = \vec{F}_G + \vec{F}_R \tag{6.16}$$

is examined with $\vec{F} = m_T \vec{a} = m_T \dot{\vec{v}}$ and where

$$\vec{F}_G = m_T \vec{g} \tag{6.17}$$

is the weight-force with the mean mass m_T of the waterdrops and

$$\vec{F}_R = \frac{1}{2} c_w \varrho_L A v^2 \hat{e}_i \tag{6.18}$$

the air resistant for fast velocities $\vec{v}$ of bodies in fluids and $\hat{e}_i$ the unit vector of the air resistant. Where A is the cross-section area of the body in moving direction, ϱ_L the densitiy of the air and c_w the resistance coefficient of the body, which depends on the streamlined shape of the body. For a good streamline shape it is $c_w < 1$, for a sphere it is $c_w \approx 1$ and for a bad streamline shape it is $c_w > 1$. Based on the high velocity it is in the limits a turbulent flow. The utilised coordinate system is also shown in Fig. 6.1. For a simplification the flow direction of the waterdrops and the air flow is along the z-axis.

With (6.17), (6.18) and the simplifications $\vec{v} = -v\hat{e}_z$ and $\vec{g} = -g\hat{e}_z$ the equation (6.16) can be written as

$$-m_T\dot{v}\hat{e}_z = -m_T g\hat{e}_z + \frac{1}{2}c_w\varrho_L A v^2\hat{e}_z. \tag{6.19}$$

Now it can be rewritten

$$\dot{v} = -\frac{c_w\varrho_L A}{2m_T}v^2 + g. \tag{6.20}$$

This is a kind of a Riccati ODE [Bro08]

$$y' = P(x)y^2 + Q(x)y + R(x) \tag{6.21}$$

with $P(x) = P < 0$, $Q(x) = 0$ and $R(x) = R = \text{const.} > 0$. It can be solved with the approach:

$$y = z(x) + u(x) \quad \Rightarrow \quad y' = z' + u' \tag{6.22}$$

This equation can be inserted in (6.21)

$$z' + u' = P(z+u)^2 + R = Pz^2 + 2Pzu + Pu^2 + R. \tag{6.23}$$

The coefficient for the z^0 term disappears for a homogenous solution in z

$$Pu^2 + R = 0 \quad \Rightarrow \quad u = \pm\sqrt{-\frac{R}{P}}. \tag{6.24}$$

Only the + value of the root is considered, because of the side condition of P and R. As can be seen the solution $u = \sqrt{-\frac{R}{P}}$ solves with $z = 0$ the ODE (6.21). It is a constant solution for the ODE. With the substitution (6.22) the Riccati ODE can be transferred into a Bernoulli ODE

$$z' = Pz^2 + 2Pz\sqrt{-\frac{R}{P}} = Pz^2 - 2\sqrt{-PR}z, \tag{6.25}$$

the standard root rules cannot be utilized, because the value of the radicand of the root is negative and the exponent of the root is even. This new ODE can be solved with division by z^2 and implementation of $a = 1/z$ and $z' = -\frac{1}{a^2}a'$ [Bro08]. With this substitution it is a linear ODE, which can easily be solved:

$$\frac{z'}{z^2} = P - \frac{2\sqrt{-PR}}{z} \quad \Rightarrow \quad a' = 2\sqrt{-PR}a - P \tag{6.26}$$

This can be solved with the variation of the constants [Bro08, Sch02]. It is valid that:

$$y' = \tilde{P}y + \tilde{Q} \quad \Rightarrow \quad y = \mu\left(\int\frac{\tilde{Q}}{\mu}\,\mathrm{d}x + c\right) \quad \text{with} \quad \mu = \exp\left(\int\tilde{P}\,\mathrm{d}x\right) \tag{6.27}$$

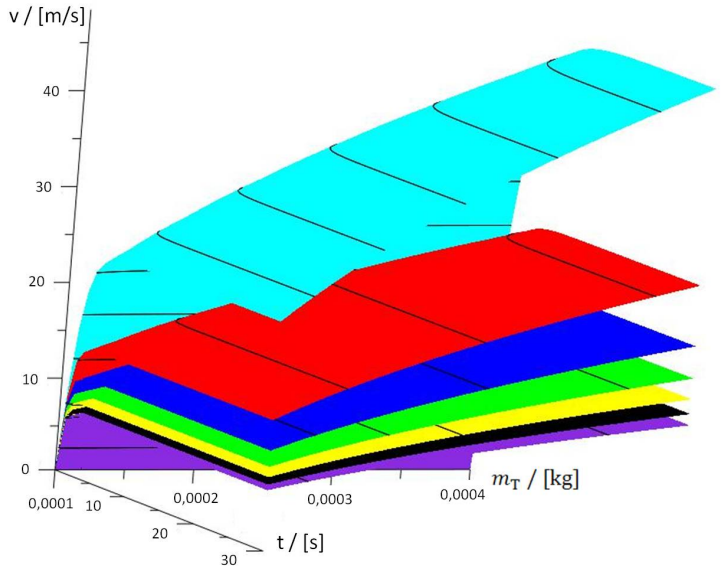

Fig. 6.4.: Velocity of waterdrops inside the WDU in dependency of drag coefficient and mass over a short time period.

In this situation it is $\tilde{Q} = -P$ and $\tilde{P} = 2\sqrt{-PR}$. The solution can be calculated with the first re-substitution and due to the value of the radicand it is:

$$\begin{aligned} a &= -\frac{1}{2}\sqrt{\frac{-P}{R}} + c\exp\left(2\sqrt{-PR}x\right) = \frac{1}{z} \\ \Rightarrow z &= \frac{-2}{\sqrt{\frac{-P}{R}} - 2c\exp\left(2\sqrt{-PR}x\right)} \end{aligned} \tag{6.28}$$

The final solution of the ODE (6.21) can now be calculated with (6.22) and (6.24)

$$y(x) = -\frac{2}{\sqrt{\frac{-P}{R}} - 2c\exp\left(2\sqrt{-PR}x\right)} + \sqrt{\frac{-R}{P}}. \tag{6.29}$$

For the final solution the constant c must be determined with the initial condition $y(x_0) = y_0$. With (6.20) it is $P = -\frac{c_w \varrho_L A}{2m_T}$ and $R = g$ and now the maximum speed in dependency of different variables can be approximated. The limits depend on the kind of the waterdrops. Fig. 6.4 shows the possible solution for the fixed values $A = (3 \cdot 10^{-3})^2\,\pi\ \mathrm{m}^2$, $g = 9.81\,\mathrm{m/s^2}$ and $\varrho_L = 1.183\,\mathrm{kg/m^3}$ (25 °C). The fallen waterdrops have a velocity of 0.42 m/s and in this figure the mass of the waterdrops m_T varies between $1 \cdot 10^{-4}$ kg and $4 \cdot 10^{-4}$ kg. The c_w value is between 0.1 in cyan and 1.3 in blue violet. This figure is plotted for a timeframe of 30 s. As can be seen in Fig. 6.4 the speed reaches a maximum value, which depends on the mass and on the drag coefficient of the waterdrops. The smaller the drag coefficient and the higher the mass, the higher is the maximum velocity of it. Small waterdrops with a high drag coefficient have a much lower velocity. If all drops would have the same size and the same drag coefficient, it could be

possible to define a maximum velocity inside the WDU. The advantage would be that the air flow can be adjusted in a way that a maximum amount of water is evaporated inside the WDU. In reality the waterdrops are all different, this is well-founded in the chaotic behaviour inside the WDU. Therefore it is only possible to do series of measurements to adjust the best airflow inside the WDU, but the theoretical limits are shown in Fig. 6.4. The problem is, if the air flow is too high small saltwaterdrops inside the WDU can be blown from the left to the right chamber of the WDU and then the produced freshwater is polluted with saltwater. In the worst case the water can no longer be used and it must be desalinated again. The problem can be fixed in a way that a membrane separates the left chamber from the right chamber. It must be such a membrane, that only water vapour can pass it from the left to the right side of the WDU. The saltwaterdrops can settle and rain down again. With this membrane a contamination of the freshwater with saltwater can be avoided and furthermore the air speed can be adjusted higher compared to a system without a membrane.

6.2. Distribution of water and the density in the pipes

The saltwater enters the WDU at the right side of the component and it is transported in a pipe from the bottom to the top, as it can be seen in Fig. 6.1. During this transportation the water is heated up by the air and the evaporated water from the left side, which condenses in the right chamber. At the middle of the WDU a bypass is included, which extracts hot water from the left chamber and it injects the hot saltwater into the pipe in the right chamber. This is done with a controllable 3-way-valve. The saltwater enters the WDU with the lowest temperature $T_{min} = T_{S,in}$ and leaves the pipe with a higher temperature $T_{S,3}$ at the top of the right chamber. The saltwater enters the pipe with a density $\varrho = \varrho_{S,in}$. Due to the temperature rise the density depends on the position in the pipe, therefore it is a $\varrho(\vec{r})$ and it passes a pipe with the length l and the radius $R = 0.02\,\mathrm{m}$. Due to different temperatures at different locations a temperature field $T(\vec{r})$ can be considered for the calculation. Due to the cylindrical problem cylindrical coordinates B.1.2 are used.
The first step is to calculate the mass of the head of water for an increasing temperature

$$M = \int_{V_0} \varrho(\vec{r})\,\mathrm{d}V = \int_{V_0} \varrho(\vec{r}) r\,\mathrm{d}r\,\mathrm{d}\varphi\,\mathrm{d}z. \tag{6.30}$$

For the calculation a uniform increasing water temperature field $T(\vec{r})$ is considered, which only depends in this model on the z position:

$$T(\vec{r}) = \frac{\triangle T}{\triangle z} z = \frac{\triangle T}{l} z \qquad \Rightarrow \nabla T(\vec{r}) = \frac{\triangle T}{l} \hat{e}_z \tag{6.31}$$

As can be seen the change of the temperature field is along the z-axis, where ∇ is in cylinder coordinates (B.8). Along r and φ the temperatures are constant. For the

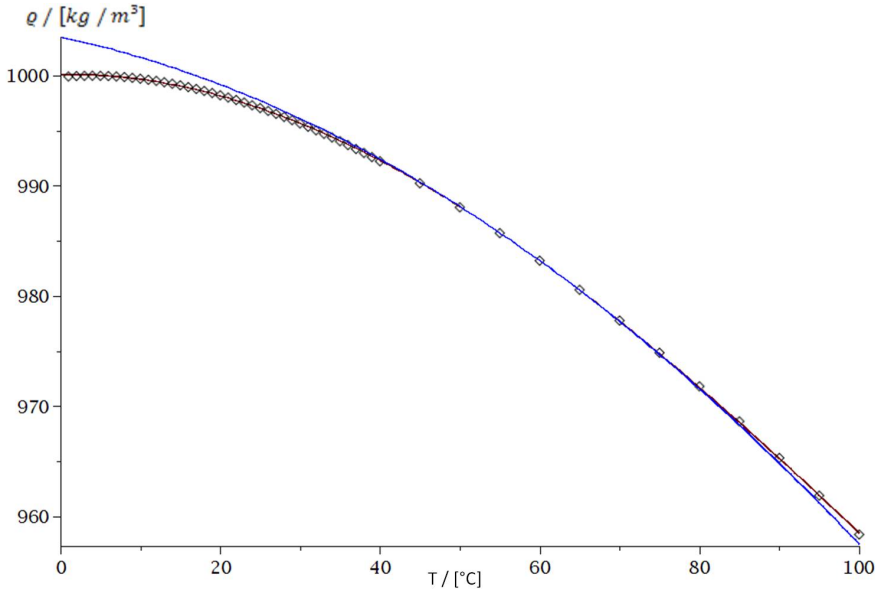

Fig. 6.5.: Density of water in the range between 0 °C and 100 °C.

calculation the temperature-dependent density function of water is necessary. The data in Tab. C.9 are used for a least square polynomial approximation of the order 3:

$$\varrho = 1000.045624 + 0.01740584493T - 0.005926393447T^2 + 0.00001597007T^3 \qquad \left[\frac{\text{kg}}{\text{m}^3}\right] \tag{6.32}$$

With this approximation a good calculation of the density between the freezing point and the boiling point of water is possible. For a temperature range between 20 °C and 100 °C a polynomial with the order 2 can be used:

$$\varrho_{\text{taylor}} = 1014.48 - 0.52T - 0.0031(T - 60)^2 \qquad \left[\frac{\text{kg}}{\text{m}^3}\right] \tag{6.33}$$

Due to the water anomaly at 4 °C the curve in the temperature range between 0 °C and 100 °C is much more complicated compared to the temperature range between 20 °C and 100 °C. This is based on the fact that the highest density of water is at 4 °C. This is also called the anomaly of water. An overview of the water density can be found in Fig. 6.5. Now an adoption is done for different frame conditions:

$$T = T_{min} + T(\vec{r}) = T_{min} + \frac{\triangle T}{l} z \tag{6.34}$$

With this equation and (6.32) the mass in the pipe (6.30) can be calculated:

$$M = \int_{V_0} \varrho \, \mathrm{d}V = \pi R^2 \int_0^l \varrho(\vec{r}) \, \mathrm{d}z$$

$$= \frac{1}{2}\Big(0.000025 \triangle T^3 - 0.012 \triangle T^2 + 0.0001 T_{min} \triangle T^2 - 0.037 T_{min} \triangle T + 0.055 \triangle T + 0.00015 T_{min}^2 \triangle T + 0.11 T_{min} - 0.037 T_{min}^2 + 0.0001 T_{min}^3 + 6283.47\Big) R^2 l \qquad [\text{kg}] \tag{6.35}$$

Inside the right chamber of the WDU the water flows through a pipe and will be heated up to a higher temperature. This happens again in the external heat exchanger, which can be found at the top in Fig. 6.1. Due to a higher temperature the water has a lower density, this is still valid, if the temperature is above 4 °C. During the heating the volume of the pipe is nearly constant and therefore the velocity of the water at the end of the pipe must be higher compared to the incoming velocity of the water. For this calculation the continuity equation (3.34) is solved in cylindrical coordinates (B.6) and for a static situation. The water flows in z direction with the speed $\vec{v} = v_z(z)\hat{e}_z$ and furthermore the density is then independent of time $\frac{\mathrm{d}\varrho}{\mathrm{d}t} = 0$. Only the density $\varrho(\vec{r})$ depends on the location in z and in this model the density allocation is independent of the radial direction. Therefore only the derivation (B.8) in the z direction is unequal zero. For the divergence of $\vec{v}(z)$ equation (B.9) must be used. In this static situation the solution of the continuity equation can be written as:

$$\nabla \cdot (\varrho \vec{v}) = 0 \quad \Rightarrow \quad \varrho \nabla \cdot \vec{v} + \vec{v} \cdot \nabla \varrho = 0 \quad \Rightarrow \quad \varrho \frac{\partial v_z}{\partial z} + v_z \frac{\partial \varrho}{\partial z} = 0 \tag{6.36}$$

This is an ODE, which can easily be solved for v_z and for the substitution $u = \varrho(z)$ and $\mathrm{d}u = \frac{\partial \varrho}{\partial z}\,\mathrm{d}z$

$$v_z = \exp\left(-\int \frac{1}{\varrho}\frac{\partial \varrho}{\partial z}\,\mathrm{d}z\right) c = \exp\left(-\int \frac{1}{u}\,\mathrm{d}u\right) c = \frac{c}{\varrho(z)}. \tag{6.37}$$

Finally it can be solved with the initial condition. For this, the speed of the water v_0 at the beginning of the pipe $z = 0$ is considered

$$v_z(0) = v_0 \quad \Rightarrow \quad v_z = \frac{c}{\varrho(0)} = v_0 \quad \Rightarrow \quad c = v_0 \varrho(0). \tag{6.38}$$

The final solution of the equation is now

$$v(z) = \frac{v_0 \varrho(0)}{\varrho(z)}. \tag{6.39}$$

As it can be seen the speed of the water depends on the location on the z axis. The lower the density, the higher the speed of the fluid. This equation is not only valid for liquids, it is also valid for air. If there is a phase change in the fluids it must be calculated in a different way, because of the volume expansion during the phase change. The growth of the speed is proportional to $1/\varrho(z)$. For water the dependency is not very essential, because the density of liquid water (Tab. C.9) varies just a little bit over the temperature. Therefore this density correction later on is not considered for water.

6.3. Distribution of air and the density in the WDU

Inside the WDU is air, which is used to transport the evaporated water from the left chamber to the right chamber. The way of the air is included in Fig. 6.1. It is accelerated with a ventilator, which is installed at the bottom of the WDU. The ventilator takes the air from the right chamber and blows it into the left chamber. It rises there from the bottom to the top and on this path the air is heated up by the saltwater. At the top the air is transferred via a channel from the left to the right chamber. On the right side of the WDU the air cools down and drops to the ground. At the ground the air is again transferred from the right to the left chamber. Therefore the same air is used again. Due to the heating process inside the WDU the densities of the air are different. At the bottom the air has the lowest temperature and therefore the highest density. The temperature is close to the temperature of the incoming saltwater. At the top of the left chamber the air has the highest temperature inside the WDU. It is close to the maximum saltwater temperature $T_{max} = T_{S,4}$ in the whole system. Due to the higher temperature the air has the lowest density. Based on the different temperatures in the system the contribution of the temperatures can also be described with a temperature gradient $\nabla\phi(x, y, z)$, where $\phi(x, y, z)$ is a potential, which describes the profile of the temperature distribution. It is similar to the water temperature gradient (6.31). Due to the temperature rise along the z axis, the main direction of the gradient is also along the z axis. The gradient of the density is the other way round. Due to the different densities in the system the speed of the air is not only accelerated by the ventilator. During the heating the density of the air becomes smaller and rises in the system. Due to these differences it is also accelerated along the temperature gradient. The velocity dependency of the air flow can also be calculated with (6.39). In contrast to the density correction of water the density correction of air must be considered, because the variation of the temperature-dependent density is much higher. For the estimation of the air inside the WDU it is considered in the first step as an ideal and dry gas. The density can then be calculated with

$$\varrho = \frac{p}{R_l T}, \tag{6.40}$$

where p is the ambient pressure, $R_l = 287.058\,\mathrm{J/(kg\,K)}$ the universal gas constant and T the temperature in Kelvin. For wet air this equation must be slightly modified. The universal gas constant for dry air R_l must be modified and exchanged with R_f for wet air

$$R_f = \frac{R_l}{1 - \varphi\frac{e_s}{p}\left(1 - \frac{R_l}{R_w}\right)}, \tag{6.41}$$

where φ is the relative humidity between 0 and 1, $R_w = 461\,\mathrm{J/(kg\,K)}$ is the universal gas constant for water and e_s is the saturation vapour pressure of water, which can be calculated with (3.42). For 20 °C a density is calculated with $1.193\,\mathrm{kg/m^3}$ and for 95 °C it is $0.657\,\mathrm{kg/m^3}$. Due to this huge difference the density correction should be considered during the simulation of the WDU. It can also be calculated with (6.39). The air is accelerated at the bottom of the WDU with a ventilator and therefore the

initial velocity v_0 of the air is needed. This can be calculated with the mass conservation inside the WDU

$$Q_0 = A_0 v_0 = A_1 v_1 = Q_1, \tag{6.42}$$

where A_1 and v_1 is the area and the flow rate of the ventilator. This can be solved with the needed initial speed for the density correction (6.39):

$$v_0 = \frac{A_1}{A_0} v_1 = \frac{Q_1}{A_0} \quad \Rightarrow \quad v(z) = \frac{A_1 v_1}{A_0} \frac{\varrho(0)}{\varrho(z)} = \frac{Q_1}{A_0} \frac{\varrho(0)}{\varrho(z)}, \tag{6.43}$$

where Q_1 is the volume flow of the ventilator. This equation can also be written as an z axis dependent volume flow

$$Q_0(z) = Q_1 \frac{\varrho(0)}{\varrho(z)} \tag{6.44}$$

This density correction is necessary for the calculation of the real volume flow, which could flow at the top from the left chamber to the right chamber. Due to losses in the system, this is only the maximum value, which is theoretically possible. The losses in the system could be turbulences in the chambers and frictions of the molecules with other molecules, with the outerwalls of the housing or resistances inside the chambers. The chaotic behaviours are not calculable at the moment, because this topic is at the early beginning in scientific research. Therefore other possibilities must be found to include it into the simulation.

6.4. Energy distribution in the WDU

In the following section a short summary of the energy distribution in the system is given. The distribution of the salt- and freshwater inside the system can be seen in Fig. 6.1. The temperature of a fluid reflects the intrinsic energy of the fluid (6.50). Furthermore the amount of energy is also characterised by the volume flow. The hotter the fluid and the higher the volume flow, the more energy is stored in the fluid. The saltwater enters the WDU at a relatively low temperature T_{min}. At the building site in Hurghada the saltwater temperature is in the range between 20 °C and 30 °C, as it can be seen in Fig. 5.4. For an operation with a high efficiency the saltwater must be heated up to the operation temperature T_{max} of the WDU. It is close to 95 °C. In the following the heating due to friction is neglected in the overview, because the friction reduces the volume flow, but the temperature is increased slightly. Due to the closed system no energy is lost in the WDU. The water is heated up in the right chamber by an energy transfer from the hot air to the water on the one hand and on the other hand it is heated up by mixing it up with water from the left chamber, which is done inside the flow mixer. In the right chamber the energy of the saltwater increases from the bottom to the top and the energy of the air is reduced from the top to the bottom. Then the saltwater passes an external heat exchanger. In the external heat exchanger the saltwater is heated up to the maximum temperature T_{max} in the system. In this heat

exchanger an energy transfer takes part from the external heat source to the saltwater. The heat source enters this heat exchanger with a temperature close to the boiling point and it releases its energy to the saltwater. Finally it leaves the heat exchanger with a lower temperature. At the end of the heat exchanger the saltwater has the highest energy. In the left chamber the water rains down and releases its energy to the air on the one hand and on the other hand it is cooled down by evaporation. It is also called evaporation heat loss. This heat loss is considered during the simulation with an additional heat exchanger, which transfers a part of the energy from the left chamber to the saltwater in the right chamber. It can be justified in a way, that the energy for the evaporation heat loss is stored in the evaporated water and during the condensation in the right chamber it is released again. This happens in a normal phase change from gas to liquid. The WDU is a closed system and therefore a loss of energy cannot happen. Part of the saltwater is separated in the flow diverter. One part leaves the WDU and the other part is mixed up with the incoming and cold saltwater. Due to the bypass a part of the energy can be reused and therefore the efficiency is raised. At the top of the left chamber the energy of the saltwater has its maximum value and at the bottom the water has the lowest intrinsic energy. The same energy distribution is for the air. At the bottom it has the lowest energy and at the top it has the highest energy in the system. The energy distribution for the saltwater and the air can also be described with $\nabla\varphi_w$ or $\nabla\varphi_a$, where φ_i depends on the location z inside the WDU and ∇ is the gradient.

6.5. Model of the water desalination unit

In the following section the modelling of the WDU is shown. A rough overview of the model can be seen in Fig. 6.6. The model of the system consists of different components. It starts with different heat exchangers, which will be discussed in the following subsection and other components like a flow mixer and a flow diverter. Furthermore the air and its density correction 6.3 is included during the modelling. Additionally the production of freshwater is also implemented in the system. The complete model was invented and improved by the author.
The nomenclatures of the heat exchangers in Fig. 6.6 and in the model are the following. If the water is hotter than the air, it is a W / A - Heat exchanger and if it is vice versa it is written as A / W - Heat exchanger. Only the external heat exchanger is a special case, because both fluids are water. Inside the pipe of the solar thermal part is water and it heats up the saltwater inside the WDU, therefore it is called a W / W - Heat exchanger, but the first W also stands for the water in the heat source.
The saltwater enters the WDU in the right chamber and is transported inside a pipe from the bottom to the top. This chamber is also called the condensation chamber, because the evaporated water condenses there. The flow direction of the saltwater (blue line) is shown with arrows. At this position the air temperature T_a is higher than the temperature of the saltwater T_w, therefore thermal energy is transferred from the air to the water, which is consistent with the thermodynamic laws. This energy transfer

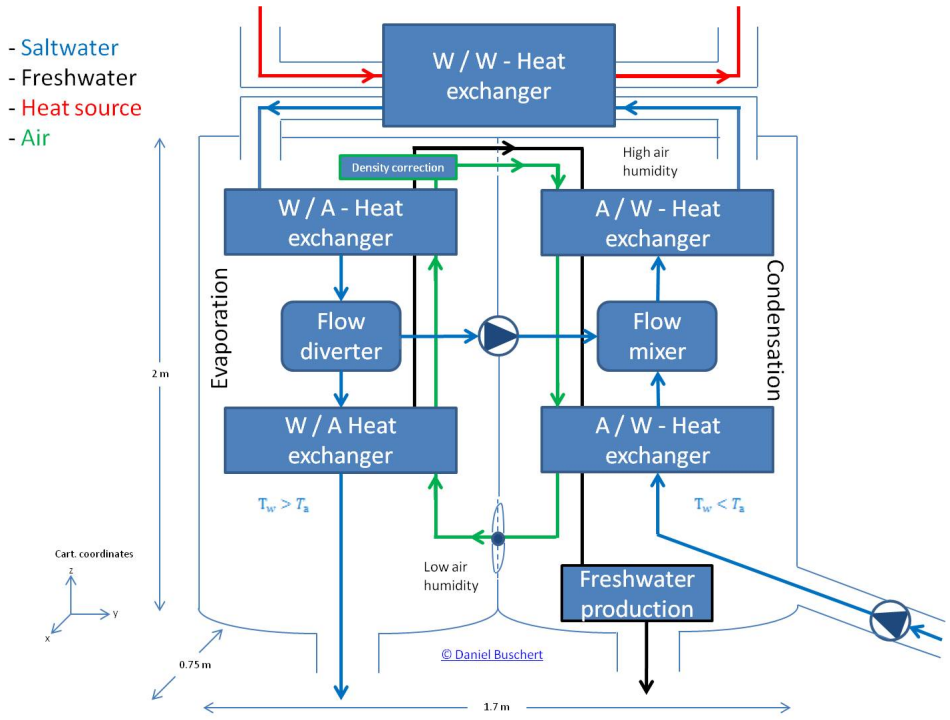

Fig. 6.6.: Model of the WDU with all components, which are necessary for the simulation.

is described and calculated with a heat exchanger at the bottom right. The preheated water passes the flow mixer in the next step. The entered saltwater is mixed up with a part of the hot water, which comes from the flow diverter in the left chamber. This chamber is also called evaporation chamber, because the saltwater evaporates there. The flow mixer can easily be calculated. At this point only two different volume flows with different temperatures are combined and stream together to the next heat exchanger on the right. The new temperature can be calculated with the law of conservation of energy

$$\begin{aligned} Q_{\text{delivered}} &= Q_{\text{absorbed}} \\ m_1 c_{p_1}(T_1 - T_m) &= m_2 c_{p_2}(T_m - T_2), \end{aligned} \tag{6.45}$$

where m_i is the mass of the two flows in a short time period $\mathrm{d}t$, T_i is its temperature, c_{p_i} is the heat capacity of the different flows and T_m is the resulting temperature of the leaving flow in this short time period. This equation is solved to T_m:

$$T_m = \frac{m_1 c_{p_1} T_1 + m_2 c_{p_2} T_2}{m_1 c_{p_1} + m_2 c_{p_2}} \tag{6.46}$$

For the simplification it can be set at this position, that $c_{p_1} = c_{p_2}$, because saltwater is mixed up with saltwater. Only the temperature is slightly different. Now the final equation for the leaving temperature is

$$T_m = \frac{m_1 T_1 + m_2 T_2}{m_1 + m_2}. \tag{6.47}$$

It is also called the rule of mixture from Richmann and it is valid if no state of aggregation is changed. The calculation of the new stream in a short time period $\mathrm{d}t$ is much easier to calculate

$$m_m = m_1 + m_2, \tag{6.48}$$

where m_i is the mass of the different volume elements. During the simulation it is observed time-discrete.
After passing the flow mixer the water passes again another heat exchanger. At this point the saltwater temperature is lower than the air temperature and therefore the energy is transferred from the air to the water. This is once again included in the simulation with a heat exchanger. Afterwards the water passes the external heat exchanger of the WDU. In this heat exchanger the water is heated up with an external heat source to the maximum saltwater temperature in the system. It leaves the external heat exchanger and rains down in the evaporating chamber. At the top of this chamber once again a heat exchanger is included, because at this point the saltwater has a higher temperature than the air and therefore the energy is transferred in contrast to the condensations chamber from the saltwater to the air. Then it passes a flow diverter, which splits the saltwater flow into two different volume flows. The one volume flow is injected into the cold saltwater stream, which is in the right chamber and the other volume flow continues its way inside the WDU. The flow diverter is adjustable and therefore it can be calculated with

$$m_1 = m_2 + m_3 = am_1 + bm_1 = am_1 + (1-a)m_1 \tag{6.49}$$

where m_1 is the mass of the incoming volume flow in a short time period and m_2 and m_3 the leaving masses of the two volume flows in the same time interval. It is valid $a + b = 1$. The temperatures are the same for all volume flows. As was mentioned before, one volume flow is injected into the incoming saltwater stream and the other stream leaves the WDU, but first the leaving saltwater flow once again passes another heat exchanger. At the bottom of the evaporation chamber the water is again warmer than the air and therefore the energy is transferred from the water to the air.
The flow direction of the external heat source (red line) is also plotted in Fig. 6.6. It enters the external heat exchanger on the left, it runs through it and leaves it on the right. Afterwards the leaving water will be heated up again by the solar thermal roof and can be reused. This was already described in section 4.2.
Inside the WDU the air is on a counter flow compared to the saltwater. In Fig. 6.6 the path is depicted in green and the arrows show the direction of the volume flows. It starts in the left chamber at the bottom with the minimum temperature $T_{L,1}$. It is heated up by the saltwater and streams to the top. On the one hand it gets its velocity from the ventilator at the bottom and the other hand warmer air raises due to the density differences and therefore it is accelerated. As can be seen in section 6.3 the difference is not insignificant. Therefore a density correction is included in the simulation for the air, this was done in contrast to the saltwater, because for liquids it is not so important as can be seen in section 6.2. It is included at the top of the left chamber. At the top of the chamber the air is transferred from the evaporation chamber to the condensation

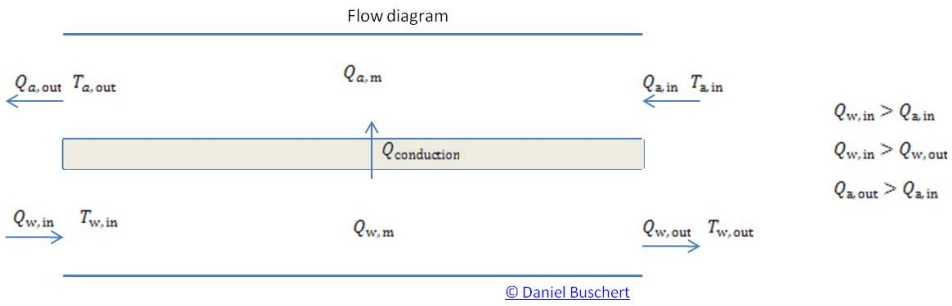

Fig. 6.7.: Model of a counter flow heat exchanger with different input and output variables.

chamber. In the right chamber the air cools down and drops to the bottom. At the bottom the air is again blown with the ventilator from the right chamber to the left chamber and the path starts again.
Meanwhile the saltwater evaporates in the left chamber of the WDU and rises with the air to the top of this chamber. The air is the supporting medium for the transportation. Only water evaporates in the left chamber, but the salt stays in the liquid water and leaves the WDU with the saltwater. Saltwater with a higher salt content is also called brine. It leaves the WDU and must be depolluted. The path of the freshwater in Fig. 6.6 is plotted in black. At the bottom the air has a very low humidity and at the top the humidity reaches the maximum of 100 %, but the temperature is higher compared to the bottom. Therefore more water can be stored in the air, because the possibility to store evaporated water depends on the temperature. It is described with (3.42). The air passes a channel from the left to the right chamber. In the entire right chamber the temperature is lower than in the left chamber, therefore the air cools down and releases the stored energy to the saltwater. Besides the cooling of the air the water condenses as freshwater. Due to the beginning velocity and the lower temperature of the air, the air drops to the bottom. The condensed water streams to the ground of the condensation chamber and leaves it as usable freshwater. Afterwards it can be used as normal freshwater, but it must be accumulated with trace elements first. The purity of the freshwater is very high and the drinking of this water can induce deficiency symptoms. The calculation for the production of freshwater is done in one of the next sections.

6.5.1. Heat exchangers

In the following section the modelling of the heat exchangers is discussed. It can be calculated with the conservation of energy. For this the system is observed in a way that there is no interaction with the environment. In the whole system, as shown in Fig. 6.6, there are only counter flow heat exchangers. An overview of different variables for the heat exchanger can be found in Fig. 6.7. The fluid with the higher temperature $T_{w,in}$ enters the heat exchanger at the left, runs through the whole heat exchanger and

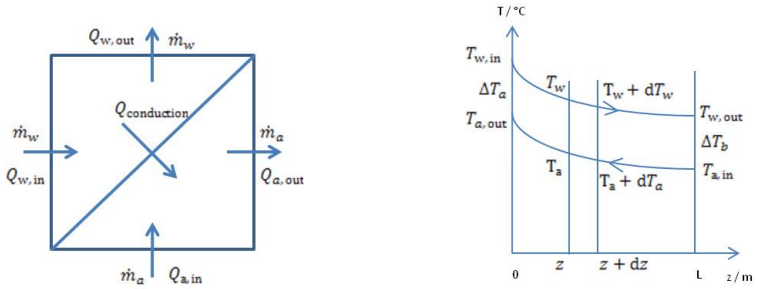

(a) (b)

Fig. 6.8.: a) Energy transfer in a counter flow heat exchanger with input and output variables. b) Temperatures in a counter flow heat exchanger.

passes it on the right with a lower temperature $T_{w,out}$. In contrast to the first fluid, the other fluid enters the heat exchanger on the right with a lower temperature $T_{a,in}$, flows through the whole heat exchanger and leaves it on the left with a higher temperature $T_{a,out}$. The entering heat source on the left has the thermal energy $Q_{w,in}$ and leaves it with the lower energy $Q_{w,out}$. The other fluid has the energy $Q_{a,in}$ at the beginning and the higher energy $Q_{a,out}$ at the end. During the transportation of these fluids through the heat exchanger, the energy $Q_{conduction}$ is transferred from the hot fluid through the dividing wall to the colder fluid. Inside the heat exchanger in a static situation the stored energy is $Q_{a,m}$ and $Q_{w,m}$, which is constant during the operation. During the initialisation the following general condition are given $Q_{w,in} > Q_{a,in}$, $Q_{w,in} > Q_{w,out}$ and $Q_{a,out} > Q_{a,in}$. A different illustration can be found in Fig. 6.8a. In this figure the different energies are listed and additionally the mass flows are shown, which flow through the heat exchanger. The mass flow in the heat source is $\dot{m}_w$ and the mass flow in heat sink is $\dot{m}_a$. The continuity equation (3.34) is valid, because the mass flow, which enters the heat exchanger, will also leave it and it will not disappear inside the heat exchanger. This is valid for the sink and the source. During the transfer through the heat exchanger the energy $Q_{conduction} = Q_{cond}$ is conducted from the one side to the other side. Both fluids are separated by a wall, which only allows the conduction of thermal heat. A mass transport is not possible. Fig. 6.8b shows the temperature distribution in the heat exchanger $T_{i,in}$ and $T_{i,out}$, where i is either w or a. The temperature distribution is as expected. $T_{w,out} > T_{a,in}$ and $T_{w,in} > T_{a,out}$. Furthermore it is also valid for a non-idealised heat exchanger, that it is $T_{w,in} > T_{a,out}$ and $T_{w,out} > T_{a,in}$. For an idealised counter flow heat exchanger the $>$ can be exchanged with $\geq$, but the final temperatures depend on the heat capacities, the volume flows of the fluids and the heat exchanger material and its arrangement [Bae08]. For later realisations the temperature differences $\triangle T_a = T_{w,in} - T_{a,out}$ and $\triangle T_b = T_{w,out} - T_{a,in}$ are very important. The relation between the stored energy and mass in a defined temperature area is

$$Q = c_p m \triangle T, \tag{6.50}$$

where c_p is the heat capacity of the fluid and $\triangle T = T_2 - T_1$ is the difference of the temperature ranges. In this simulation only two different heat capacities are used:

$$c_{p,w} = 4185 \frac{\mathrm{J}}{\mathrm{kg\,K}} \tag{6.51}$$

$$c_{p,l} = 1003 \frac{\mathrm{J}}{\mathrm{kg\,K}} \tag{6.52}$$

Where $c_{p,w}$ is the heat capacity of water and $c_{p,l}$ is the heat capacity of air. The difference in the heat capacity in saltwater and freshwater is disregarded due to the low amount of salt in the water. Due to the conservation of energy the equations for the two volume flows can be written as:

$$Q_{w,out} = Q_{w,in} - Q_{cond} \tag{6.53}$$

$$Q_{a,out} = Q_{a,in} + Q_{cond} \tag{6.54}$$

The intrinsic energy (6.50) of fluids will be rewritten for later usage. With this adaption the following equations will be much easier, because less terms must be considered. For the next calculations the intrinsic energy (6.50) corresponds to absolute zero at $T_a = 0\,\mathrm{K} = -273.15\,^{\circ}\mathrm{C}$ and therefore (6.50) can be written as

$$Q = c_p m(T_2 - T_a) = c_p m T_2. \tag{6.55}$$

With the examination of one volume flow inside the heat exchanger the following equation can be assembled

$$Q_{in} = Q_m + Q_{out} + Q_{cond}, \tag{6.56}$$

where Q_{in} is the energy of the entering flow, Q_m is the energy stored in the heat exchanger with the mass m_m, Q_{out} is the energy, which leaves it and Q_{cond} is the energy, which is transferred from or to this fluid. In this case the energy Q_{cond} can be positive or negative, if it is positive it is an energy donator based on Q_{in} and if it is negative, it is an energy acceptor. With (6.55) it can be rewritten as

$$c_p m_{in} T_{in} = c_p m_m T_m + c_p m_{out} T_{out} + Q_{cond} \tag{6.57}$$

For the time dependency this equation is derived in time t. The heat capacities in this derivation are constant. The other terms will be evaluated below and it is now:

$$c_p \dot{m}_{in} T_{in} + c_p m_{in} \dot{T}_{in} = c_p \dot{m}_m T_m + c_p m_m \dot{T}_m + c_p \dot{m}_{out} T_{out} + c_p m_{out} \dot{T}_{out} + \dot{Q}_{cond} \tag{6.58}$$

In the static situation the heat exchanger is filled with water and therefore it is $\dot{m}_m = 0$. Furthermore in this situation the input and output temperatures are constant and they will not vary during the operation. Therefore the derivation in time for the inlet temperature $\dot{T}_{in}$ and the outlet temperature $\dot{T}_{out}$ disappear. $\dot{T}_m$ varies in the heat exchanger over the time and location and therefore it appears in the equation. Additionally mass flows $\dot{m}_{in}$ and $\dot{m}_{out}$ are not zero, because the characteristic of the heat exchanger depends on it. Now the equation is

$$c_p \dot{m}_{in} T_{in} = c_p m_m \dot{T}_m + c_p \dot{m}_{out} T_{out} + \dot{Q}_{cond}. \tag{6.59}$$

This equation can be simplified with the continuity equation (3.34). It is $\operatorname{div} \vec{j} = 0$, because the whole fluid, which enters the heat exchanger, will also leave it and due to the relative constant water density (Tab. C.9) it can be summarised as:

$$\frac{\partial \varrho}{\partial t} = 0 \quad \Rightarrow \quad \varrho = \text{const.} \quad \Rightarrow \quad \dot{m}_{in} = \dot{m}_{out} = \dot{m} \tag{6.60}$$

The final equation for the heat exchanger is now

$$c_p \dot{m} T_{in} = c_p m_m \dot{T}_m + c_p \dot{m} T_{out} + \dot{Q}_{cond} \tag{6.61}$$

and after solving for the heat exchanger's internal variables it is:

$$\begin{aligned} \Rightarrow c_p m_m \dot{T}_m &= c_p \dot{m} T_{in} - c_p \dot{m} T_{out} - \dot{Q}_{cond} \\ &= c_p \dot{m} \left(T_{in} - T_{out}\right) - \dot{Q}_{cond} \end{aligned} \tag{6.62}$$

The heat transfer is described by the power

$$P = \dot{Q}_{cond} = kA \left(T_1 - T_2\right) = kA \vartheta_{cond}, \tag{6.63}$$

where k is the heat transfer coefficient and A is the corresponding area. ϑ_{cond} is the operation characteristic, which depends on the temperature in the corresponding volume elements in the one side and the other side of the heat exchanger. It will be discussed in the next subsection. Now the equations for the heat exchangers are given. For the heat emission side it is

$$c_p m_m \dot{T}_m = c_p \dot{m} \left(T_{in} - T_{out}\right) - kA \vartheta_{cond} \tag{6.64}$$

and for the heat absorption side it is

$$c_p m_m \dot{T}_m = c_p \dot{m} \left(T_{in} - T_{out}\right) + kA \vartheta_{cond}. \tag{6.65}$$

The temperature rate of change $\dot{T}_m$ is incapable of measurement. This problem in the simulation can be solved in a way that $\dot{T}_m$ can be exchanged with $\dot{T}_{out}$, because the $\dot{T}_m$ reaches the specific outlet temperatures $\dot{T}_{out}$ in the heat exchanger. With the labelling like in Fig. 6.7 both equations are:

$$\frac{\mathrm{d}T_{w,out}}{\mathrm{d}t} = \frac{\dot{m}_w}{m_{w,m}} \left(T_{w,in} - T_{w,out}\right) - \frac{kA}{c_{p,w} m_{w,m}} \vartheta_{cond} \left(T_{w,in}, T_{w,out}, T_{a,in}, T_{a,out}\right) \tag{6.66}$$

$$\frac{\mathrm{d}T_{a,out}}{\mathrm{d}t} = \frac{\dot{m}_a}{m_{a,m}} \left(T_{a,in} - T_{a,out}\right) + \frac{kA}{c_{p,a} m_{a,m}} \vartheta_{cond} \left(T_{w,in}, T_{w,out}, T_{a,in}, T_{a,out}\right) \tag{6.67}$$

Right now it can be seen, that a system of differential equations must be solved to calculate the output temperatures from the heat source and the heat sink. Another problem is, that ϑ_{cond} depends on the different input and output temperatures. In the next section the work characteristic of this variable is analysed.

Work characteristic

The calculation of the work characteristic is based on [Bae08]. It is calculated with the analysis of the temperature profile in a heat exchanger. For this calculation Fig. 6.8b is considered. The temperatures depend on the z coordinate of the heat exchanger and the flow direction. At the position z the temperature in the one fluid is T_1 and in the other fluid T_2. At $z + \mathrm{d}z$ is the temperature $T_1 + \mathrm{d}T_1$ or $T_2 + \mathrm{d}T_2$. With the main theorem the heat flow for the two different volume elements at the position z through the infinitely small area $\mathrm{d}A$ can be calculated with (6.50):

$$\mathrm{d}\dot{Q} = -\dot{m}_w c_{p,w}\,\mathrm{d}T_w = -\dot{W}_w\,\mathrm{d}T_w \tag{6.68}$$

$$\mathrm{d}\dot{Q} = -\dot{m}_a c_{p,a}\,\mathrm{d}T_a = -\dot{W}_a\,\mathrm{d}T_a \tag{6.69}$$

$\dot{W}_i$ is the heat capacity rate for $i \in \{a,\, w\}$

$$\dot{W}_w := \dot{m}_w c_{p,w}, \tag{6.70}$$

$$\dot{W}_a := \dot{m}_a c_{p,a} \tag{6.71}$$

and $\mathrm{d}T_i$ is the infinitesimal change of the temperature at both points. The $\mathrm{d}\dot{Q}$ is eliminated with the valid approach for the heat transfer [Ger02]

$$\mathrm{d}\dot{Q} = k\,(T_w - T_a)\;\mathrm{d}A = kA\,(T_w - T_a)\,\frac{\mathrm{d}z}{L}. \tag{6.72}$$

It is only a valid equation in case that the temperature difference is small. If the temperature difference is larger, the radiative procedure must be calculated with the Stefan-Boltzmann-equation with the difference between the radiative power of the one fluid $P_w = A\sigma T_w^4$ and the radiative reflection power of the other fluid $P_a = A\sigma T_a^4$. It is $\sigma = 5.7 \cdot 10^{-8}\,\mathrm{W/(m^2\,K^4)}$ the Stefan-Boltzmann-constant. In this case the temperature differences are below 100 °C and therefore the first equation can be used. With (6.68) and (6.69) it can be written as:

$$\mathrm{d}T_w = -\,(T_w - T_a)\,\frac{kA}{\dot{W}_w}\frac{\mathrm{d}z}{L} = -\,(T_w - T_a)\,N_w\frac{\mathrm{d}z}{L} \tag{6.73}$$

$$\mathrm{d}T_a = -\,(T_w - T_a)\,\frac{kA}{\dot{W}_a}\frac{\mathrm{d}z}{L} = -\,(T_w - T_a)\,N_a\frac{\mathrm{d}z}{L} \tag{6.74}$$

N_i is the Number of Transfer-Units (NTU) with

$$N_w := \frac{kA}{\dot{W}_w} \quad \text{and} \quad N_a := \frac{kA}{\dot{W}_a}. \tag{6.75}$$

For the calculation of the work characteristic, the difference of (6.73) and (6.74) is calculated and afterwards this equation is divided by $T_w - T_a$

$$\frac{\mathrm{d}\,(T_w - T_a)}{T_w - T_a} = (N_a - N_w)\,\frac{\mathrm{d}z}{L}. \tag{6.76}$$

After integration from the beginning of the heat exchanger $z = 0$ to the end $z = L$ it is

$$\ln\left(\frac{(T_w - T_a)_L}{(T_w - T_a)_0}\right) = \ln\left(\frac{T_{w,out} - T_{a,in}}{T_{w,in} - T_{a,out}}\right) = N_a - N_w. \tag{6.77}$$

The first equal sign is justified with the evaluation of Fig. 6.8b and the frame condition at $z = 0$ and $z = L$. For a later calculation the logarithm is evaluated. It is valid

$$\frac{T_{w,out} - T_{a,in}}{T_{w,in} - T_{a,out}} = \frac{T_{w,in} - T_{a,in} - (T_{w,in} - T_{w,out})}{T_{w,in} - T_{a,in} - (T_{a,out} - T_{a,in})} = \frac{1 - \epsilon_w}{1 - \epsilon_a} \tag{6.78}$$

with the simplifications

$$\epsilon_w := \frac{T_{w,in} - T_{w,out}}{T_{w,in} - T_{a,in}} \quad \text{and} \quad \epsilon_a := \frac{T_{a,out} - T_{a,in}}{T_{w,in} - T_{a,in}}. \tag{6.79}$$

These equations are unit-free measures and reflect the temperature change of both fluids in the heat exchanger. Only unit-free measures are sufficient to calculate many important state variables in the thermodynamic. The two equations link the input temperatures and the output temperatures with the temperature differences of the heat exchanger input temperatures.
For the next calculation (6.68) and (6.69) are again considered. Due to a closed system, the energy, which is released from one fluid, is absorbed by the other fluid. Therefore this equations can be written as

$$\dot{Q} = \dot{W}_w \left(T_{w,in} - T_{w,out}\right) = \dot{W}_a \left(T_{a,out} - T_{a,in}\right). \tag{6.80}$$

Based on Fig. 6.8b two terms must be swapped and in this version all terms have the same sign. With (6.63) it can be summarised

$$\dot{Q} = kA\vartheta_{cond} = \dot{W}_w \left(T_{w,in} - T_{w,out}\right) = \dot{W}_a \left(T_{a,out} - T_{a,in}\right) \tag{6.81}$$

and it is here

$$\vartheta_{cond} := \frac{1}{A}\int_A (T_w - T_a)\,\mathrm{d}A. \tag{6.82}$$

In this case, ϑ_{cond} is the mean temperature in the heat exchanger of the corresponding volume elements with the local temperature differences $T_w - T_a$. At the moment it is not possible to calculate this value, because the temperature differences are unknown. Therefore another possibility must be found to estimate the mean temperature difference ϑ_{cond}. For this (6.81) is divided by kA and $T_{w,in} - T_{a,in}$

$$\frac{\vartheta_{cond}}{T_{w,in} - T_{a,in}} = \frac{\dot{W}_w}{kA}\frac{T_{w,in} - T_{w,out}}{T_{w,in} - T_{a,in}} = \frac{\dot{W}_a}{kA}\frac{T_{a,out} - T_{a,in}}{T_{w,in} - T_{a,in}} \tag{6.83}$$

This can be written with the new unit-free measure

$$\Theta := \frac{\vartheta_{cond}}{T_{w,in} - T_{a,in}}. \tag{6.84}$$

It can be simplified with (6.75) and (6.79) as

$$\Theta = \frac{\epsilon_w}{N_w} = \frac{\epsilon_a}{N_a}. \tag{6.85}$$

Now the difference of N_a and N_w can be calculated:

$$\begin{aligned} N_a - N_w &= \frac{\epsilon_a - \epsilon_w}{\Theta} = \frac{T_{a,out} - T_{a,in} - (T_{w,in} - T_{w,out})}{\vartheta_{cond}} \\ &= \frac{T_{w,out} - T_{a,in} - (T_{w,in} - T_{a,out})}{\vartheta_{cond}} \end{aligned} \tag{6.86}$$

With (6.77) the final version of the mean temperature difference in the heat exchanger between both fluids is now

$$\vartheta_{cond} = \frac{T_{w,out} - T_{a,in} - (T_{w,in} - T_{a,out})}{\ln\left(\frac{T_{w,out} - T_{a,in}}{T_{w,in} - T_{a,out}}\right)}. \tag{6.87}$$

This is the so-called logarithm mean and as can be seen the temperature behaviour of the heat exchanger depends only on the input and output temperatures of the two fluids. Furthermore this equation is symmetric in the output and input temperatures. With this equation the model of the heat exchanger is complete and the whole model of the heat exchanger can now be summarised:

$$\frac{\mathrm{d}T_{w,out}}{\mathrm{d}t} = \frac{\dot{m}_w}{m_{w,m}}\left(T_{w,in} - T_{w,out}\right) - \frac{kA}{c_{p,w}m_{w,m}}\vartheta_{cond}\left(T_{w,in}, T_{w,out}, T_{a,in}, T_{a,out}\right) \tag{6.88}$$

$$\frac{\mathrm{d}T_{a,out}}{\mathrm{d}t} = \frac{\dot{m}_a}{m_{a,m}}\left(T_{a,in} - T_{a,out}\right) + \frac{kA}{c_{p,a}m_{a,m}}\vartheta_{cond}\left(T_{w,in}, T_{w,out}, T_{a,in}, T_{a,out}\right) \tag{6.89}$$

with

$$\vartheta_{cond} = \frac{T_{w,in} - T_{a,out} - T_{w,out} - T_{a,in}}{\ln\left(\frac{T_{w,in} - T_{a,out}}{T_{w,out} - T_{a,in}}\right)} \tag{6.90}$$

As can be seen in this equation of the heat exchanger model, it is a system of ODEs, which cannot be solved analytically, because the $T_{i,out}$ appear in the time derivation and also in the logarithmic mean of the temperature behaviour of the heat exchanger. Therefore only a numerical calculation of the output temperatures $T_{i,out}$ is possible. This model is implemented several times in the WDU model (Fig. 6.6) to calculate the different temperatures inside the WDU. For the implementation different general conditions of the heat exchangers must be considered. If the values are out of range the values must be caught, otherwise the simulation of the heat exchanger ends with an error.

6.5.2. Evaporation and freshwater production

Inside the WDU, the saltwater evaporates in the left chamber and due to the moving air it rises to the top of this chamber. At the top the evaporated water is transported

from the left to the right chamber, where it condenses as freshwater. The condensed freshwater leaves the WDU and it can finally be used. At the bottom the air has a very low temperature and therefore the amount of evaporated water is very low. During the movement of the air from the bottom to the top the air temperature rises. Due to the higher temperature more water can be transported compared to the bottom of the chamber. This was already discussed in section 3.3. Another effect is that the speed inside the WDU rises, as can be seen in section 6.3. The maximum water content of the air depends on the air temperature. The higher the temperature, the higher is the water content. The curve of the maximum water content in dependency of the temperature can be found in the saturation vapour pressure curve in Fig. 3.5 or it can directly be calculated with (3.42). This is the maximum water content in the air, which can evaporate and can be transported with the air. Therefore it can be used to calculate the freshwater output of the WDU. For the calculation of the freshwater output the maximum relative humidity at the bottom and the top is considered and with these values the possible freshwater output is calculable. Only the difference of the water content is condensed as freshwater. The absolute humidity ρ_w can be calculated with

$$\rho_w = \frac{e_s}{R_w T} = \frac{m_w}{V_{tot}}, \tag{6.91}$$

where R_w was already used in (6.41), e_s in (3.42) and V_{tot} is the volume of the transported air. This equation can be solved to m_w and can be evaluated at the top and at the bottom of the WDU. The difference reflects the possible condensed freshwater. During this approximation it is considered, that the relative humidity φ at the bottom and at the top is 100 %

$$\varphi = \frac{\rho_w}{\rho_{w,max}} = 1, \tag{6.92}$$

but due to different temperatures the water contents are different. This principle is included in the model of the WDU to calculate the freshwater output.
The efficiency of the WDU can be raised, if for example the air is dehumidified at the bottom of the WDU. The air temperature has the lowest temperature, but there is still water vapour in it. This water vapour could be extracted and then the efficiency is raised. Afterwards the dehumidified air can be used to transport more evaporated water. In this case the relative humidity φ is below 100 %. Due to (3.42) the difference is slightly, but all in all it is an interesting option.

6.6. Start and end time of the WDU operation

In the following subsection the possible start and end point of the WDU operation is calculated. The problem is that in the morning not enough thermal heat is produced to operate the water desalination unit during the entire time. After sunrise the solar radiation is too low to produce the needed volume flows and temperatures for the operation and for the optimisation and a high efficiency the produced thermal heat should be

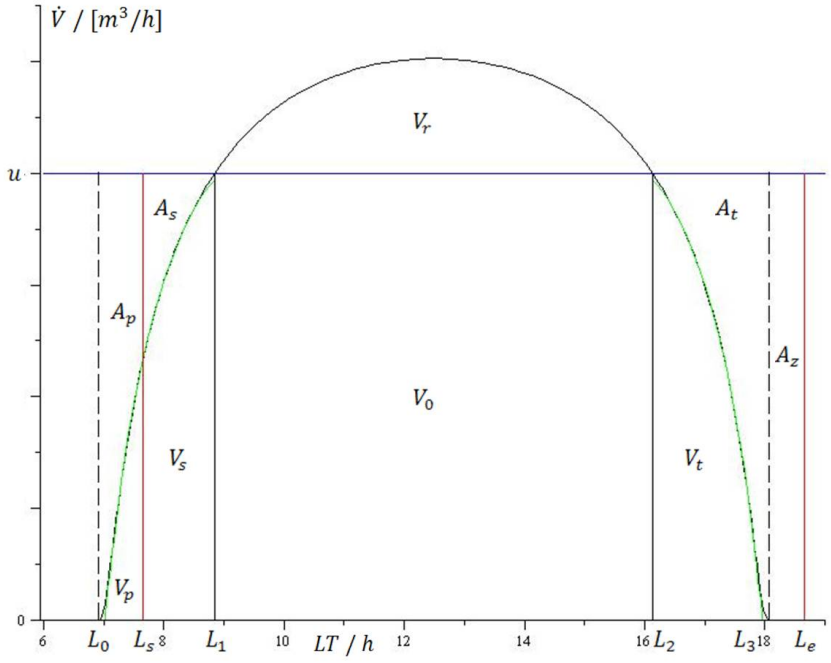

Fig. 6.9.: Calculation of the start and end time of the WDU operation.

buffered for a later usage. The same problem once again occurs before sunset. During this time the volume flow drops, which comes from the solar thermal roof and therefore the surplus energy during the noon time is necessary for the operation of the water desalination unit. A short overview of the behaviour can be seen in Fig. 4.3. For this calculation a symmetric curve like in this figure is advantageous, but the calculation with an unsymmetrical curve is also possible. In the real demonstration plant the curve will have another curve progression, because the Sun does not shine during the whole day. Sometimes there are clouds in the sky or the solar collectors are shadowed. Therefore the following integrals can be exchanged with small sums or a continuous integration method could be used for the calculation of the start and end time, but this is not such a big problem. The real calculation depends on measured data, for the theoretical examination a continuous and easy calculable curve is enough. The curve depends on the solar radiation and therefore a simple modified equation for the solar radiation (3.22) is used as a basic approach. A modified curve for Hurghada was used on the 50^{th} day in the year. The used variables in this section, the assignments and the curves are shown in Fig. 6.9. Due to the high complexity of this curve, the curve segment between sunrise and the intersection with the horizontal line at u is approximated with a Taylor series T_1 with the order 4 and another Taylor series T_2 with the order 4 is also calculated for the curve segment between the intersection of the curve and the horizontal line at u and the sunset:

$$T_1 = -11.93942837 + 1.873565313LT - 1.008855389(LT - 7.874410966)^2 + 0.5289023703(LT - 7.874410966)^3 - 0.2622295839(LT - 7.874410966)^4 \quad (6.93)$$

$$T_2 = 34.85665220 - 1.873565313LT - 1.008855389(LT - 17.10261025)^2 - 0.5289023703(LT - 17.10261025)^3 - 0.2622295839(LT - 17.10261025)^4 \quad (6.94)$$

The needed intersection points in a real plant can for example be taken from the previous days. A different approximation is possible, but it is very difficult, due to different environmental conditions. The previous days can be used, because in minor cases the weather will not completely be different on two consecutive days. The horizontal line at u represents the theoretical energy demand of the WDU. If the produced volume flow and the needed temperature is below this value, it cannot directly be operated and the produced energy must be buffered. At first it is soughed for the starting time L_s. It is the time when enough energy is in the system for a continuous operation of the WDU untill the evening. It can be defined with Fig. 6.9, that the area above the curve and below the horizontal line at u and between sunrise L_0 and L_s is A_p. Below it is V_p. The area above the curve and below the horizontal line at u and between L_s and the intersection with the vertical line L_1 is A_s. Below it is V_s. The total area above the curve and below u and between L_0 and L_1 is $A_{ges} = A_p + A_s$. Below it is $V_{ges} = V_p + V_s$. For a continuous operation the produced energy in the time between L_0 and L_s must be the same as the needed area A_s and therefore the first approach is found

$$A_s = V_p \quad \Rightarrow \quad \int_{L_s}^{L_1} u \, \mathrm{d}LT - \int_{L_s}^{L_1} T_1 \, \mathrm{d}LT = \int_{L_0}^{L_s} T_1 \, \mathrm{d}LT. \quad (6.95)$$

This equation must be solved to L_s and then the starting time of the WDU is approximated. For this example and for $u = 4\,\mathrm{m^3/h}$ the start time of the WDU is at $L_s = 7.66\,\mathrm{h}$. During L_1 and the second intersection with the horizontal line at u (L_2) the produced volume flow of the STR is above the needed volume flow for the WDU operation. The difference between the horizontal line and the curve is the surplus energy V_r, which must be stored for a later operation. It can easily be calculated with

$$V_r = \int_{L_1}^{L_2} IG \, \mathrm{d}LT - \int_{L_1}^{L_2} u \, \mathrm{d}LT, \quad (6.96)$$

where IG is the complete function of the curve. For $u = 4\,\mathrm{m^3/h}$ it is $V_r = 5.33\,\mathrm{m^3}$. The final step is to calculate the end time of the WDU operation L_e. In the last area the surplus energy between L_1 and L_2 can be used to extend the working time of the WDU. The energy, which is produced between L_2 and the sunset L_3, can also be used in this time for the operation of the WDU. The final shut down of the WDU L_e depends on the produced energy at noon time and the curve progression after the second intersection with the horizontal line u. It can easily be calculated, where A_t is the area above the curve and V_t is the area below the curve. Furthermore it is possible, if enough energy is available in the heat storage tanks and additional the consideration of the thermal heat production after the intersection with L_2, that the WDU can be operated between L_3

and L_e. This associated area is called A_z. The working time after L_2 can be calculated with

$$A_t = \int_{L_2}^{L_3} u \, \mathrm{d}LT - V_t, \tag{6.97}$$

where

$$V_t = \int_{L_2}^{L_3} T_2 \, \mathrm{d}LT \tag{6.98}$$

and if enough energy is available the working time after sunset can now be calculated as

$$A_z = V_r - A_t = \int_{L_3}^{L_e} u \, \mathrm{d}LT. \tag{6.99}$$

This equation can again be solved to L_e and then the shut-down time is calculated. If the difference in (6.99) is negative the WDU must be shut down before sunset L_3, because not enough hot water is available in the system. In this example and for $u = 4\,\mathrm{m^3/h}$ the calculated shut down time is at $L_e = 18.66\,\mathrm{h}$. Therefore the whole running time of the WDU is $L_e - L_s = 11\,\mathrm{h}$. Within this time, if the described water desalination unit is used, which has a freshwater output of 209 l/h, a total amount of $V = 2300\,\mathrm{l/d} = 2.3\,\mathrm{m^3/d}$ is possible.

For an optimisation of the WDU it is one good possibility to reduce the hourly demand of hot water. If the needed value is reduced from $4\,\mathrm{m^3/h}$ to $3.5\,\mathrm{m^3/h}$ or even lower than $3\,\mathrm{m^3/h}$ the working time can easily be extended with the same set-up, if the heat storage tanks are large enough. Due to the lower energy demand the system can start much faster and work longer, because less energy is needed in the morning and the amount of the surplus energy in the noon time is much higher. Additionally due to the reduced energy demand a longer operation is possible. As it can be seen in Fig. 6.10 the production of the surplus energy does not increase linearly. Therefore an optimisation in this combination between solar thermal roof and WDU is significant. This can for example be achieved by improving the insulation materials of the WDU and other improvements in efficiencies, such as reducing the output temperatures of the brine and the freshwater. The better the insulation to avoid the heat losses or other actions to increase the efficiency, the better is the possible gain of the WDU.

If the WDU energy demand at 90 °C is reduced from $4\,\mathrm{m^3/h}$ to $3\,\mathrm{m^3/h}$ the working time increases from 11 h to 14.7 h, which is a difference of more than 750 l of freshwater every day and this a real noticeable value. Another possibility is to increase the solar thermal roof. If the STR is increased or optimised the needed volume flows are generated earlier during the day and in the afternoon more hot process water is produced, but it must be buffered for later usage. This additional water can be used to extend the operation after sunset. Another advantage is that the second intersection point is later in the afternoon and therefore the buffered hot water must be tapped later. With this extension the operation time of the WDU can easily be extended.

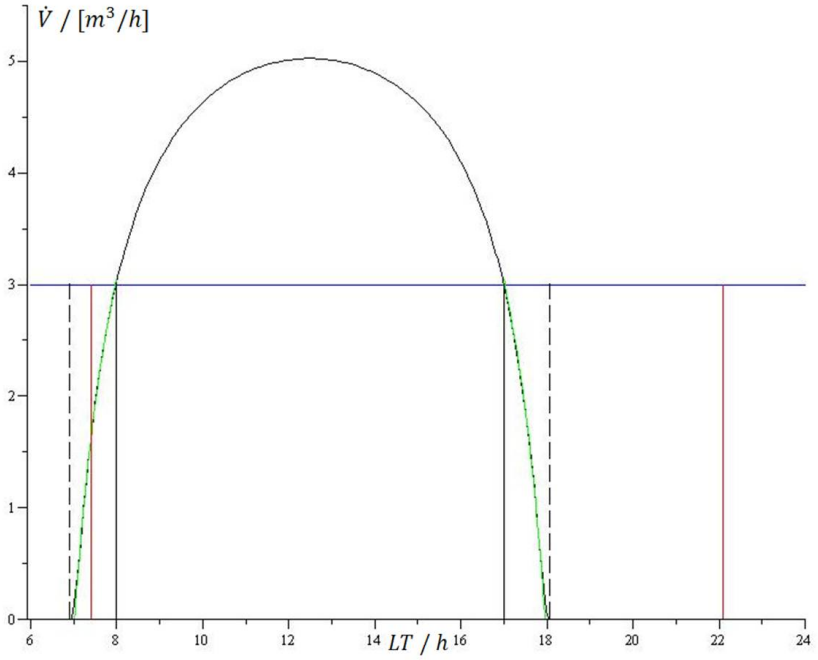

Fig. 6.10.: Enhanced WDU freshwater output for a lower energy demand is essential.

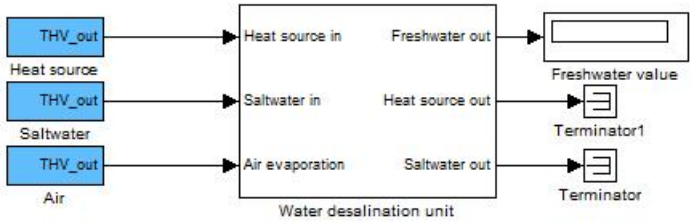

Fig. 6.11.: Overview of the highest level of the WDU simulation with THV input and out vectors and a display.

6.7. Final model of the WDU

In the following section the final model of the WDU is presented. The model was created in Simulink and with the help of Maple. For the implementations of different components only standard Simulink blocks are used. These are for example mathematical operators like multiplication, division and integration blocks. For a better overview the different parts of the simulation are arranged in sub- and subsub-blocks. Fig. 6.11 shows the highest level of the simulated WDU. Inside the white box the complete WDU is simulated. The needed information for the simulation is included in 3 THV vectors, which contain the information for the heat source, the saltwater and the air. With the THV vector for the air the circulation of the ventilator inside the WDU can be modified. The utilised values of the THV vectors for the simulation are only the temperatures and

the volume flows of the external heat source, the air and the saltwater. Furthermore 3 outputs are included into the WDU simulation block. The display shows the exact amount of the produced freshwater, which has been produced during the run, and the other outputs, which are connected with a terminator, are THV vectors for the saltwater output and the heat source output. They contain for example the temperatures and the volume flows of the system after the WDU operation.
Fig. 6.12 shows the next level of the WDU model. It consists of different modules and submodules. The idea of the water desalination model was shown in Fig. 6.6. In this Simulink model different heat exchangers are included. Two heat exchangers can be found in the right part of the model and two at the left. They are the still above-mentioned water / air (W/ A) and the air / water (A / W) heat exchangers. If the water temperature is lower than the air temperature in this figure they are called *Heat exchanger Tw < Ta* and *Heat Exchanger Tw < Ta1*. For the vice versa situation the heat exchangers are called *Heat exchanger Tw > Ta* and *Heat exchanger Tw > Ta1*. At the top there is the 5^{th} heat exchanger, which is shown in Fig. 6.6. This heat exchanger is called *Heat exchanger Water:Water*. It is the external heat exchanger of the WDU, which is used to raise the temperature of the saltwater to its maximum value. At the bottom there is a 6^{th} heat exchanger, which is not shown in Fig. 6.6. This heat exchanger is called *Heat exchanger Water:Water1*. This heat exchanger is justified with the evaporative cooling. During the evaporation the water cools down, as it is normal in nature. It happens for example during sweating[1]. Due to a closed system the heat stays in the system and is transferred from the left side to the right side, because the saltwater evaporates in the left chamber and it condenses as freshwater in the right chamber. Included salt stays in the left chamber and leaves the WDU with the brine. This can be equated with a direct energy transfer between both chambers. This associated heat exchanger is included between the lowest heat exchanger in the right chamber and the bypass on the one hand and on the other hand after the exit of the lowest heat exchanger in the left chamber of the WDU. With this heat exchanger the temperature of the leaving brine can be adjusted. The temperature level and the volume flow characterise the energy, which leaves the WDU and which is lost. The leaving volume flow depends on the incoming water of the WDU, which was shown in section 6.1, and therefore this temperature reflects only the lost energy. This heat exchanger is used to adjust the brine temperature to the real output temperature of the WDU. Additionally a flow diverter and a flow mixer are included in this model. The flow diverter can be adjusted in the range between 0 and 1. For 1 the whole water stays in the system and for 0 the bypass is deactivated. Values higher than a certain level are uninteresting and impracticable, because such a high value increases the stored water inside the system and the water volume could be larger than the storage volume of the complete WDU, but it is a very interesting theoretical approach. The dependency was shown in Fig. 6.2. In this figure and during the simulation the separator is set to 0.5. On the right side of Fig. 6.12 is the already mentioned density correction module and the water production module, as explained in section 6.3. The freshwater production of the WDU is calculated with the

[1] A lot of creatures regulate their body temperature with sweating, this includes humans.

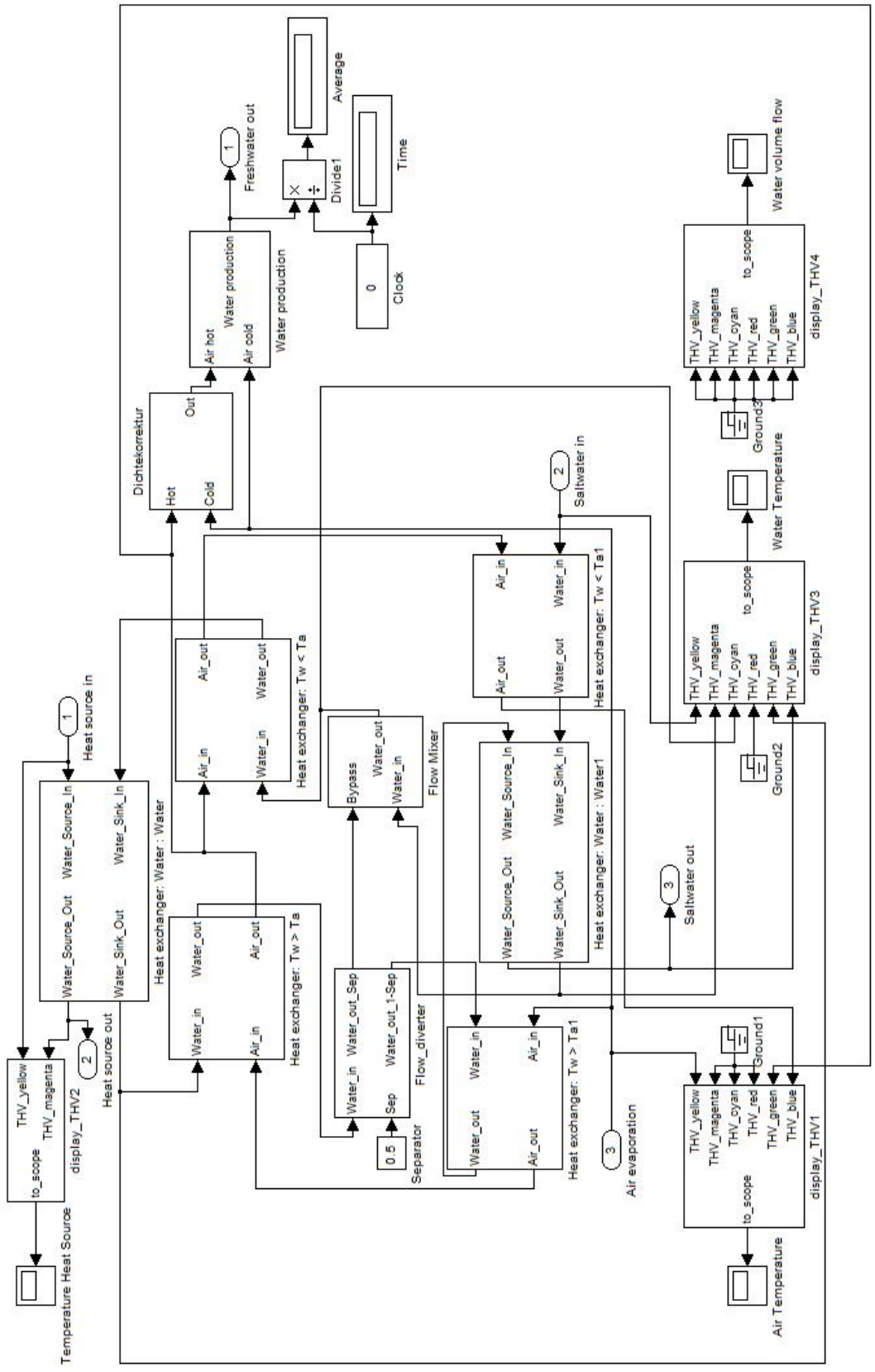

Fig. 6.12.: Model of the WDU, implemented in Simulink with different submodules like heat exchangers, calculation of the freshwater production and control and display modules.

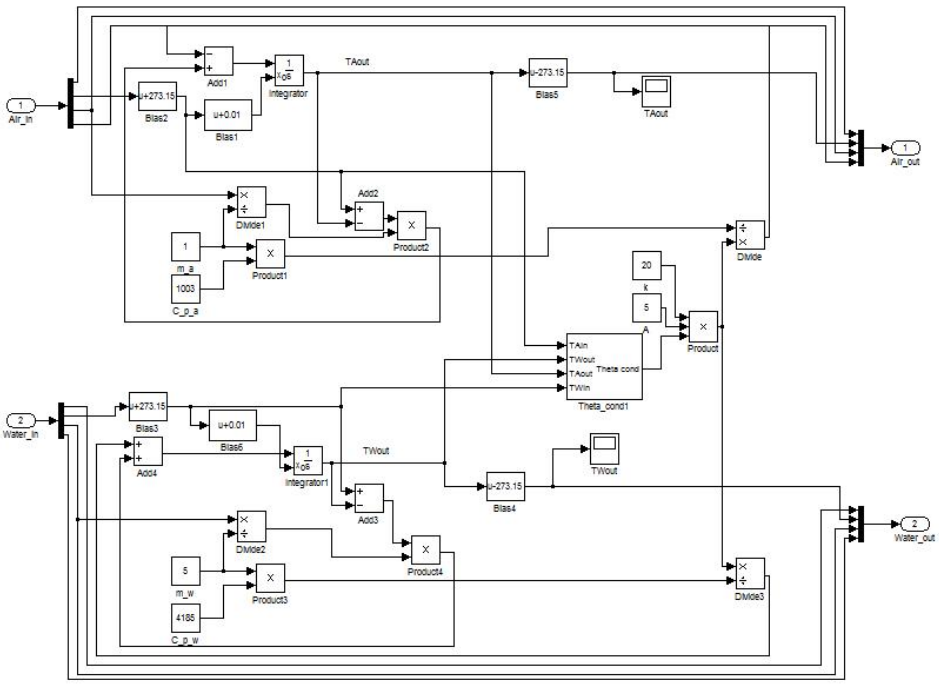

Fig. 6.13.: Model of the heat exchanger, which is used for the simulation of the WDU.

temperature difference and the volume flow of the air at the bottom and at the top. It was described in subsection 6.5.2. Furthermore a few blocks exist to evaluate different connecting vectors. These blocks can for example be used to compare the input and output temperatures of different modules or other states in the system. It is for example used for the external heat exchanger. Other modules are used to show the temperatures of the saltwater or the air at different positions inside the WDU. These modules are included in Fig. 6.12 at the bottom left and the middle. Finally there is also the possibility to show different volume flows inside the system, but in this figure this module is not connected with the other modules. It can be found at the bottom right. At the top right the average of the freshwater is calculated. The oval modules are the inputs and outputs for a higher level. They can be used to transfer the values from a higher level to this level of the model or vice versa.
Fig. 6.13 shows the model of one utilised heat exchanger. The mathematical background was explained above in subsection 6.5.1. It is a system of ODEs with a logarithmic mean in the input and output temperatures. Their constant of integrations is the input variable of the fluids. It was implemented in Simulink with standard mathematical blocks, which are for example modules for integration, multiplication, addition and constant factors. The heat capacities for water and air are directly included in the calculation. This heat exchanger also consists of a submodule for the heat characteristic, which was calculated above in subsection 6.5.1. Fig. 6.14 shows the work characteristic of the heat exchanger. It was also implemented with standard mathematical operators. Furthermore different logical operators are used to come up with the frame conditions of the

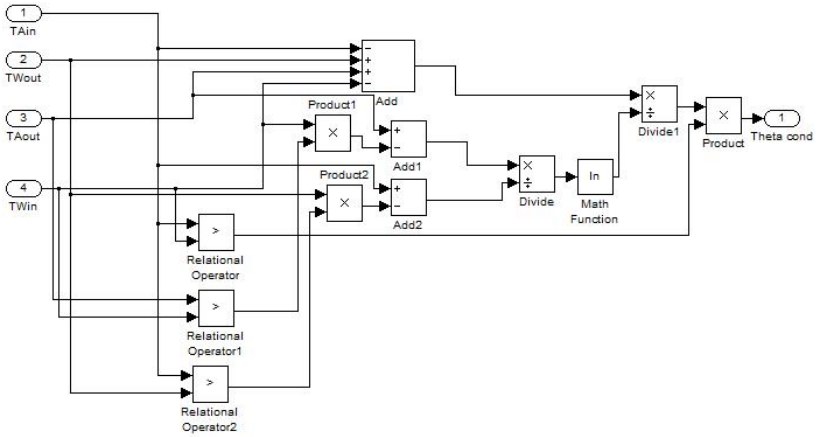

Fig. 6.14.: Work characteristic of the heat exchanger with logical operators.

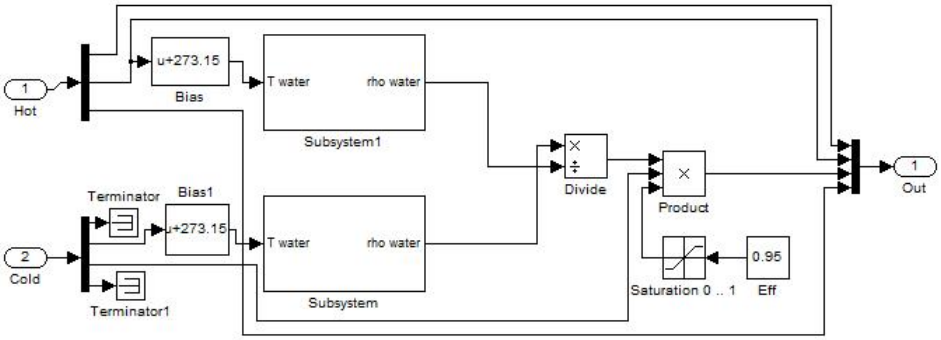

Fig. 6.15.: Density correction of the air for a more exact calculation of the freshwater output.

work characteristic. As input variables the input and output temperatures of the different fluids are needed and it calculates the ϑ_{cond}, which is needed for the linked ODE. Another module, which can be found in Fig. 6.12, is the calculation of the density correction of the air, as was already discussed. It is necessary for the optimisation of the WDU. An overview of this module can be found in Fig. 6.15. This module was included in the simulation, because during the first runs the calculated freshwater output of the WDU model was too low compared to the real desalination unit. With this optimisation a better value during the simulation of the WDU could be reached. This module contains two subsystems, which are equal below the surfaces. Furthermore there is the possibility to adjust the calculation to real values, because in real life there are a lot of physical losses included in the system. The included submodule for the density correction can be found in Fig. 6.16. It calculates with the given air temperatures at the bottom or at the top the corresponding densities of water in the air. This model itself consist of another submodule, which is the Groff-Gratch equation, which was introduced in (3.42). An overview of this implemented equation can be found in Fig. 6.17. It contains a lot of basic mathematical blocks and a lot of constants. The equation is again incorporated in Simulink, by combining a lot of different mathematical operators.

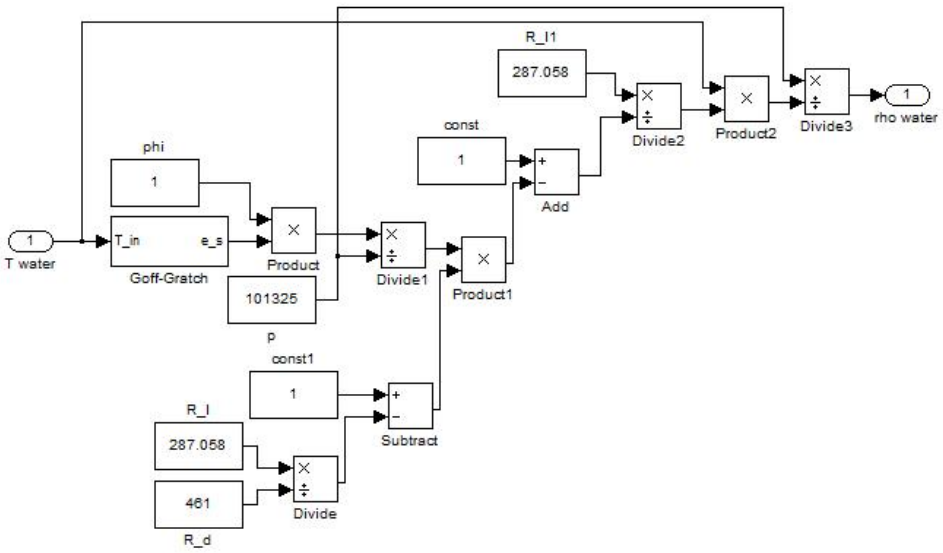

Fig. 6.16.: Calculation of the temperature-dependent density of the air.

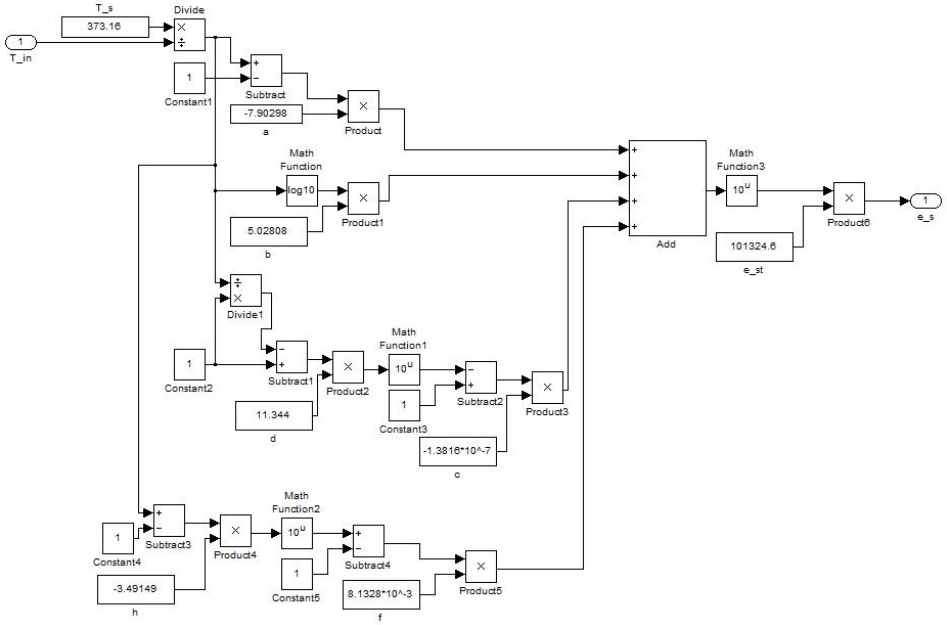

Fig. 6.17.: Goff-Gratch equation implemented in Simulink to calculate the vapour pressure curve of water.

The last module, which is implemented into the simulation of the WDU, is the production of freshwater. It contains one module with different submodules. An overview of the highest level can be found in Fig. 6.18. It calculates the freshwater output in dependency of the volume flows and the temperatures of the air. This is done with the temperature difference at the bottom and at the top of the WDU. This module includes another submodule, which calculates the temperature-dependent water content in the

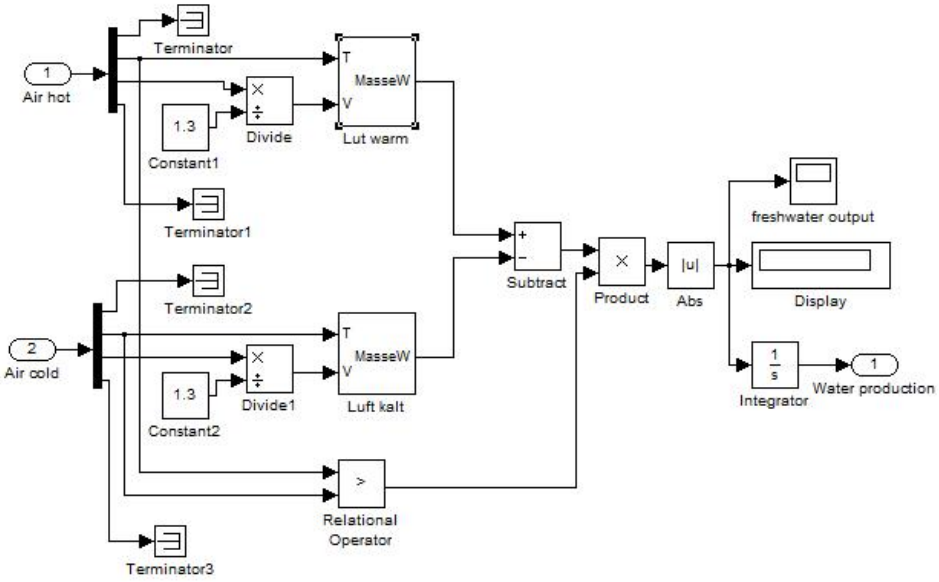

Fig. 6.18.: Calculation of the freshwater production in dependency of the temperatures and the volume flows.

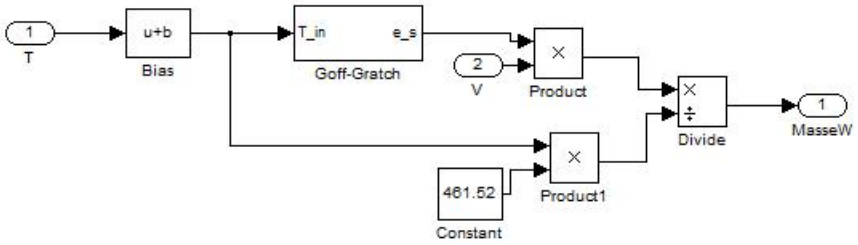

Fig. 6.19.: Calculation of the water content in the air in dependency of the volume flow and the temperature.

air. One module is used for the air at the top, which has a higher temperature and another module is used to calculate it for the colder air, which is at the bottom. An overview of these modules can be found in Fig. 6.19. As can be seen in this figure an already known module is included in this calculation. It is once again the Goff-Gratch-equation. The result of the produced freshwater is extracted to the highest level of the WDU model, but before the average of the freshwater production is calculated at the next higher level. At the highest level the total amount of the freshwater production is shown. The maximum amount is calculated with a continuous integration block.
With this overview the different modules for the simulation of the whole WDU are shown. They were created step by step with the equations, which were presented at the first pages of chapter 6. The modelling of the WDU takes a lot of time, because different solutions for the modelling must be found, which were not available at the University in Soest. Additionally many problems must be solved during the implementation in

Simulink. It was done step by step and when a module was created and checked another module was implemented in the simulation. Finally the model of the WDU was created and the results are very promising. The simulation of this WDU takes a lot of time. For one working hour of the WDU more than 45 min are necessary for the simulation. For a stable and correct simulation the step size must be very small. This is based on the coupled ODEs and the highly complex sub-modules.
During the creation of these modules a crosscheck with the expected results were done and finally they were optimised to reflect the actual water desalination system. A few data came from the real demonstration plant and others came from theoretical considerations during the project life-time with different partners and industrial companies. Additionally the previously calculated solutions were used for the crosscheck.
In the model there are still a lot of different variables available, which can be used to fine-tune the whole simulation of the WDU. Therefore this simulation could be used for later applications and to find additional improvements.

6.8. Simulation of other components

In the following section the model of the solar thermal part is discussed. An overview of the final model can be found in Fig. 6.20. This model of the demonstration plant is based on Fig. 4.1. It was built with the toolbox Carnot [Car10] for Simulink, which is available for Matlab. This toolbox consists of different parts to calculate and simulate different components of heating systems with regards to conventional and regenerative elements. It is organized in blocksets. This toolbox consists of two different libraries, the Carsys and the Carnot blocksets. Carsys can be used for simulations of heating systems with commercially available components and Carnot can be used for more sophisticated simulations and analysis of heating systems. It contains elements, which can be user-defined and includes some basic functions, which facilitate the modelling. Additionally components for Real-Time-Workshop models are also included in this toolbox.
For the Sunwater simulation a few blocksets from the Carnot library were used. The mainly used parts in this simulation are for example the solar thermal roof with the necessary input data, heat storage tanks, pumps and control blocks. Other blocks are also included in this toolbox, but they were not necessary and therefore not included in the simulation of this demonstration plant. In other models they can be used to simulate for example radiators or a room floor heating. Furthermore pipes are also included in this package to simulate connecting pipes. Due to the simulation limitation, the pipes were not considered during this application. Most blocksets can directly be adjusted in the program. This includes the most important general condition, these are for example the initial temperatures or the losses. The settings depend on the kind of the blockset. Other blocksets need an additional input file with necessary simulation data. This is for example the blockset for the solar thermal collector. Without this input file the simulation cannot be started. An overview of the input data for the collectors can be found in Tab. 6.1. For unknown values in this table, it is possible to set the value -9999.

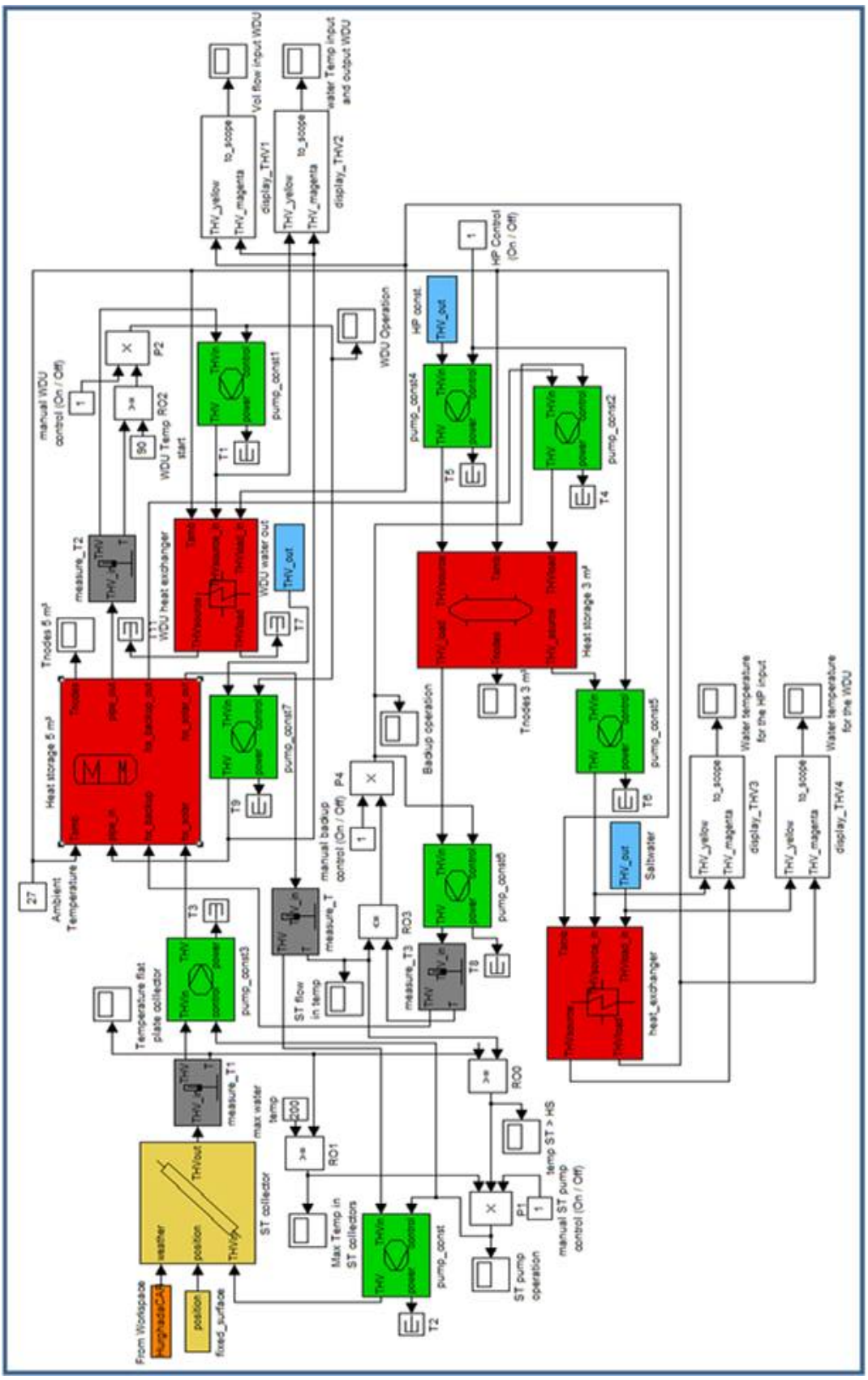

Fig. 6.20.: Final model in Carnot of the solar thermal part of the demonstration plant.

Tab. 6.1.: Weather vector with the needed values for the simulation in Carnot.

Column	Description	Unit
1	time	s
2	timevalue, format YYYYMMDDHHMM	—
3	zenith angle of Sun (at time, not averaged)	°
4	azimuth angle of Sun (0° south, east negative)	°
5	incidence angle on surface (0° vertical)	°
6	direct solar radiation on surface	W/m^2
7	diffuse solar radiation on surface	W/m^2
8	ambient temperature	°C
9	radiation temperature of sky	°C
10	relative humidity	%
11	precipitation	m/s
12	cloud index (0 no cloud, 1 covered sky)	—
13	station pressure	pascal
14	mean wind speed	m/s
15	wind direction (0° north, 270° west)	°
16	incidence angle in plane of vertical and main surface axis	degree
17	incidence angle in plane of vertical and second surface axis	°

It is used for a few values in the simulation database, but it makes no sense to set the most important data to this value. These are for example the daily solar radiation or other weather conditions. An overview of the simulation data can be found in Tab. C.10. The needed values for the simulation are included into one file, which must be opened in Matlab. Due to the high variability of this toolbox, it was chosen for the simulation of the solar thermal part, although it was not programmed for this kind of application. It was adapted to this kind of project, because it is a good basic engineering concept. During the simulation of the demonstration plant many problems had to be solved, but they were ultimately solved.
For the simulation data different sources were tapped to get the needed data. Some information were bought from a weather institute [Met09] and other information were taken from a weather service in the internet [Wet09]. An overview can be found in the annex C, but not all needed figures could be found, especially at the beginning of the project. Therefore a simulation for the global solar radiation in W/m^2 was necessary. The difficult calculation of the solar radiation in W/m^2 can be found in section 3.1. All

values for the simulation must be given exactly on the hour. Estimated and mean values cannot be used for the simulation. The simulation of the solar radiation was used to get exact values at the desired time. The file was created as explained in the guide. The data for the simulation with Carnot can be found in Tab. C.10. Furthermore another input for the solar collectors was necessary, which includes the azimuth, slope and rotation of the solar collectors. The best values for the simulation were previously estimated and then entered into the appropriated blocks. Other values of the solar collectors were changed directly in the collector's block. These are for example the size of the solar collectors, the optical efficiency, different loss coefficients and the initial temperature.
Another important component, which is included in the model of the solar thermal part, is a heat storage tank, which can be found in Fig. 6.20 at the top in the middle. For the simulation one heat storage tank with $5\,m^3$ was used. In the block different parameters can be changed and adjusted to the given situation. These are for example the diameter, initial temperature and the heat loss coefficients. Furthermore the number of nodes can be changed for the simulation. Nodes reflect the amount of layers during the simulation. Another heat storage tank with just $3\,m^3$ can be found at the bottom right in Fig. 6.20. This storage tank was considered as a buffer tank for the heat pump, which was planned at the beginning of the project. In contrast to the other storage tank, this storage tank has only 2 inputs and outputs. In contrast to this heat storage tank the other has 3 inputs and outputs. Both tanks are theoretically connected in this model with pipes. Furthermore the ambient temperature must be set for the simulation of the heat storage tank. For this simulation a constant temperature of $27\,°C$ during the whole day was used. This value reflects a mean basic condition at the building site. During the day it is hotter and during the night it is below the used temperature.
On the smaller heat storage tank a modelled heat pump was connected. This heat pump was implemented in this simulation to show, if it is possible to use a waste heat heat pump for the operation of the WDU or to extend the working time of the demonstration plant. Due to problems in the Carnot toolbox with the included heat pump, a modelled heat pump was added in this model of the demonstration plant. It was just modelled with a constant and very low volume flow, which was controllable with a pump. This heat pump has just a constant flow temperature of $90\,°C$. The technical values for this heat pump came from a German heat pump manufacturer [The10], which can produce the needed heat pumps. The high temperature heat pumps are still under development and they are very expensive at the moment. Therefore it was on the one hand not included into the project and on the other hand there was unfortunately the problem, that the support for the pump was not given all the time, especially in a foreign country.
Additionally a heat exchanger was implemented in the model of the solar thermal part to check, if this heat pump can be operated in the system. The reason is that the returning volume flow (heat sink) to the heat pump must be below a certain level. Otherwise it cannot be operated. The heat exchanger shown at the bottom left is used to reduce the incoming heat sink temperature for the heat pump. The energy is transferred from the solar thermal part to the saltwater, which is used for the desalination and therefore it is not lost in the system. The innovative idea of the heat pump is again that it uses the stored energy in the brine and thus an increase in efficiency is possible. During differ-

Tab. 6.2.: Components of the THV vector in Carnot [Car10].

No.	Description	Abbreviation	Units	Remarks
1	flow identifier	flow-ID	—	set by the simulation
2	temperature	T	°C	
3	mass flow	mdot	kg/s	
4	pressure	p	Pa	
5	fluid type	fluid-ID	—	set in the pump
6	mixture of fluid	fluid-mix 0..1	—	set in the pump
7	diameter last piece	c	m	
8	const. coeff. press. drop	l	—	
9	linear coeff. press. drop	q	s/kg	
10	quadratic press. drop	dpqua	s^2/kg^2	
11	not used			
⋮	⋮			
20	not used			

ent simulations it was seen, that such a heat pump can be used to extend the working time of the demonstration plant. In later realisations such an implementation is a very interesting aspect.
The water flow inside the pipes can be controlled with pumps. They can be switched off and on and furthermore the volume flow can be adjusted in the blocks itself. The pumps are necessary to circulate the water inside the solar thermal part. The control of the pumps were combined with logical operators. They will only be activated if a special frame condition is reached. For example the output temperature of the solar collector must be higher than the input temperature otherwise the pump is switched off. Other frames are needed to control the other pump in the system. This is the heat delivery pump for the WDU or the pump for the included heat pump.
All components in the system like the storage tanks, pumps heat exchangers are connected with vectors, which are called Thermo-Hydraulic Vector (THV). These vectors contain the needed parameters for the simulation. An overview of the THV's structure can be found in Tab. 6.2. Additionally different other components are included in the model of the solar part of the demonstration plant. These are for example blocks to extract the fluid temperatures or blocks with logical operators to controll the pumps in the system. The logical blocks are necessary, because it makes no sense to pump hot water through the collector, if the output temperature is lower than the input temperature. Furthermore it is also uninteresting to pump water from the smaller heat storage

tank, which is used for the heat pump, to the other heat storage tank, if the temperature is lower. With these simple logical operations the temperature levels for the start and stop values could be set. The logical operations for the pumps were not included in the original Carnot toolbox and therefore it was artificially added in this simulation. During a few runs the different logical operations were optimised to get the best results.
Other blocks are used to extract the needed values for the analysis or to store the simulation results in different files or in Matlab. The files could be evaluated in other programs like Maple or Excel. With these programmes different simulation results can be combined in one graph for a better and faster analysis. With this analysis the best opportunity for a realisation of the demonstration plant is possible. Additionally different set-ups of the demonstration plant can be played through and finally the best realisation can be chosen for a new and better realisation.
With this model of the demonstration plant it is possible to simulate different working conditions. It is for example possible to deactivate the heat pump, the bye-pass between both systems and / or the STR. Additionally it is possible to adjust the system to different frame conditions. This starts with the adjustment of the heat storage tanks or the size of the solar thermal roof. Furthermore different weather conditions can be used in different simulations. Therefore the model can be used for a wide area of applications.

6.8.1. Simulation of the dynamic and static heat storage tank

The first module is the larger heat storage tank. Its symbol can be found in Fig. 6.20 and a closer view in Fig. 6.21a. The heat storage tank consists of different inputs and outputs. These are for example an input for the ambient temperature, which is a scalar quantity and an output with the temperatures in the different nodes. This output is an ordinary vector, which can easily be displayed. Furthermore different THV input vectors from other blocks can be connected with the heat storage tank and the following blocksets can be connected with this heat storage tank via the THV vectors. They are for example the input and output vectors from and for the solar thermal roof or the connection vectors for a backup system. It could also be a standard heating system. The input vector contains the initial values of the fluid for the calculations and the output vectors contain the results after the calculation. The old values are processed with the blockset and were exported with the new THV vector. This vector can be used as a input vector for another blockset. The heat storage tank is modelled with a multiport one-dimensional node and every node can be calculated with the following ODE

$$\begin{aligned}\rho c\frac{\mathrm{d}T_{\mathrm{node}}}{\mathrm{d}t} = &\frac{U_{\mathrm{loss}}A_{\mathrm{loss}}}{V_{\mathrm{node}}}\left(T_{\mathrm{amb}}-T_{\mathrm{node}}\right)+\frac{\lambda_{\mathrm{eff}}}{d_h^2}\left(T_{\mathrm{node\ above}}+T_{\mathrm{node\ below}}-2T_{\mathrm{node}}\right)\\ &+\frac{c\dot{m}_{\mathrm{up}}}{V_{\mathrm{node}}}\left(T_{\mathrm{node\ below}}-T_{\mathrm{node}}\right)+\frac{c\dot{m}_{\mathrm{down}}}{V_{\mathrm{node}}}\left(T_{\mathrm{node\ above}}-T_{\mathrm{node}}\right)\\ &+\frac{U_{\mathrm{hx}}A_{\mathrm{hx}}}{V_{\mathrm{node}}}\left(T_{\mathrm{hx}}-T_{\mathrm{node}}\right),\end{aligned} \tag{6.100}$$

where:

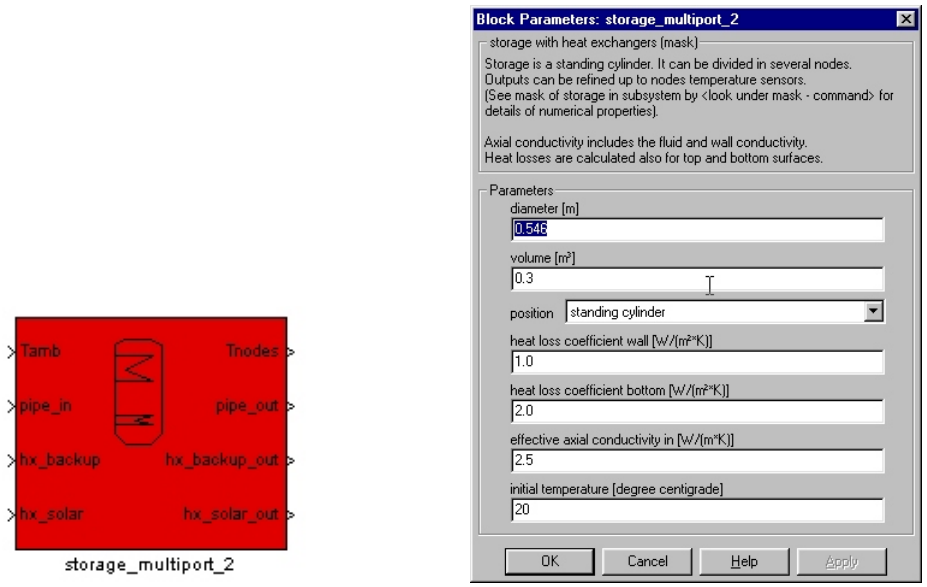

(a) (b)

Fig. 6.21.: a) Symbol of the lager heat storage tank in the Carnot toolbox [Car10].
b) Adjustment of the lager heat storage tank.

Symbol	Used for	Unit
A_{loss}	surface area for losses of one storage node	m^2
A_{hx}	surface area of heat exchanger per storage node	m^2
λ_{eff}	effective axial thermal conduction	$\text{W}/(\text{m}\,\text{K})$
c	heat capacity	$\text{J}/(\text{kg}\,\text{K})$
d_h	distance between two nodes	m
$\dot{m}$	mass flow rate ("up" or "down" is 0 acc. to sum of flowrates)	kg/s
ρ	density	kg/m^3
T	temperature (amb: ambient, hx: heat exchanger, node)	K
t	time	s
U_{loss}	heat loss coefficient	$\text{W}/(\text{m}^2\,\text{K})$
U_{hx}	heat transfer coefficient of heat exchanger	$\text{W}/(\text{m}^2\,\text{K})$
V_{node}	node volume	m^3

Additionally it is possible to change a few parameters in a parameter mask. This mask can be found in Fig. 6.21b. It is for example possible to change the diameter and the volume of the heat storage tank. Additionally different heat loss coefficients and its initial temperature can be adjusted. Due to a huge amount of possibilities this heat storage blockset can be used for a lot of different applications.

The second heat storage tank is similar to this heat storage tank, but instead of three inputs and outputs only two are available. The block parameters are equal to this one and they are also directly included into the calculation and simulation.
For a static situation without a volume flow the temperature decreases with an exponential form. This is for example shown in [Bae08]. The temperature drops in the heat storage tanks with

$$T_F = T_{\text{amb}} + (T_{FO} - T_{\text{amb}}) \exp\left(-\frac{kA}{M_F C_F} t\right). \tag{6.101}$$

The constant fluid in the heat storage tank has the mass M_F and the heat capacity c_F. Under a static situation theses values are constant. It can additionally be seen in this equation, that the heat transfer coefficient k and the surface area A of the heat storage tank have an essential part in the calculation. The lower the value of A and k, the better is it for the heat storage. The temperature drop depends also on the fluid temperature T_F and the ambient temperature T_{amb}. The bigger the difference, the better must be the insulation of the heat storage tank, which has the initial temperature T_{F0}. For $t > 0$ and $t \to \infty$ the temperature reaches the ambient temperature. Further changes can only be reached, if energy is transferred into or from the tank. This can for example be done with cooling or heating.

6.8.2. Simulation of the solar thermal roof

Another module, which was used during the simulation, is the module for the solar thermal collector. In the simulation a flat plate collector was used. The symbol of this collector can be found in Fig. 6.22a. It consist of 3 input vectors and just one THV output vector. The input vectors are a weather vector, which must be prepared before the simulation and it must previously be opened with Matlab, a position vector, which contains the information of the orientation of the flat plate collectors, and finally two THV input and output vectors, which contain the information of the fluid before and after the calculation. A few parameters of the solar thermal roof can be changed directly in the flat plate collector block. The overview of the parameters can be found in Fig. 6.22b. It is possible to change the collector surface, the optical efficiency and different heat loss coefficients. With this huge amount of parameters the flat plate collector module can be adopted to a wide range of different applications.
The parameters have a direct effect during the simulation. The model for the collector is a one-dimensional multinode model. Its parameters are based on real measurements for example collector test results. It is divided into nodes, which can be defined in the parameter overview. During the calculation the water is equally distributed in the risers. The results are calculated with an ODE

$$\begin{aligned} c_{\text{coll}} \frac{\mathrm{d}T}{\mathrm{d}t} = \dot{q}_{\text{solar}} + \frac{\dot{m} \cdot c}{A_{\text{coll}}} (T_{\text{lastnode}} - T) + u_1 (T_{\text{amb}} - T) - u_2 (T_{\text{amb}} - T)^2 \\ + u_{\text{wind}} \cdot v_{\text{wind}} (T_{\text{amb}} - T) + u_{\text{sky}} (T_{\text{sky}} - T), \end{aligned} \tag{6.102}$$

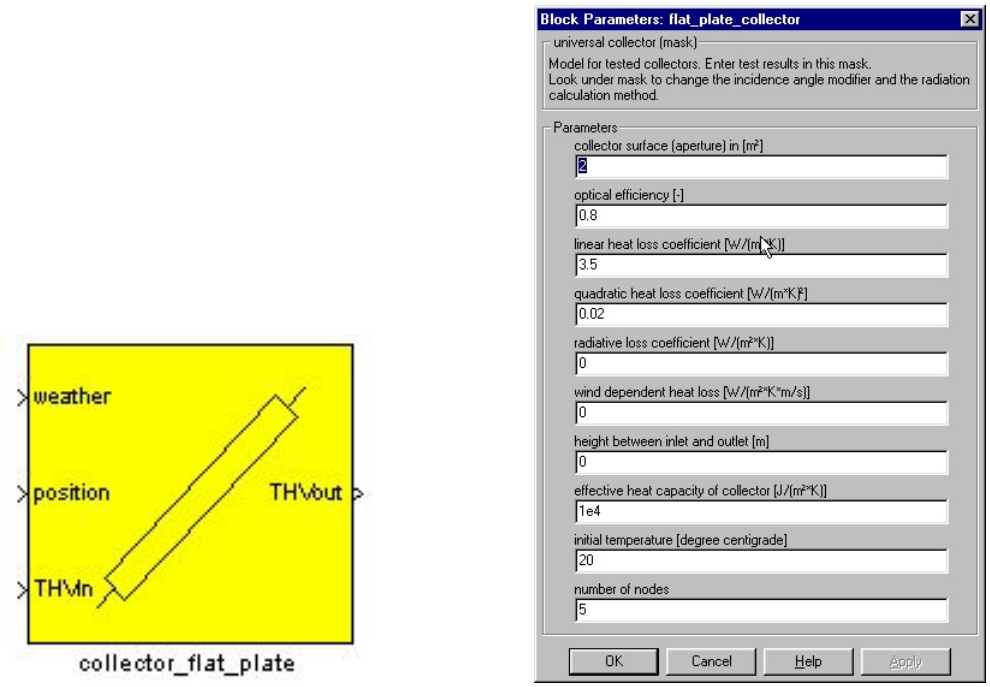

(a) (b)

Fig. 6.22.: a) Symbol of the flat plate collector in the Carnot toolbox [Car10]. b) Adjustment of the flat plate collector.

where:

Symbol	Used for	Unit
c	heat capacity of fluid	$\mathrm{J/(kg\,K)}$
c_{coll}	heat capacity of collector per surface	$\mathrm{J/(m^2\,K)}$
A_{coll}	collector area	$\mathrm{m^2}$
$\dot{m}$	mass flow rate	kg/s
$\dot{q}_{\mathrm{solar}}$	power input per surface area from Sun	$\mathrm{W/m^2}$
T	temperature	K
t	time	s
u_1	linear heat loss coefficient	$\mathrm{W/(m^2\,K)}$
u_2	quadratic heat loss coefficient	$\mathrm{W/(m^2\,K^2)}$
u_{wind}	wind speed dependant heat losses	$\mathrm{W\,s/(m^3\,K)}$
u_{sky}	linear heat loss coefficient	$\mathrm{W/(m^2\,K)}$
v_{wind}	wind speed	m/s

7. Simulations, measurements and results

In the following section the results of the Sunwater project are presented. This includes the simulations, which were done in Simulink or Maple and a few measurements, which were done at the building site in Egypt during the project life-time at the end of 2010. Furthermore an interlink between both aspects is given. There are just a few measurements available, because of the revolution at the beginning of 2011 in Egypt. After the end of the project the author tried to get more measuring results, but he was promised to a later point in time and therefore only a few measuring results are available at the moment. At the end of this chapter the results of this section are summarised.
During a later conservation the author got the information, that the demonstration plant was dismantled and had been transported to Cairo. In Cairo the system will be rebuilt for a new demonstration plant, but therefore it takes too much time for newer measurements. The new system will hopefully be ready in the first half-year 2012.

7.1. Solar radiation and ambient conditions

In chapter 3.1 the calculation of the daily solar radiation was shown. It was necessary, because no data were available at that time, which reflect the needed information in the right units. Therefore a simulation of the daily solar radiation was done at the beginning of the project. For a few days in a year the simulation results are shown in Fig. 3.3. After the installation of the demonstration plant a few measurements were done of the ambient conditions, which also includes the daily solar radiation. Fig. 7.1 shows the measured solar radiation and the ambient temperature. Two days are presented there, which are measured at the end of 2010. On these days the solar radiation was with 600 W/m^2 very low compared to the whole year with an expected maximum solar radiation of more than 1000 W/m^2. Compared to the data, which came from [Met09] the measured values for the solar radiation are slightly lower. The curve progression is very steeply rising and steeply sloping with a maximum value at noon. These steeply curve progressions were expected at the beginning of the Sunwater project.
On this day the sunrise was at 6 o'clock in the morning and the sunset at 18 o'clock in the afternoon. Therefore the day is split into 12 h night and 12 h day. The temperature on these days is in the range between 15 °C at night and 27 °C during the day. Compared to Tab. C.2 and Tab. C.3 the measured values are lightly higher. It is very interesting

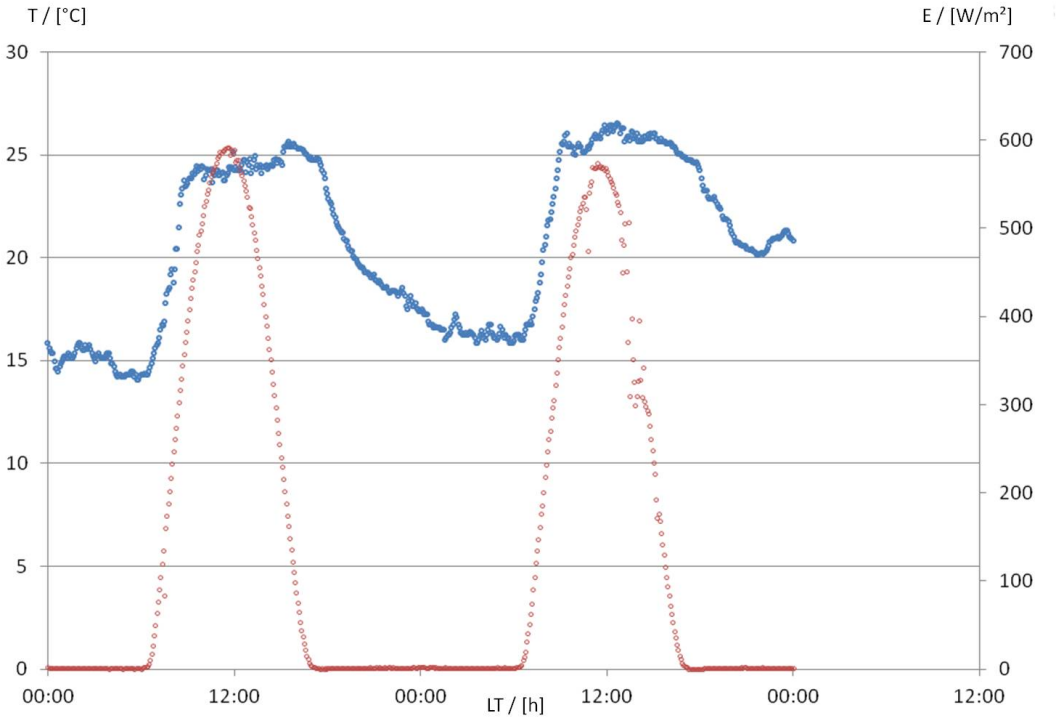

Fig. 7.1.: Solar radiation and temperature measurements at the building site on two days in the winter.

that the temperatures are higher compared to previous years, but the solar radiation is slightly lower. Normally there is a direct relation between both values, but it seems to be at the moment that there were on the previous days dirty weather. In the afternoon and the night the temperature drops exponentially and in the early morning there is a small fluctuation in the temperature measurements. The ambient temperature in the morning increases relatively fast. As can be seen, it is coupled with the solar radiation. If the solar radiation rises, the ambient temperature also rises. In the evening the behaviour is a little bit different. The temperature curve drops more slightly than the solar radiation. This can again be explained with an exponential drop of the ambient temperatures. It is similar to (6.101).
Fig 7.2 shows a comparison between the simulation, the data from the MeteoGroup and the measured data from the building site in Egypt. As can be seen the different curves are a little bit different. The actual measured solar radiation in this graph is the lowest curve. It is followed by the data from the MeteoGroup, which were measured at the beginning of 2009. The highest is the simulated curve at the end of the year. Only the sunrise, sunset and the duration of the day can exactly be calculated. The simulated solar radiation is too high compared to the measured data. As it was mentioned before, the calculation of the simulated data is very difficult, because many different aspects must be considered during the simulation. Furthermore a lot of impacts are uncalculable.

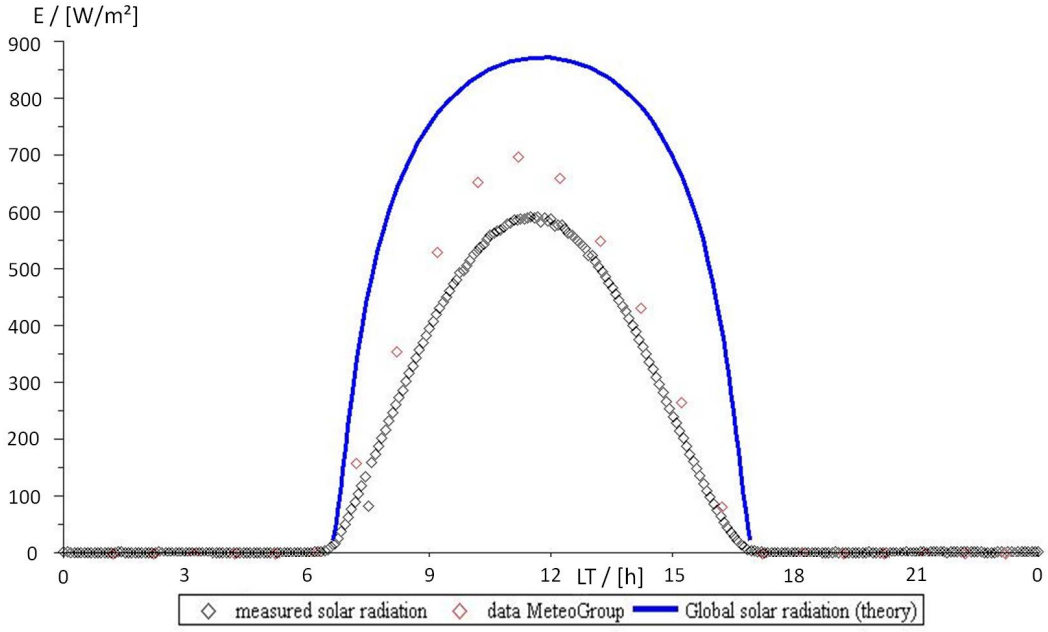

Fig. 7.2.: Comparison between measured and simulated solar radiation data.

Therefore the solar radiation simulation can only show a direction and not the real result. The simulation of the daily solar radiation can be improved, but it will never show the actual situation. It depends on too many variables. One aspect is, that the angle widening in the morning and the evening is not considered in this calculation (accordingly Fig. 3.1).

7.2. Solar thermal collectors

After the installation of the demonstration plant at the building site a few measurements were done with the solar thermal roof. For the measurement the input and the output temperatures of the solar thermal roof were measured. The results are plotted with the actual solar flow into one graph. It can be found in Fig. 7.3. As can be seen in this Figure the water input temperature of the solar thermal collector is between 60 °C and 70 °C during the sunshine hours, which reflects Fig. 7.1 and the existing volume flow during the operation time of the solar thermal pump. The water is heated up in the collectors to a temperature higher than 80 °C. The desired target for the Sunwater project, which is higher than 90 °C, is neither reached on the first nor on the second day. On the one hand the temperature is high enough to operate the WDU, but the volume flow in this temperature range is just round about 40 l/min at maximum. This volume flow is too low to operate the WDU in a continuous state, but the produced water can be stored in the heat storage tanks and this water can be used to operate the water desalination unit for a short time. Within this time freshwater can be produced. On these days

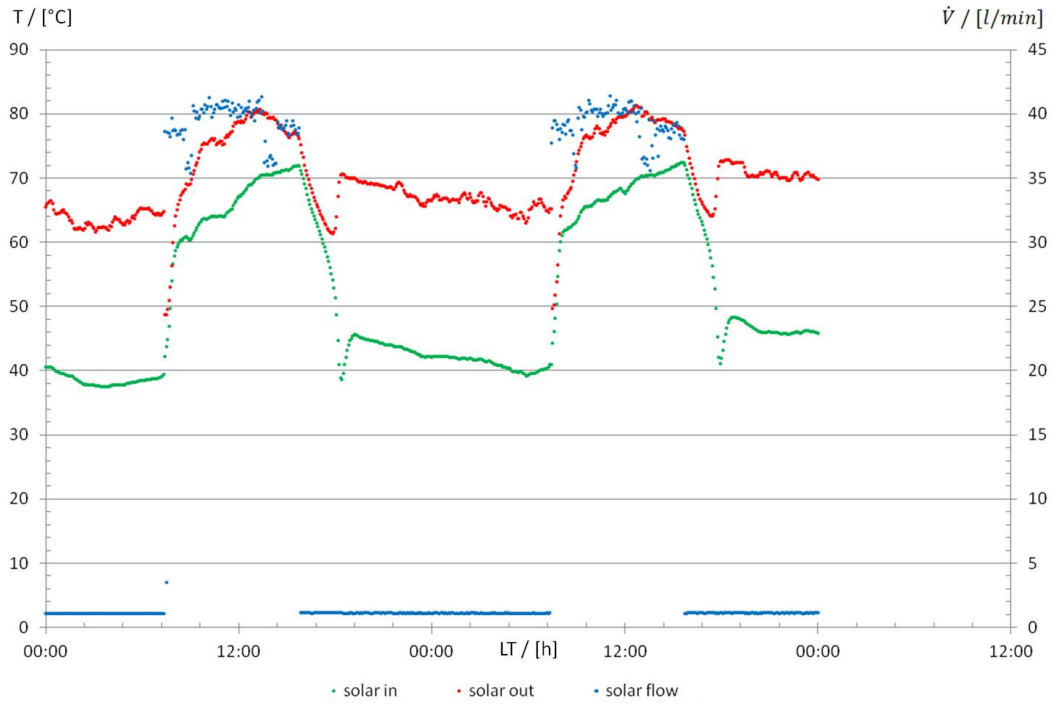

Fig. 7.3.: Volume flow and temperature measurements with the vacuum tube collectors at the building site in Egypt.

the solar radiation was very low, but in the summer more hot water can be produced with the same installation, because the expected maximum solar radiation is higher than 1000 W/m^2. The difference with regard to the actual measured solar radiations is round about 400 W/m^2. With this big difference higher temperatures and higher volume flows are possible.
After the solar thermal pump stops the water temperature in the system drops to a level below 40 °C and then it is constant. At the moment and due to the short measurement time, it is not finally clarified why the temperature drops to such a low level. The measurements of the volume flows through the collectors show, that the value is not zero. Therefore the idea is at the moment, that the hot water circulates in the pipes during the night. The hot water rises in the pipes to the solar thermal roof and there the stored energy is dissipated to the environment. The process water with the lost energy drops in the system and other hot water can flow to the STR. This circulation can for example be prevented by installing solenoid valves in the pipes from the collectors to the heat storage tanks and from the heat storage tanks to the collectors. The same should be installed for the pipes from and to the WDU. Another trick could be to arrange the pipes in a turned U-pipe and then the volume flow through the collectors can be reduced to a minimum.
During the project a few simulations of the demonstration plant were done with the Carnot toolbox for one day. The model of the demonstration plant was presented in Fig. 6.20. With this setup different simulations were done to plan the desalination

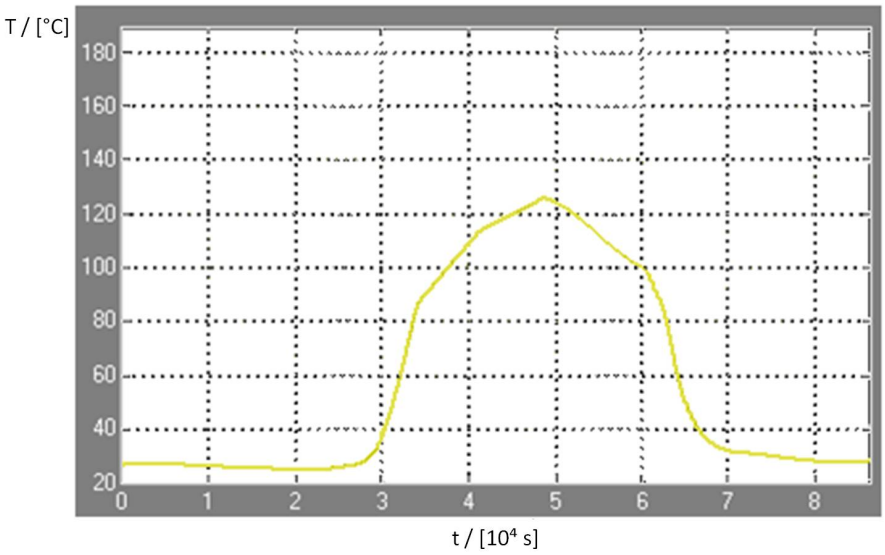

Fig. 7.4.: Simulation of the solar thermal collector with Carnot.

demonstration plant. With this model the output temperatures and the working time of the solar collectors were simulated. A simulation result of the temperatures can be found in Fig. 7.4. During this run the WDU was activated and the heat pump was deactivated. As can be seen, the start temperature of the simulation is the ambient temperature with more than 20 °C. During the morning the temperature rises to a value close to 90 °C. Later during the day the temperature rises to a temperature higher than 120 °C. This temperature level could only be reached, when the pressure in the system is increased, otherwise the water would boil in the collectors. This aspect is not considered during the simulation with the Carnot toolbox. The water temperature is raised without respect to physics. During the simulation the pressure in the system is during the entire time 1000 hPa. This serious problem must be solved by the persons, who built the Carnot toolbox, but finally it can be seen, that the needed temperatures for the operation of the WDU can be reached with the solar thermal collectors. In the actual realisation temperatures higher than 95 °C can be prevented, if the volume flow through the collectors is controllable, which is not possible with Carnot. In the evening the process water temperature drops again to the ambient temperature, because the stored heat is emitted to the environment. Fig. 7.4 shows that the solar thermal pump works for several hours on this day. It was controlled in a way, that it only works, when the output temperature of the collector is higher than the input temperature of the process water. If the output temperature is lower, the pump stops.
In the simulation tool Carnot, a variable volume flow could not be implemented. Only a fixed value could be set. If the volume flow could be adjustable, the output temperature could be fixed at a constant value. This has the advantage that the volume flow during the noon time could be increased and reduced in the morning and the evening. With this implementation the needed volume flows for the desalination process could be generated.

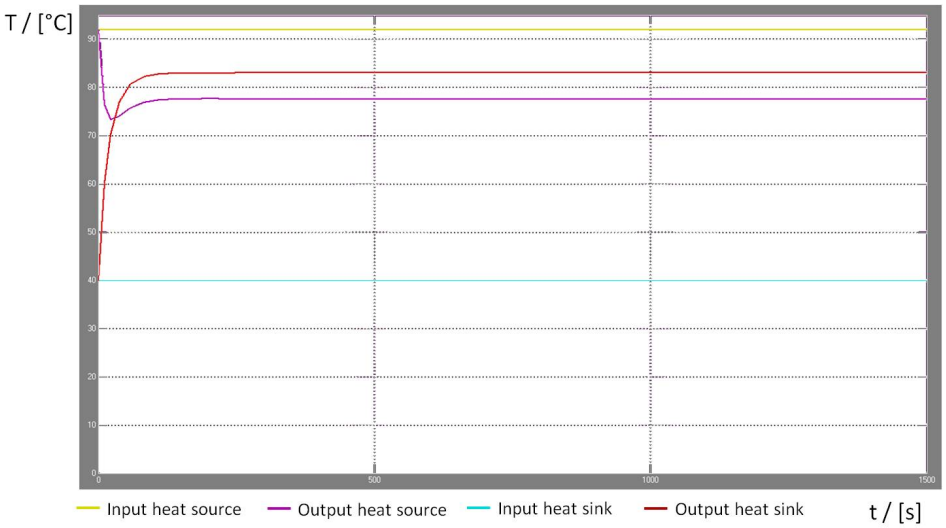

Fig. 7.5.: Simulation of the heat exchanger with a comparison of the input (yellow / magenta) and output (cyan / red) temperatures.

7.3. Heat exchangers

One main and difficult aspect during the project was the simulation of the needed heat exchangers for the WDU. The model of the heat exchanger is presented in section 6.5.1. It consists of different combined ODEs. After implementation in Simulink different simulations were done. A result for one simulation can be found in Fig. 7.5. For the simulation of this heat exchanger a constant temperature at 90 °C and a volume flow with 3.33 kg/s was used for the heat source (yellow). For the heat sink (cyan) a volume flow with 1.11 kg/s and a temperature with 40 °C was included in the calculation. As can be seen in Fig. 7.5 the temperature of the leaving heat source (magenta) drops to a value below 80 °C and simultaneously the output temperature of the heat sink (red) rises to a temperature higher than 80 °C. At the beginning the temperature of the heat source drops to a value below 75 °C, but later it stabilises at a constant and higher temperature. As can be seen in this figure the temperature of the heat sink does not reach the temperature of the heat source. It is a few degrees below the temperature of the heat source. This is justified with the heat transfer co-efficient of the used materials. This means that for a desired temperature of the heat sink a higher temperature of the heat source is necessary. Otherwise the needed temperature cannot be reached. This means for the solar thermal water desalination plant, that the water from the collectors must be higher than 90 °C to reach the optimal operation temperature of 90 °C for the evaporation desalination unit. This disregards the heat losses during the transport of the process water from the collectors to the WDU. If this heat loss is regarded the process water temperature must be much higher than the operation temperature. In the worst case the solar thermal roof must be operated with overpressure to get the needed volume flow temperatures.

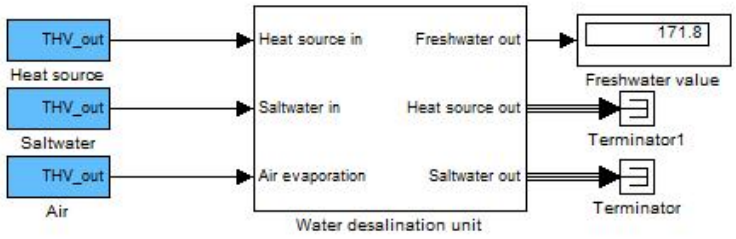

Fig. 7.6.: Simulation result of the modelled WDU in Simulink with a calculated freshwater output of 171.8 l.

7.4. Water desalination unit

During the realisation of the demonstration plant a simulation of the water desalination unit was done. The idea was presented in section 6.7. It consists of different parts, which were necessary for the simulation. In different modules there are a lot of different constants, which must be adjusted for the final simulation results. This includes for example the integration constants, which are necessary for the heat exchangers. For one heat exchanger two different integration constants are indispensable. The model consists of several heat exchangers and therefore a lot of constants must only be adjusted for them. Other constants are used for the dissipation of the wet air in the WDU and the calculation of the freshwater output. After this initialisation the simulation gives a result of the produced freshwater in the real range, which is mentioned in the technical data. Based on this, the freshwater output is round about 209 l/h, but this nominal value depends on the frame conditions. Fig. 7.6 shows the freshwater output for the simulated WDU after one hour. The calculated value is lower than 200 l, because the temperature inside the WDU must be increased from ambient conditions to the maximum working temperature. This takes a few minutes and therefore the freshwater output is lower. If the temperature inside the WDU has the right working temperature at the beginning, the calculated freshwater output is much higher. The freshwater output can also be optimised and adjusted with the constants, which are necessary for the simulation. The simulated output is valid for a continuous operation of the demonstration plant.
With the model in Carnot the working time of the WDU can be calculated. The result can be found in Fig. 7.7. If the value in this graph is one, the heat delivery pump for the WDU is activated and if the value is zero, the pump is deactivated. At the beginning and the end of the graph the pump is deactivated, because it is night and no thermal energy is produced. In the morning and the evening the graph jumps between the values 0 and 1, because there is not enough heat in the system for a continuous operation of the desalination unit. It can be interpreted in that way, that the needed operation temperature can be reached, but the volume flow is not high enough for a continuous operation. Therefore the hot water must be buffered and later the buffered process water can be used to operate the WDU. During the noon time there is a high

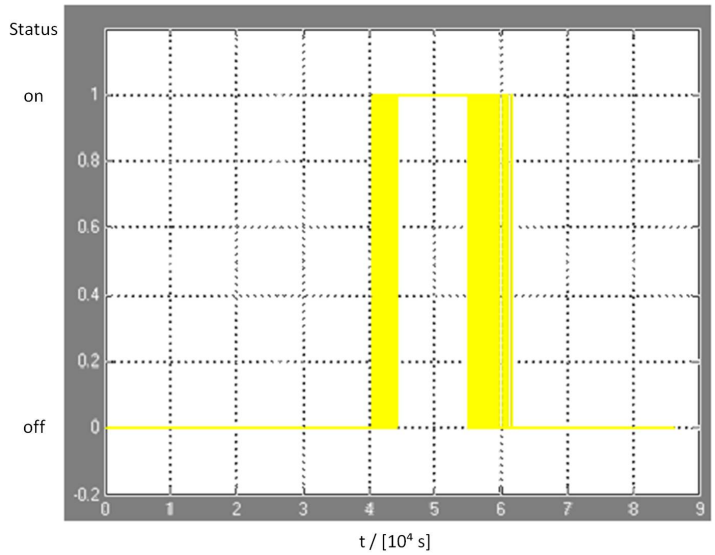

Fig. 7.7.: Calculation of the working time with Carnot. It is plotted WDU operation versus time in seconds.

volume flow, which is high enough for the operation of the WDU. The surplus energy is stored in the heat storage tanks and it is later be used for the operation. Unfortunately the system cannot be simulated in Carnot in that way, that the WDU is started, when enough hot water is available in the system. In this toolbox only the temperature at the top or at the bottom of the heat storage tanks can be used for logical operations. Other possibilities are not given. This is the reason, why the status of the heat delivery pump in the morning and the evening jumps between the states 0 and 1. If other temperature measurement points in the heat storage tanks could be used or if the amount of the stored water is considered for the heat pump's logical operation, the number of jumps between the different states can be reduced or prevented.
During the simulation different temperature states in the WDU were calculated. The results for the water temperatures in the system can be found in Fig. 7.8a. As it can be seen in this figure, there are different saltwater temperatures in the system. At the inlet of the saltwater (yellow), the water has a temperature of 20 °C. The next measurement point is after the first heat exchanger and the fluid mixer (cyan). At this point and after a few minutes the water has a constant temperature higher than 70 °C, but this value includes also the energy, which is transferred due to evaporation from the left to the right chamber. Normally the energy is completely absorbed in the whole right chamber, but due to the closed system it can be transferred in only one point. The transferred energy is the difference between the saltwater input temperature in yellow and the line in magenta. The associated heat exchanger is included between the lower air-water heat exchanger and the fluid mixer. After the external heat exchanger there is another measuring point (green). At this position the saltwater reaches its highest temperature value in the system. It is calculated with more than 80 °C. During this simulation the heat source input temperature has a value close to 90 °C and its output temperature is adjusted to

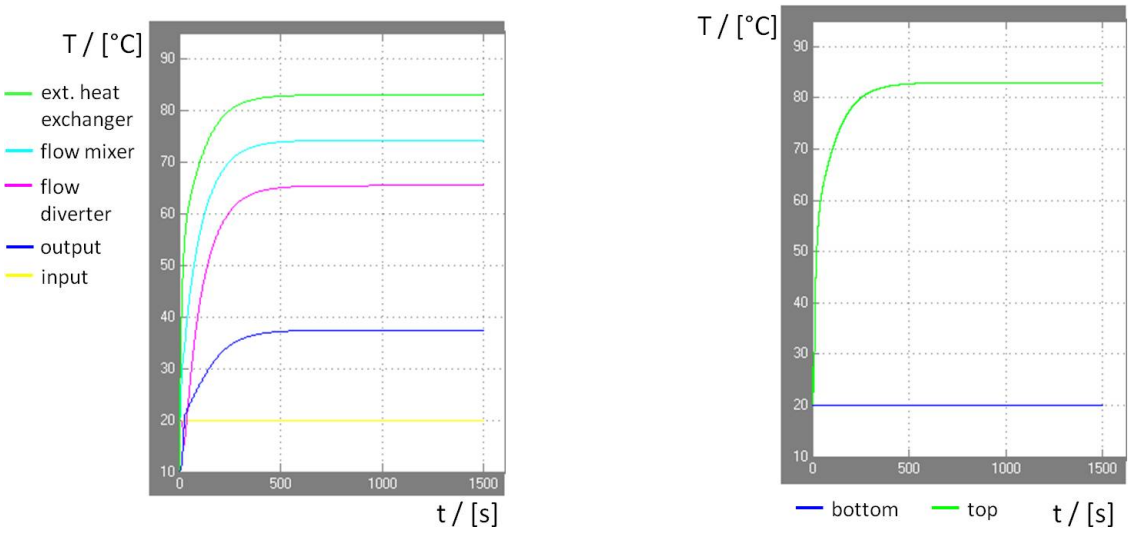

(a) (b)

Fig. 7.8.: a) Water and b) air temperatures inside the simulated WDU.

80 °C. The last measuring point in the system is the temperature of the leaving brine. The brine leaves the WDU with a temperature below 40 °C. The input temperature of the saltwater and the output temperature of the brine were optimised with the technical data, which came from the weather institute or from the manufacturing company.
In Fig. 7.8b the different air temperatures in the system are presented. One measuring point is at the bottom of the WDU. Another measuring point is at the top. At the bottom the air has a temperature of 20 °C and at the top it is close to 85 °C. This temperature difference is very important, because the higher the temperature difference, the higher is the possible freshwater output. In the first order it is very important to increase the air temperature to a maximum value. The content of the evaporated water is very sensitive to this value. It can be explained with (3.42). The lower temperature has only a minor effect.
For a better freshwater production rate, the top temperature value of the air inside the WDU must be increased as much as possible. This can only be done, if the temperature of the saltwater is increased close to the boiling point. For this the temperature level of the heat source must be raised to a temperature, which is higher than the boiling point at ambient pressure. This is due to a difference between the input and output temperatures of the heat source and the heat sink, as it was shown in the previous section. This temperature level can only be reached, if the solar thermal part is operated with overpressure or if another process fluid with a higher boiling point is used. This could for example be oil or water with other additives. The increase of the boiling point could be a new aspect during another innovative project.

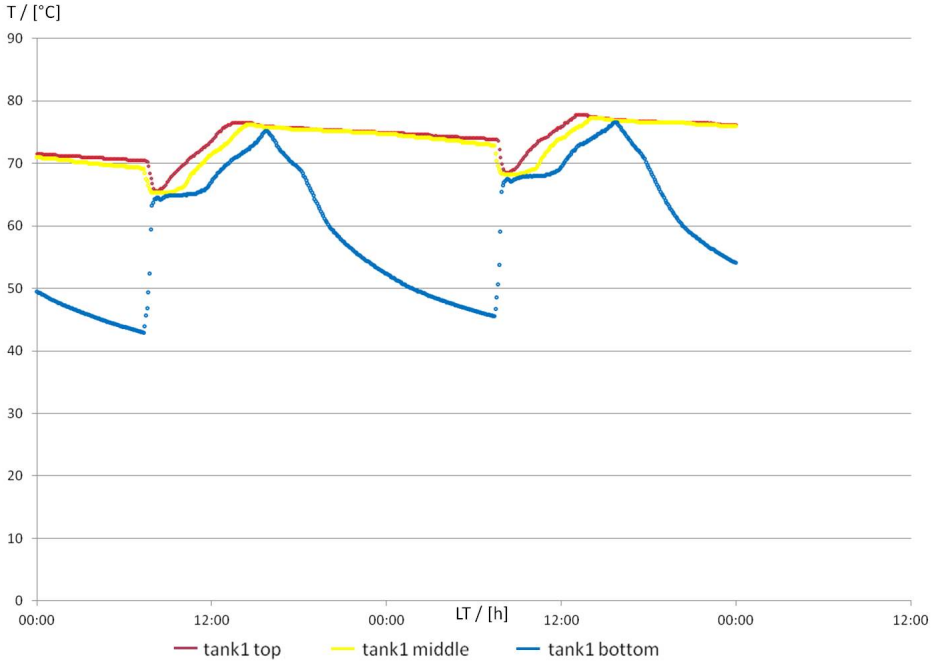

Fig. 7.9.: Measurements of the heat storage tank temperatures at 3 different positions, one at the top, one in the middle and one at the bottom.

7.5. Heat storage tanks

In the following section the temperature in the heat storage tanks is discussed. During the operation of the solar thermal part a few measurements of the desalination unit were taken. The results for 2 days can be found in Fig. 7.9. As can be seen in this figure, the heat storage tanks work as expected. The hot water from the solar thermal roof is buffered. In the morning the temperature at the bottom is 42 °C and the temperatures in the middle and at the top are 70 °C. The orders of the different temperatures are as expected. At the top is the hottest water, in the middle the water is a little bit colder and at the bottom is the coldest temperature in the heat storage tank. Surprisingly the temperature at the bottom is much lower than it was expected during the planning of the demonstration plant.
When the solar thermal pump starts the temperature at the bottom increases to 65 °C and the other temperatures drop to the same value. This is an indication, that the water is mixed up in the different layers. The cold water is extracted from the bottom of the heat storage tanks and the water in the other layers sinks down and thus it is mixed up in the different layers. As can be seen in Fig. 7.3, the volume flow is relatively constant during the day and therefore a constant volume flow is generated through the collectors. Later during the day it can be seen in Fig. 7.9, that different temperature layers are induced in the heat storage tank. At the top is the hottest temperature and at the bottom it is colder. The temperature differences between the different measuring points are just a few degrees.

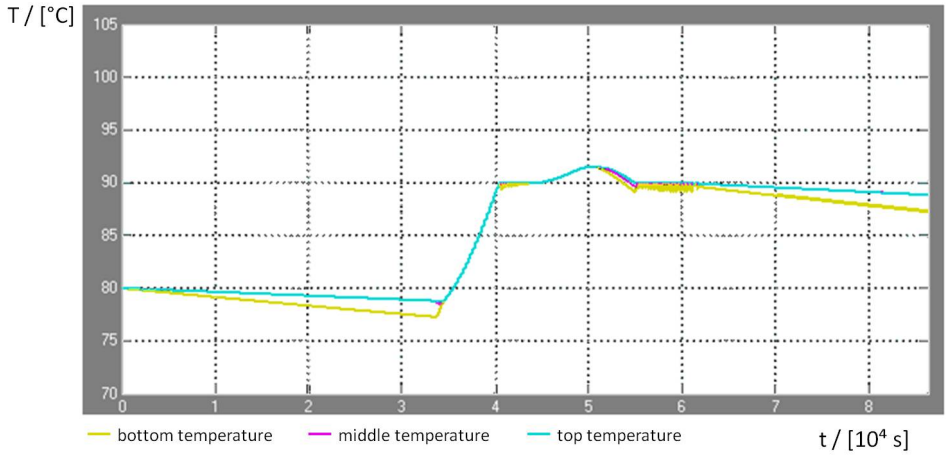

Fig. 7.10.: Simulation result of the heat storage tank in Carnot for different layers.

At the end of the sunny day the heat storage tanks are 75 °C in all layers. At this time the heat storage tanks are fully loaded for the generated volume flows, which comes from the STR. The maximum temperatures in the heat storage tanks are a little bit lower than the maximum output temperature of the collectors. This is on the one hand justified with temperature losses in the pipes and on the other hand the mixture of the volume flow with the stored water in the heat storage tanks.
After the solar thermal pump stops the temperature sensor at the bottom drops extremely. It is somewhat interesting, because the other two temperature layers are relatively stable at the maximum temperature. The temperature at the bottom drops within a few hours to a temperature higher than 45 °C. This can be justified with a volume flow inside the pipes, after the solar thermal pump was stopped. It is also reflected by the measurements, because there is a continuous volume flow through the pipes, which are connected with the solar roof and the WDU. It is measured with the two installed flow meters. The hot water rises to the solar thermal roof and cools down. The cold water flows back to the heat storage tanks, and therefore the temperature at the bottom drops.
Another aspect is the standard temperature losses based on the environmental conditions. For a better heat storage the insulation of the heat storage tanks and the pipes must be improved. This can for example be done with a vacuum insulation or with an enlargement of the existing insulation. Due to the high temperature differences between the environment and the process water it is favourable. Furthermore the installation of solenoid valves could also help to prevent the convection of hot water in the system, but it must be shown in later realisations. Two solenoid valves were bought, but they were not installed in the demonstration plant by the Egyptian partners. Additionally the improvement of the pipe layout could help. This can for example be tested in later realisations.
Next to measurements at the building site different simulations with Carnot were done in Simulink. Fig. 7.10 shows a simulation result. As can be seen the initial temperature of the heat storage tank is 80 °C. The simulation starts at midnight and runs for 24 h. During the first hours the temperatures drop in the heat storage tank. It must

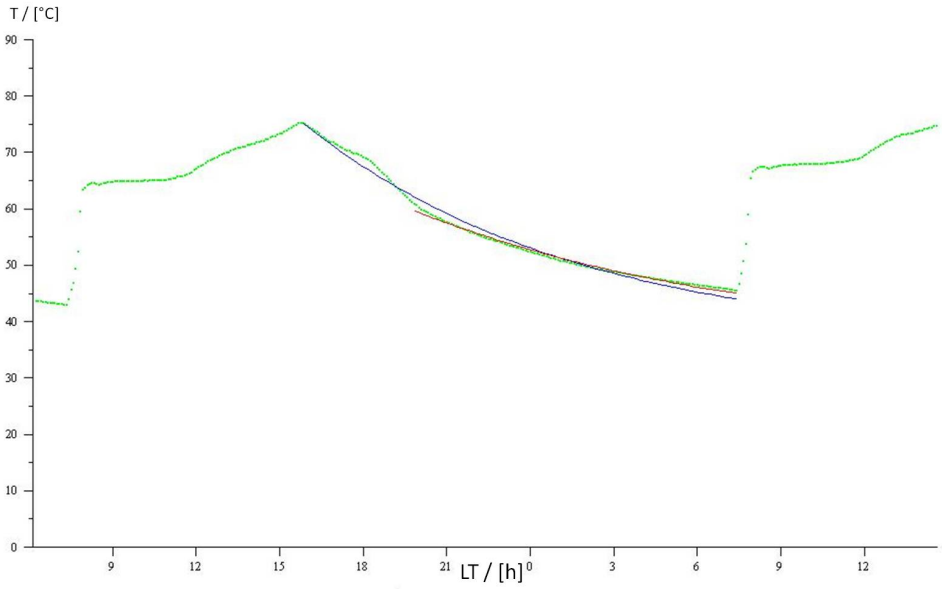

Fig. 7.11.: Hourly temperature profile in the heat storage tanks with two exponential fits in red and blue.

be different between the top, the middle and the bottom of the tank. The top and the middle are more or less stable and only the temperature at the bottom drops to 75 °C. In comparison to the real system, here the temperature losses are much lower. This is justified in the simulation, because there is no convection of hot water in the system. When the pumps starts the temperatures in the heat storage tanks rise to more than 90 °C. In the late afternoon and the night the temperature drops again in the system. The curve progression is similar to the measured data, but the temperature rise is much faster in the simulation compared to the real measured data. For the simulation a day in September was used, which has a higher solar radiation. The used data for the simulation can be found in Tab. C.10. Due to the higher solar radiation a higher water output temperature is expected with the collectors. Furthermore it can also be seen, that the water in the heat storage tank splits into different temperature layers. The results between the measuring at the demonstration plant and the simulation are comparable.
In subsection 6.8.1 it was forecasted that the temperature drops exponentially. This can be seen in Fig. 7.9. For a better overview the interesting part of the figure was fitted with the exponential curve (6.101). The result can be found in Fig. 7.11, but for a better result an additional and constant term must be inserted into the function. Without this term the curve cannot be fitted. The additional term shows, that another aspect is also responsible for the cooling of the process water and not only the temperature difference between ambient and the process water. The higher temperature losses can for example be explained with an convection of hot water through the pipes and the solar thermal roof. Another solution could be different insulation materials. The exact details must be confirmed during later realisations and measurements.

7.6. Results and optimisations

The results of the simulations and the measurements are very promising, that the freshwater production with solar thermal energy is possible. The needed hot water can be produced with the solar thermal roof and this process water could be stored in heat storage tanks. This produced process water was already used to operate the water desalination unit and to generate freshwater out of saltwater. During the short measuring time of the project just a few litres of freshwater were produced, but this is the first step towards a future-proof and environmentally friendly system. In the future a few aspects of the system must be optimised for a better efficiency. This includes for example an optimisation of the volume flows from the STR and its energy yield. Furthermore the volume flows must be increased for a longer operation of the WDU. Otherwise the working time is too short for an efficient and cost-effective operation. For this a larger STR must be installed and the heat storage must be optimised. It could for example be a stratified storage tank. Furthermore other environmentally friendly energy sources are interesting for an operation. This could for example be the already planned, but not included heat pump. It was shown in the simulation, that the operation of a waste heat heat pump can extend the working time of the water desalination unit. On the one hand the WDU can start earlier in the morning, because the temperature drop during the night is lower and the produced energy during the day can be used in the evening. If this heat pump is powered with green electrical energy, the freshwater production is still environmentally friendly. The needed electrical energy can come from PV or from biomass power plants. On the other hand it is also possible to use nuclear power as an environmentally friendly energy supply. Unfortunately, this energy source is heavily discussed at the moment [N24]. Additionally fusion technology and the associated power generation are unlikely before 2040 [Ite12].
As it was seen in this project the operation of the WDU depends extremely on the sunshine duration. It only makes sense to use ST in areas with a very high daily solar radiation. In countries with a low solar radiation the needed temperatures can hardly be obtained and therefore it is very uninteresting to install such a system there, but there could be the possibility to combine ST and a heat pump. A solar roof could be used to produce volume flows with temperatures in the range between 60 °C and 80 °C. The temperature difference to 95 °C can then be raised with the usage of a heat pump. This combination of two different environmentally friendly components are also very interesting and future-proof. This idea could for example be included into an additional international project. Another important advantage is, that this combination can also be used in areas with a lower solar radiation. It can for example be installed in Germany or other countries.
As was seen, the missing solenoid valves accelerate the temperature losses in the system. Therefore it is very interesting to include such a component in the system to prevent energy losses during the night or on cloudy days. The control of the different temperatures in the system must also be optimised. During one day the volume flow temperature from the solar thermal roof was higher than 100 °C and then one of the flow sensors

was damaged. With more experience in the temperature and volume flow behaviour of the STR concerning the solar radiation and other environmental frame conditions, this problem should be solvable in later realisations. To prevent this excessive temperature more sensors could be installed at the solar thermal roof, because one row consists of more than one solar collector. In this constellation it is not enough to measure the temperature only at the outlet of the whole conglomerate of the collectors. If the temperature reaches the limit, it could be too late. With the additional temperature sensors a better overview and control is feasible.
In the next step the simulation of the daily solar radiation can be improved to make a better forecast. This would help to plan and control other solar thermal demonstration plants. With this information the control of the pumps and the forecast of the produced freshwater is easier. With this information the size of the desalination plant for a special application can be estimated.

8. Future prospects and summary

In the following chapter different improvements for a later realisation are discussed, which are interesting to optimise the system. It starts with a tracking system for the solar collectors or other interesting add-ons for the solar thermal desalination system. Furthermore alternative possibilities for the heat source are identified and explained. Another important aspect is a summary of the complete project with advantages and disadvantages of the installed system.

8.1. Tracking of the collectors

At the moment most solar collectors are fixed mounted. Currently they are not movable, because it is too expensive, too complicated and too accident-sensitive for most installations. Nowadays they are installed in a way that the most solar collectors at the northern hemisphere have a southerly orientation and the solar collectors in the southern hemisphere have a northerly orientation. This is rooted in the movement of the Sun during the whole year. For the operation of the collectors the surface must be orientated towards the Sun. The best performance can be harvested, when the angle of incidence of the Sun is perpendicular on the surface, especially at noon and the early afternoon. For a regular installation of the collectors an angle is chosen, which reflects the best performance during the whole year. The chosen angle between the applications PV and solar thermal could be different, because in the winter more thermal energy is needed compared to the summer. Therefore the angle of inclination should be slightly bigger compared to PV, because this higher angle guarantees a better performance in the winter time in contrast to the summer time. The best angle for the installation can be found in reference books and it depends on the region of the installation. As can be seen in section 3.1 the movement of the Sun varies during the whole year. In the summer the angle of incidence is smaller compared to the winter time, then the optimal angle is bigger. Due to the fixed angle for the collectors, they have only for a few hours on a few days during the whole year the best orientation towards the Sun. Then it is the best time for gathering electrical or thermal energy. Furthermore in the morning and in the evening most collectors are illuminated from the side and therefore the angle of impact is not optimal and thus the rate of yield is reduced. For a higher efficiency it is also important to harvest this energy. For an optimisation for the energy gathering it is very interesting to install a tracking system for the collectors. At the moment there are 3 different possibilities for tracking systems:

- North-South tracking system
- East-West tracking system
- Full tracking system

The first and the second options are 1-axis tracking systems and the third option is a two or 3D axis tracking system. The North-South tracking system is a tracking system, which changes the angle of inclination during the whole year. In the winter the inclination angle is bigger compared to the summer. Due to the tracking system a better performance can be obtained in contrast to a fixed installed system, but the energy harvesting is still not optimal. During the morning and during the evening a lot of energy is squandered, because the angle of impact is not perpendicular. The hardware demand for a one axis tracking system is relatively low. Furthermore the calculation time of the tracking is also very easy, because the angle of impact depends only on the declination of the Sun and these are fixed values during the whole year.
The next and slightly more complex tracking system is an East-West tracking system. The collectors are installed with a fixed angle of inclination, but they can be rotated around the high axis. In the morning the collectors are eastward orientated and during the day they follow the Sun. In the evening the collectors are more westerly orientated compared to the morning. The speed of rotation, the start point and the end point depends on the season, because the Sun has different paths on the sky during the year. In the night the collectors must be rotated back to its initial state. The initial state, the final state and the speed during the whole year must be calculated for every day in a year. Therefore the calculation time for the best tracking is more complex compared to the first possibility. The hardware demand for the tracking system is in the area of the first possibility.
The most complex tracking system is a two-axis tracking system, but this system can be used to harvest the most energy during the day. This tracking system unifies both tracking systems. The collectors can be rotated in the North-South and additionally in the East-West direction. Therefore the angle of impact can be adjusted in a way, that it is always perpendicular during the whole time. This is possible as long as the Sun is above the horizon and it is also needed if concentrating solar thermal collectors are used to harvest the solar radiation at a fixed point. The energy is for example collected at the top of a tower like in the Desertec project. The hardware demand compared to the other tracking systems is much higher, because two independent systems are needed to control both axis and to reach the desired positions. Furthermore the computing time of the tracking is much more complicated, because the calculation for the two axis are dependent on each other. This calculation must also be done for every day in a year. The advantage is, that the energy yield is much higher compared to a fixed mounting or to a one axis tracking system. Furthermore more technical problems can happen compared to a fixed installation, which does not need a control or management system.

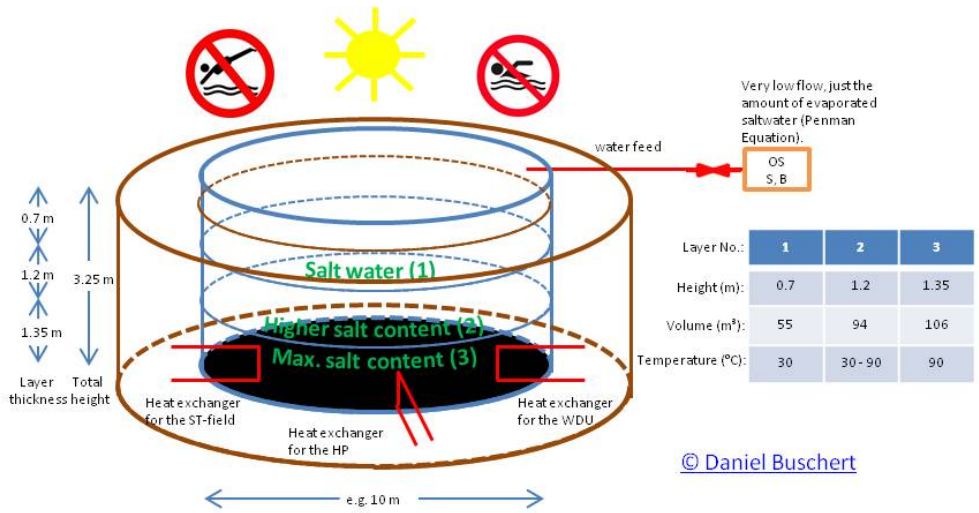

Fig. 8.1.: A solar pond can be used to harvest and store thermal heat

8.2. Solar pond

Another interesting idea is to use a so called solar pond as a heat source. A solar pond can be used as a collector and / or as a heat storage tank. The idea was to implement such a solar pond in the Sunwater project instead of a heat storage tank. Due to the complexity and the unavailable expertise it was rejected by the other project members. This special storage technology is based on the density, temperature and concentration gradient between the bottom and the surface of the reservoir. It is also observable in natural salt lakes like in the *Solar Lake* close to the Red Sea in Egypt [Coh75]. The solar radiation in this solar pond produces a maximum temperature of 60.5 °C at a depth of 2.5 m − 3 m with a decreasing temperature down to 40 °C at the bottom in 5 m. This natural solar pond is protected with a mountain ridge against wind. The height of the ridge is 100 m above the sea level. Furthermore the lake is separated from the Red Sea by a 60 m wide gravel bar. Seeping water through the gravel bar feeds the solar lake, because a lot of water evaporates during the year.
The nature behind this solar lake can be used to build an artificial solar pond as a heat source for the desalination plant. At the top of the pond the temperature is nearly ambient temperature, but in the depth the temperature can rise up to 90 °C and higher. This heat source and storage can be tapped as a heat source for the desalination unit. Furthermore it should be possible to store the produced heat inside the solar pond for later usage, which comes from a heat pump or from the solar thermal collectors. This could for example be the surplus and unused energy in the afternoon.
A rough overview of a solar pond can be found in Fig. 8.1. The idea is that in the solar pond different water layers with different salinities are present at the same time. At the bottom is the layer with the highest salinity and at the top there is a layer with the lowest salinity. Between both layers a salinity gradient can be established. Without any outer impact the solar pond is stable, because the water with the highest salinity has

the highest density and therefore the layer is at the bottom of the pond. At the top is the water with the lowest salinity and therefore it has the lowest density. The solar radiation enters the pond from the top and then it is absorbed at a light absorbing layer at the bottom of the solar pond, where the solar radiation is converted into heat. Due to the different salinities the heat is captured at the bottom and will not be released to the environment. The temperature increases continuously. Warmer water has a lower density compared to colder water. Therefore it should normally climb to the surface and release the stored heat. It cools down and should descend to the ground. Due to the different salinities the hot water cannot climb to the surface and stays at the ground and therefore the temperature difference at the surface between the liquid and the air is relatively low and thus the energy losses are reduced. Herewith a natural heat insulation is established. With this easy trick temperatures higher than 90 °C are possible at the bottom. The problem is, that for a stable temperature layering and a good heat insulation no turbulences, water waves or flows are desirable inside the pond, which destroy the different layers in the pond. Therefore the surface should be covered with a transparent foil or with wind breaking mechanisms, such as rings for example. Furthermore the evaporated water must be refilled with freshwater and an eye must be kept on the salt content and its distribution. For the heat extraction and the heat conduction heat exchangers can be used, as can be seen in the Fig. 8.1. With the brine and the saltwater of a desalination system, especially an evaporation system, it should be possible to build such an innovative solar pond. With different possibilities the efficiency of the solar pond could be raised. Furthermore the solar pond can still be operated in the winter when the outside temperature is below the freezing point.

8.3. Concentrating solar thermal systems

During the planning of this project the first idea was to install simple flat plate collectors, but later the decision was to install vacuum tube collectors. The fear was that the flat plate collectors would not produce the needed heat source temperature for the water desalination unit. With the vacuum tube collectors it is possible to produce temperatures up to 100 °C and higher, as can be seen in Fig. 7.3.
The next step could be to replace the vacuum tube collectors with for example parabolic-trough collectors. These collectors use parabolic mirrors to focus sunlight on a dark surface tube. Inside the tube a fluid is transported, which collects the energy. The advantage is, that the pipe can be operated with overpressure and therefore higher storage temperatures are obtainable. The hot water can be stored with overpressure in heat storage tanks or in solar ponds. The maximum fluid temperature depends on the fluid itself and the pressure. The higher the pressure, the higher is the possible fluid storage temperature. With higher storage temperatures less volumes inside the storage tanks are needed to store the same amount of energy. Inside the heat storage tanks temperatures higher than 150 °C and much more are possible. Due to the situation, that this evaporation desalination unit only needs temperatures around 90 °C, the stored

water with a temperature of more than 90 °C must be reduced to the needed heat source temperature and the operation pressure of the WDU. Due to higher temperatures in the heat storage tanks the operation time of the WDU can be extended. With a controlled volume flow, for example with the included 3-way valve in the demonstration plant, the desired temperature can be set.
A next step could be to use a huge field of independent mirrors to reflect the sunlight to a well-defined point. This point is due to the geometrics at a head of a tower and at this point the energy can be harvested. The solar energy can be bundled there to reach much higher temperatures compared to flat plate, vacuum tube and parabolic-trough collectors, because a much higher effective area can be used to gather energy. In this case temperatures higher than several 100 °C are no problem. At the moment temperatures higher than 1000 °C can be reached. Then the energy can be stored in highly efficient heat storage tanks or can be used to produce freshwater and / or electrical energy. For the tracking of the solar collectors a two-axis tracking system is necessary to reflect the solar radiation during the whole day to the fixed point at the tower. If the area of mirrors is relative large, the mirrors must independently be controlled, because small differences have a big effect on the optical path between the mirrors and the receivers and with a bad alignment a lot of energy is lost [Des11].

8.4. Waste heat or environmentally friendly energy for desalination

Next to solar energy other (environmentally friendly) energy sources can also be used to operate the desalination unit. One interesting option is to use waste heat sources, which are normally unused. This can for example come from power plants or the heavy industries, which need high temperatures. High temperatures are needed in blast furnaces or in steel works. On a lot of premises there are small power plants which produce the energy for internal purposes and furthermore there are a lot of external power plants, which produce waste heat during their normal energy production. In most cases this thermal energy is unused and released via big cooling towers to the environment and then it is lost. For internal usages the temperature respectively the energy densities of the energy sources are too low, but this energy can be used to produce freshwater with the evaporation desalination unit from TW. For the used desalination unit relative moderate temperatures and volume flows are necessary, which can be operated with this waste heat. If there is a huge amount of waste energy a lot of water desalination units can be operated, if there is just a small amount of waste energy only a few desalination units can be included in the system. The quantities of the units can be scaled to the demand of freshwater and the available energy sources. Furthermore if the desalination units are combined with an environmentally friendly energy source, for example wind or nuclear power plants, the produced freshwater does not accelerate the global warming. Therefore the freshwater can be sold to the community without any misgivings in

contrast to the actual produced freshwater, which is normally produced with fossil fuels. The burning of fossil fuels is again responsible for the global warming and the green house effect. At the moment there are only a few possibilities to produce freshwater in an environmentally friendly way, because the technology is in the fledgling stages. In the next years the kind of environmentally friendly technologies are more important than ever, because the costs for fossil fuels will rise continuously. In the next decades many oil or gas sources will run dry.
Another possible energy source to convert saltwater into freshwater can for example be geothermal or biomass sources. The geothermal sources is available in volcano regions or in other anomalous regions like in areas with a high heat transmission rate, in fracture zones or in sediment basins, where disposable warm and hot water is available. The geothermal heat is rooted in the genesis of the Earth and the natural radioactive decays, which have been present for millions of years.
In civilisation a lot biological wastes are produced every day and this biowaste can be used to generate the needed thermal energy with biomass power plants. One possibility is to produce bioethanol, biopetroleum and biogas with different production processes. The secondary energy carriers can be used to operate the desalination unit. The advantage of these fuels is, that they can be produced with renewable primary products and therefore they are environmentally friendly and do not accelerate the greenhouse effect. They only emit as much carbon dioxide as they have absorbed during the growing. Both energy sources, the geothermal and the biomass sources, are predestined to produce environmentally friendly freshwater.

8.5. Wastewater treatment and common salt production

Desalination can also be used to clean wastewater and to produce common salt for daily life. In a lot of applications wastewater is generated during the manufacturing or in the normal course of life. In a lot of companies the vehicle has only a low contaminations. This can for example be paint impurities, chemicals or other very small particles. If the water contains impurities with bigger grain size or other larger substances it must first be pre-filtered with coarse and fine screens, because these substances can damage the desalination unit or they cannot be transported inside the WDU. Finally the rest can be treated with the desalination unit. In a lot of cases it is very difficult and / or too expensive to remove it with other standard methods. Therefore the complete wastewater must be depolluted and this can be very expensive, because in most cases the disposal must be paid by volume. If the amount were reduced and separated into wastewater and clean and residue-free water, it could be a profitable solution for a lot of companies. Especially if the companies have a waste heat source, which can be tapped for the desalination process. With the desalination unit it is possible to reduce in a lot of cases the vehicle and thus the amounts of polluted fluids are reduced. Consequently the costs for the waste disposal is also reduced. If the desalination process is repeated frequently the vehicle can be reduced to its minimum. The condensing freshwater can

easily be disposed off or can again be reused for the same process, which again has a financial benefit.
With this WDU it is also possible to produce common salt directly from the saltwater or the remaining brine. On the one hand several desalination units can be cascaded to raise the concentration of the salt in the water until the maximum salinity in the water is reached, which can be treated with the desalination units. Another possibility is that only one desalination unit is enough to concentrate the salinity in the fluid. Always the same fluid is desalinated again and again and so the maximum concentration is obtainable with this single system. After the concentration it is much easier and faster to remove the remaining water from the fluid. This suspension can be cost-effectively dehumidified with for example sunlight or artificial heat sources in open reservoirs. In the reservoirs the still remaining water is reduced to the minimum and then the salt precipitates. Finally it can be skimmed for later usage. A welcome side effect is that the 'waste product' during the common salt production is usable freshwater.

8.6. Heat storage made of PCM or sand

Another innovative idea is to use phase change materials (PCM) in the system for the heat storage. During the phase change between two different phases more energy can be stored compared to an exclusive temperature rise in a fluid or in a solid. For example 1 kg ice at 0 °C needs 333 kJ for melting. If the same energy amount is added to the liquid after melting, it increases its temperature to 80 °C. The energy, which is needed for melting, is called latent heat and it is characteristic for all phase changes [Phy11]. Additionally the phase changes can be repeated several times without a problem. The technology is already used in construction materials and was already discussed in the international Smart-Eco project [Sma10]. For the heat storage for the Sunwater project the phase change from solid to liquid must be in the range between 80 °C and 110 °C. Therefore ice and liquid water cannot be used, but there is the possibility to use sugar alcohols or paraffins, which have a phase change in this temperature range. The enthalpy of fusion is in the range between 200 kJ/l and 400 kJ/l. For temperatures up to 200 °C nitrates or hydroxides can be used, which have a higher enthalpy of fusion. It is in the range between 200 kJ/l and 700 kJ/l. This technology can for example be included in later demonstration plants or in other worldwide realisations.
Another cheap realisation for a heat storage tank can for example be sand, which can be found in deserts. This material is very cheap and with the right technology it can be used as a heat buffer. The sand itself works as an insulation material. For these the ground must be divided into different layers. The highest layer is for the insulation and the other layers can be used as a heat storage system. For this realisations, pipes (heat exchangers) must be installed in the ground, which transfer the energy from the solar collectors to the heat storage materials. The same pipes can also be used to extract the stored energy. The technology is still in development, but in the future it could be ready for the market [Spi10].

8.7. Desalination with magnetic (and electric) fields

Another possibility is to convert saltwater with magnetic fields. This can for example be combined with electric fields. Due to the dissociation of salt crystals into anions and kations (2.2.1) magnetic fields can be used to separate the ions from the water. This can be explained with the Lorentz force F_L. The electric fields generated between the different ions could for example be compensated with an external electric field. If the set-up of the magnetic field and the volume flow is perpendicular, the ions inside the water are shifted into the third direction in space. The anions and kations are shifted due to different charges into an opposites direction. Now the three different streams can be separated from each other. One contains water with anions, the other contains water with kations and the middle layer is water without any ions. With this constellation usable freshwater can be produced. This innovative idea can also combined with superconductive magnets, which could reduce the electricity costs.

9. Conclusion of the Sunwater project and future prospects

During this project it was shown, that it is possible to produce freshwater with a solar desalination. This was the aim of this project, as can be seen in section 1.1. The solar energy can be tapped in a lot of areas to produce enough thermal heat to operate an evaporation desalination unit to produce high-quality freshwater. The quality is high enough for the daily life in private homes and agriculture, which is very important for the health of the people and the supply with foods. During this project different prospects were shown, which should be taken into account during a later realisation and for a commercial use.
During this project different objectives, as can be seen in section 1.1, had to be solved and were solved. At the beginning a project consortium was found, who wanted to contribute in this great project. Another solved aspect of this project was the system model of the complete system and a model of the solar desalination based on the solar thermal part and the WDU. Furthermore all needed data were found or simulated to simulate the solar thermal part and the WDU in Simulink. Additionally the complete demonstration plant was installed in Egypt. At the end of the project life time a few measurements were done in Egypt. With these measurements an optimisation of the complete system could be realised. Future prospects were also theoretically added to improve later realisations. Finally the schedule of the complete project was met and all objectives were achieved.
During this project it was not possible to install a heat pump at the demonstration plant which has a flow temperature of 90 °C or higher, because only one company was found in Germany who can produce such a heat pump. This technology is still in development and therefore this company was not interested in joining this project. Due to this unavailability the heat pump was not installed at the final demonstration plant and due to this reason the heat exchangers were not necessary. During the project a few solenoid valves were planed at the building site, but they were finally not installed, because the Egyptian partner did not see the importance of these components. On bigger problem during the measurements was that the temperature increases to temperatures higher than 120 °C and due to this a volume flow sensor was damaged. Later this was avoided by reducing the operation temperature of the solar thermal roof to temperatures below 85 °C.Only a few measurements were done at the demonstration plant, because the revolution started in Egypt and this was at the end of the project life time. Unfortunately different aspects could not be tested and measured.

The solar energy has enough potential to operate numerous solar desalination units. An important problem, which was seen during this project was, that the Sun only shines for a few hours a day and within this time only a few hours can directly be used to produce the needed operation temperature and volume flows for the operation of the demonstration plant. During other times the needed thermal energy should come from alternative energy sources like from waste heat or from another environmentally friendly energy source. If the desalination unit should be operated 24 h/d with solar energy, the solar area must be planned much bigger. During the short time period at noon and the early afternoon enough thermal energy must be produced and stored to operate the whole system during the time with a low solar radiation. With a bigger solar area more energy can be harvested, but the storage of this thermal energy is relatively difficult, as was shown. The energy density and the storage volume must be improved. The energy density can for example be expanded, if the process water is stored with overpressure and thus the temperature level can be raised. Later the water can be mixed up with colder water to generate the needed volume flows in the system and to get the needed process temperatures for the water desalination unit. With this trick the needed volume flows can be generated and additionally the lower volume flow through the storages, which is based on the higher temperatures, improves the efficiencies of the heat storage tanks. The efficiencies are improved, because less turbulences are induced in them. Additionally new heat storages could be used, which have a better efficiency. An innovative idea is the usage of PCMs or sand. If the phase change of the PCMs is in the right temperature range, much more energy can be stored compared to materials without a phase change. The heat transfer could be initialised with heat exchangers, which are installed inside the well-insulated heat storage tanks.
Another larger problem was the storage of the produced heat for later usage. For a short time period, the heat storage tanks can be used, but for a long storage time other possibilities must be considered. Due to the high temperature differences between the environment and the process water, special heat storage aspects must be considered to keep the process water temperature at a high level. Regular insulation materials are not good enough for an adequate insulation, which was reflected due to the high temperature losses during the night. At this temperature level special materials or technologies are necessary. One possibility could be the usage of vacuum as an insulation material like for Helium Dewar vessels. Additionally very thick insulation materials with a very low heat transfer coefficient could be helpful. Otherwise a lot of energy is lost to the environment, as was seen in the measuring results. Another bigger problem is the convective flow of hot water inside the pipes and the heat storage tanks. This also has an essential effect on the energy losses in the system. Especially in the night the water rises to the collectors and the stored energy is released to the environment. This can for example be prevented with an installation of solenoid valves in the pipes. One should be installed in the supply line and one in the return line. One solenoid valve is not enough to stop the convection in the whole system, because the water can flow in lager pipes parallel in both directions. On the one side it rises to the collectors and on the other side it drops.
For a better and a higher efficiency, vacuum tube collectors should be used to generate the needed volume flows. It can for example be combined with mirrors to increase the output

temperatures. Another very innovative idea could be to use a concentrating solar thermal system. With this technology temperatures higher than 1000 °C are possible. The produced thermal flow can be mixed up with colder fluids to generate the needed volume flows to operate the water desalination unit. Furthermore there is also the possibility to combine this technology with power generation. The generated high temperature volume flows can be used in the first step to generate electrical power and the remaining thermal energy is normally high enough to operate the water desalination unit. This combination is very future-proof and could help to generate environmentally friendly electrical energy and in addition needed freshwater. This installation can for example be done in countries with a very high solar radiation and normally there is also a high demand on freshwater.

During the simulation of the water desalination it was observed, that it is very important to raise the temperature inside the WDU to a very high temperature. It must be as close as possible below the boiling temperature of saltwater. As was shown the water vapour pressure curve has an exponential form and therefore a few degrees more or less have an important impact on the freshwater production rate. Due to the heat exchangers and the heat transfer the temperature of the heat source must be higher than the desired temperature in the desalination unit. With the continuous control and a continuous coordination of the heat source temperature in the system and the saltwater temperature in the WDU the efficiency of the desalination unit can be raised. Additionally the ambient pressure could be consulted for an optimisation, because the boiling temperature depends on this condition. Furthermore the volume flow of the air inside the WDU could be optimised to a higher freshwater output. A few possibilities were already presented in this document. The maximum volume flow of the air depends on the size of the saltwater drops and the available energy for the desalination process. Finally the project was successful and the freshwater production with solar thermal energy was shown. A lot of problems were solved and new aspects can be included in later realisations. Now the system can be used to generate freshwater with a very high quality. Later implementations in hotel chains or in smaller towns are possible, but more scientific work is necessary for improvements and design matching.

The environmentally friendly production of freshwater can help secure the future, but first a high capital investment is necessary. The first steps are met with this project and the results are promising for the future ...

A. Equation of Time

It is commonly known, that the orbit of the Earth around the Sun is on a elliptical path. The Sun is in one of the two focal points of the ellipse [Fli01]. It is described in the first Kepler's law B.5. During the path through the solar system the speed of the Earth varies, because of the acceleration and deceleration of the Earth on this path. This is mainly based on the gravitational force of the Sun. This has the effect that in the same timescale the speed of the position vector between the Sun and the Earth varies over the year according to Kepler's 2nd law (B.23). In the same period of time $\mathrm{d}t$ the covered area $\mathrm{d}A$ is always the same. It can be written as ${}^{\mathrm{d}A}/_{\mathrm{d}t} = \text{const}$. This means that the angular velocity of the Earth is different throughout the whole year, but it is valid

$$t\frac{\mathrm{d}A}{\mathrm{d}t} = \frac{t}{T}\pi ab \quad \text{with} \quad 0 \leq t \leq T, \tag{A.1}$$

where a and b are the semi-major and semi-minor axis of the ellipse, T is the time of circulation and t the running time. The square of the orbital period of a planet T is directly proportional to the cube of the semi-major axis a of its orbit. This can be shown with the third Kepler's law (B.24). The semi-major axis of the Earth has $a = 149.598\,\mathrm{Gm}$ and the semi-minor axis $b = 149.577\,\mathrm{Gm}$. This has the effect that the numerical eccentricity of the Earth e is just

$$e = \frac{\sqrt{a^2 - b^2}}{a} = \sqrt{1 - \frac{b^2}{a^2}} = 0.0167. \tag{A.2}$$

This value is close to zero and so the path is nearly circular and therefore the speed varies slightly during the year. The perihelion is the nearest position of the Sun with 147.1 Gm and the aphelion is the farthest position of the Sun with 152.1 Gm. The length of the semi-major axis is the mean of both values. Other gravitational effects from other planets, relativistic effects and the quadrupole moment of the Sun are neglected in the following calculations. Another important effect is the orbital inclination of the Earth which must be considered during the calculation of the Equation of Time. At the moment the angle between the axis of rotation and the ecliptic is $\epsilon = 23°26'21.45''$. In 40 000 years the ecliptic varies between $21°55'$ and $24°18'$ [Chi04]. These are two reasons why the apparent local time differs from the mean solar time. The apparent local time is the time when the Sun is in the local meridian or rather exactly in the astronomic south. This time is defined as 12 o'clock or noon. This position is also called upper culmination. Another definition is based on the lower culmination, which defines the start of the day. The apparent time is the time which is shown on a solar clock. It

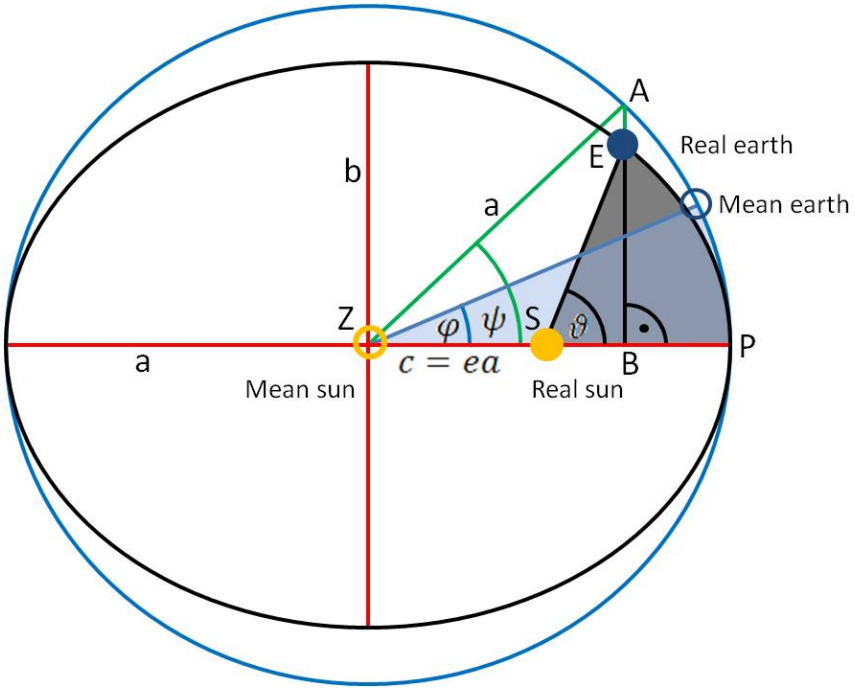

Fig. A.1.: Comparison between mean Earth and Sun (blank) and real Earth and Sun (unfilled). Furthermore the different angles φ, ϑ and ψ are shown, which are used in the calculation. This diagram is not true to scale.

varies from location to location if it is not on the same longitude. During the year the difference between local time and mean time which is measured for example with mechanical or atomic clocks, can be between 16 min in autumn and −14 min in spring. The difference between the apparent time and the local time can be calculated with the Equation of Time (EoT). Due to the large period, the nutation and precession will not be considered in the following calculations. During one year and the long period of the effects, the Earth can be assumed to have the same direction in the universe.
The following section is based on [Mue93] and the calculations are presented in more detail compared to the original paper. In addition a few calculations were slightly modified to make it more clear. The idea is to present the calculation step by step, which includes the necessary intermediate steps and for example the necessary additional theorems.
Kepler was the first person who had the idea to compare the real path of the Earth with the path of an Earth which is on a circular orbit around the Sun. The speed of the mean Earth around the Sun is always the same in contrast to the real Earth. For this situation different angles are considered. A short overview can be seen in Fig. A.1. The distance between the mean Sun and the real Sun is $c = ea$. The angle φ is the angle between the semi-major axis and the mean Earth based on the mean Sun. This angle is called *mean anomaly*. On the other side is ϑ the angle between the real Earth and the same axis, but this angle is based on the real Sun. This angle is called *true anomaly*. The last angle which is shown in Fig. A.1, is ψ. ψ is the angle between the

mean Sun and the perpendicular projection of the real Earth referred to the semi-major axis onto the path of the mean Earth. The intersection is in A. This angle is called *eccentric anomaly* and it can be used to calculate the area of the elliptic sectors. It was introduced by Kepler. For the following calculation it is assumed, that both, the true and the mean Earth, start in point P and run on different paths around the Sun. P is also called the perihelion. The time of circulation is for both T. In a defined time the real Earth covers the angle ϑ and the angle φ of the mean Earth is swept in the same time. This is justified with Kepler's 2nd law and (A.1). For the angle φ is valid

$$\varphi = 2\pi\frac{t}{T}. \tag{A.3}$$

It is $t = 0$ in P and for one period of circulation, t is between 0 and T. Fig. A.1 shows the relation

$$\tan(\vartheta) = \frac{\overline{EB}}{\overline{SB}} = \frac{\frac{b}{a}\overline{AB}}{\overline{ZB} - \overline{ZS}} = \frac{\frac{b}{a}a\sin(\psi)}{a\cos(\psi) - ea} = \frac{b}{a}\frac{\sin(\psi)}{\cos(\psi) - e} \overset{(A.2)}{=} \frac{\sqrt{1-e^2}\sin(\psi)}{\cos(\psi) - e}. \tag{A.4}$$

The second equal sign is justified by the parametric representation of the circle and the ellipse. It can also be seen with (B.41) and (A.4)

$$\begin{aligned}\cos(\vartheta) &= \sqrt{\frac{1}{1+\tan^2(\vartheta)}} = \sqrt{\frac{(\cos(\psi)-e)^2}{(\cos(\psi)-e)^2 + (1-e^2)\sin^2(\psi)}} \\ &= \frac{\cos(\psi)-e}{\sqrt{\cos^2(\psi) - 2e\cos(\psi) + e^2 + \sin^2(\psi) - e^2\sin^2(\psi)}} \\ &\overset{(B.50)}{=} \frac{\cos(\psi)-e}{\sqrt{1 - 2e\cos(\psi) + e^2(1-\sin^2(\psi))}} \overset{(B.50)}{=} \frac{\cos(\psi)-e}{1-e\cos(\psi)}.\end{aligned} \tag{A.5}$$

With the trigonometric function for the half angle (B.52) can be calculated

$$\begin{aligned}\tan\left(\frac{\vartheta}{2}\right) &= \sqrt{\frac{1-\cos(\vartheta)}{1+\cos(\vartheta)}} = \sqrt{\frac{1 - e\cos(\psi) - \cos(\psi) + e}{1 - e\cos(\psi) + \cos(\psi) - e}} = \sqrt{\frac{(1+e)(1-\cos(\psi))}{(1-e)(1+\cos(\psi))}} \\ &= \sqrt{\frac{1+e}{1-e}}\sqrt{\frac{1-\cos(\psi)}{1+\cos(\psi)}} \overset{(B.52)}{=} \sqrt{\frac{1+e}{1-e}}\tan\left(\frac{\psi}{2}\right).\end{aligned} \tag{A.6}$$

In the following it will be substituted:

$$\text{const.} = \sqrt{\frac{1-e}{1+e}} =: \cos(\alpha), \qquad \frac{\vartheta}{2} =: y, \qquad \frac{\psi}{2} =: x \tag{A.7}$$

For e between 0 and 1 the function of the first term is a bijective function in the codomain between 0 and 1. Therefore the function can be described by a cosine, because this

function is also bijective between 0 and π. In this case it is enough to limit the α domain between 0 and $\pi/2$. In the following (A.6) and (A.7) can be combined:

$$\tan(y) = \frac{\tan(x)}{\cos(\alpha)} \quad \Rightarrow \quad y = \arctan\left(\frac{\tan(x)}{\cos(\alpha)}\right) \tag{A.8}$$

This will be differentiated with the respect to x:

$$\begin{aligned}
\frac{\mathrm{d}y}{\mathrm{d}x} &\overset{(B.56)}{\underset{(B.55)}{=}} \frac{1}{1+\frac{\tan^2(x)}{\cos^2(\alpha)}} \cdot \frac{1}{\cos(\alpha)\cos^2(x)} = \frac{\cos(\alpha)}{\cos^2(\alpha)\cos^2(x)+\sin^2(x)} \\
&\overset{(B.44)}{\underset{(B.45)}{=}} \frac{\cos(\alpha)}{\frac{1}{2}\cos^2(\alpha)\left(1+\cos(2x)\right)+\frac{1}{2}\left(1-\cos(2x)\right)} \\
&\overset{(B.50)}{=} \frac{\cos(\alpha)}{\frac{\cos^2(\alpha)}{2}+\frac{\left(1-\sin^2(\alpha)\right)\cos(2x)}{2}+\frac{1}{2}-\frac{\cos(2x)}{2}} \\
&= \frac{2\cos(\alpha)}{1-\sin^2(\alpha)\cos(2x)+\cos^2(\alpha)} =: f(x)
\end{aligned} \tag{A.9}$$

This equation can be simplified with (B.43):

$$\begin{aligned}
f(x) &= \frac{2\cos(\alpha)}{1+\cos^2(\alpha)-\sin^2(\alpha)\left(\cos^2(x)-\sin^2(x)\right)} \\
&\overset{(B.50)}{=} \frac{2\cos(\alpha)}{1+\cos^2(\alpha)-\sin^2(\alpha)\cos^2(x)+\sin^2(\alpha)\left(1-\cos^2(x)\right)} \\
&\overset{(B.50)}{=} \frac{2\cos(\alpha)}{2-2\sin^2(\alpha)\cos^2(x)} = \frac{\cos(\alpha)}{1-\sin^2(\alpha)\cos^2(x)}
\end{aligned} \tag{A.10}$$

This equation is a periodical function and therefore it can be expanded into a Fourier series (B.27) with the corresponding coefficient (B.28) and (B.29). The first coefficient a_0 can easily be calculated with

$$a_0 = \frac{1}{\pi}\int_0^{2\pi} f(x)\,\mathrm{d}x = \frac{1}{\pi}\int_0^{2\pi}\frac{\mathrm{d}y}{\mathrm{d}x}\,\mathrm{d}x = \frac{1}{\pi}\int_0^{2\pi}\mathrm{d}y = 2. \tag{A.11}$$

With the first coefficient the first term in (B.27) has the value $\frac{a_0}{2} = 1$. In the following calculations of a_n and b_n the indices n start in both cases with $n = 1$. The next step is to calculate the values of the a_n for the function (A.9). For this it is necessary to replace the cosine terms in (B.28) with (B.40)

$$a_n = \frac{1}{\pi}\int_0^{2\pi}\frac{\cos(\alpha)\left(\exp(\mathrm{i}\,nx)+\exp(-\mathrm{i}\,nx)\right)}{1+\cos^2(\alpha)-\sin^2(\alpha)\frac{\exp(\mathrm{i}\,2x)+\exp(-\mathrm{i}\,2x)}{2}}\,\mathrm{d}x. \tag{A.12}$$

With the substitution

$$z = \exp(\mathrm{i}\,2x) \quad \Rightarrow \quad \frac{\mathrm{d}z}{\mathrm{d}x} = \mathrm{i}\,2\exp(\mathrm{i}\,2x) \quad \Rightarrow \quad \mathrm{d}x = \frac{dz}{\mathrm{i}\,2\exp(\mathrm{i}\,2x)} = -\mathrm{i}\,\frac{\mathrm{d}z}{2z} \tag{A.13}$$

the equation will be

$$a_n = -\frac{\mathrm{i}}{\pi}\oint \frac{\cos(\alpha)\left(z^{n/2}+z^{-n/2}\right)}{2z(1+\cos^2(\alpha))-\sin^2(\alpha)\,(z^2+1)}\,\mathrm{d}z$$
$$= \frac{\mathrm{i}}{\pi}\oint \frac{\cos(\alpha)\left(z^{n/2}+z^{-n/2}\right)}{\sin^2(\alpha)\left(z^2-\frac{2(1+\cos^2(\alpha))}{\sin^2(\alpha)}z+1\right)}\,\mathrm{d}z. \tag{A.14}$$

Due to the complex substitution, the integral changes to a closed integral, because the integration is now twice the unit circle. This is based on the substitution and the limits of the integral (A.12). The next step is to calculate the roots of the denominator, it is based on z

$$z^2 - \frac{2(1+\cos^2(\alpha))}{\sin^2(\alpha)}z + 1 = 0. \tag{A.15}$$

The polynomial is standardised and the results are

$$z_{1,2} = \frac{1+\cos^2(\alpha)}{\sin^2(\alpha)} \pm \sqrt{\frac{(1+\cos^2(\alpha))^2}{\sin^4(\alpha)} - 1}$$
$$= \frac{1+\cos^2(\alpha)}{\sin^2(\alpha)} \pm \sqrt{\frac{1+2\cos^2(\alpha)+\cos^4(\alpha)-\sin^4(\alpha)}{\sin^4(\alpha)}}.$$

This equation can be simplified with (B.47) and (B.48)

$$z_{1,2} = \frac{1+\cos^2(\alpha)}{\sin^2(\alpha)}$$
$$\pm \frac{\sqrt{1+2\cos^2(\alpha)+\frac{1}{8}\left(\cos(4\alpha)+4\cos(2\alpha)+3\right)-\frac{1}{8}\left(\cos(4\alpha)-4\cos(2\alpha)+3\right)}}{\sin^2(\alpha)}$$
$$= \frac{1+\cos^2(\alpha)}{\sin^2(\alpha)} \pm \frac{1}{\sin^2(\alpha)}\sqrt{1+2\cos^2(\alpha)+\cos(2\alpha)}.$$

With (B.43) it can be evaluated:

$$z_{1,2} = \frac{1+\cos^2(\alpha)}{\sin^2(\alpha)} \pm \frac{1}{\sin^2(\alpha)}\sqrt{1+2\cos^2(\alpha)+\cos^2(\alpha)-\sin^2(\alpha)}$$
$$\overset{(B.50)}{=} \frac{1+\cos^2(\alpha)}{\sin^2(\alpha)} \pm \frac{1}{\sin^2(\alpha)}\sqrt{1+3\cos^2(\alpha)-1+\cos^2(\alpha)}$$
$$= \frac{1+\cos^2(\alpha)}{\sin^2(\alpha)} \pm \frac{2\cos(\alpha)}{\sin^2(\alpha)} = \frac{1\pm 2\cos(\alpha)+\cos^2(\alpha)}{\sin^2(\alpha)} = \left(\frac{1\pm\cos(\alpha)}{\sin(\alpha)}\right)^2 \tag{A.16}$$

Now the solutions of the denominator (A.14) can be listed:

$$z_1 = \left(\frac{1+\cos(\alpha)}{\sin(\alpha)}\right)^2 \overset{(B.53)}{=} \cot^2\left(\frac{\alpha}{2}\right) \tag{A.17}$$

$$z_2 = \left(\frac{1-\cos(\alpha)}{\sin(\alpha)}\right)^2 \overset{(B.52)}{=} \tan^2\left(\frac{\alpha}{2}\right) \tag{A.18}$$

With this, solution (A.14) can be written as

$$a_n = \frac{\mathrm{i}}{\pi} \oint \frac{\cos(\alpha)}{\sin^2(\alpha)} \frac{z^{n/2} + z^{-n/2}}{\left(z - \tan^2\left(\frac{\alpha}{2}\right)\right)\left(z - \cot^2\left(\frac{\alpha}{2}\right)\right)} \,\mathrm{d}z. \tag{A.19}$$

For the solution of this equation, the denominator will be expanded into a partial fraction:

$$\begin{aligned} &\frac{1}{\left(z - \tan^2\left(\frac{\alpha}{2}\right)\right)\left(z - \cot^2\left(\frac{\alpha}{2}\right)\right)} = \frac{A}{z - \tan^2\left(\frac{\alpha}{2}\right)} + \frac{B}{z - \cot^2\left(\frac{\alpha}{2}\right)} \\ &= \frac{A\left(z - \cot^2\left(\frac{\alpha}{2}\right)\right) + B\left(z - \tan^2\left(\frac{\alpha}{2}\right)\right)}{\left(z - \tan^2\left(\frac{\alpha}{2}\right)\right)\left(z - \cot^2\left(\frac{\alpha}{2}\right)\right)} = \frac{(A+B)z - A\cot^2\left(\frac{\alpha}{2}\right) - B\tan^2\left(\frac{\alpha}{2}\right)}{\left(z - \tan^2\left(\frac{\alpha}{2}\right)\right)\left(z - \cot^2\left(\frac{\alpha}{2}\right)\right)} \end{aligned} \tag{A.20}$$

With the comparison of the coefficients follow the values for A and B. The first term implicates

$$A + B = 0 \quad \Rightarrow \quad A = -B \tag{A.21}$$

and the second term gives:

$$\begin{aligned} &- A\cot^2\left(\frac{\alpha}{2}\right) - B\tan^2\left(\frac{\alpha}{2}\right) = 1 \\ &\Rightarrow A\left(\tan^2\left(\frac{\alpha}{2}\right) - \cot^2\left(\frac{\alpha}{2}\right)\right) = 1 \\ &\Rightarrow A = \frac{1}{\tan^2\left(\frac{\alpha}{2}\right) - \cot^2\left(\frac{\alpha}{2}\right)} = -B \end{aligned} \tag{A.22}$$

With these results, the equation (A.19) can be written as

$$a_n = \frac{\mathrm{i}}{\pi} \oint \frac{\cos(\alpha)}{\sin^2(\alpha)} \frac{z^{n/2} + z^{-n/2}}{\tan^2\left(\frac{\alpha}{2}\right) - \cot^2\left(\frac{\alpha}{2}\right)} \left(\frac{1}{z - \tan^2\left(\frac{\alpha}{2}\right)} - \frac{1}{z - \cot^2\left(\frac{\alpha}{2}\right)}\right) \mathrm{d}z. \tag{A.23}$$

At the moment it is not possible to find a closed-form expression. For the evaluation of the integral, the integrand must be simplified. Therefore the denominator of the second fraction will be simplified with (B.52) and (B.53):

$$\begin{aligned} &\tan^2\left(\frac{\alpha}{2}\right) - \cot^2\left(\frac{\alpha}{2}\right) = \left(\frac{1-\cos(\alpha)}{\sin(\alpha)}\right)^2 - \left(\frac{1+\cos(\alpha)}{\sin(\alpha)}\right)^2 \\ &= \frac{1 - 2\cos(\alpha) + \cos^2(\alpha) - 1 - 2\cos(\alpha) - \cos^2(\alpha)}{\sin^2(\alpha)} = -\frac{4\cos(\alpha)}{\sin^2(\alpha)} \end{aligned} \tag{A.24}$$

With this short calculation the integral (A.23) can now be written as

$$a_n = -\frac{\mathrm{i}}{4\pi} \oint \left(z^{n/2} + z^{-n/2}\right) \left(\frac{1}{z - \tan^2\left(\frac{\alpha}{2}\right)} - \frac{1}{z - \cot^2\left(\frac{\alpha}{2}\right)} \right) \mathrm{d}z. \tag{A.25}$$

With the following side consideration, the above equation can also be simplified. For the evaluation of the first fraction the infinite geometrical series (B.25) is used. With $x = \frac{a}{z}$ and $a_0 = \frac{1}{z}$ it can be calculated

$$\frac{1}{z} \sum_{k=0}^{\infty} \left(\frac{a}{z}\right)^k = \frac{1}{z} \frac{1}{1 - \frac{a}{z}} = \frac{1}{z - a}. \tag{A.26}$$

With the substitution $a = \tan^2\left(\frac{\alpha}{2}\right)$ the first fraction in (A.25) is

$$\frac{1}{z - \tan^2\left(\frac{\alpha}{2}\right)} = \frac{1}{z} \sum_{i=0}^{\infty} \left(\frac{\tan^2\left(\frac{\alpha}{2}\right)}{z} \right)^i. \tag{A.27}$$

Now the second fraction of (A.25) will be analysed with an infinite Taylor series. Due to the constant number of $\cot^2\left(\frac{\alpha}{2}\right)$ the term can be written as:

$$f(z) = -\frac{1}{z - \frac{1}{a}} \qquad \text{with } a = \text{const.} \tag{A.28}$$

For the Taylor series the first derivations are necessary:

$$f^{(1)}(z) = \frac{1}{\left(z - \frac{1}{a}\right)^2} \tag{A.29}$$

$$f^{(2)}(z) = -\frac{2\left(z - \frac{1}{a}\right)}{\left(z - \frac{1}{a}\right)^4} = -\frac{2}{\left(z - \frac{1}{a}\right)^3} \tag{A.30}$$

$$f^{(3)}(z) = \frac{6\left(z - \frac{1}{a}\right)^2}{\left(z - \frac{1}{a}\right)^6} = \frac{6}{\left(z - \frac{1}{a}\right)^4} \tag{A.31}$$

$$\vdots$$

$$f^{(i)}(z) = (-1)^{i+1} \frac{i!}{\left(z - \frac{1}{a}\right)^{i+1}} \qquad \text{for } i \in \mathbb{N}_0 \tag{A.32}$$

With the last equation, the i-th derivation of the function $f(z)$ can be calculated. These derivations will be used in the infinite Taylor series (B.26) with the expansion point $z_0 = 0$. This Taylor series is also called Maclaurin series:

$$f(z) = a + a^2 z + a^3 z^2 + \ldots = \sum_{i=0}^{\infty} a^{i+1} z^i = a \sum_{i=0}^{\infty} (az)^i \tag{A.33}$$

With $\frac{1}{a} = \cot^2\left(\frac{\alpha}{2}\right)$ and therefore $a = \frac{1}{\cot^2\left(\frac{\alpha}{2}\right)} = \tan^2\left(\frac{\alpha}{2}\right)$ the equation (A.28) can be written as

$$-\frac{1}{z - \cot^2\left(\frac{\alpha}{2}\right)} = \tan^2\left(\frac{\alpha}{2}\right) \sum_{i=0}^{\infty} \left(\tan^2\left(\frac{\alpha}{2}\right) z\right)^i . \tag{A.34}$$

The terms (A.27) and (A.34) can also be calculated the other way around and now the solutions can be inserted into the integrand (A.25)

$$-\frac{\mathrm{i}}{4\pi}\left(z^{n/2} + z^{-n/2}\right)\left(\frac{1}{z}\sum_{i=0}^{\infty}\left(\frac{\tan^2\left(\frac{\alpha}{2}\right)}{z}\right)^i + \tan^2\left(\frac{\alpha}{2}\right)\sum_{i=0}^{\infty}\left(\tan^2\left(\frac{\alpha}{2}\right) z\right)^i\right). \tag{A.35}$$

With the next intermediate thought it is easier to evaluate the equation (A.35). For $0 \le x \le 2\pi$ and the substitution used (A.13), the new limits are $1 = \exp(\mathrm{i}\,0) \le z \le \exp(\mathrm{i}\,4\pi)$. The first calculation is for $P \neq -1$:

$$\begin{aligned}\oint z^P \,\mathrm{d}z = \int_1^{\exp(\mathrm{i}\,4\pi)} z^P \,\mathrm{d}z = \frac{z^{P+1}}{P+1}\bigg|_1^{\exp(\mathrm{i}\,4\pi)} &= \frac{\exp(\mathrm{i}\,4\pi)^{P+1}}{P+1} - \frac{1}{P+1} \\ = \frac{1}{P+1} - \frac{1}{P+1} = 0 \qquad &\text{for } P \neq -1\end{aligned} \tag{A.36}$$

The case $P = -1$ has a different solution:

$$\oint z^P \,\mathrm{d}z = \oint \frac{1}{z}\,\mathrm{d}z = \int_1^{\exp(\mathrm{i}\,4\pi)} \frac{1}{z}\,\mathrm{d}z = \ln(z)\Big|_1^{\exp(\mathrm{i}\,4\pi)} = \mathrm{i}\,4\pi \qquad \text{for } P = -1 \tag{A.37}$$

These solutions can be summarised as:

$$\oint z^P \,\mathrm{d}z = \int_1^{\exp(\mathrm{i}\,4\pi)} z^P \,\mathrm{d}z = \begin{cases} 0 & \text{for } P \neq -1 \\ \mathrm{i}\,4\pi & \text{for } P = -1 \end{cases} \tag{A.38}$$

As can be seen in the summary, the integral has only a result, if the integrand has the form of $h(\alpha)/z$. Therefore the values of n and i in (A.35) can further be evaluated. All other terms can be neglected, because the other terms disappear after integration. As was defined above, it is still $n \ge 1$. For the next simplification the term (A.35) will be expanded and simplified:

$$\begin{aligned}&-\frac{\mathrm{i}}{4\pi}\left(z^{n/2-1}\sum_{i=0}^{\infty}\left(\frac{\tan^2\left(\frac{\alpha}{2}\right)}{z}\right)^i + \tan^2\left(\frac{\alpha}{2}\right) z^{n/2}\sum_{i=0}^{\infty}\left(\tan^2\left(\frac{\alpha}{2}\right) z\right)^i\right. \\ &\left. + z^{-n/2-1}\sum_{i=0}^{\infty}\left(\frac{\tan^2\left(\frac{\alpha}{2}\right)}{z}\right)^i + \tan^2\left(\frac{\alpha}{2}\right) z^{-n/2}\sum_{i=0}^{\infty}\left(\tan^2\left(\frac{\alpha}{2}\right) z\right)^i\right) \\ &= -\frac{\mathrm{i}}{4\pi}\left(\sum_{i=0}^{\infty}\tan^{2i}\left(\frac{\alpha}{2}\right) z^{n/2-1-i} + \tan^2\left(\frac{\alpha}{2}\right)\sum_{i=0}^{\infty}\tan^{2i}\left(\frac{\alpha}{2}\right) z^{n/2+i}\right.\end{aligned}$$

$$+\sum_{i=0}^{\infty}\tan^{2i}\left(\frac{\alpha}{2}\right)z^{-n/2-1-i}+\tan^2\left(\frac{\alpha}{2}\right)\sum_{i=0}^{\infty}\tan^{2i}\left(\frac{\alpha}{2}\right)z^{-n/2+i}\Bigg) \tag{A.39}$$

At this time every summand of the above term can be evaluated on its own with the result (A.38). The exponent of z must be -1 to get a contribution to the integral. For the evaluation the different exponents can be separately evaluated and with this result, it is possible to define the value of i. The value of i depends only on the value of n. For a given n there is only one possible i. This can be summarised as:

$$\begin{array}{llll|l}
1.\ \text{term} & \frac{n}{2}-1-i=-1 & \Rightarrow i=\frac{n}{2} & & >0 \text{ for } n=2k \text{ with } k\in\mathbb{N}\\
2.\ \text{term} & \frac{n}{2}+i=-1 & \Rightarrow i=-1-\frac{n}{2} & & <0 \text{ for } n=2k \text{ with } k\in\mathbb{N}\\
3.\ \text{term} & -\frac{n}{2}-1-i=-1 & \Rightarrow i=-\frac{n}{2} & & <0 \text{ for } n=2k \text{ with } k\in\mathbb{N}\\
4.\ \text{term} & -\frac{n}{2}+i=-1 & \Rightarrow i=-1+\frac{n}{2} & & \geq 0 \text{ for } n=2k \text{ with } k\in\mathbb{N}
\end{array} \tag{A.40}$$

As can be seen in the right column the value of n must be even. If n is odd, the value of i is not an integer and therefore the sum over i is not defined. In the second term it can be seen that for all even n the value of i is negative. Negative numerical values of i are not included in the sum and so this term completely disappears in the calculation. The third term also disappears, because n is greater than or equal to 2. For these values the numerical values of i are again negative and this is not covered with the infinite sum used. In the fourth term i is always greater than or equal to 0 and therefore this term must be considered in the integral. The results in (A.40) can be included in (A.39)

$$\begin{aligned}
&-\frac{\mathrm{i}}{4\pi}\left(\tan^n\left(\frac{\alpha}{2}\right)\frac{1}{z}+\tan^2\left(\frac{\alpha}{2}\right)\tan^{2(-1+n/2)}\left(\frac{\alpha}{2}\right)\frac{1}{z}\right)\\
&=-\frac{\mathrm{i}}{4\pi}\left(\tan^n\left(\frac{\alpha}{2}\right)\frac{1}{z}+\tan^n\left(\frac{\alpha}{2}\right)\frac{1}{z}\right)=-\frac{\mathrm{i}}{2\pi}\tan^n\left(\frac{\alpha}{2}\right)\frac{1}{z}.
\end{aligned} \tag{A.41}$$

This simplified term can be inserted into the integral (A.25) and now it is possible to determine it

$$\begin{aligned}
a_n&=-\frac{\mathrm{i}}{2\pi}\tan^n\left(\frac{\alpha}{2}\right)\int_1^{\exp(\mathrm{i}\,4\pi)}\frac{1}{z}\,\mathrm{d}z=-\frac{\mathrm{i}}{2\pi}\tan^n\left(\frac{\alpha}{2}\right)\mathrm{i}\,4\pi\\
&=2\tan^n\left(\frac{\alpha}{2}\right)\qquad\text{for } n=2k \text{ with } k\in\mathbb{N}.
\end{aligned} \tag{A.42}$$

The coefficients a_n were found which are necessary to calculate the Fourier series (B.27). The next steps are used to calculate the b_n which are also necessary for the calculation of the EoT. The coefficients can be calculated with (B.29). The principle is similar to the calculation of the a_n. The b_n also starts with $n=1$ and they will be rewritten with (A.9), (B.40) and (B.39)

$$b_n=-\frac{\mathrm{i}}{\pi}\int_0^{2\pi}\frac{\cos(\alpha)\left(\exp(\mathrm{i}\,nx)-\exp(-\mathrm{i}\,nx)\right)}{1+\cos^2(\alpha)-\sin^2(\alpha)\frac{\exp(\mathrm{i}\,2x)+\exp(-\mathrm{i}\,2x)}{2}}\,\mathrm{d}x. \tag{A.43}$$

It will be substituted again

$$z = \exp(\mathrm{i}\,2x) \quad \Rightarrow \quad \frac{\mathrm{d}z}{\mathrm{d}x} = \mathrm{i}\,2\exp(\mathrm{i}\,2x) \quad \Rightarrow \quad \mathrm{d}x = -\mathrm{i}\,\frac{\mathrm{d}z}{2z} \tag{A.44}$$

and b_n can now be written as:

$$\begin{aligned} b_n &= -\frac{\mathrm{i}}{\pi}\int_0^{\exp(\mathrm{i}\,4\pi)} \frac{\cos(\alpha)\left(z^{n/2}-z^{-n/2}\right)}{1+\cos^2(\alpha)-\sin^2(\alpha)\left(\frac{z}{2}+\frac{1}{2z}\right)}\frac{\mathrm{d}z}{\mathrm{i}\,2z} \\ &= \frac{1}{\pi}\oint \frac{\cos(\alpha)\left(z^{n/2}-z^{-n/2}\right)}{\sin^2(\alpha)\left(z^2-\frac{2(1+\cos^2(\alpha))}{\sin^2(\alpha)}z+1\right)}\,\mathrm{d}z \end{aligned} \tag{A.45}$$

The solutions in z of the denominator can be found in (A.17) and (A.18). Therefore the b_n can again be simplified with partial fraction expansion (A.22) and the term (A.24)

$$\begin{aligned} b_n &= \frac{1}{\pi}\oint \frac{\cos(\alpha)}{\sin^2(\alpha)}\frac{z^{n/2}-z^{-n/2}}{\left(z-\tan^2\left(\frac{\alpha}{2}\right)\right)\left(z-\cot^2\left(\frac{\alpha}{2}\right)\right)}\,\mathrm{d}z \\ &= \frac{1}{\pi}\oint \frac{\cos(\alpha)}{\sin^2(\alpha)}\frac{z^{n/2}-z^{-n/2}}{\tan^2\left(\frac{\alpha}{2}\right)-\cot^2\left(\frac{\alpha}{2}\right)}\left(\frac{1}{z-\tan^2\left(\frac{\alpha}{2}\right)}-\frac{1}{z-\cot^2\left(\frac{\alpha}{2}\right)}\right)\mathrm{d}z \\ &= -\frac{1}{4\pi}\oint \left(z^{n/2}-z^{-n/2}\right)\left(\frac{1}{z-\tan^2\left(\frac{\alpha}{2}\right)}-\frac{1}{z-\cot^2\left(\frac{\alpha}{2}\right)}\right)\mathrm{d}z. \end{aligned} \tag{A.46}$$

The next step is to replace the fractions in the integral with (A.27) and (A.34). Afterwards it can be simplified:

$$\begin{aligned} &\Rightarrow -\frac{1}{4\pi}\oint \left(z^{n/2}-z^{-n/2}\right)\left(\frac{1}{z}\sum_{i=0}^{\infty}\left(\frac{\tan^2\left(\frac{\alpha}{2}\right)}{z}\right)^i+\tan^2\left(\frac{\alpha}{2}\right)\sum_{i=0}^{\infty}\left(\tan^2\left(\frac{\alpha}{2}\right)z\right)^i\right)\mathrm{d}z \\ &= -\frac{1}{4\pi}\oint \left(\sum_{i=0}^{\infty}\tan^{2i}\left(\frac{\alpha}{2}\right)z^{n/2-1-i}+\tan^2\left(\frac{\alpha}{2}\right)\sum_{i=0}^{\infty}\tan^{2i}\left(\frac{\alpha}{2}\right)z^{n/2+i}\right. \\ &\left.-\sum_{i=0}^{\infty}\tan^{2i}\left(\frac{\alpha}{2}\right)z^{-n/2-1-i}-\tan^2\left(\frac{\alpha}{2}\right)\sum_{i=0}^{\infty}\tan^{2i}\left(\frac{\alpha}{2}\right)z^{-n/2+i}\right)\mathrm{d}z \end{aligned} \tag{A.47}$$

Every term can be evaluated separately like above. The results are the same as in (A.40) and with these, the b_n can be written as:

$$b_n = -\frac{1}{4\pi}\oint \left(\tan^n\left(\frac{\alpha}{2}\right)\frac{1}{z}-\tan^n\left(\frac{\alpha}{2}\right)\frac{1}{z}\right)\mathrm{d}z = 0 \tag{A.48}$$

As can be seen in the above equation, all coefficients b_n disappear. The infinite Fourier series (B.27) only consists of even coefficients a_n. With the already calculated coefficient a_0, this complete series can be written as

$$f(x) = \frac{\mathrm{d}y}{\mathrm{d}x} = 1 + 2\sum_{k=1}^{\infty}\tan^{2k}\left(\frac{\alpha}{2}\right)\cos(2kx). \tag{A.49}$$

The n was replaced by $2k$, because of the even numerical value of n. After integration the result is:

$$y = x + \sum_{k=1}^{\infty} \frac{1}{k} \tan^{2k}\left(\frac{\alpha}{2}\right) \sin(2kx) + \text{const.} \tag{A.50}$$

The absolute term will be calculated later. In the following, the term (B.52) will be rewritten with (A.7) and then the fraction will be expanded so that the 3rd binomial formula can be used

$$\begin{aligned}\tan^2\left(\frac{\alpha}{2}\right) &= \frac{1-\cos(\alpha)}{1+\cos(\alpha)} = \frac{1-\sqrt{\frac{1-e}{1+e}}}{1+\sqrt{\frac{1-e}{1+e}}} = \frac{1-2\sqrt{\frac{1-e}{1+e}}+\frac{1-e}{1+e}}{1-\frac{1-e}{1+e}} \\ &= \frac{1+e-2\sqrt{1-e^2}+1-e}{1+e-1+e} = \frac{1-\sqrt{1-e^2}}{e}.\end{aligned} \tag{A.51}$$

Now the term $\sqrt{1-e^2}$ will be expanded into a Taylor series (B.26) with the expansion point $e_0 = 0$ up to the 4th order:

$$\begin{aligned}\sqrt{1-e^2} &= \sqrt{1-e^2}\Big|_{e_0=0} + \frac{-e}{\sqrt{1-e^2}}\Big|_{e_0=0} e + \frac{1}{2!}\left(\frac{-1}{\sqrt{1-e^2}} + \frac{-e^2}{(1-e^2)^{3/2}}\right)\Big|_{e_0=0} e^2 \\ &+ \frac{1}{3!}\left(\frac{-e}{(1-e^2)^{3/2}} + \frac{-2e}{(1-e^2)^{3/2}} + \frac{-3e^3}{(1-e^2)^{5/2}}\right)\Big|_{e_0=0} e^3 \\ &+ \frac{1}{4!}\left(\frac{-3}{(1-e^2)^{3/2}} + \frac{-9e^2}{(1-e^2)^{5/2}} + \frac{-9e^2}{(1-e^2)^{5/2}} + \frac{-15e^4}{(1-e^2)^{7/2}}\right)\Big|_{e_0=0} e^4 \\ &+ \mathcal{O}(e^5) \\ &= 1 - \frac{e^2}{2} - \frac{e^4}{8} + \mathcal{O}\left(e^5\right)\end{aligned} \tag{A.52}$$

With this Taylor series the equation (A.51) can be written as

$$\tan^2\left(\frac{\alpha}{2}\right) = \frac{e}{2} + \frac{e^3}{8}. \tag{A.53}$$

The equation (A.50) yields with the back substitution (A.7):

$$y = x + \sum_{k=1}^{\infty} \frac{1}{k}\left(\frac{e}{2} + \frac{e^3}{8}\right)^k \sin(2kx) + \text{const.} \tag{A.54}$$

$$\Rightarrow \vartheta = \psi + 2\sum_{k=1}^{\infty} \frac{1}{k}\left(\frac{e}{2} + \frac{e^3}{8}\right)^k \sin(k\psi) + \text{const.} \tag{A.55}$$

With the side condition, that the mean Earth and the real Earth start at the same point, the absolute term can be calculated. The side condition is $\vartheta(\psi = 0) = 0$ and so the solution is

$$\vartheta(\psi = 0) = \text{const.} = 0. \tag{A.56}$$

Now the equation can be written as

$$\begin{aligned}\vartheta(\psi) &= \psi + 2\sum_{k=1}^{\infty}\frac{1}{k}\left(\frac{e}{2}+\frac{e^3}{8}\right)^k \sin(k\psi)\\ &\approx \psi + \left(e+\frac{e^3}{4}\right)\sin(\psi) + \frac{e^2}{4}\sin(2\psi) + \frac{e^3}{12}\sin(3\psi) + \mathcal{O}(e^4).\end{aligned} \tag{A.57}$$

The angle ψ is in this case very helpful, because the angle describes the projection of the Earth around the Sun on a circular orbit. Due to Kepler's 2nd law (B.23), the speed of the Earth is always different. Only the angle φ is linear in time t instead of the other angles mentioned. With the linear angle, the calculation of the non-linear angles ϑ and ψ are possible. For the next calculations the geometrical issue is considered. The grey shaded area F in Fig. A.1 is

$$\begin{aligned}F &= \text{elliptic sector } SEP = \frac{b}{a}\left(\text{sector } ZAP - \text{triangle } ZAS\right)\\ &= \frac{b}{a}\left(\frac{\psi}{2\pi}\text{area}_{\text{circle}} - \frac{\overline{ZS}\,\overline{AB}}{2}\right) = \frac{b}{a}\left(\frac{\psi}{2}a^2 - \frac{ea^2\sin(\psi)}{2}\right)\\ &= \frac{ab}{2}\left(\psi - e\sin(\psi)\right).\end{aligned} \tag{A.58}$$

With Kepler's 2nd law of areas (B.23) it can be written as

$$F = \frac{t}{T}\pi ab \quad \text{and } \varphi = \frac{t}{T}2\pi \quad \Rightarrow F = \frac{ab}{2}\varphi. \tag{A.59}$$

(A.58) and (A.59) implies

$$\psi = \varphi + e\sin(\psi). \tag{A.60}$$

This equation is called Kepler's equation. This equation cannot be solved in closed form, only approximations are possible. This means that the real position of the Earth can only be approximated and it cannot exactly be calculated. The approximation can for example be done with the Lagrange reversion theorem (B.37) respectively (B.38). With the Lagrange reversion theorem the equation (A.60) can be expanded into a function of ψ with the variables e and φ. With

$$x = \psi, \quad t = \varphi, \quad m = e, \quad f(x) = \sin(x) \Rightarrow f(\varphi) = \sin(\varphi), \tag{A.61}$$

$$g(x) = g(\psi) = \psi \text{ (identity) and } g(t) = g(\varphi) = \varphi \text{ (identity)} \tag{A.62}$$

this equation can now be written as

$$\begin{aligned}\psi &= \varphi + \sum_{k=1}^{\infty}\frac{e^k}{k!}\frac{\partial^{k-1}}{\partial\varphi^{k-1}}\sin^k(\varphi) = \varphi + e\sin(\varphi) + \frac{e^2}{2!}\frac{\partial}{\partial\varphi}\sin^2(\varphi) + \frac{e^3}{3!}\frac{\partial^2}{\partial\varphi^2}\sin^3(\varphi) + \mathcal{O}(e^4)\\ &\overset{(B.46)}{=} \varphi + e\sin(\varphi) + \frac{e^2}{2}2\sin(\varphi)\cos(\varphi) + \frac{e^3}{6}\frac{\partial^2}{\partial\varphi^2}\frac{1}{4}\left(3\sin(\varphi) - \sin(3\varphi)\right) + \mathcal{O}(e^4)\end{aligned}$$

$$\overset{(B.42)}{=} \varphi + e\sin(\varphi) + \frac{e^2}{2}\sin(2\varphi) + \frac{e^3}{8}\left(3\sin(3\varphi) - \sin(\varphi)\right) + \mathcal{O}(e^4). \tag{A.63}$$

The expression ϑ in (A.57) can be rewritten in dependency of φ. For the complete substitution the terms $\sin(\psi)$, $\sin(2\psi)$ and $\sin(3\psi)$ must be calculated first. The term $\sin(\varphi)$ can easily be calculated with (A.60) and (A.63)

$$\sin(\psi) = \frac{\psi - \varphi}{e} = \sin(\varphi) + \frac{e}{2}\sin(2\varphi) + \frac{e^2}{8}\left(3\sin(3\varphi) - \sin(\varphi)\right) + \mathcal{O}(e^3). \tag{A.64}$$

Slightly more difficult is the calculation of the term $\sin(2\psi)$. For this the equation (B.37) and (A.61) can be used, but (A.62) must be modified. The modification is:

$$g(t) = \sin(2t) \quad \Rightarrow \quad g'(t) = 2\cos(2t) \tag{A.65}$$

The wanted term will be approximated up to the order e

$$\begin{aligned}
\sin(2\psi) &= \sin(2\varphi) + 2e\sin(\varphi)\cos(2\varphi) + \mathcal{O}\left(e^2\right) \\
&\overset{(B.44)}{=} \sin(2\varphi) + 2e\sin(\varphi)\left(1 - 2\sin^2(\varphi)\right) + \mathcal{O}\left(e^2\right) \\
&= \sin(2\varphi) + 2e\sin(\varphi) - 4e\sin^3(\varphi) + \mathcal{O}\left(e^2\right) \\
&\overset{(B.46)}{=} \sin(2\varphi) + 2e\sin(\varphi) - e\left(3\sin(\varphi) - \sin(3\varphi)\right) + \mathcal{O}\left(e^2\right) \\
&= \sin(2\varphi) + e\left(\sin(3\varphi) - \sin(\varphi)\right) + \mathcal{O}\left(e^2\right).
\end{aligned} \tag{A.66}$$

The last wanted term can be found with (B.37) and (A.61), but (A.62) must be modified again:

$$g(t) = \sin(3t) \quad \Rightarrow \quad g'(t) = 3\cos(3t) \tag{A.67}$$

This function will be calculated in this case up to the order e^0. This is only the first term in (B.37) and therefore it is

$$\sin(3\psi) = \sin(3\varphi) + \mathcal{O}\left(e\right). \tag{A.68}$$

The equations (A.63), (A.64), (A.66) and (A.68) will be used in (A.57)

$$\begin{aligned}
\vartheta = {} & \varphi + e\sin(\varphi) + \frac{e^2}{2}\sin(2\varphi) + \frac{e^3}{8}\left(3\sin(3\varphi) - \sin(\varphi)\right) \\
& + \left(e + \frac{e^3}{4}\right)\left(\sin(\varphi) + \frac{e}{2}\sin(2\varphi) + \frac{e^2}{8}\left(3\sin(3\varphi) - \sin(\varphi)\right)\right) \\
& + \frac{e^2}{4}\left(\sin(2\varphi) + e\left(\sin(3\varphi) - \sin(\varphi)\right)\right) + \frac{e^3}{12}\sin(3\varphi)
\end{aligned} \tag{A.69}$$

After simplification the equation up to the order e^3 is

$$\vartheta \approx \varphi + 2e\sin(\varphi) + \frac{5}{4}e^2\sin(2\varphi) + \frac{e^3}{4}\left(-\sin(\varphi) + \frac{13}{3}\sin(3\varphi)\right) + \mathcal{O}\left(e^4\right). \tag{A.70}$$

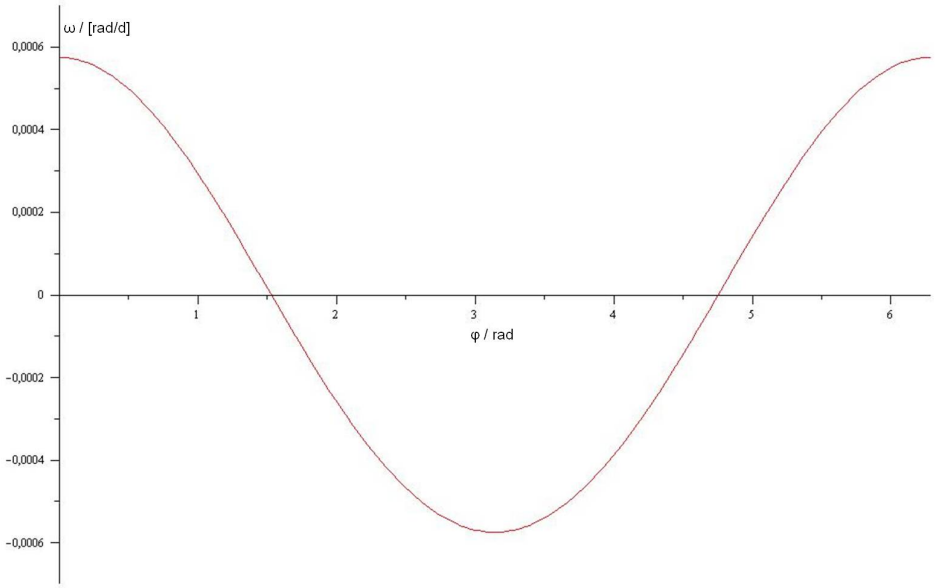

Fig. A.2.: Standardised angular velocity of the real Earth during the whole year based on the mean Earth on a circular orbit.

The above equation calculates the angle ϑ in dependency of the angle φ, this means the movement of the real Earth in dependency of the mean Earth. This relation can be seen in Fig. A.1. The formula can be truncated after the order of e^3, because the numerical value of e is very small (A.2). With $e = 0.0167$ the approximation is very exact. The main difference between the circular orbit and the elliptic orbit is just $2e$. So the difference between both paths is less than 3.5 %. With this formula the angular velocity of the Earth can be calculated. With the time dependency of φ (A.3) and the chain rule it can be determined as

$$\begin{aligned}\omega(t) &= \frac{\mathrm{d}\vartheta}{\mathrm{d}t} = \frac{\mathrm{d}\vartheta}{\mathrm{d}\varphi}\frac{\mathrm{d}\varphi}{\mathrm{d}t} = \frac{2\pi}{T}\frac{\mathrm{d}\vartheta}{\mathrm{d}\varphi} \\ &= \frac{2\pi}{T}\left(1 + 2e\cos(\varphi) + \frac{5}{2}e^2\cos(2\varphi) + \frac{e^3}{4}\left(-\cos(\varphi) + 13\cos(3\varphi)\right)\right). \end{aligned} \tag{A.71}$$

Fig. A.2 shows the standardised angular velocity of the Earth. It is based on the mean angular velocity of the mean Earth which is about 0.017 rad/d. The difference between the maximum and the minimum angular velocity of the real Earth during the whole year is less than 0.0012 rad/d. The curve starts at point P in Fig. A.1 and describes the behaviour of the angular velocity in an anti-clockwise rotation. The minimum is reached on the left side in this figure. The intersection points are at $\varphi_1 = 1.53$ rad and at $\varphi_2 = 4.75$ rad. The mean angular velocity is reached a little bit before $\varphi_1 = 90°$ and a little bit after $\varphi_2 = 270°$. The results are in accordance with the position of the Sun, because the real Sun is not in the centre of ellipse, but in one of the two focal points. The mean angular velocity is reached above and below the real Sun, which is based on the semi-major axis.

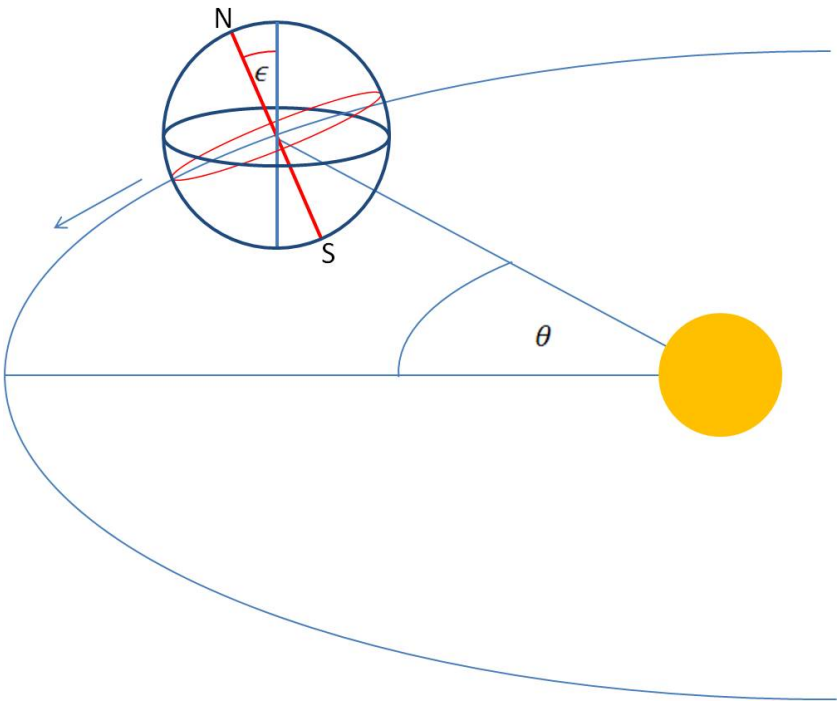

Fig. A.3.: Definition of the angles θ and ϵ. Marked in red is the axis of rotation and the red ellipse is the equator of the Earth. Marked in pale blue is the surface normal of the Earth's orbit.

The direction of the axis of the Earth in the solar system can be described with two angles. The first angle is ϵ, this is the angle between the surface normal of the Earth's orbit and the axis of rotation of the Earth. As was mentioned before, this angle is at the moment $\epsilon = 23°26'21.45''$. This angle is called *obliquity of the ecliptic*. The second angle is the angle θ, which is necessary for the calculation. This is the angle between the semi-major axis of the Earth's orbital plane and the projection of the axis of the Earth onto this plane. θ is at the moment 12.25°. It is also the angle between the winter solstice (21. or 22. December) and the perihelion (2. until 4. January). This angle is referred to the Sun. An overview can be found in Fig. A.3. The Earth runs on a path around the Sun in an anti-clockwise manner. N and S are the North and the South Pole of the Earth. Due to the conservation of momentum the axis are stable. The stable rotation axis is overlaid with the nutation and precession. The nutation has a periodic time of 18.6 a and an amplitude of 9.2″ perpendicular to the ecliptic and 6.8″ parallel to the ecliptic. The precession has a periodic time of 25 780 a. Both are excited by the momentum of a torque, which is borne by gravitational force of the Sun and the Moon, because the shape of the Earth differs from a spherical shape. Another representation can be found in Fig. A.4. It is a geocentric view of the Earth and the Sun. In this figure the North Pole of the Earth is at the top and the South Pole below. X is the winter solstice with its projection X^P onto the celestial equator. During one year the Sun follows the complete ellipse around the Earth. Meanwhile the Earth rotates around

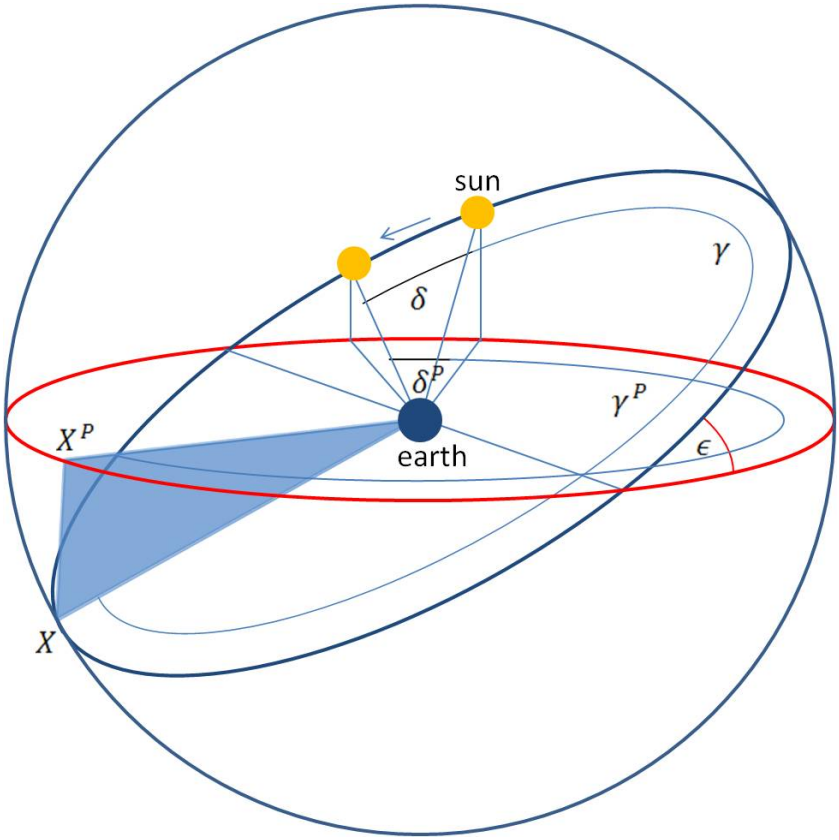

Fig. A.4.: Geocentric view of the Earth with the angles γ, δ and ϵ. The variables with the superior P are the orthogonal projections onto the celestial equator.

its own axis in 24 hours. γ is the angle, which is measured from the winter solstice and γ^P is its projection onto the plane. During a short period of time the Sun covers the angle δ with its orthogonal projection δ^P. In this figure the difference between the solar day (24 hours) and the sidereal day (23 hours, 56 minutes, 4 seconds) can easily be observed. ϵ is the same angle like in Fig. A.3. In Fig. A.4 the intersection points between the orbital plane and the celestial equator can also be seen. They are called vernal and autumnal equinox. For the Equation of Time the projected angle γ^P is needed which is a projection of θ and ϑ. These angles are already described and calculated above and it is responsible for the necessary angle widening and shortening. This deforming factor is described by ϵ. With spherical trigonometry can be found in Fig. A.4 the relation

$$\tan(\gamma) = \tan\left(\gamma^P\right)\cos(\epsilon) \tag{A.72}$$

and

$$\tan(\gamma+\delta) = \tan\left(\gamma^P+\delta^P\right)\cos(\epsilon). \tag{A.73}$$

With the angles γ and ϵ the projection factor f can be calculated for a small angle δ:

$$f(\gamma) = \lim_{\delta\to 0}\frac{\delta^P}{\delta} = \lim_{\delta\to 0}\frac{\arctan\left(\frac{\tan(\gamma+\delta)}{\cos(\epsilon)}\right) - \arctan\left(\frac{\tan(\gamma)}{\cos(\epsilon)}\right)}{\delta} \tag{A.74}$$

For $\delta \to 0$ the numerator and the denominator are 0. Therefore the equation can be evaluated with the rule of l'Hospital. The derivation of the denominator is

$$\frac{\mathrm{d}\delta}{\mathrm{d}\delta} = 1 \tag{A.75}$$

and the derivation of the numerator is with (B.56) and (B.55)

$$\begin{aligned}
&\frac{\mathrm{d}}{\mathrm{d}\delta}\left(\arctan\left(\frac{\tan(\gamma+\delta)}{\cos(\epsilon)}\right) - \arctan\left(\frac{\tan(\gamma)}{\cos(\epsilon)}\right)\right) = \frac{1}{\left(1+\frac{\tan^2(\gamma+\delta)}{\cos^2(\epsilon)}\right)\cos^2(\gamma+\delta)\cos(\epsilon)} \\
&= \frac{\cos(\epsilon)}{\cos^2(\gamma+\delta)\cos^2(\epsilon)+\sin^2(\gamma+\delta)} \overset{(B.50)}{=} \frac{\cos(\epsilon)}{\cos^2(\gamma+\delta)\left(1-\sin^2(\epsilon)\right)+\sin^2(\gamma+\delta)} \\
&\overset{(B.50)}{=} \frac{\cos(\epsilon)}{1-\sin^2(\epsilon)\cos^2(\gamma+\delta)}.
\end{aligned} \tag{A.76}$$

Now (A.74) has a limit

$$f(\gamma) = \lim_{\delta\to 0}\frac{\cos(\epsilon)}{1-\sin^2(\epsilon)\cos^2(\gamma+\delta)} = \frac{\cos(\epsilon)}{1-\sin^2(\epsilon)\cos^2(\gamma)}. \tag{A.77}$$

This is a related equation like in (A.10) with $\alpha = \epsilon$ and $x = \gamma$ and therefore it can also be transferred into a Fourier series (B.27). As seen in Fig A.1, Fig. A.3 and Fig A.4 the angle γ consists of θ and ϑ in the form $\gamma = \theta + \vartheta$. Finally the result of this Fourier series was still calculated and the result can be found in (A.49)

$$f(\gamma) = f(\theta+\vartheta) = 1 + 2\sum_{k=1}^{\infty}\tan^{2k}\left(\frac{\epsilon}{2}\right)\cos(2k(\theta+\vartheta)) \tag{A.78}$$

This projection factor is plotted in Fig. A.5. It shows the projection factor of the Sun during the whole year. In the summer and the winter the Sun has the maximum elevation above and below the celestial equator. There are the ecliptic angles stretched maximally and at the equinoxes the angles are shortened maximally. The angle θ was defined above in Fig. A.3 and ϑ was calculated in dependency of φ in (A.70). Due to the constant angular velocity of φ, this angle can be used as a reference value. This was the angle of the Sun based on a circular orbit. As can be seen in this figure the maxima are shifted slightly compared to Fig. A.2. The maxima are at the summer and winter solstices, where the Sun compared to the northern hemisphere has the highest or lowest position. In the minima the Sun is in the vernal and autumnal equinox. The variation of the projection is about 8 % and so this relative variation is higher than the variation caused by the different angular velocities of the Earth around the Sun.
The above equations can now be used to calculate the Equation of Time. For the final calculation the projection of the true anomalie ϑ^P is needed. γ^P consists of θ^P and ϑ^P:

$$\vartheta^P = \int \mathrm{d}\vartheta^P = \int f(\theta+\vartheta)\,\mathrm{d}\vartheta = \int 1 + 2\sum_{k=1}^{\infty}\tan^{2k}\left(\frac{\epsilon}{2}\right)\cos(2k(\theta+\vartheta))\,\mathrm{d}\vartheta$$

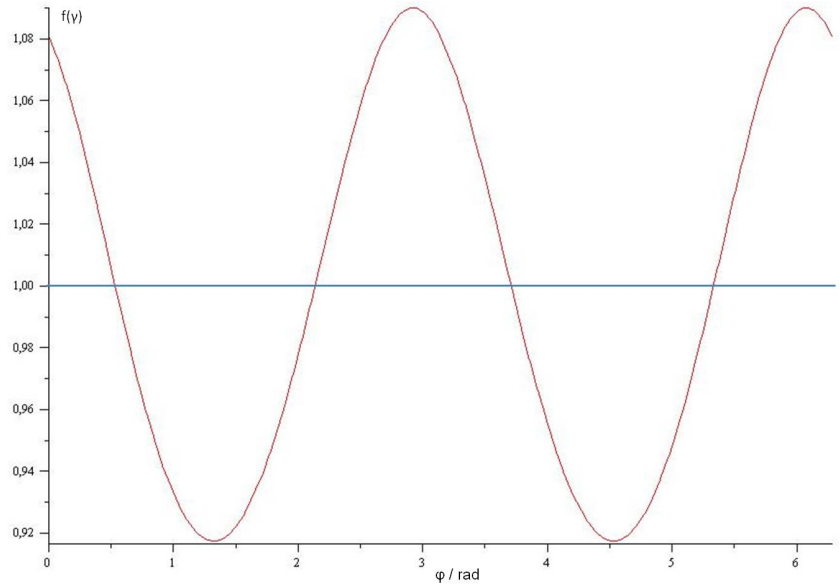

Fig. A.5.: Projection factor $f(\gamma)$ during the whole year based on the angle φ. The maxima are at the summer and winter solstice and the equinoxes are the minima.

$$= \vartheta + \sum_{k=1}^{\infty} \frac{1}{k} \tan^{2k}\left(\frac{\epsilon}{2}\right) \sin(2k(\theta+\vartheta)) + \text{const.} \tag{A.79}$$

The ϑ can be replaced by φ with (A.70):

$$\begin{aligned}
\vartheta^P &= \varphi + 2e\sin(\varphi) + \frac{5}{4}e^2\sin(2\varphi) + \frac{e^3}{4}\left(-\sin(\varphi) + \frac{13}{3}\sin(3\varphi)\right) \\
&+ \tan^2\left(\frac{\epsilon}{2}\right)\sin\left(2(\theta+\varphi) + 2\left(2e\sin(\varphi) + \frac{5e^2}{4}\sin(2\varphi) + \frac{e^3}{4}\left(-\sin(\varphi) + \frac{13}{3}\sin(3\varphi)\right)\right)\right) \\
&+ \frac{\tan^4\left(\frac{\epsilon}{2}\right)}{2}\sin\left(4(\theta+\varphi) + 4\left(2e\sin(\varphi) + \frac{5e^2}{4}\sin(2\varphi) + \frac{e^3}{4}\left(-\sin(\varphi) + \frac{13}{3}\sin(3\varphi)\right)\right)\right) \\
&+ \frac{\tan^6\left(\frac{\epsilon}{2}\right)}{3}\sin\left(6(\theta+\varphi) + 6\left(2e\sin(\varphi) + \frac{5e^2}{4}\sin(2\varphi) + \frac{e^3}{4}\left(-\sin(\varphi) + \frac{13}{3}\sin(3\varphi)\right)\right)\right) \\
&+ \mathcal{O}\left(\tan^8\left(\frac{\epsilon}{2}\right)\right) + \text{const.}
\end{aligned} \tag{A.80}$$

The big sine parts of this equation can be expanded with a Taylor polynomial (B.26) for a small value of e up to the maximum order 2. Additionally (B.49) and (B.51) are used for simplification and the appearing constant $\frac{3}{4}e^2\tan^2\left(\frac{\epsilon}{2}\right)\sin(2\theta)$ is added in const.:

$$\begin{aligned}
\vartheta^P &= \varphi + \tan^2\left(\frac{\epsilon}{2}\right)\left(1-4e^2\right)\sin(2(\theta+\varphi)) + 2e\sin(\varphi) - 2e\tan^2\left(\frac{\epsilon}{2}\right)\sin(2\theta+\varphi) \\
&+ 2e\tan^2\left(\frac{\epsilon}{2}\right)\sin(2\theta+3\varphi) + \frac{1}{2}\tan^4\left(\frac{\epsilon}{2}\right)\sin(4(\theta+\varphi)) + \frac{5}{4}e^2\sin(2\varphi)
\end{aligned}$$

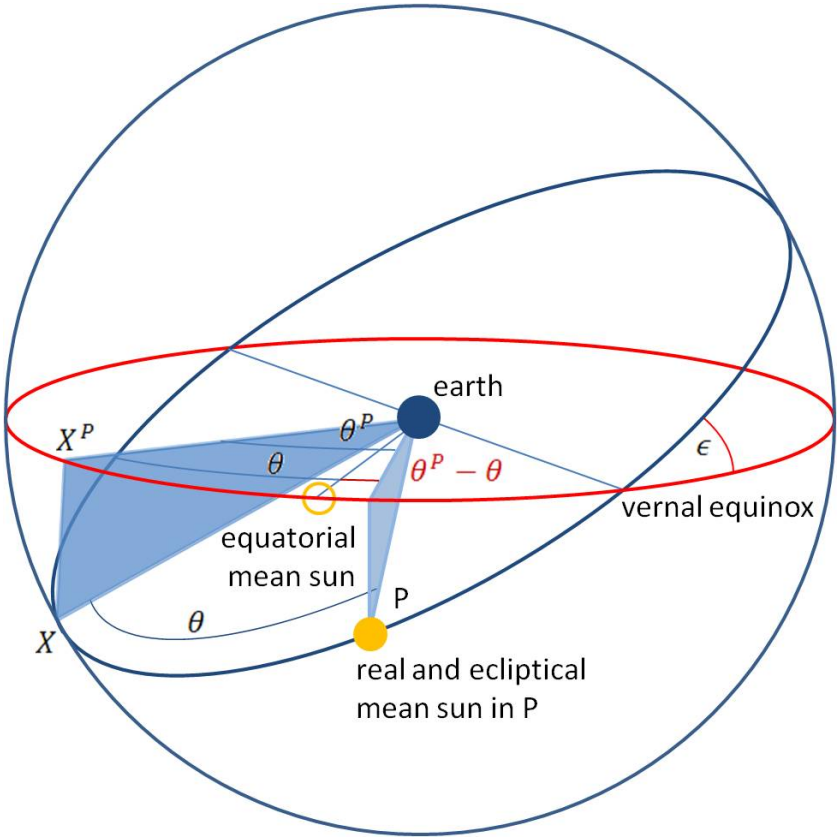

Fig. A.6.: Relation between θ and θ^P is needed to calculate the constant of integration with a geocentric view of the Earth and the Sun.

$$
\begin{aligned}
&- 2e\tan^4\left(\frac{\epsilon}{2}\right)\sin(4\theta + 3\varphi) + 2e\tan^4\left(\frac{\epsilon}{2}\right)\sin(4\theta + 5\varphi) \\
&+ \frac{13}{4}e^2\tan^2\left(\frac{\epsilon}{2}\right)\sin(2\theta + 4\varphi) + \frac{1}{3}\tan^6\left(\frac{\epsilon}{2}\right)\sin(6(\theta + \varphi)) + \mathcal{O}\left(e^3\right) + \text{const.}
\end{aligned} \tag{A.81}
$$

In this equation there is still a constant of integration. It must be determined for the final calculation of the Equation of Time. As was defined before, the real and the ecliptical mean Sun start at the same time in the perihelion P. Due to the rotation axis the equatorial mean Sun and the ecliptical mean Sun arrive at the vernal equinox at the same time. The angles of the mean Suns are always equal compared to the vernal equinox. Due to the shift ϵ of the two reference planes the projected angle θ^P is in P a little bit larger than the angle θ. An overview can be found in Fig. A.6, where red is the equatorial plane. The value can be calculated with (A.72). Based on the perihelion in point P the position of the angle ϑ is identical with the position of the angle $\theta + \vartheta$ based on the winter solstice, therefore the position of the projection of P is identical with θ^P. With the other reference point it is ϑ^P. Additionally the angles of the mean Suns are equal, therefore it can be written that a discrete angle φ matches the angle θ in the equatorial plane. The differences between the angles are the same and the result

can be summarised to calculate the missing integration constant. It can be calculated, if the passage through the perihelion P is examined:

$$\begin{aligned}\varphi - \vartheta^P = \theta - \theta^P = \theta - \int_0^\theta f(\gamma)\,\mathrm{d}\gamma = \theta - \int_0^\theta \left(1 + 2\sum_{k=1}^{\infty} \tan^{2k}\left(\frac{\epsilon}{2}\right)\cos(2k\gamma)\right)\mathrm{d}\gamma \\ = -\sum_{k=1}^{\infty}\frac{1}{k}\tan^{2k}\left(\frac{\epsilon}{2}\right)\sin(2k\theta) \qquad \text{(A.82)}\end{aligned}$$

With $t = 0$ follows with (A.3), that it is $\varphi = 0$ in (A.80) and with the insert of this equation in (A.82) the integration constant has the value 0. It can easily be seen by comparison of both sides.
Finally the Equation of Time is defined as

$$\begin{aligned}\text{Equation of Time} &= \text{‘apparent solar time’} - \text{‘mean solar time’} \\ &= \text{‘true equatorial Sun angle’} - \text{‘mean equatorial Sun angle’} \\ &= \text{‘mean anomaly’} - \text{‘true projected anomaly’} \\ &= \varphi - \vartheta^P. \qquad \text{(A.83)}\end{aligned}$$

In this equation describes the second term the geocentric view and the third term the heliocentric view. With $e = 0.0167$ and $\epsilon = 23°26'21.45''$ the Equation of Time can now be calculated as:

$$\begin{aligned}\text{Equation of Time} = \varphi - \vartheta^P = &-591.7\sin(2(\varphi+\theta)) - 459.3\sin(\varphi) + 19.8\sin(\varphi+2\theta) \\ &- 19.8\sin(3\varphi+2\theta) - 12.8\sin(4(\varphi+\theta)) - 4.8\sin(2\varphi) \\ &+ 0.9\sin(3\varphi+4\theta) - 0.9\sin(5\varphi+4\theta) - 0.5\sin(4\varphi+2\theta) \\ &- 0.4\sin(6(\varphi+\theta)) \qquad [\mathrm{s}] \qquad \text{(A.84)}\end{aligned}$$

With the help of $\theta = 12°15'0''$, the Equation of Time can be plotted in dependency of φ. The time difference in a whole year can be found in Fig. A.7. It starts in the perihelion and in the middle of the plot is the aphelion. With this formula it is now possible to calculate the difference between the true solar time and the mean solar time. The difference between minimum and maximum is round about 30 minutes. In February it is round about -14 min and in October it is round about $+16$ min. On just 4 different days during the year the mean time and the apparent time are the same.

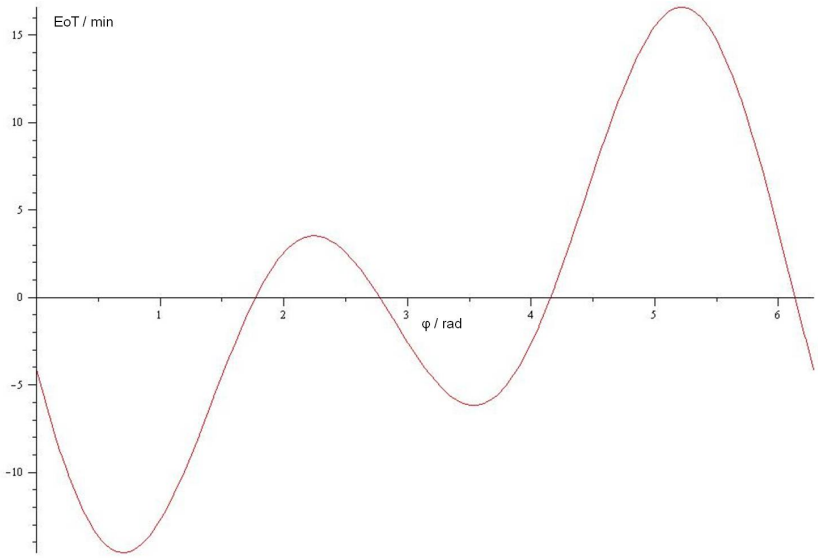

Fig. A.7.: Calculated Equation of Time with a maximum difference of −14 min in February and 16 min in October.

B. Mathematics and Physics

In the following chapter the mathematical equations used in the previous chapters are summarised. It starts with basic mathematics like different coordinate systems and the Fourier expansion. Furthermore more difficult topics will also be touched on. This includes for example the Kepler's laws, the Lagrange reversion theorem or identities. At the end the abbreviations used and a few main symbols are listed.

B.1. Coordinates and derivative operators

For the calculation of the water desalination unit and other components different coordinate systems are necessary. For a few calculations the Cartesian coordinates are necessary, for other calculations it is easier to use cylindrical or spherical coordinates. The easiest system is the Cartesian coordinate system. The other systems are more complicated. For a few calculations the Nabla operator ∇ or Laplace operator Δ are necessary, but they always have another appearance in the different coordinate systems. It also depends on the usage of the operator, if it is used as a gradient, divergence or curl. In the following section a summary can be found for 3 different coordinate systems.

B.1.1. Cartesian coordinates

The variables for the Cartesian coordinates are x, y and z in each case with the range $\pm\infty$. The ∇ and Δ operators are in this system:
Gradient:

$$\nabla U = \operatorname{grad} U = \hat{e}_x \frac{\partial U}{\partial x} + \hat{e}_y \frac{\partial U}{\partial y} + \hat{e}_z \frac{\partial U}{\partial z} \tag{B.1}$$

Divergence:

$$\nabla \cdot \vec{V} = \operatorname{div} \vec{V} = \frac{\partial V_x}{\partial x} + \frac{\partial V_y}{\partial y} + \frac{\partial V_z}{\partial z} \tag{B.2}$$

Curl:

$$\nabla \times \vec{V} = \operatorname{rot} \vec{V} = \hat{e}_x \left(\frac{\partial V_z}{\partial y} - \frac{\partial V_y}{\partial z} \right) + \hat{e}_y \left(\frac{\partial V_x}{\partial z} - \frac{\partial V_z}{\partial x} \right) + \hat{e}_z \left(\frac{\partial V_y}{\partial x} - \frac{\partial V_x}{\partial y} \right) \tag{B.3}$$

Laplace:

$$\Delta U = \nabla^2 U = \frac{\partial^2 U}{\partial x^2} + \frac{\partial^2 U}{\partial y^2} + \frac{\partial^2 U}{\partial z^2} \tag{B.4}$$

The volume element is:

$$\mathrm{d}V = \mathrm{d}x\,\mathrm{d}y\,\mathrm{d}z \tag{B.5}$$

B.1.2. Cylindrical coordinates

Below can be found the conversion of the Cylinder coordinates r, φ and z into Cartesian coordinates x, y and z

$$\begin{array}{ll} x = r\cos(\varphi) & 0 \le r < \infty \\ y = r\sin(\varphi) & 0 \le \varphi < 2\pi \\ z = z & -\infty < z < \infty \end{array} \tag{B.6}$$

and vice versa

$$\begin{array}{ll} r = \sqrt{x^2 + y^2} & -\infty < x < \infty \\ \varphi = (\mathrm{sgn}(y) + 1 - |\mathrm{sgn}(y)|)\arccos\left(\frac{x}{r}\right) & -\infty < y < \infty \\ z = z & -\infty < z < \infty \end{array}, \tag{B.7}$$

where $\mathrm{sgn}(x)$ is the Signum function. With this transformation the ∇ and Δ operators are:
Gradient:

$$\nabla U = \mathrm{grad}\, U = \hat{e}_\rho \frac{\partial U}{\partial \rho} + \hat{e}_\varphi \frac{1}{\rho}\frac{\partial U}{\partial \varphi} + \hat{e}_z \frac{\partial u}{\partial z} \tag{B.8}$$

Divergence:

$$\nabla \cdot \vec{V} = \mathrm{div}\, \vec{V} = \frac{1}{\rho}\frac{\partial}{\partial \rho}\rho V_\rho + \frac{1}{\rho}\frac{\partial V_\varphi}{\partial \varphi} + \frac{V_z}{\partial z} \tag{B.9}$$

Curl:

$$\begin{aligned} \nabla \times \vec{V} = \mathrm{rot}\, \vec{V} = \hat{e}_\rho \left(\frac{1}{\rho}\frac{\partial V_z}{\partial \varphi} - \frac{\partial V_\varphi}{\partial z}\right) + \hat{e}_\varphi \left(\frac{\partial V_\rho}{\partial z} - \frac{\partial V_z}{\partial \rho}\right) \\ + \hat{e}_z \left(\frac{1}{\rho}\frac{\partial}{\partial \rho}\rho V_\varphi - \frac{1}{\rho}\frac{\partial V_\rho}{\partial \varphi}\right) \end{aligned} \tag{B.10}$$

Laplace:

$$\Delta U = \frac{1}{\rho}\frac{\partial}{\partial \rho}\rho\frac{\partial U}{\partial \rho} + \frac{1}{\rho^2}\frac{\partial^2 U}{\partial \varphi^2} + \frac{\partial^2 U}{\partial z^2} \tag{B.11}$$

The volume element is:

$$\mathrm{d}V = r\,\mathrm{d}r\,\mathrm{d}\varphi\,\mathrm{d}z \tag{B.12}$$

B.1.3. Spherical coordinates

Below can be found the conversion of the Spherical coordinates r, φ and ϑ into Cartesian coordinates x, y and z

$$\begin{array}{ll} x = r\sin(\vartheta)\cos(\varphi) & 0 \leq r < \infty \\ y = r\sin(\vartheta)\sin(\varphi) & 0 \leq \varphi < 2\pi \\ z = r\cos\vartheta & 0 \leq \vartheta \leq \pi \end{array} \tag{B.13}$$

and vice versa

$$\begin{array}{ll} r = \sqrt{x^2+y^2+z^2} & -\infty < x < \infty \\ \varphi = \begin{cases} \arctan\left(\frac{y}{x}\right) & , \text{ for } x > 0 \\ \operatorname{sgn}(y)\frac{\pi}{2} & , \text{ for } x = 0 \\ \arctan\left(\frac{y}{x}\right) + \pi & , \text{ for } x < 0 \wedge y \geq 0 \\ \arctan\left(\frac{y}{x}\right) - \pi & , \text{ for } x < 0 \wedge y < 0 \end{cases} & -\infty < y < \infty \\ \vartheta = \arccos\left(\frac{z}{\sqrt{x^2+y^2+z^2}}\right) & -\infty < z < \infty \end{array} , \tag{B.14}$$

where $\operatorname{sgn}(x)$ is the Signum function. With this transformation the ∇ and Δ operators are:
Gradient:

$$\nabla U = \operatorname{grad} U = \hat{e}_r \frac{\partial U}{\partial r} + \hat{e}_\vartheta \frac{1}{r}\frac{\partial U}{\partial \vartheta} + \hat{e}_\varphi \frac{1}{r\sin(\vartheta)}\frac{\partial U}{\partial \varphi} \tag{B.15}$$

Divergence:

$$\nabla \cdot \vec{V} = \operatorname{div} \vec{V} = \frac{1}{r^2}\frac{\partial}{\partial r} r^2 V_r + \frac{1}{r\sin(\vartheta)}\frac{\partial}{\partial \vartheta} V_\vartheta \sin(\vartheta) + \frac{1}{r\sin(\vartheta)}\frac{\partial V_\varphi}{\partial \varphi} \tag{B.16}$$

Curl:

$$\begin{aligned} \nabla \times \vec{V} = \operatorname{rot} \vec{V} = \hat{e}_r \frac{1}{r\sin(\vartheta)}\left[\frac{\partial}{\partial \vartheta} V_\varphi \sin(\vartheta) - \frac{\partial V_\vartheta}{\partial \varphi}\right] + \hat{e}_\vartheta \frac{1}{r}\left[\frac{1}{\sin(\vartheta)}\frac{\partial V_r}{\partial \varphi} - \frac{\partial}{\partial r} r V_\varphi\right] \\ + \hat{e}_\varphi \frac{1}{r}\left[\frac{\partial}{\partial r} r V_\vartheta - \frac{\partial V_r}{\partial \vartheta}\right] \end{aligned} \tag{B.17}$$

Laplace:

$$\Delta U = \frac{1}{r^2}\frac{\partial}{\partial r} r^2 \frac{\partial U}{\partial r} + \frac{1}{r^2\sin(\vartheta)}\frac{\partial}{\partial \vartheta}\sin(\vartheta)\frac{\partial U}{\partial \vartheta} + \frac{1}{r^2\sin^2(\vartheta)}\frac{\partial^2 U}{\partial \varphi^2} \tag{B.18}$$

The volume element is:

$$\mathrm{d}V = r^2 \sin(\vartheta)\,\mathrm{d}r\,\mathrm{d}\vartheta\,\mathrm{d}\varphi \tag{B.19}$$

B.2. Galilei transformation

For $v \ll c$ the transformation between two coordinate systems which differ by a constant relative velocity, a constant spatial transformation and / or a constant time difference, can be calculated with the Galilei transformation:

$$x_i' = \sum_{j=1}^{3} \alpha_{ij} x_j - v_i t - a_i, \qquad t' = t - t_0 \tag{B.20}$$

with $v_i t$ and a_i a spatial transformation, α_{ij} a rotation and t_0 a constant time translation.

B.3. Lorentz transformation

For v in the order of c the transformation between two coordinate systems which differ by a constant relative velocity, a constant spatial transformation and / or a constant time difference, can be calculated with the Lorentz transformation:

$$x'^{\alpha} = \Lambda^{\alpha}_{\beta} x^{\beta} + b^{\alpha} \tag{B.21}$$

α und β have the values 0, 1, 2, 3 and Λ is a 4×4 matrix.

B.4. Gaussian integral theorem

This theorem combines the divergence of a vector field inside a closed surface with the flow of this vector field through this surface. It is widely used in physics and electrical engineering.

$$\int_V \operatorname{div} \vec{F} \, \mathrm{d}V = \oint_A \vec{F} \cdot \mathrm{d}\vec{A} \tag{B.22}$$

It is a special case of the more general Stokes' theorem.

B.5. Kepler's laws

1. Kepler's law: The orbit of every planet is an ellipse with the Sun at one of the two foci of the ellipse.
2. Kepler's law: A line $\vec{r}$ joining a planet and the Sun sweeps out equal areas A during equal intervals of time t:

$$\dot{A} = \frac{\mathrm{d}A}{\mathrm{d}t} = \frac{1}{2} r^2 \dot{\phi} = \frac{l}{2\mu} = \text{const.} \tag{B.23}$$

3. Kepler's law: The square of the orbital period of a planet T is directly proportional to the cube of the semi-major axis a of its orbit:

$$\frac{T^2}{a^3} = \text{const.} \tag{B.24}$$

B.6. Series

For $|x| < 1$ is valid

$$a_0 \sum_{i=0}^{\infty} x^i = a_0 \cdot \lim_{n\to\infty} \frac{1 - x^{n+1}}{1 - x} = a_0 \frac{1}{1 - x}. \tag{B.25}$$

This is the infinite geometric series for $a_0 = 1$, which converges and has a limiting value.

B.7. Taylor polynomial

With the Taylor polynomial it is possible to represent a function as an infinite sum. It is calculated with the function's derivatives at a single point. With this calculation it is possible to simplify an analytic expression, because the polynomial can be cut after a few terms with a sufficient accuracy:

$$f(x) = \sum_{n=0}^{k} \frac{f^{(n)}(x_0)}{n!} (x - x_0)^n \tag{B.26}$$

The remainder term of Schlömilch, Lagrange and Cauchy is not considered in this representation and for the Taylor series it is $k = \infty$.

B.8. Fourier series

With the Fourier series it is possible to decompose a periodic function in an interval into a sum of sines and cosines. A decomposition into complex exponentials is also possible and it is also possible for closed intervals of non-periodic functions. Real-valued it is:

$$f(x) = \frac{a_0}{2} + \sum_{k=1}^{\infty} \left(a_k \cos(kx) + b_k \sin(kx)\right) \quad \text{with } a_k,\, b_k \in \mathbb{R} \tag{B.27}$$

The constants a_k and b_k are unique defined for different functions $f(x)$:

$$a_k = \frac{1}{\pi} \int_0^{2\pi} f(x) \cos(kx)\, \mathrm{d}x \quad \text{for } k = 0,\, 1, \ldots,\, n \tag{B.28}$$

and

$$b_k = \frac{1}{\pi}\int_0^{2\pi} f(x)\sin(kx)\,\mathrm{d}x \quad \text{for } k = 1,\, 2, \ldots,\, n. \tag{B.29}$$

With the formulas

$$\cos(x) = \frac{1}{2}\left(\exp(\mathrm{i}\,x) + \exp(-\mathrm{i}\,x)\right) \quad \text{and} \quad \sin(x) = \frac{1}{2\mathrm{i}}\left(\exp(\mathrm{i}\,x) - \exp(-\mathrm{i}\,x)\right) \tag{B.30}$$

the formula above can also be written complex-valued with

$$f(x) = \sum_{k=-\infty}^{\infty} c_k \exp(\mathrm{i}\,kx). \tag{B.31}$$

Here it is:

$$c_0 = \frac{a_0}{2} \quad \text{and} \quad c_k = \frac{1}{2}(a_k - \mathrm{i}\,b_k),\ c_{-k} = \frac{1}{2}(a_k + \mathrm{i}\,b_k) = \overline{c_k} \quad \text{for } 1 \le k \le n \tag{B.32}$$

or

$$c_k := \frac{1}{2\pi}\int_0^{2\pi} f(x)\exp(-\mathrm{i}\,kx)\,\mathrm{d}x, \quad k \in \mathbb{Z}. \tag{B.33}$$

The basis functions of the Taylor series are a complete orthogonal basis with all needed characteristics. It is a Hilbert or Banach space, if it is normalised with $\sqrt{\pi}$.

B.9. Lagrange reversion theorem

For implicitly defined functions the Lagrange reversion theorem gives series or formal power series expansions of compositions with such functions [Lag71]. For a function such as

$$t = x + nf(x) \tag{B.34}$$

and for small n and any function g it is

$$g(x) = g(t) + \sum_{k=1}^{\infty} \frac{(-n)^k}{k!}\frac{\partial^{k-1}}{\partial t^{k-1}} f(t)^k g'(t). \tag{B.35}$$

With the substitution $-n = m$ the equation (B.36) can be written as

$$x = t + mf(x). \tag{B.36}$$

Therefore the equation (B.35) can also be modified

$$g(x) = g(t) + \sum_{k=1}^{\infty} \frac{m^k}{k!}\frac{\partial^{k-1}}{\partial t^{k-1}} f(t)^k g'(t). \tag{B.37}$$

If g is the identity function the above equations can be written as

$$x = t + \sum_{k=1}^{\infty} \frac{(-n)^k}{k!}\frac{\partial^{k-1}}{\partial t^{k-1}} f(t)^k = t + \sum_{k=1}^{\infty} \frac{m^k}{k!}\frac{\partial^{k-1}}{\partial t^{k-1}} f(t)^k. \tag{B.38}$$

B.10. Identities

$$\sin(\alpha) = \frac{1}{2\mathrm{i}}\left(\exp(\mathrm{i}\,\alpha) - \exp(-\mathrm{i}\,\alpha)\right) \tag{B.39}$$

$$\cos(\alpha) = \frac{1}{2}\left(\exp(\mathrm{i}\,\alpha) + \exp(-\mathrm{i}\,\alpha)\right) \tag{B.40}$$

$$\cos(\alpha) = \frac{1}{\sqrt{1+\tan^2(\alpha)}} \tag{B.41}$$

$$\sin(2\alpha) = 2\sin(\alpha)\cos(\alpha) \tag{B.42}$$

$$\cos(2\alpha) = \cos^2(\alpha) - \sin^2(\alpha) \tag{B.43}$$

$$\sin^2(\alpha) = \frac{1}{2}\left(1 - \cos(2\alpha)\right) \tag{B.44}$$

$$\cos^2(\alpha) = \frac{1}{2}\left(1 + \cos(2\alpha)\right) \tag{B.45}$$

$$\sin^3(\alpha) = \frac{1}{4}\left(3\sin(\alpha) - \sin(3\alpha)\right) \tag{B.46}$$

$$\sin^4(\alpha) = \frac{1}{8}(\cos(4\alpha) - 4\cos(2\alpha) + 3) \tag{B.47}$$

$$\cos^4(\alpha) = \frac{1}{8}(\cos(4\alpha) + 4\cos(2\alpha) + 3) \tag{B.48}$$

$$\sin(\alpha)\cos(\beta) = \frac{1}{2}\left(\sin(\alpha-\beta) + \sin(\alpha+\beta)\right) \tag{B.49}$$

$$\sin^2(\alpha) + \cos^2(\alpha) = 1 \tag{B.50}$$

$$\begin{aligned}\sin(\alpha)\sin(\beta)\sin(\gamma) = \frac{1}{4}&\left(\sin(\alpha+\beta-\gamma) + \sin(\beta+\gamma-\alpha)\right.\\ &\left.+\sin(\alpha+\gamma-\beta) - \sin(\alpha+\beta+\gamma)\right)\end{aligned} \tag{B.51}$$

$$\tan\left(\frac{\alpha}{2}\right) = \sqrt{\frac{1-\cos(\alpha)}{1+\cos(\alpha)}} = \frac{1-\cos(\alpha)}{\sin(\alpha)} \tag{B.52}$$

$$\cot\left(\frac{\alpha}{2}\right) = \frac{1+\cos(\alpha)}{\sin(\alpha)} \tag{B.53}$$

$$\exp(\mathrm{i}\,\varphi) = \cos(\varphi) + \mathrm{i}\,\sin(\varphi) \tag{B.54}$$

$$\frac{\mathrm{d}\tan(x)}{\mathrm{d}x} = \frac{1}{\cos^2(x)} \tag{B.55}$$

$$\frac{\mathrm{d}\arctan(x)}{\mathrm{d}x} = \frac{1}{1+x^2} \tag{B.56}$$

C. Tables

Tab. C.1.: Comparison between different solar collector types [Sol11].

Collector type	Conversion factor	Thermal dissipation factor [W/(m^2 °C)]	Temperature range [°C]
Absorber (uncovered)	0.82 - 0.97	10 - 30	until 40
Flat plate collector	0.66 - 0.83	2.9 - 5.3	20 - 80
Vacuum flat plate collector	0.81 - 0.83	2.6 - 4.3	20 - 120
Vacuum tube collector	0.62 - 0.84	0.7 - 2.0	50 - 120
Storage collector	about 0.55	about 2.4	20 - 70
Air collector	0.75 - 0.90	8 - 30	20 - 50

Tab. C.2.: Solar radiation and climate data of Hurghada [Ami09, Aeg11].

	Jan.	Feb.	Mar.	Apr.	May	June	July	Aug.	Sept.	Oct.	Nov.	Dec.
S	9.20	9.70	9.66	10.49	11.59	12.81	12.47	12.08	11.17	10.17	9.73	8.85
RS	0.86	0.83	0.80	0.82	0.86	0.93	0.92	0.93	0.91	0.88	0.90	0.84
G	4.26	5.36	6.53	7.41	7.88	8.27	8.18	7.75	6.96	5.56	4.48	3.91
RG	0.64	0.65	0.65	0.67	0.70	0.72	0.72	0.71	0.69	0.66	0.65	0.63
D	1.36	1.77	2.29	2.52	2.52	2.32	2.37	2.17	2.02	1.72	1.34	1.29
I	6.42	7.14	7.87	7.82	8.35	9.25	9.15	8.83	8.50	7.34	6.68	6.22
F	7.68	8.66	9.61	10.00	10.50	11.20	11.08	10.66	10.11	8.76	7.91	7.36
T_{max}	21.0	21.6	23.8	26.7	30.0	32.2	33.0	33.3	31.2	29.1	25.9	22.5
T_{min}	9.7	10.1	13.0	16.4	20.5	23.7	25.0	25.2	23.2	19.8	15.6	11.6
RH	51	49	49	47	44	43	47	47	51	55	54	54
C	1.7	1.6	1.3	1.6	1.2	0.2	0.2	0.2	0.2	0.9	1.3	1.7
WS	11.3	12.2	12.7	12.4	13.3	14.3	12.9	12.9	13.6	11.3	10.3	10.7
EV	10.0	11.0	12.1	14.1	16.3	18.8	17.7	17.1	16.2	12.6	10.7	9.8
WT	22	21	22	23	27	29	31	30	29	26	25	24
RD	0	0	0	1	0	1	0	0	0	0	0	0

with: S: Sunshine duration in h; RS: Relative sunshine duration S/S_0 with S_0 possible sunshine duration in h; G: Global radiation in kW h/(m^2 d); RG: Relative global radiation $G/G0$; D: Diffuse solar radiation in kW h/(m^2 d); I: Incidence solar radiation in kW h/(m^2 d); F: Solar energy density on full tracking systems in kW h/(m^2 d); T_{max}: Max. air temperature in °C; T_{min}: Min. air temperature in °C; RH: Relative humidity in %; C: Total sky cover in octas $(0-8)$; WS: Wind speed in knots; EV: Daily evaporation in mm; WT: Water temperature in °C; RD: Rainy days

Tab. C.3.: Weather data from the Meteo Group in 01.2009 [Met09].

date	time†	temperature [°C]	wind direction [°]	wind speed [m/s]	cloud amount [octas]	air pressure [hPa]	global radiation [kW/m^2]
2009-01-01	00:00	12.3	290	7.2	0	1019.0	0.000
2009-01-01	01:00	12.2	290	7.1	0	1019.2	0.000
2009-01-01	02:00	12.1	290	6.8	0	1019.4	0.000
2009-01-01	03:00	12.1	290	6.7	0	1019.6	0.000
2009-01-01	04:00	12.2	290	6.5	0	1019.8	0.000
2009-01-01	05:00	12.5	290	6.3	0	1020.0	0.000
2009-01-01	06:00	12.8	290	6.2	0	1020.2	0.158
2009-01-01	07:00	13.3	300	7.3	0	1020.0	0.355
2009-01-01	08:00	14.0	300	8.4	1	1019.9	0.530
2009-01-01	09:00	15.3	165	9.5	2	1019.7	0.652
2009-01-01	10:00	16.8	310	10.7	2	1019.5	0.698
2009-01-01	11:00	18.1	310	11.7	2	1019.4	0.660
2009-01-01	12:00	19.0	310	12.9	3	1019.2	0.549
2009-01-01	13:00	18.8	340	11.9	2	1019.7	0.431
2009-01-01	14:00	18.2	340	11.0	2	1020.1	0.265
2009-01-01	15:00	17.3	320	10.0	2	1020.6	0.081
2009-01-01	16:00	15.8	330	9.1	1	1021.1	0.000
2009-01-01	17:00	14.7	310	8.1	0	1021.5	0.000
2009-01-01	18:00	13.6	290	7.2	0	1022.0	0.000
2009-01-01	19:00	13.4	290	7.4	0	1022.1	0.000
2009-01-01	20:00	13.1	290	7.6	0	1022.2	0.000
2009-01-01	21:00	12.7	310	7.7	0	1022.3	0.000
2009-01-01	22:00	12.4	280	7.9	0	1022.4	0.000
2009-01-01	23:00	12.1	280	8.1	0	1022.5	0.000

† in UTC

Tab. C.4.: Weather data from the Meteo Group in 03.2009 [Met09].

date	time†	temperature [°C]	wind direction [°]	wind speed [m/s]	cloud amount [octas]	air pressure [hPa]	global radiation [kW/m^2]
2009-03-01	00:00	15.9	280	5.1	0	1015.9	0.000
2009-03-01	01:00	15.7	280	6.3	0	1016.3	0.000
2009-03-01	02:00	15.6	280	7.6	1	1016.7	0.000
2009-03-01	03:00	15.5	280	8.8	1	1017.1	0.000
2009-03-01	04:00	15.6	300	9.9	1	1017.6	0.000
2009-03-01	05:00	15.7	300	11.2	2	1018.0	0.054
2009-03-01	06:00	15.9	310	12.4	2	1018.4	0.250
2009-03-01	07:00	16.2	300	12.5	2	1018.4	0.470
2009-03-01	08:00	16.6	300	12.5	1	1018.5	0.682
2009-03-01	09:00	17.4	320	12.6	1	1018.5	0.848
2009-03-01	10:00	18.3	360	12.7	1	1018.5	0.940
2009-03-01	11:00	19.1	360	12.8	0	1018.6	0.941
2009-03-01	12:00	19.6	360	12.9	0	1018.6	0.848
2009-03-01	13:00	19.4	360	12.1	0	1019.0	0.682
2009-03-01	14:00	19.0	350	11.3	0	1019.4	0.470
2009-03-01	15:00	18.3	335	10.6	0	1019.9	0.245
2009-03-01	16:00	17.4	330	9.8	0	1020.3	0.040
2009-03-01	17:00	16.6	310	9.0	0	1020.7	0.000
2009-03-01	18:00	15.8	320	8.2	0	1021.1	0.000
2009-03-01	19:00	15.3	300	7.6	0	1021.2	0.000
2009-03-01	20:00	14.8	270	6.8	0	1021.4	0.000
2009-03-01	21:00	14.3	295	6.2	0	1021.5	0.000
2009-03-01	22:00	13.8	270	5.5	0	1021.7	0.000
2009-03-01	23:00	13.3	270	4.8	0	1021.9	0.000

† in UTC

Tab. C.5.: Weather data from the Meteo Group in 05.2009 [Met09].

date	time†	temperature [°C]	wind direction [°]	wind speed [m/s]	cloud amount [octas]	air pressure [hPa]	global radiation [kW/m^2]
2009-05-01	00:00	21.3	290	7.7	0	1010.4	0.000
2009-05-01	01:00	21.6	305	7.8	0	1010.8	0.000
2009-05-01	02:00	21.9	310	7.9	0	1011.1	0.000
2009-05-01	03:00	22.4	300	8.0	0	1011.5	0.000
2009-05-01	04:00	22.9	300	8.1	0	1011.8	0.059
2009-05-01	05:00	23.4	310	8.1	0	1012.1	0.246
2009-05-01	06:00	24.1	320	8.2	0	1012.5	0.460
2009-05-01	07:00	24.4	315	9.0	0	1012.1	0.676
2009-05-01	08:00	24.9	335	9.8	1	1011.8	0.864
2009-05-01	09:00	25.7	335	10.6	2	1011.5	0.993
2009-05-01	10:00	26.7	330	11.3	2	1011.1	1.046
2009-05-01	11:00	27.5	325	12.1	2	1010.8	1.014
2009-05-01	12:00	28.1	360	12.9	3	1010.4	0.897
2009-05-01	13:00	28.1	320	12.3	3	1010.7	0.734
2009-05-01	14:00	27.9	330	11.7	3	1010.9	0.531
2009-05-01	15:00	27.5	320	11.1	2	1011.2	0.319
2009-05-01	16:00	26.7	330	10.5	2	1011.5	0.124
2009-05-01	17:00	26.2	310	9.9	2	1011.7	0.000
2009-05-01	18:00	25.6	320	9.3	2	1012.0	0.000
2009-05-01	19:00	25.0	220	8.6	2	1012.1	0.000
2009-05-01	20:00	24.4	150	7.9	1	1012.1	0.000
2009-05-01	21:00	23.7	155	7.2	1	1012.2	0.000
2009-05-01	22:00	23.1	150	6.5	1	1012.3	0.000
2009-05-01	23:00	22.4	145	5.8	0	1012.3	0.000

† in UTC

Tab. C.6.: Weather data from the Meteo Group in 07.2009 [Met09].

date	time†	temperature [°C]	wind direction [°]	wind speed [m/s]	cloud amount [octas]	air pressure [hPa]	global radiation [kW/m^2]
2009-07-01	00:00	32.8	290	6.2	0	1006.0	0.000
2009-07-01	01:00	33.0	330	6.0	0	1006.1	0.000
2009-07-01	02:00	33.2	310	5.8	0	1006.3	0.000
2009-07-01	03:00	33.4	340	5.7	0	1006.4	0.000
2009-07-01	04:00	33.7	330	5.5	0	1006.5	0.077
2009-07-01	05:00	34.1	315	5.3	0	1006.7	0.255
2009-07-01	06:00	34.5	360	5.1	0	1006.8	0.458
2009-07-01	07:00	34.8	320	5.1	0	1006.6	0.664
2009-07-01	08:00	35.1	325	5.1	0	1006.4	0.848
2009-07-01	09:00	35.8	335	5.1	0	1006.1	0.982
2009-07-01	10:00	36.6	360	5.1	0	1005.9	1.046
2009-07-01	11:00	37.2	335	5.1	0	1005.7	1.031
2009-07-01	12:00	37.7	360	5.1	0	1005.5	0.939
2009-07-01	13:00	37.8	360	5.3	0	1005.5	0.783
2009-07-01	14:00	37.6	335	5.5	0	1005.6	0.588
2009-07-01	15:00	37.3	335	5.7	0	1005.6	0.380
2009-07-01	16:00	36.7	330	5.8	0	1005.7	0.185
2009-07-01	17:00	36.2	325	6.0	0	1005.8	0.021
2009-07-01	18:00	35.7	330	6.2	0	1005.8	0.000
2009-07-01	19:00	35.3	300	6.7	0	1005.9	0.000
2009-07-01	20:00	34.8	300	7.2	0	1006.0	0.000
2009-07-01	21:00	34.3	300	7.7	0	1006.0	0.000
2009-07-01	22:00	33.8	295	8.2	0	1006.1	0.000
2009-07-01	23:00	33.3	305	8.8	0	1006.2	0.000

† in UTC

Tab. C.7.: Weather data from the Meteo Group in 09.2009 [Met09].

date	time†	temperature [°C]	wind direction [°]	wind speed [m/s]	cloud amount [octas]	air pressure [hPa]	global radiation [kW/m^2]
2009-09-01	00:00	27.6	300	10.3	0	1008.8	0.000
2009-09-01	01:00	27.9	305	10.3	0	1009.0	0.000
2009-09-01	02:00	28.2	300	10.3	0	1009.1	0.000
2009-09-01	03:00	28.6	305	10.3	0	1009.3	0.000
2009-09-01	04:00	29.1	310	10.3	0	1009.5	0.001
2009-09-01	05:00	29.7	315	10.3	0	1009.6	0.188
2009-09-01	06:00	30.4	330	10.3	0	1009.8	0.407
2009-09-01	07:00	30.6	320	10.7	0	1009.4	0.633
2009-09-01	08:00	31.0	325	11.0	0	1009.0	0.834
2009-09-01	09:00	31.7	325	11.3	0	1008.6	0.979
2009-09-01	10:00	32.5	350	11.7	0	1008.2	1.045
2009-09-01	11:00	33.2	330	12.0	0	1007.8	1.020
2009-09-01	12:00	33.7	360	12.4	0	1007.4	0.909
2009-09-01	13:00	34.0	335	10.3	0	1007.3	0.731
2009-09-01	14:00	34.0	330	8.2	0	1007.3	0.512
2009-09-01	15:00	33.9	360	6.2	0	1007.2	0.286
2009-09-01	16:00	33.4	335	6.8	0	1007.7	0.082
2009-09-01	17:00	32.9	325	7.6	0	1008.1	0.000
2009-09-01	18:00	32.3	320	8.2	0	1008.6	0.000
2009-09-01	19:00	31.7	305	8.3	0	1008.6	0.000
2009-09-01	20:00	31.0	305	8.4	0	1008.7	0.000
2009-09-01	21:00	30.4	310	8.5	0	1008.7	0.000
2009-09-01	22:00	29.7	305	8.6	0	1008.7	0.000
2009-09-01	23:00	29.0	305	8.6	0	1008.8	0.000

† in UTC

Tab. C.8.: Weather data from the Meteo Group in 11.2009 [Met09].

date	time†	temperature [°C]	wind direction [°]	wind speed [m/s]	cloud amount [octas]	air pressure [hPa]	global radiation [kW/m²]
2009-11-01	00:00	21.3	280	5.1	0	1012.0	0.000
2009-11-01	01:00	21.8	155	5.0	0	1012.0	0.000
2009-11-01	02:00	22.3	145	4.8	0	1012.1	0.000
2009-11-01	03:00	22.8	145	4.6	0	1012.1	0.000
2009-11-01	04:00	23.5	10	4.5	0	1012.1	0.000
2009-11-01	05:00	24.1	130	4.3	0	1012.2	0.084
2009-11-01	06:00	24.9	260	4.1	0	1012.2	0.292
2009-11-01	07:00	25.4	145	4.2	0	1011.7	0.502
2009-11-01	08:00	25.9	285	4.3	0	1011.3	0.684
2009-11-01	09:00	27.0	320	4.4	0	1010.8	0.807
2009-11-01	10:00	28.2	305	4.5	0	1010.3	0.849
2009-11-01	11:00	29.3	220	4.5	0	1009.9	0.804
2009-11-01	12:00	30.0	120	4.6	0	1009.4	0.679
2009-11-01	13:00	29.9	210	4.2	0	1009.7	0.495
2009-11-01	14:00	29.4	230	3.8	0	1010.1	0.284
2009-11-01	15:00	28.6	230	3.3	0	1010.4	0.078
2009-11-01	16:00	27.4	215	2.9	0	1010.7	0.000
2009-11-01	17:00	26.4	210	2.5	0	1011.1	0.000
2009-11-01	18:00	25.4	170	2.1	0	1011.4	0.000
2009-11-01	19:00	24.7	150	2.7	0	1011.4	0.000
2009-11-01	20:00	24.0	310	3.2	0	1011.4	0.000
2009-11-01	21:00	23.3	310	3.9	0	1011.3	0.000
2009-11-01	22:00	22.5	285	4.5	0	1011.3	0.000
2009-11-01	23:00	21.8	295	5.0	0	1011.3	0.000

† in UTC

Tab. C.9.: Density of water in the range between 0 °C and 100 °C [Wte11]

Temperature [°C]	Density [kg/m^2]	Comment	Temperature [°C]	Density [kg/m^2]	Comment
0	918	ice	27	996.51	
0	999.84		28	996.23	
1	999.90		29	995.94	
2	999.94		30	995.64	
3	999.96		31	995.34	
4	999.97		32	995.02	
5	999.96		33	994.70	
6	999.94		34	994.37	
7	999.90		35	994.03	
8	999.85		36	993.68	
9	999.78		37	993.32	
10	999.70		38	992.96	
11	999.60		39	992.59	
12	999.50		40	992.21	
13	999.38		45	990.21	
14	999.24		50	988.03	
15	999.10		55	985.69	
16	998.94		60	983.19	
17	998.77		65	980.55	
18	998.59		70	977.76	
19	998.40		75	974.84	
20	998.20		80	971.79	
21	997.99		85	968.61	
22	997.77		90	965.30	
23	997.54		95	961.88	
24	997.29		100	958.35	
25	997.04		100	0.590	vapour at 1013 hPa
26	996.78				

Tab. C.10.: Selection of different data for the simulation in Carnot.

time [s]	time value†	zenith angle of Sun [°]	azimuth angle of Sun [°]	direct solar radiation [W/m^2]	diffuse solar radiation [W/m^2]	ambient temperature [°C]	mean wind speed [m/s]	wind direction [°]
0	2009092000	152	-170	0	0	28	6.1	293
3600	2009092001	147	-142	0	0	27	6.1	293
7200	2009092002	137	-123	0	0	27	5.3	293
10800	2009092003	125	-111	0	0	26	5.3	293
14400	2009092004	112	-102	0	0	26	5.6	293
18000	2009092005	99	-95	0	0	25	5.3	270
21600	2009092006	86	-88	0	0	25	5.3	270
25200	2009092007	72	-81	456	46	27	5.6	270
28800	2009092008	59	-73	698	70	29	5.3	293
32400	2009092009	47	-62	807	81	30	5.3	305
36000	2009092010	36	-46	865	87	32	6.1	338
39600	2009092011	29	-22	896	90	33	6.1	0
43200	2009092012	28	11	906	91	33	6.1	0
46800	2009092013	33	39	900	90	33	6.1	23
50400	2009092014	43	57	877	88	33	7.2	0
54000	2009092015	55	69	828	83	33	7.2	0
57600	2009092016	68	78	738	74	33	8.3	0
61200	2009092017	81	86	552	55	33	4.2	0
64800	2009092018	94	92	39	4	31	1.9	135
68400	2009092019	118	99	0	0	30	1.1	270
72000	2009092020	120	108	0	0	31	3.1	305
75600	2009092021	133	118	0	0	29	3.1	270
79200	2009092022	144	134	0	0	28	3.6	293
82800	2009092023	151	150	0	0	28	3.6	293
86400	2009092024	152	170	0	0	28	6.1	293

† in YYYYMMDDHH

References

My references

[Bus05] Daniel Buschert, *X-Band-ESR-Spektroskopie polarisierbarer Targetmaterialien bei tiefen Temperaturen*, diploma thesis, Ruhr-Universität-Bochum, Germany 2005

[Bus08] Daniel Buschert, *Optimization of energy parks with biomass plants and water desalination*, UPEC 2008, Padua, Italy 2008

[Bus09a] Daniel Buschert, *Concept for optimization and simulation of renewable energy parks with desalination*, ICREPQ'09, Valencia, Spain 2009

[Bus09b] Daniel Buschert, B. Bitzer, *Report 2: Analysis of the gathered data*, South Westphalia University of Applied Sciences, Campus Soest, Germany 2009

[Bus10] Daniel Buschert, *Modeling a solar desalination*, ICREPQ'10, Granada, Spain 2010

[Bus11] Daniel Buschert, *Water desalination with evaporation from environmentally friendly waste heat source*, UPEC 2011, Soest, Germany 2011

[Bus14] Daniel Buschert, *Sunwater and beyond*, ICREPQ'14, Cordoba, Spain 2014

General references

[Aeg11] www.aegypten-spezialist.de

[Aki11] www.akitarescueoftulsa.com/phase-diagram-of-water-superphase/

[Ako09] Technical data: Vacuum tube collectors, AkoTech, Germany 2009

[Aet14] www.alternative-energy-tutorials.com

[Ami09] Amr M. A. Amin, *Report 1: Hurghada's Weather Profile*, Helwan University, Sunwater project, Egypt 2009

[Aqu07] Franz Trieb, *Concentrating Solar Power for Seawater Desalination*, Deutsches Zentrum für Luft- und Raumfahrt e.V. (DLR), Stuttgart, Germany 2007

[Bac11] Robert Bach, *Anwendung von Hochtemperatursupraleitern (HTSL) in elektrischen Energieversorgungsnetzen* Hochschule Soest, Germany 2011

[Bae08] Hans Dieter Baehr, Karl Stephan, *Wärme- und Stoffübertragung*, Springer, Germany 2008

[Bar10] lexikon.astronomie.info/zeitgleichung, Arnold Barmettler

[Bro08] Ilja Nikolajewitsch Bronstein, *Taschenbuch der Mathematik*, Verlag Harri Deutsch, Germany 2008

[Bjo11] www.buschjostventile.de

[Car10] Carnot Blockset, *Conventional and renewable energy systems optimization blockset*, Solar Institute Jülich, version 1.0

[Cer11] www.cern.ch

[Chi04] Rolf Chini, *Astronomie I + II*, Ruhr-Universität-Bochum, Germany 2004

[Coh75] Yehuda Cohen, Wolfgang E. Krumbein et al., *Solar Lake (Sinai). 1. Physical and chemical limnology*, Department of Microbiological Chemistry, Israel 1975

[Dar08] M. A. Darwish, *Towards sustainable seawater desalting in the Gulf area*, Mechanical Engineering Department, Kuwait University, Kuwait 2008

[Daw12] Mohamed A. Dawoud, *Environmental Impacts of Seawater Desalination: Arabian Gulf Case Study*, Water Resources Department, Environment Agency, Abu Dhabi, United Arab Emirates 2012

[Des10] *Water resources, withdrawal and pollution*, Statistisches Bundesamt, Statistisches Jahrbuch 2010

[Des11] Max Voß, *Desertec, renewable energy from the desert*, RWE AG Research and Development, UPEC 2011, Germany

[DPG10] Deutsche Physikalische Gesellschaft, *Elektrizität: Schlüssel zu einem nachhaltigen und klimaverträglichen Energiesystem*, DPG, Bad Honnef, Germany 2010

[Dwd11] www.dwd.de

[Ebe11] www.erneuerbareenergien.de

[End05] Endohousing - Endothermic technology for energy efficient housing in the European Union, int. project, Soest, Germany

[Ett06] Mohamed Al-bahou, Zamzam Al-Rakaf, Hassan Zaki, Hisham Ettouney, *Desalination experience in Kuwait*, Kuwait 2006

[Faz06] *Öl oder Wasser - was versiegt zuerst?*, www.faz.de 2006

[Fli01] Torsten Fließbach, *Mechanik, Lehrbuch zur Theoretischen Physik I*, Spektrum Akademischer Verlag, Heidelberg, Germany 1999

[Fli02] Torsten Fließbach, *Elektrodynamik, Lehrbuch zur Theoretischen Physik II*, Spektrum Akademischer Verlag, Heidelberg, Germany 2000

[Fli04] Torsten Fließbach, *Statistische Physik, Lehrbuch zur Theoretischen Physik IV*, Spektrum Akademischer Verlag, Heidelberg, Germany 1999

[Fli06] Torsten Fließbach, Hans Walliser, *Arbeitsbuch zur Theoretischen Physik I - IV*, Spektrum Akademischer Verlag, Heidelberg, Germany 2008

[For99] Otto Forster, *Analysis 1*, Vieweg Studium, Germany 1999

[Gas96] Andreas Gassel, *Beiträge zur Berechnung solarthermischer und exergieeffizienter Energiesysteme*, Dissertation, Dresden, Germany 1996

[Ger02] Dieter Meschede, *Gerthsen Physik*, Springer-Verlag, Berlin, Heidelberg, Germany 2002

[GJJ76] L. A. Guildner, D. P. Johnson, F. E. Jones, *Vapor Pressure of Water at Its Triple Point*, Institute for Basic Standards, National Bureau of Standards, Washington D. C., USA 1976

[Gof46] J. A. Goff, S. Gratch, *Low-pressure properties of water from -160 to* 212 °F, in Transactions of the American Society of Heating and Ventilating Engineers, New York, United States 1946

[Goo11] maps.google.de

[Gre14] www.greencollarjobtraining-free.com

[Gre11] www.greenpeace.de

[Gru10] Technical data: UPS 31-120 F, Grundfos, Egypt 2010

[Gru11] www.grundfos.de

[Gtz09] Deutsche Gesellschaft für Technische Zusammenarbeit (GTZ) GmbH, *Technische und Wirtschaftliche Potenziale Windgetriebener Wasserentsalzung*, Eschborn, Germany 2009

[Gtz10] Deutsche Gesellschaft für Technische Zusammenarbeit (GTZ) GmbH, *Wasser*, edition 03 - 04 / 2010, Eschborn, Germany 2010

[Hei07] www.heise.de

[Hep08] Michael Heppelmann, *Innovative optimisation of a solar assisted heat pump system*, dissertation, Soest, Germany 2008

[Hoa09] Manh Hoang, *Desalination in Australia*, CSIRO Materials Science and Engineering, Australia 2009

[Ire12] IEA-ETSAP and IRENA Technology Brief I12, *Water Desalination - Using Renewable Energy*, The International Renewable Energy Agency, www.etsap.org, www.irena.org, 2012

[Ite12] www.iter.org

[Jax11] www.jaxa.jp

[Kob10] Technical data: DUK flow meters, Kobold, Germany 2010

[Kob11] www.kobold.de

[Lag71] Joseph Louis Lagrange, Œuvre de Lagrange, mémoires extraits des recueils de l'académie royale des sciences et belles-lettres de Berlin 1869, publication 1771

[Lgi02] Technical data: iG5 Series, LG Industrial Systems, Egypt 2002

[Loe10] Martin Lödl, *Abschätzung des Photovoltaik-Potentials auf Dachflächen in Deutschland*, 11. Symposium Energieinnovation, Graz, Austria 2010

[Luc10] www.lucom.de

[Mag10] Technical data: Solenoid valves, Buschjost, Germany 2010

[Maple] www.maplesoft.com, Waterloo Maple Inc. 2012

[Mdr12] Mena Development Report, *Renewable Energy Desalination - An Emerging Solution to Close the Water Gap in the Middle East and North Africa*, International Bank for Reconstruction and Development / The World Bank, Washington DC, USA 2012

[Mee98] Jean Meeus, *Astronomical Algorithms*, Willmann-Bell, Richmond 1998

[Met07] Meteotest, *Datenbank Meteonorm*, (www.meteonorm.com), Switzerland 2007

[Met09] www.meteogroup.de

[Mic09] Giorgio Micale, Lucio Rizzuti and Andrea Cipollina, *Seawater Desalination*, Springer 2009

[Mit11] Ken Gethard, Ornthida Sae-Khow, Somenath Mitra, *Water Desalination Using Carbon-Nanotube-Enhanced Membrane Distillation*, New Jersey Institute of Technology, United States 2011

[Mue93] Markus Müller, *Equation of time - Problem in astronomy*, awarded paper in the II International Competition in First Step to Nobel Prize in Physics, Münchenstein, Switzerland 1993

[N24] www.n24.de

[Nat11] www.nature.com

[Opp86] Chr. von Oppel, *Wasserentsalzung mit elektrochemischen Membranverfahren*, VGB Kraftwerkstechnik, Germany 1986

[Pac06] Heather Cooley, Peter H. Gleick and Gary Wolff, *Desalination, with a grain of salt*, Pacific Institute, United States 2006

[Pen47] Howard L. Penman, *Natural evaporation from open water, bare soil and grass*, Harpenden, Herts, UK 1947

[Pet03] Marcus Petermann, "Mit Sonnenlicht zum Trinkwasser", Lehrstuhl für Partikeltechnologie und Partikeldesign der Ruhr-Universität Bochum, Bochum, Germany 2003

[Phy11] Physik Journal 10.2011

[Phy12] Physik Journal 11.2012

[Pic02] Keith A. Pickering, *The Southern Limits of the Ancient Star Catalog and the Commentary of Hipparchos*, Watertown, Minnesota, United States 2002

[Pvc11] www.pveducation.org/pvcdrom

[Qad09] Mohammed Redha Qader, *Electricity Consumption and GHG Emissions in GCC Countries*, Applied Studies College, University of Bahrain, Kingdom of Bahrain 2009

[Raw92] Dennis Rawlins, *Tycho 1004-Star Catalog's Completion Was Faked*, DIO 2.1, 1992

[Sch02] Otto Schafmeister, *Mathematik I - IV*, Vorlesung, Ruhr-Universität-Bochum, Germany 2000 - 2002

[Sch09] Reinhard Schlickeiser, *Theoretische Physik II: Elektrodynamik*, Vorlesung, Ruhr-Universität-Bochum, Germany 2009

[Sma10] Smart-ECO consortium, *Sustainable Smart Eco-Buildings in the EU*, international project 2008 - 2010

[Sol08] Susan Solomona, Gian-Kasper Plattnerb, Reto Knuttic Pierre Friedlingstein, *Irreversible climate change due to carbon dioxide emissions*, United States 2008

[Sol10] www.solaregypt.com

[Sol11] www.solarserver.de

[Spe71] J. W. Spencer, *Fourier series representation of the position of the sun*, Melbourne, Victoria, Australia 1971

[Spi10] www.spiegel.de

[Ter10] Nicolas Heyn, *Terrawater*, www.terrawater.de, Kiel 2009 - 2011

[The10] www.thermea.de

[Tip00] Paul A. Tipler, *Physik*, Spektrum Akademischer Verlaf, Heidelberg, Germany 2000

[Tos10] Technical data: Weather sensors, Toss GmbH, Germany 2010

[Tos11] www.toss.de

[Tre08] Technical data: Trend IQ3 Web-DDC-Station, Trend controls, Germany 2008

[Tre09] Technical data: Trend IQView4 Touch Screen Display, Trend controls, Germany 2009

[Tre11] www.trendcontrols.com

[Tri01] Trinkwasserverodnung, Germany 2001

[Twt11] www.thewatertreatments.com

[Uni06] www.unicef.de

[Was11] www.wasserstiftung.de

[Wel11] www.welthungerhilfe.de

[Wet09] www.wetter24.de

[Wte11] www.wissenschaft-technik-ethik.de

[Wwf09] WWF, The Facts on Water in Africa, www.panda.org

[Zoh06] Hartmut Zohm, *Theoretische Hydrodynamik*, Max-Planck-Institute for Plasmaphysics, Garching, Germany 2006